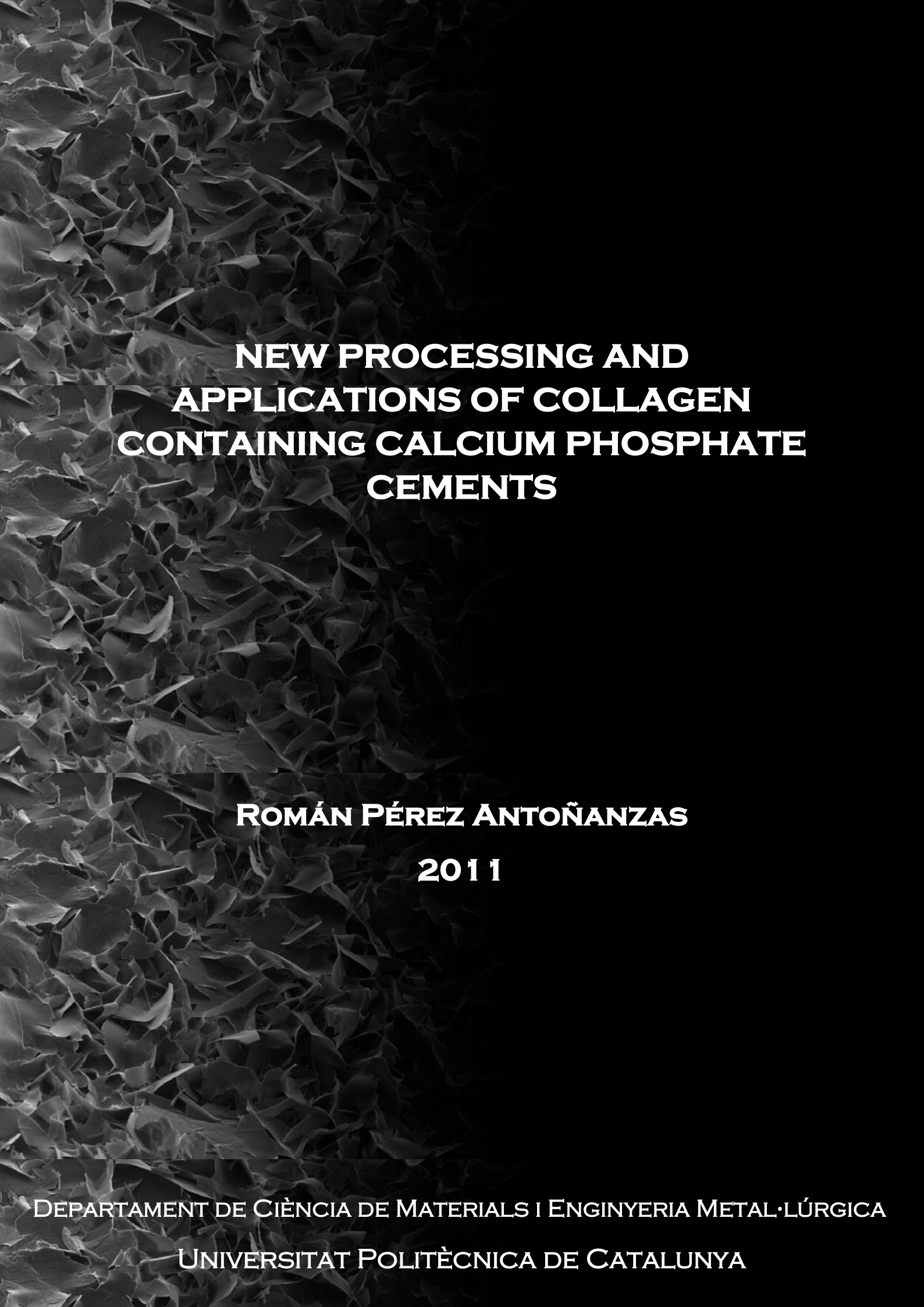


**ADVERTIMENT.** La consulta d'aquesta tesi queda condicionada a l'acceptació de les següents condicions d'ús: La difusió d'aquesta tesi per mitjà del servei TDX ([www.tesisenxarxa.net](http://www.tesisenxarxa.net)) ha estat autoritzada pels titulars dels drets de propietat intel·lectual únicament per a usos privats emmarcats en activitats d'investigació i docència. No s'autoritza la seva reproducció amb finalitats de lucre ni la seva difusió i posada a disposició des d'un lloc aliè al servei TDX. No s'autoritza la presentació del seu contingut en una finestra o marc aliè a TDX (framing). Aquesta reserva de drets afecta tant al resum de presentació de la tesi com als seus continguts. En la utilització o cita de parts de la tesi és obligat indicar el nom de la persona autora.

**ADVERTENCIA.** La consulta de esta tesis queda condicionada a la aceptación de las siguientes condiciones de uso: La difusión de esta tesis por medio del servicio TDR ([www.tesisenred.net](http://www.tesisenred.net)) ha sido autorizada por los titulares de los derechos de propiedad intelectual únicamente para usos privados enmarcados en actividades de investigación y docencia. No se autoriza su reproducción con finalidades de lucro ni su difusión y puesta a disposición desde un sitio ajeno al servicio TDR. No se autoriza la presentación de su contenido en una ventana o marco ajeno a TDR (framing). Esta reserva de derechos afecta tanto al resumen de presentación de la tesis como a sus contenidos. En la utilización o cita de partes de la tesis es obligado indicar el nombre de la persona autora.

**WARNING.** On having consulted this thesis you're accepting the following use conditions: Spreading this thesis by the TDX ([www.tesisenxarxa.net](http://www.tesisenxarxa.net)) service has been authorized by the titular of the intellectual property rights only for private uses placed in investigation and teaching activities. Reproduction with lucrative aims is not authorized neither its spreading and availability from a site foreign to the TDX service. Introducing its content in a window or frame foreign to the TDX service is not authorized (framing). This rights affect to the presentation summary of the thesis as well as to its contents. In the using or citation of parts of the thesis it's obliged to indicate the name of the author



**NEW PROCESSING AND  
APPLICATIONS OF COLLAGEN  
CONTAINING CALCIUM PHOSPHATE  
CEMENTS**

**ROMÁN PÉREZ ANTOÑANZAS**

**2011**

**DEPARTAMENT DE CIÈNCIA DE MATERIALS I ENGINYERIA METAL·LÚRGICA  
UNIVERSITAT POLITÈCNICA DE CATALUNYA**



# ACTA DE QUALIFICACIÓ DE LA TESI DOCTORAL

Reunit el tribunal integrat pels sota signants per jutjar la tesi doctoral:

Títol de la tesi: .....

Autor de la tesi: .....

Acorda atorgar la qualificació de:

- No apte
- Aprovat
- Notable
- Excel·lent
- Excel·lent Cum Laude

Barcelona, ..... de/d'..... de .....

El President

El Secretari

.....  
(nom i cognoms)

.....  
(nom i cognoms)

El vocal

El vocal

El vocal

.....  
(nom i cognoms)

.....  
(nom i cognoms)

.....  
(nom i cognoms)



UNIVERSITAT POLITECNICA DE CATALUNYA

# NEW PROCESSING AND APPLICATIONS OF COLLAGEN CONTAINING CALCIUM PHOSPHATE CEMENTS

ROMÁN PÉREZ ANTOÑANZAS

PHD THESIS

THESIS SUPERVISOR: PROF DRA MARIA PAU GINEBRA MOLINS

DEPARTAMENT DE CIENCIA DELS MATERIALS I ENGINYERIA  
METL·LURGICA

ESCOLA TECNICA SUPERIOR D'ENGINYERIA INDUSTRIAL DE BARCELONA

BARCELONA, 2011





# Acknowledgments

Parece que fue ayer cuando empecé a trabajar en la tesis en el campo de los biomateriales. Esos fueron los comienzos de una nueva etapa o ciclo, y el ciclo finaliza aquí, con la lectura de la tesis. Durante estos años, de manera directa o indirecta, ha sido mucha la gente que ha contribuido para que esta llegase a su fin. Es por ello que estas personas se merecen unas líneas.

En primer lugar se encuentra mi directora de tesis, Prof Maria Pau Ginebra. Ella es la que me ha guiado durante estos años. Le agradezco su paciencia y al mismo tiempo su nivel de exigencia. Este nivel de exigencia es lo que realmente me ha hecho esforzarme cada día al máximo para conseguir decir y hacer las cosas de la manera más eficiente. Sin embargo, lo que más le agradezco y lo que más valoro es el trato que ha tenido hacia mí, el entusiasmo y la alegría que me ha transmitido, las conversaciones del día a día. Por ello, aunque nuestras carreras científicas se separen, siempre recordaré que es una buena persona. Gracias.

Al mismo tiempo, este comentario lo hago extensivo al Prof. Javier Gil quien, a pesar de que no he tenido interacción desde un punto de vista científico, siempre ha tenido el buen clima de trabajo y el buen ambiente en el grupo de investigación como prioridad y, sin duda, el lo ha sabido transmitir. Es por ello que el grupo de BIBITE es un sitio donde me he sentido a gusto, y agradezco a todas las personas que han contribuido a que reine este ambiente y que siempre me han animado durante la tesis. Es más, llegó un momento en que muchas de las personas dejaron de ser compañeros de trabajo para convertirse en amigos. Éste es el recuerdo con el que me quedaré durante muchos años.

I'm also very thankful to Prof Myron Spector, for accepting me in his lab and for his kindness. He always had time for me, even in his busiest moments. He always had a smile for me and all the group members. For all his wise advices and his will to always help. I have great memories of the nine months I stayed in his lab in Boston. I also want to thank the rest of the people at tissue engineering lab for treating me as another member of the group.

También me gustaría agradecer el trato recibido por el Prof Josep Anton Planell, el cual en su momento también me recibió con entusiasmo en el grupo y que también me ha permitido desarrollar parte de mi investigación en el centro que dirige, el IBEC.



También le agradezco la simpatía y alegría que siempre me ha transmitido. I would also like to thank George Altankov for all the advices he has given me and the discussions we have had that have helped me advance during these years.

Agradecer a Jordi Franch y a todo su equipo de la facultad de veterinaria de la UAB por las implantaciones de los materiales desarrollados en la tesis. No simplemente el haber trabajado juntos, sino también el buen humor que tienen, a pesar de que las implantaciones fueron duras. Estos resultados no están incluidos en la tesis, pero es una gran satisfacción ver que los materiales pueden llegar a ser prometedores.

Por supuesto que ha habido personas con las que he tenido más interacción que con otras y con las que he tenido grandes momentos, tanto dentro como fuera del trabajo. Los compañeros de la línea de cementos, Edgar, Gemma, Yassine, David, Montse, Cristina, Sara y Maite, con los cuales he interactuado con gran frecuencia y siempre han tenido buenos consejos. En su momento también fueron Sergio y Tania, los cuales me enseñaron mucho sobre los cementos en mis inicios. También a los estudiantes de ingeniería/master que hicieron el proyecto final conmigo y con los cuales trabajé más directamente codo con codo, como Kiara, Ferran y Cécile. Mis compañeros de despacho durante este final de tesis, Jordi, María, Noelia y Marta G, los cuales siempre han tenido palabras de apoyo, risas y sobretodo, buenos momentos. Marta P, que a pesar de no estar directamente en el mismo despacho, cada día tenía una sonrisa y aportaba más felicidad, si cabe, al despacho. Marc y Luis, con los que siempre compartía unas risas y los cuales siempre me animaban en todo lo que hacía. Txell, por ayudar siempre en todo lo que podía, por hacer los pedidos incluso antes de pedírselos y por su buena disposición. Pablo y Aleix por tener siempre buena predisposición. La gente con la que compartía buenos momentos en las comidas, en las cuales siempre, se hablara del tema del que se hablara, siempre reíamos.

Me gustaría también tener unas líneas para la gente del IBEC con quien compartí buenas conversaciones y momentos. Miguel, del cual me acordaré siempre por su sonrisa constante y por ser una gran persona. Al lado de Miguel siempre estaba Óscar, y sabía que siempre que los veía juntos, dirían alguna de las suyas para estar riendo un rato. Eli, con la que también compartí buenos momentos. Melba, por la alegría constante que transmitía a la gente que estaba alrededor. Finalmente gente con la que

tuve menos contacto, pero que de alguna manera u otra, siempre han estado ahí, como Damien, Jérôme, Clara, Andy, Andrea, Tiziano, Dencho, George T, Nuno y Marta M.

Agradecer también a la gente del departamento de ciencia de materiales la ayuda brindada en cuando ha sido requerida. Esto incluye las horas de SEM con Dr José María Manero, Montse e Isaac, las cuales nunca eran fáciles, pero con su paciencia y experiencia, siempre conseguíamos obtener buenas imágenes. También a las secretarías del departamento, Olga, Lluisa y Esther, por solventar los problemas burocráticos con eficiencia.

Por supuesto, tengo que hacer una mención especial al deporte, ya que ha sido uno de mis grandes apoyos a lo largo de la tesis. No sólo el deporte como tal, sino también las personas que me han ayudado y los amigos que he conseguido a través del fútbol. Entre ellos quisiera destacar a Fede, Ferran y Eric, con los que he compartido muchos grandes momentos y aprecio mucho y, obviamente, toda la gente que está jugando conmigo o que han jugado a lo largo de estos años.

Finalmente, agradecer el apoyo de la familia a lo largo de toda la tesis, mis padres Juanje e Isabel, mi hermano Alberto, mis abuelos Santiago e Isabel, mi tía Belén y mis primos Marc y Cristina. Por haber estado juntos, tanto en los buenos momentos, como en los malos. En especial a mi hermano, ya que, gracias a él, creo que he tenido la fuerza para salir siempre adelante. Ya que, como él bien dijo, de pequeños eramos yo y él contra el mundo. Gracias a la rivalidad y competitividad que hemos tenido desde siempre, en todo lo que hemos hecho, siempre me he esforzado para poder ganarle: en el fútbol, corriendo, jugando a cualquier juego, incluso a las canicas. Muchas veces no lo conseguía, pero cada vez estaba más preparado para la próxima vez. Siempre me esforzaba un poco más. Todo este espíritu de superación también ha sido una de las constantes en la tesis que yo creo que él, sin saberlo, me inculcó.

Agradecer al Ministerio de Ciencia e innovación la beca concedida para realizar la tesis doctoral por 4 años con la beca pre-doctoral BES-2007-16427 dentro del proyecto MAT-2006-16427. A su vez, al IBEC, por otorgarme una beca pre-doctoral de Febrero de 2007 a Enero de 2008.



# Abstract

When bone regeneration is needed, natural bone grafts are widely used. They are the best option since they present the same composition to that of bone, contain living cells with osteogenic potential, growth factors that induce cell differentiation into osteoblasts and extracellular matrix proteins that facilitate bone healing. However, this system presents some drawbacks, such as pain, morbidity, possible transmission of diseases in some cases, as well as limited availability. That is why synthetic bone grafts are one of the main objectives of the research in regenerative medicine and tissue engineering. This new discipline is based on the development of new biomaterials and on the comprehension of the interactions between the cells and the material in order to enhance the bone healing response.

The present thesis is focused on calcium phosphate cements-based materials. CPC have the ability to transform an injectable paste made of calcium phosphates, into a phase similar to that of bone, hydroxyapatite. The CPC are well known for their osteoconductive properties. Nevertheless, these may be improved from a biological point of view and can be further processed to obtain materials with new morphologies and different applications. Therefore, the incorporation of collagen in these CPC was thought as a way to enhance their biological performance. Furthermore, new processing approaches were studied, as well as their applications in new fields. The thesis is divided in three main parts: i) injectable composite cements; ii) composite macroporous scaffolds for tissue engineering and iii) composite microcarriers.

In the first part, the fabrication of injectable composite cements is described as well their physico-chemical and morphological features. It is observed that the setting reaction is delayed in the presence of collagen during the initial minutes of reaction. Already after 1 hour the kinetics are similar in the presence and absence of collagen, without affecting the final product of reaction. The presence of collagen increases the injectability of the cements, whereas the mechanical properties decrease as the collagen concentration increases. From a biological point of view, the addition of collagen results in an increase in the initial cell adhesion as well as an increase in the cell proliferation rates. In the second part, macroporous scaffolds made of collagen and CPC are fabricated. These scaffolds are prepared through the freeze-drying of a collagen-CPC slurry. Different amounts of CPC are incorporated in the scaffolds. When mesenchymal

stem cells are cultured on these scaffolds, it is observed that as the CPC content increases in the scaffolds, the cell differentiation increases, whereas the proliferation decreases. Further improvement of the scaffolds can be achieved through the incorporation of a BMP-7 gene into the scaffolds, in order to stimulate their osteoinductivity. The results show that as the gene incorporated in the scaffolds increases, there is an increase in the BMP-7 production, although this increase is associated with an increase in cell proliferation. In the third and final part, spherical microcarriers containing either gelatin or collagen are produced through the setting reaction of the CPC in a water in oil emulsion. The emulsion and CPC compositions can be adjusted in order to control the final features of the microcarriers. The *in vitro* characterization of the microcarriers reveals that under static and dynamic culturing conditions, microcarriers are able to support cell attachment, proliferation and differentiation.

## Resumen

Cuando la regeneración ósea es necesaria, los injertos de hueso natural son ampliamente utilizados. Son la mejor opción debido a que presentan la misma composición que el hueso, contienen células vivas con potencial osteogénico, factores de crecimiento que inducen la diferenciación de las células a osteoblastos y proteínas de la matriz extracelular que facilitan la regeneración ósea. A pesar de esto, este sistema presenta algunos inconvenientes, tales como el dolor, morbidez, posible transmisión de enfermedades en algunos casos, al igual que una disponibilidad limitada. Por ello, los injertos de hueso sintético son uno de los principales objetivos de la investigación en medicina regenerativa e ingeniería de tejidos. Esta nueva disciplina se basa en el desarrollo de nuevos biomateriales y en la comprensión de las interacciones entre las células y los materiales con el fin de incrementar la regeneración ósea.

La presente tesis se centra en materiales basados en los cementos de fosfato de calcio (CPC). Los CPC tienen la habilidad de transformar una pasta inyectable formada por fosfatos de calcio, en una fase similar a la del hueso, que es la hidroxiapatita. Los CPC son bien conocidos por sus propiedades de osteoconductividad. Sin embargo, estos se pueden mejorar desde un punto de vista biológico y pueden ser procesados con el fin de obtener nuevos materiales con nuevas morfologías y aplicaciones. Por ello, la incorporación de colágeno en estos CPC fue pensada como una manera de incrementar el comportamiento biológico. Se estudiaron nuevas rutas de procesamiento, al igual que sus aplicaciones. La tesis está dividida en tres partes: i) cementos compuesto inyectables; ii) andamios compuestos macroporosos para ingeniería de tejidos y iii) microtransportadores compuestos.

En la primera parte, se describe la fabricación del cemento de fosfato de calcio compuesto y la caracterización físico-química y morfológica del material. Se observa que la reacción de fraguado se retrasa en presencia del colágeno durante los minutos iniciales de reacción. Sin embargo, después de solamente una hora, se observa como la presencia de colágeno no afecta a la cinética de reacción ni al producto final de reacción. La presencia del colágeno incrementa la inyectabilidad de los cementos, mientras que las propiedades mecánicas bajan al incrementar la concentración de colágeno. Desde un punto de vista biológico, la incorporación de colágeno resulta en un incremento de la adhesión celular inicial y un incremento de la proliferación celular. En

la segunda parte, se fabrican andamios macroporosos de colágeno con CPC. Estos andamios se preparan a través de la liofilización de mezclas de colágeno y CPC. Se incorporan diversas cantidades de CPC en los andamios. Cuando se cultivan células mesenquimales en los andamios, se ve que a medida que se incrementa la cantidad de CPC en el andamio, la diferenciación celular se incrementa, mientras que la proliferación disminuye. Los andamios se pueden mejorar mediante la incorporación de un gen para expresar la proteína BMP-7 con el fin de incrementar la osteoinducción. Los resultados muestran que al aumentar la cantidad de gen incorporado en el andamio, se incrementa la producción de BMP-7, aunque este incremento va asociado con un incremento en la proliferación celular. En la tercera y última parte, se fabrican microtransportadores esféricos que contienen gelatina o colágeno mediante la reacción de fraguado del CPC en una emulsión de agua en aceite. La emulsión y la composición del CPC se pueden ajustar con el fin de controlar las propiedades finales de los microtransportadores. La caracterización *in vitro* de los microtransportadores revela que bajo condiciones de cultivo estáticas y dinámicas, los microtransportadores son capaces de soportar adhesión celular, proliferación y diferenciación.

## Thesis objectives

The aim of the thesis is to develop new materials with enhanced properties for bone regeneration. The thesis is based on calcium phosphate cements combined with collagen. Calcium phosphate cements have been widely studied, although the incorporation of this extracellular matrix protein has not been extensively investigated. Three specific objectives were established:

- To fabricate an injectable calcium phosphate cement/collagen composite.
- To fabricate macroporous collagen/calcium phosphate cement scaffolds for tissue engineering and gene delivery applications.
- To fabricate hybrid calcium phosphate/gelatin or collagen microcarriers.

These three main objectives can be considered as three different approaches to design biomaterials for bone regeneration. Relevant milestones can be identified within each of these three issues:

1. Fabrication of an injectable calcium phosphate cement/collagen composite
  - To optimize the L/P ratio to obtain an injectable and mouldable paste with good handling and setting properties.
  - To determine effect of collagen in the physico-chemical properties and morphology of the CPC.
  - To determine the effect of collagen concentration and its initial morphology in the CPC properties.
  - To determine the *in vitro* response of osteoblasts on the composite CPC.
2. Fabrication of macroporous collagen/calcium phosphate cement scaffolds for tissue engineering
  - To determine the effect of CPC incorporation in the collagen sponge properties.
  - To study the behavior of mesenchymal stem cells on scaffolds with different fractions of CPC.
  - To determine the effect of incorporating a bone morphogenetic protein 7 gene in the scaffolds on the mesenchymal stem cells response.



3. Fabrication of hybrid calcium phosphate cement/gelatin or collagen microcarriers through a water in oil emulsion.
- To optimize the processing parameters to obtain a low viscosity CPC paste adequate for microcarrier fabrication.
  - To introduce collagen or gelatin in the low viscosity CPC to fabricate composite microcarriers.
  - To optimize the emulsion parameters in order to obtain inorganic or composite microcarriers with desired features.
  - To determine *in vitro* cell viability of osteoblastic cells cultured on inorganic and composite microcarrier under static conditions.
  - To determine the ability of the microcarriers to be injected when mixed with an adequate gel.
  - To optimize *in vitro* conditions in spinner flask dynamic cultures to ensure cell viability on the microcarriers.

## Publications

Espanol M, Pérez RA, Montufar EB, Marichal C, Sacco A & Ginebra MP. Intrinsic porosity of calcium phosphate cements and its significance for drug delivery and tissue engineering applications. *Acta Biomaterialia* **5** 2752-2762 (2009).

Ginebra MP, Espanol M, Montufar EB, Pérez RA & Mestres G. New Processing Approaches In Calcium Phosphate Cements And Their Applications In Regenerative Medicine. *Acta Biomaterialia* **6** 2863–2873 (2010)

Pérez RA, Del Valle S, Altankov G & Ginebra MP. Porous Hydroxyapatite and Gelatin/Hydroxyapatite Microspheres Obtained by Calcium Phosphate Cement Emulsion. *Journal of Biomedical Biomaterials Research B: Applied Biomaterials* **97** 156-166 (2011).

Perez RA, Ginebra MP & Spector M. Cell Response to Collagen-Calcium Phosphate Cement Scaffolds Investigated for Nonviral Gene Delivery. *Journal of Materials Science: Materials in Medicine* **22** 887-897 (2011).

Pérez RA, Altankov G, Jorge-Herrero E & Ginebra MP. Micro- and nanostructured hydroxyapatite/collagen microcarriers for bone tissue engineering applications. *Journal of Tissue Engineering and Regenerative Medicine* (submitted).

## Conference Participation

Pérez RA, Del Valle S, Altankov G & Ginebra MP. Calcium Phosphate Cement Microcarriers. *8<sup>th</sup> World Biomaterials Congress* 28<sup>th</sup> May- 1<sup>st</sup> June 2008, Amsterdam, Holland (Poster Presentation).

Pérez RA, Del Valle S, Altankov G & Ginebra M.P. Desarrollo de microtransportadores de cement de fosfato de calcio para la regeneración ósea. *X Congreso Nacional de Materiales* 18-20<sup>th</sup> June 2008, San Sebastián, Spain (Oral Presentation).

Pérez RA, Del Valle S, Altankov G & Ginebra MP. Hydroxyapatite and Hydroxyapatite/Gelatine Microcarriers Obtained by Calcium Phosphate Cement Emulsion. *2nd China-Europe Symposium on Biomaterials in Regenerative Medicine* 16-20<sup>th</sup> November 2009, Barcelona, Spain (Oral Presentation).

Pérez RA, Del Valle S, Altankov G & Ginebra MP. Porous Hydroxyapatite Microspheres as Cell Microcarriers for Bone Augmentation. *The International Association for Dental Research General Session & Exhibition* 14<sup>th</sup>-17<sup>th</sup> July 2010, Barcelona, Spain (Oral presentation).

Pérez RA, Ginebra MP & Spector M. Collagen-Calcium Phosphate Cement Scaffolds for Nonviral Gene Delivery. *23rd European Conference on Biomaterials (ESB 2010)* 11-15<sup>th</sup> September 2010, Tampere, Finland (Oral Presentation).

Pérez RA, Ginebra MP & Spector M. Collagen-Calcium Phosphate Cement Scaffolds for Nonviral Gene Delivery. *Symposium ITREN 2011* 15<sup>th</sup> January 2011, Cheonan, South Korea (Oral Presentation).

<b>Acknowledgments</b>	<b>I</b>
<b>Abstract</b>	<b>V</b>
<b>Resumen</b>	<b>VII</b>
<b>Objectives</b>	<b>IX</b>
<b>Publications and Conference Participation</b>	<b>XI</b>
<b>Chapter 1: Introduction</b>	<b>1</b>
1.1. Mythology and Science	1
1.2. Bone	3
1.2.1. Composition	3
1.2.1.1. Bone cells	4
1.2.2. Function	6
1.2.3. Structure	7
1.2.4. Bone remodeling	9
1.3. Bone substitutes	11
1.3.1. Bone graft	11
1.3.1.1. Autograft	12
1.3.1.2. Allograft	12
1.3.1.3. Xenografts	13
1.3.1.4. Synthetic Bone grafts	13
1.3.2. Tissue engineering and regenerative medicine	14
1.4. Biomaterials for bone tissue engineering and regenerative medicine	15
1.4.1. Calcium phosphates	15
1.4.2. Calcium phosphate cements	19
1.4.3. Collagen	21
1.4.4. Calcium phosphate/collagen composites for bone regeneration	24
1.5. Cell interactions with biomaterials	30
1.5.1. Collagen-integrins interaction	31
1.5.2. Recognition sites in triple helical and denatured collagen	33
1.6. References	34
<b>Chapter 2: Calcium Phosphate Cement-Collagen for Bone Regeneration</b>	<b>49</b>
2.1. Introduction	49
2.2. Objectives	51
2.3. Materials and methods	51
2.3.1. Powder phase	51
2.3.1.1. Synthesis and preparation	51
2.3.1.2. Characterization of powder	54

2.3.2. Liquid phase	55
2.3.2.1. Preparation of collagen solutions	55
2.3.2.2. Collagen characterization	56
2.3.3. Characterization of the setting reaction	57
2.3.3.1. Setting and cohesion times	57
2.3.3.2. Differential Scanning Calorimetry	59
2.3.3.3. pH evolution	59
2.3.4. Calcium phosphate cement properties	60
2.3.4.1. Collagen liberation during setting	60
2.3.4.2. Collagen distribution	61
2.3.4.3. Scanning electron microscopy	61
2.3.4.4. Fourier Transformed Infrared Spectroscopy	62
2.3.4.5. X-Ray diffraction	62
2.3.4.6. Helium pycnometry	63
2.3.4.7. Mercury intrusion porosimetry	63
2.3.4.8. Injectability	64
2.3.4.9. Mechanical properties	64
2.3.4.10. Statistical analysis	65
2.4. Results	65
2.4.1. Powder phase	65
2.4.1.1. Thermal treatment	65
2.4.1.2. Particle size distribution	66
2.4.2. Liquid phase	67
2.4.3. Characterization of the setting reaction	68
2.4.3.1. Setting and cohesion times	69
2.4.3.2. Differential scanning calorimetry	69
2.4.3.3. pH evolution	71
2.4.4. Calcium phosphate cement properties	73
2.4.4.1. Collagen release during the setting reaction	73
2.4.4.2. Collagen distribution	73
2.4.4.3. Scanning electron microscopy	76
2.4.4.4. Fourier Transformed Infrared Spectroscopy	78
2.4.4.5. X-Ray diffraction	82
2.4.4.6. Helium pycnometry	86
2.4.4.7. Porosimetry	87
2.4.4.8. Injectability	91
2.4.4.9. Mechanical properties	93
2.5. Discussion	95
2.5.1. Collagen processing	95
2.5.2. Setting reaction	98

2.5.3. Collagen release and collagen distribution	102
2.5.4. Microstructure	103
2.5.5. Phase evolution and CPC-collagen interaction	104
2.5.6. Density and porosity	106
2.5.7. Injectability	108
2.5.8. Mechanical properties	109
2.6. Conclusions	110
2.7. References	111

### **Chapter 3: Cell Response to Injectable CPC/Collagen Composites** **121**

3.1. Introduction	121
3.2. Objectives	122
3.3. Materials and methods	122
3.3.1. Materials	122
3.3.2. Cells	123
3.3.3. Cell behaviour on CPC/collagen composites	123
3.3.3.1. Initial adhesion	123
3.3.3.2. Cell proliferation and cell differentiation	124
3.3.4. Characterization	124
3.3.4.1. Proliferation	124
3.3.4.2. Differentiation	125
3.3.4.3. Fluorescence Diacetate staining	125
3.3.4.4. Scanning Electron Microscopy	126
3.3.5. Statistical analysis	126
3.4. Results	126
3.4.1. Initial cell adhesion	126
3.4.2. Cell proliferation and cell differentiation	128
3.4.2.1. Proliferation	128
3.4.2.2. Differentiation	129
3.4.2.3. Overall cell morphology	130
3.5. Discussion	132
3.6. Conclusions	136
3.7. References	137

### **Chapter 4: Cell Response to Collagen-Calcium Phosphate Cement Scaffolds Investigated for Nonviral Gene Delivery** **141**

4.1. Introduction	141
4.2. Objectives	143
4.3. Materials and methods	144
4.3.1. Collagen preparation	144

4.3.2. Calcium phosphate cement powder	144
4.3.3. Preparation of the scaffolds	144
4.3.3.1. Scaffold characterization	145
4.3.4. Plasmid preparation	145
4.3.5. MSC culture	147
4.3.6. <i>In vitro</i> behavior of scaffolds containing different HA content	147
4.3.6.1. Proliferation	148
4.3.6.2. Differentiation	148
4.3.6.3. Cell morphology	149
4.3.7. Plasmid incorporation	149
4.3.8. Statistical analysis	150
4.4. Results	150
4.4.1. Microstructure of the scaffolds	150
4.4.2. Plasmid characterization	152
4.4.3. Cell response to collagen scaffolds with different HA contents	153
4.4.4. BMP-7 expression	158
4.5. Discussion	160
4.6. Conclusions	164
4.7. References	165
<b>Chapter 5: Porous Hydroxyapatite and Gelatin/Hydroxyapatite Microcarriers Obtained by Calcium Phosphate Cement Emulsion</b>	<b>171</b>
5.1. Introduction	171
5.2. Objectives	174
5.3. Materials and methods	174
5.3.1. Microcarriers preparation	174
5.3.2. Microcarriers characterization	176
5.3.3. Cell cultures	177
5.3.3.1. Overall cell morphology	178
5.3.3.2. Cell proliferation	178
5.3.3.3. Cell differentiation	179
5.3.3.4. Statistical analysis	179
5.4. Results	179
5.4.1. Inorganic Microcarriers	179
5.4.2. Gelatine-Hydroxyapatite Microcarriers	183
5.4.3. Cellular response	185
5.5. Discussion	189
5.6. Conclusions	194
5.7. References	195

<b>Chapter 6: Hydroxyapatite/collagen Microcarriers for Bone Tissue Engineering Applications</b>	<b>201</b>
6.1. Introduction	201
6.2. Objectives	203
6.3. Materials and methods	203
6.3.1. Microcarrier preparation	203
6.3.2. Microcarriers characterization	204
6.3.3. <i>In vitro</i> culture test	205
6.3.3.1. Morphology	205
6.3.3.2. Cell proliferation	206
6.3.3.3. Cell differentiation	206
6.3.4. Statistical analysis	206
6.4. Results	206
6.4.1. Microcarrier characterization	206
6.4.2. <i>In vitro</i> culture test	209
6.4.2.1. Overall morphology and proliferation	209
6.4.2.2. Cell differentiation	212
6.5. Discussion	213
6.6. Conclusions	215
6.7. References	216
<b>Chapter 7: Dynamic In Vitro Characterization CPC Composite Microcarriers</b>	<b>221</b>
7.1. Introduction	221
7.2. Objectives	223
7.3. Materials and methods	223
7.3.1. Materials	223
7.3.2. Culturing cells on MC in dynamic cultures	223
7.3.2.1. Cell proliferation	226
7.3.2.2. Cell morphology	226
7.3.2.3. Statistical analysis	226
7.3.3. MC-containing alginate gels	227
7.4. Results	228
7.4.1. Dynamic culture	228
7.4.1.1. Short-time dynamic and static culture	229
7.4.1.2. Long-term dynamic and static culture	233
7.4.2. MC-containing alginate gels	236
7.5. Discussion	240
7.6. Conclusions	247
7.7. References	248
<b>Conclusion and Future Perspectives</b>	<b>253</b>





# Chapter 1: Introduction

## 1.1. Mythology and Science

In the ancient Greek mythology, Prometheus was a Titan, the son of Iapetus and Themis. He stole fire from Zeus to give it to the mortals. Zeus punished him for this crime and bounded him to a rock while a great eagle ate his liver every day (Figure 1.1). The most striking thing was that Prometheus' liver was able to grow back or regenerate every night<sup>1</sup>. Nowadays, biomedical researchers are trying to develop the Promethean ability to regenerate organs. Actually, there are several companies in the biomedical field which have inspired their name in the Greek mythology (e.g. Prometheus: Therapeutics and diagnostics).

Nowadays, this Promethean ability to regenerate tissue is called tissue engineering and refers to the use of human cells to restore, maintain or repair human tissue. Bone, muscle, or skin tissue can be formed with the use of tissue engineering tools. This tissue engineering approach is becoming promising for the replacement of these tissues, since the supply of organs from donors cannot keep up with the demand. For this purpose, scientists deal with the extraction of cells and how to make them form a specific tissue with a



Figure 1.1. Prometheus and his brother Atlas punished by Zeus.

determined function. Cells have the genetic material needed to become the desired tissue, but they need the right cues. A code made of 3.000.000 letters (gene sequence) will give directions to cell of when to live, when to grow and when to die. These cells, moreover, need a structure (scaffold) to guide the regeneration, nutrients and oxygen.

One of the key issues in tissue engineering is the ability of the cells to grow on these types of structures called scaffolds. These cells need to be maintained on these scaffolds *ex vivo*, simulating the conditions *in vivo*. This was already achieved 100 years ago. Rudolf Virchow in the late 1850's published his work *Cellularpathologie*<sup>2</sup>, in which he described that tissue regeneration was dependent on cell proliferation, work in which he also cultivated cells outside the body (nowadays known as *in vitro* first suggested by Leo Loeb<sup>3</sup>). CA Ljunggren and J Jolly were the first researchers to attempt the *in vitro* cultivation<sup>4</sup>, but it was not until the work done by RG Harrison in 1910 that demonstrated the active growth of cells in culture<sup>5</sup>. This was one of the key points in science and especially in tissue engineering.

The promethean ability to regenerate an organ did not succeed until the 70s'. WT Green undertook some experiments to generate new cartilage by implanting chondrocytes seeded on a scaffold in nude mice<sup>6</sup>. He did not succeed, but he set the theoretical and practical concept of connecting cells with a scaffold. He concluded that with the improvement of biomaterials science and the loading of cells into these biomaterials, it would be possible to

produce or regenerate tissues<sup>6</sup>. Burke and Yannas generated skin by a culture of dermal fibroblasts or keratinocytes on protein scaffolds and using them for the regeneration of burn wounds. The bases of the new biomedical discipline were established in the article by Langer and Vacanti<sup>7</sup>. Tissue engineering was even more advertised when BBC explored the potential of tissue-engineered cartilage, which included images of the mouse with the ear on its back from the laboratory of Dr Charles Vacanti (Figure 1.2.). This Vancanti mouse



*Figure 1.2. Vacanti's mouse with an ear on its back.*

helped to promote the idea of creating new tissues and organs. Since then, tissue engineering has been considered one of the most promising technologies of the century.

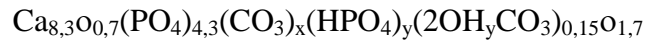
The present thesis will deal with tissue engineering and regenerative medicine applied to bone. As will be seen, the combination of the main components of bone was thought of an interesting approach to regenerate bone.

## 1.2. Bone

### 1.2.1. Composition

Bone is a living and dynamic tissue composed mainly of collagen, stiffened with calcium phosphate crystals embedded in its structure. Bone also contains water, proteins, cells and macromolecules. The bone matrix is composed of an organic matrix, which is 30% of the total bone weight, and mainly composed of collagen (90-95%) and 5-8% of non-collagenous proteins such as osteocalcin, osteonectin, proteoglycans, bone morphogenetic protein, proteolipids and phosphoproteins. The mineral phase constitutes 60% of the bone weight and is composed almost entirely of carbonated hydroxyapatite having small amounts of magnesium, sodium, potassium, fluorides and chlorides. The 10% missing for the total bone weight is attributed to water.

The hydroxyapatite is able to precipitate on the gaps left by the collagen fibers presenting the following formula<sup>8</sup>:



Where o represents a vacant and  $x + y = 1,7$

It presents the following characteristics<sup>8</sup>:

- It is calcium deficient
- It presents  $\text{CO}_3^{2-}$  in its structure (substitution for groups  $\text{PO}_4^{3-}$ )
- It has a non-stoichiometric composition, presenting  $\text{HPO}_4^{2-}$  groups and  $\text{Na}^+$ ,  $\text{Mg}^{2+}$ ,  $\text{K}^+$ ,  $\text{F}^-$  and  $\text{Cl}^-$  which are incorporated in its structure
- It has low crystallinity (250-500 x 30 Å)
- It has high specific surface area

Bones also contain blood vessels. Most of the bones are hollow and contain hematopoietic or fatty marrow, which will allow for new cell formation. Tendons and ligaments insert into the bone substance. The ends of the bones are often covered by a thin layer of cartilage for lubrication.

The membrane that lines on the outside of the bone is called periosteum, as for the membrane found inside the bone is called endosteum.

#### *1.2.1.1. Bone cells*

The cellular part of bone is composed of three cell types that derive from the marrow cells found inside the bones, namely, osteoblasts, osteocytes and osteoclasts.

Osteoblasts derive from bone-lining cells and are responsible for the formation of bone. The word comes from the Greek words bone (osteo) and embryonic (blast). They initially lay down the collagenous matrix, osteoid, in which mineral is later deposited. These kind of cells are able to produce type I collagen, osteocalcin and sialoproteins.

Osteoprogenitors cells are induced to differentiate to osteoblasts under the influence of growth factors, especially bone morphogenetic proteins. Osteoblasts have big rough endoplasmatic reticulum. The rough endoplasmatic reticulum is composed of ribosomes which are the organules in charge of protein synthesis. They also have a large Golgi apparatus and a large and spherical nucleus. Osteoblasts that become trapped in the bone matrix become osteocytes<sup>9</sup>.

Osteocytes are the cells in the body of the bone and their density may vary from 90.000  $\text{mm}^{-3}$  in rats to 30.000  $\text{mm}^{-3}$  in cows. In general, as the animal is bigger, the lower the density of osteocytes will be<sup>10</sup>. Unlike osteoblasts, osteocytes have a high nucleus/cytoplasm ratio, meaning that they contain fewer organules due to their low activity in synthesis and are involved in the routine turnover of bony matrix, through various mechanosensory mechanisms. As mentioned before, they derive from osteoblasts and are imprisoned in the hard tissue and connect with neighboring osteocytes and with bone lining cells, by means of processes that are housed in little channels, named canaliculi, of about 0.2-0.3  $\mu\text{m}$  in diameter. The connections with neighboring cells are by means of gap junctions that allow small molecules through easily.

The word osteoclast comes from the Greek for the words bone and broken. They are bone destroying cells, are large and multinucleated, derived from precursor cells circulating in the blood. They have a cytoplasm with a high concentration of vesicles and vacuoles. The ways in which they act is by clamping themselves to the bone's surface and leave a space underneath named ruffled border that is very mobile and beneath which, the bone is known to dissolve through the release of protons coming from the osteoclast. Debris, both organic and mineral, are packed into vesicles and pass through the cells body of the osteoclast and is dumped into the space above. The mineral portion of the matrix which is endocytosided is then secreted into the extracellular fluid increasing levels of ions in the blood. Once osteoclasts have dissolved old bone, they disappear and die<sup>11</sup>.

## 1.2.2. Function

The bones are known to have three main functions: mechanical, synthetic and metabolic functionalities. Regarding the mechanical functionality, it has to be taken into account that bone does not only protect the internal organs, but also helps to maintain body shape, transfer movement and even in the transduction of sound. These functionalities are described in Table 1.1.

<b>Function</b>	<b>Importance</b>
<i>Protection</i>	Serve to protect internal organs, such as the skull, which protects the brain, or the ribs, which protect the heart and the lungs
<i>Shape</i>	Provide a frame to keep the body supported
<i>Movement</i>	Bones, in junction with skeletal muscles, tendons, ligaments and joints function together to generate and transfer forces so that individual body parts or the whole body can be manipulated in three-dimensional space
<i>Sound transduction</i>	Important in the mechanical aspect of over shadowed hearing

Table 1.1. Mechanical functions of bone<sup>12</sup>.

The synthetic functionalities of bone are described on Table 1.2.

<b>Function</b>	<b>Importance</b>
<i>Blood production</i>	The marrow, located within the medullar cavity of long bones and interstices of cancellous bone, produces blood cells in a process called hematopoiesis

Table 1.2. Synthetic functions of bone<sup>12</sup>.

The metabolic functionalities of bone are described on Table 1.3.

<b>Function</b>	<b>Importance</b>
<i>Mineral storage</i>	Act as reserves of minerals for the body, most notably calcium and phosphorous
<i>Growth factor storage</i>	Mineralized bone matrix stores important growth factors, such as insulin-like growth factors, transforming growth factors, bone morphogenetic proteins and others
<i>Fat storage</i>	The yellow bone marrow acts as a storage reserve of fatty acids
<i>Acid-base balance</i>	Buffers the blood against excessive pH changes by absorbing or releasing alkaline salts
<i>Detoxification</i>	Bone tissues can also store heavy metals and other foreign elements, removing them from the blood and reducing their effects on other tissues. These can later be gradually released for excretion

Table 1.3. Metabolic functions of bone<sup>12</sup>.

### 1.2.3. Structure

Bone is structured in a hierarchized form, and it is this hierarchy, that gives the optimum functional properties. The different levels at which bone may be studied can be observed in Figure 1.3.<sup>13</sup>:

- 1- The macrostructure: cancellous and cortical bone
- 2- The microstructure (from 10 to 500  $\mu\text{m}$ ): Haversian systems, osteons, single trabeculae
- 3- The sub-microstructure (1-10  $\mu\text{m}$ ): lamellae
- 4- The nanostructure (from hundred nanometers to 1  $\mu\text{m}$ ): fibrillar collagen and embedded mineral
- 5- Sub-nanostructure (below few hundred nanometers): molecular structure of constituent elements, such as mineral, collagen and non-collagenous organic proteins.



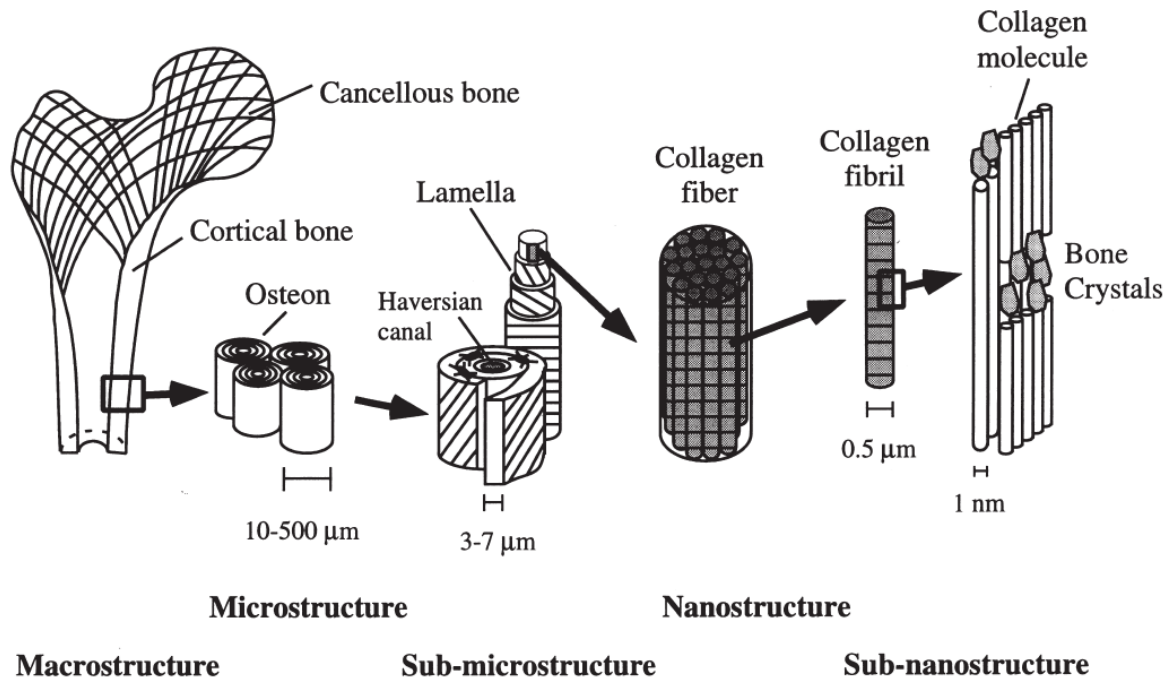


Figure 1.3. Structure of bone from its macrostructure to its sub-nanostructure<sup>13</sup>.

This organization of bone and the resulting structure leads to excellent properties in the z direction, but with rather anisotropic and heterogeneous properties.

At macroporous level, bone is distinguished between cortical or compact bone and cancellous or trabecular bone<sup>14</sup>. The end of a long bone has a dense cortical shell with a porous cancellous interior. As a first approximation, visual differences can appear when comparing cancellous and cortical bone, although the true differences appear at the microstructure. Cortical bone is composed of well structured osteons, which are concentric structures on the center of which, the Haversian channels may be found. The sub-microstructure of cortical bone is composed of regular, cylindrically shaped lamellae. Each of the lamellas are composed of collagen fibers, and these collagen fibers, are the matrix onto which the HA may precipitate. The HA precipitates in the gaps left by the collagen, which are the gaps that are found between collagen fibers, separated by a typical 67 nm distance.

Some researchers consider cortical and cancellous bone as a single morphological material which can be characterized by a highly variable porosity or apparent density<sup>15-17</sup>. In

general, cancellous bone is much more active metabolically, being remodeled much more often than cortical and therefore, can be considered as younger, on average, than the cortical bone.

Cortical bone comprises 80% of the skeleton in mass and has a higher resistance to bending and torsion, due to its high density and its compact structure. The major part is calcified and its main function is to provide mechanical strength and protection. It can also participate in metabolic responses, particularly when there is severe or prolonged mineral deficit. On the other hand, trabecular bone represents 20% of the skeletal mass and is less dense, more elastic, and has a higher turnover than cortical bone, having a higher metabolic function. Trabecular bone serves as mechanical support in the case of vertebrae and provides the initial supplies in acute deficiency states<sup>18</sup>. It is important to take into account that the differences in structure will lead to differences in the mechanical behavior of bone and the values for maximum strength and Young modulus are shown in Table 1.4.

	Young Modulus (GPa)	Compressive strength (MPa)
<i>Cortical bone</i>	7-30	100-230
<i>Cancellous bone</i>	0.05-0.5	2-12

Table 1.4. Young modulus and compressive strength for cortical and cancellous bone<sup>19</sup>.

### 1.2.4. Bone remodeling

Bone is a living organ that undergoes remodeling throughout life. Bone remodeling arises from the action of osteoblasts and osteoclasts that repair bone defects such as microfractures. In a hemostatic equilibrium, resorption and bone formation should be balanced, continuously replacing old bone by new bone formation. Bone remodeling is the process by which there is a bone turnover and that allows for bone to maintain the shape, quality and size of the skeleton.

The remodeling cycle is shown in Figure 1.4 and consists of three consecutive phases: resorption, reversal and formation. The first phase, resorption, starts when partially differentiated mononuclear preosteoclasts migrate to the bone surface, where they form multinucleated osteoclasts. After the completion of this osteoclastic resorption, there is a

reversal phase where mononuclear cells appear on the bone surface. These cells are the ones that prepare the surface for new osteoblasts to begin bone formation and provide signals for osteoblasts differentiation and migration. The formation phase follows, with osteoblasts laying down bone until the resorbed bone is completely replaced by new one. When this phase is completed, the surface is covered with flattened lining cells and a prolonged resting period begins, until a new remodeling cycle is initiated. It has to be mentioned that the stages of remodeling cycle have different lengths. Resorption takes place probably in about 2 weeks, followed by 4 or 5 weeks for the reversal phase and finally, formation can take place for about 4 months, until the new bone is completely created.

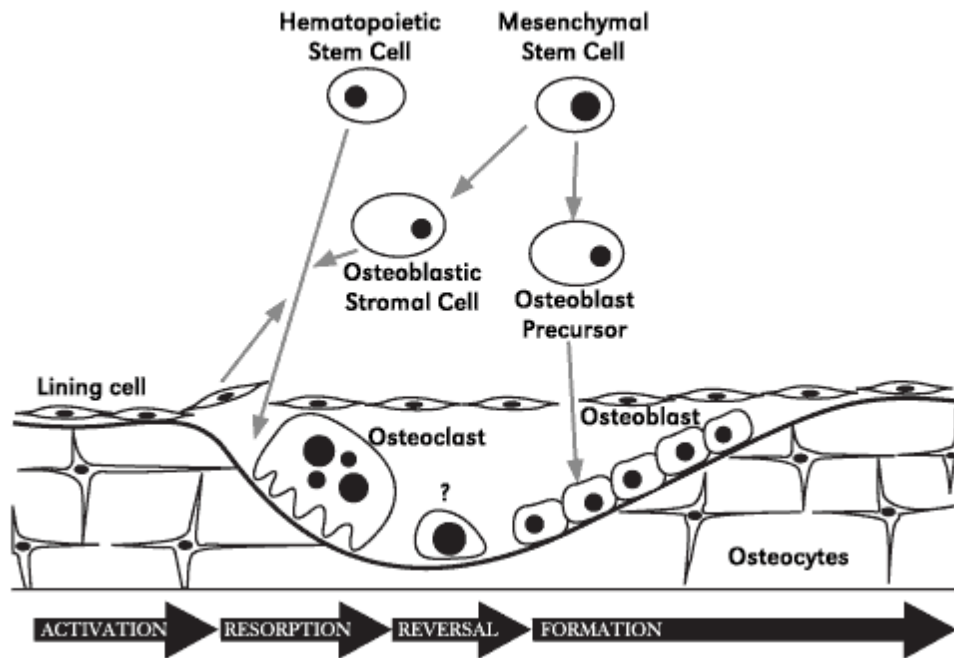


Figure 1.4. Representation of bone remodeling by osteoclasts and osteoblasts. Osteocytes are represented as mature osteoblasts which form part of the ECM<sup>12</sup>.

The principle underlying bone remodeling is still unclear, but a well accepted theory for bone remodeling is based on the fact that bone has electrical properties, which is named piezoelectricity. Piezoelectricity is the coupling between mechanical deformation and electrical polarization of a material. The origin of piezoelectricity lies in the presence of asymmetric charged groups in the material. As the material is deformed, the charges move

respect to each other so that change in dipole moment occurs. It is collagen that gives the piezoelectric properties of bone. What happens in bone is that, when there is a tension or compression force, small electrical impulses are produced: the zones in which there is compression (concave parts of bone), these are charged negatively and new bone tissue is deposited in these zones, whereas in the zones that suffer tension (convex parts), these are positively charged and tissue is resorbed in this zone. This is the explanation for the monograph published in 1892 by Julius Wolff on bone remodeling, which is nowadays known as Wolff's law and establishes that bone is reshaped in response to the forces acting on it<sup>20</sup>.

## **1.3. Bone substitutes**

### **1.3.1. Bone graft**

The high regenerative capacity of bone previously explained due to its bone remodeling and since it is a dynamic system, makes it an ideal tissue for the healing of fractures without the need of a major intervention. This can only be applied in small fractures. In the case of having larger fractures, as those observed after bone tumors resections and nonunion fractures, the bone cells have no guide through which they can direct bone reconstruction. That is why these require a surgical intervention.

Bone graft is the second most common transplanted tissue, being blood the first one. More than 500.000 bone grafting procedures are done annually in the United States and 2,2 million worldwide in order to solve injuries related to orthopedics, neurosurgery and dentistry<sup>21</sup>. Spinal fusions, filling defects following removal of bone tumors and several congenital diseases may require bone grafting.

The gold standard of bone grafting is harvesting autologous cortical and cancellous bone from the iliac crest. Although autologous bone and other forms of bone grafting have disadvantages, and as such, their use is not optimal. The main properties that can be found in a bone graft from natural bone are briefly described, as well as the possible bone substitutes that can be used from other natural bones.

Osteogenesis, osteoinduction and osteoconduction are the three essential elements of bone regeneration, along with the osteointegration. Osteoprogenitor cells living within the donor graft could proliferate and differentiate to osteoblasts. These cells represent the osteogenic potential of the graft<sup>22</sup>. Osteoinduction is the stimulation and activation of host mesenchymal stem cells from the surrounding tissue, which differentiate into bone-forming osteoblasts. Osteoconduction is associated with the facilitation and orientation of blood vessel and the creation of the new Haversian systems into the bone scaffold. And finally, osteointegration describes the surface bonding between the host bone and the grafting material<sup>23</sup>.

### *1.3.1.1. Autograft*

Autograft is considered the gold standard since it provides optimal osteoconductivity and osteoinductivity, as well as osteogenic properties. Iliac crest is the most frequently chosen donor site as it provides easy access to good quality and quantity cancellous bone. Harvesting autologous bone from the iliac crest has disadvantages, such as pain and aesthetic deformities, as well as longer surgical procedures<sup>24-27</sup>. There is also the fact that most of the cellular elements will not survive the transplantation, which will reduce the osteogenic properties of the graft<sup>28</sup>. Besides this, autograft may also be associated with complications such as hematoma formation, blood loss, nerve injury, hernia formation, infection, arterial injury, urethral injury, fracture, pelvis instability, cosmetic defects, tumor transplantation, and sometimes chronic pain at the donor site<sup>24,26,29-32</sup>.

### *1.3.1.2. Allograft*

Allografts are grafts coming from an external donor and are considered as the most frequently chosen bone substitute<sup>33</sup>. It accounts for one third of bone grafts performed in the United States<sup>34</sup>. The benefit of using an allograft is that it avoids the pain from the donor site, but still presents some limitations and some risks. Allograft may carry the risk of transferring viral diseases. The allograft can be processed to reduce the risk, but in that case, the biological, such as its osteogenic potential, and mechanical characteristics can be reduced<sup>35-41</sup>.

Allograft can be prepared in fresh, frozen or freeze-dried forms, cortical or cancellous. Fresh allografts are rarely used, since they increase the probabilities to elicit an immune response or transmit diseases<sup>42</sup>. The concern regarding viral disease transmission is practically eliminated through tissue processing and sterilization. Freezing and irradiation that eliminate the cellular phase of the allograft modify the processes of graft incorporation and affect its structural strength. Frozen and freeze-dried allograft is more osteoconductive but is considered to have weak osteoinductive capabilities compared to fresh allograft. The method of preparation of the allograft is done in a way to reduce the risk of immune response, but eliminates any viable cells, reducing its osteogenic properties. The risk is still lower than in the case of blood transfer, but still exists<sup>43</sup>. It has been estimated that the risk of being infected with HIV virus in screened allograft is, 1 in 1,6 million, compared to that of blood, which is 1 in 450,000, which is still low, but existing<sup>34,44,45</sup>.

### *1.3.1.3. Xenografts*

Xenografts are derived from other species, having the organic components completely removed. Upon removal of the organic components, no possible immunological reaction can appear. The inorganic part, which is the only one remaining, can act as an structural scaffold, as well as a source of calcium<sup>46</sup>. The inorganic phase is also responsible for the physical dimension of the augmentation during remodeling phases<sup>47</sup>. Surgeons have used xenografts due to the introduction of a calcium phosphate source, offering the mechanical and architectural components of bone that lacked in the synthetics. Obviously, it fails to satisfy the standards set by autogenous bone because it does not have the organic or the cellular components.

### *1.3.1.4. Synthetic Bone grafts*

As was previously seen, autografts seem very promising as bone grafts since they can provide support, fill voids and enhance biologic repair of skeletal defects. Although these promising characteristics, autografts present serious counterparts, such as donor site morbidity and the fact of not having enough amount or not in the adequate shape. That is why, nowadays, many synthetic bone grafts are under current investigations. Synthetic

bone graft materials are used in order to overcome the natural grafts drawbacks. In this sense, the materials are designed so that they meet similar features to those of natural grafts, such as osteoconductivity (e.g. calcium phosphates), osteoinductivity (e.g. incorporating growth factors) or osteogenicity (e.g. incorporating cells)<sup>48,49</sup>.

### 1.3.2. Tissue engineering and regenerative medicine

Tissue engineering is a multidisciplinary field that involves chemistry, biology, medicine and materials science among others. This multidisciplinary implies applying principles and methods used in engineering as well as in biological sciences in order to understand the relationship between structure and function in tissues and develop biological substitutes which may be able to reestablish, maintain or improve a tissue<sup>50</sup>. The main idea is to overcome the limitations involved in the natural grafts and the simple implantation of biomaterials<sup>7</sup>. In order to do so, the basic principles of tissue engineering are shown in Figure 1.5, in which it can be seen that the process starts by extracting cells of the patient through a biopsy. These cells are then expanded *in vitro* and cultured afterwards on a scaffold or construct. The scaffold is then placed in a bioreactor to simulate the physiological conditions for cells to proliferate and differentiate into the cell lineage desired. The scaffold loaded with cells, is finally implanted into the patient.

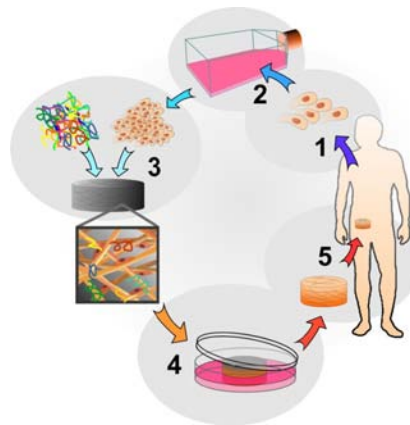


Figure 1.5. Scheme of tissue engineering principles. 1. Extraction of stem cells from the patient through a biopsy. 2. Expansion of cells *in vitro*. 3. Seeding the cells with growth factors on a scaffold. 4. Cell proliferation and differentiation *ex vivo* in a bioreactor to simulate physiological environment. 5. Implantation of the cell loaded scaffold on the patient<sup>51</sup>.

The materials implanted in the past were intended to be bio-inert. Scientist have now evolved to the fabrication of bioactive materials that integrate with biological molecules or cells and regenerate tissues<sup>7,52</sup>.

The term regenerative medicine has similar concepts of those of tissue engineering, but with the only difference that in this case, the grafts or scaffolds can incorporate some type of signaling (e.g. growth factors) which will then be implanted by minimally invasive surgery into the defect. Therefore, in this approach, the scaffolds are implanted directly into the organism without the need of *in vitro* cultures<sup>53</sup>.

## **1.4. Biomaterials for bone tissue engineering and regenerative medicine**

Up to now, science has only been able to replace tissue with physiological tolerance, biocompatibility and long term stability, with relative success. This demonstrates that we are still far from obtaining a really biomimetic material and shows the superiority and complexity of natural structure<sup>54</sup>. It is important to distinguish the difference between a biological material and a biomaterial. Biological materials are the materials fabricated by biological systems, such as bones, whereas the biomaterials are materials that are designed and fabricated by scientist that can produce a beneficial effect on living tissues. In the latter case, biomimetic materials are a branch of biomaterials which are considered as biomaterials that are not made by living organisms, but have similar composition, structure and properties.

### **1.4.1. Calcium phosphates**

The use of calcium phosphates as bone biomaterial is due to the similarity with the mineral phase of bone and teeth. CaPs have been used for more than 90 years with medical objectives. The first CaP used for bone healing was proposed by Albee and Morrison in 1920<sup>55</sup>. Later on, in 1951, Ray implanted HA in rats and Guinea pigs<sup>56</sup>. It was not until 1970, in which they started to be synthesized, characterized and implanted.



Calcium orthophosphates are considered as bioactive materials. The meaning for bioactive is that, these are materials that will promote the formation of a biological apatite before interfacing directly with the tissue at the atomic level, resulting in the formation of a direct chemical bond with bone. At the same time, in some cases CaP will be able to dissolve and allow newly formed tissue to grow. Bioceramics made of dense HA may be considered as bioactive, whereas porous scaffolds made of biphasic CaP, may be used as bioresorbable materials. The general applications of these materials are the use in non-loading bearing implants, such as filling bone defects in oral or orthopedic surgery, middle ear surgery or even coatings for metallic prosthesis. These materials are opposite to those considered as the first generation of biomaterials or bioinert, which would provoke the formation of a fibrous capsule isolating the material from the body.

There are two main types of CaP: the ones obtained by precipitation of an aqueous solution at room temperature and the ones obtained by thermal treatment. The specific type of CaP that formed depends on the solubility of the CaP in aqueous medium. The name and composition of the main compounds that can be obtained at low temperature in aqueous systems, as well as the compounds obtained by thermal treatment, appear in Table 1.5:

Name	Formula	Ca/P	Mineral	Symbol
Monocalcium phosphate monohydrate	$\text{Ca}(\text{H}_2\text{PO}_4)_2 \cdot \text{H}_2\text{O}$	0.50	-	MCPM
Dicalcium phosphate	$\text{CaHPO}_4$	1.00	Monetite	DCP
Dicalcium phosphate dihydrate	$\text{CaHPO}_4 \cdot 2\text{H}_2\text{O}$	1.00	Brushite	DCPD
Octacalcium phosphate	$\text{Ca}_8\text{H}_2(\text{PO}_4)_6 \cdot 5\text{H}_2\text{O}$	1.33	-	OCP
Precipitated hydroxyapatite	$\text{Ca}_{10-x}(\text{HPO}_4)_x(\text{PO}_4)_{6-x}(\text{OH})_{2-x}$	1.33-1.67	-	PHA
Precipitated amorphous calcium phosphate	$\text{Ca}_3(\text{PO}_4)_2 \cdot n\text{H}_2\text{O}$ where $n=3-4.5$	1.50	-	ACP
Monocalcium phosphate	$\text{Ca}(\text{H}_2\text{PO}_4)_2$	0.50	-	MCP
$\alpha$ -Tricalcium phosphate	$\alpha\text{-Ca}_3(\text{PO}_4)_2$	1.50	-	$\alpha$ -TCP
$\beta$ -Tricalcium phosphate	$\beta\text{-Ca}_3(\text{PO}_4)_2$	1.50	-	$\beta$ -TCP
Sintered hydroxyapatite	$\text{Ca}_{10}(\text{PO}_4)_6(\text{OH})_2$	1.67	Hydroxyapatite	SHA
Oxyapatite	$\text{Ca}_{10}(\text{PO}_4)_6\text{O}$	1.67	-	OXA
Tetracalcium phosphate	$\text{Ca}_4(\text{PO}_4)_2\text{O}$	2.00	Hilgenstockite	TetCP

Table 1.5. Calcium phosphates that may be obtained at low temperature (top 6) or through high temperature sintering (bottom six)<sup>57</sup>.

The first six compounds correspond to those compounds which can be obtained by precipitation in aqueous medium, whereas the last 6 correspond to those obtained by thermal treatment.

The key feature that will prognosticate what the behavior of the CaP will be *in vivo*, will depend on their solubility<sup>58</sup>. In general, if a CaP is less soluble than the mineral phase of bone, it will take long period of time to degrade, if ever degrading. If the solubility of the CaP is higher than that of the mineral phase of bone, it will degrade. Although it is also worth highlighting that *in vivo*, there will also be the effect of the cells, such as osteoclasts that will enhance the dissolution of the CaP.

Before advancing in the description of the different solubilities of the CaP, first of all, it is important to understand the concept of solubility. An example is given in the general case of having a compound with formula AX in aqueous solution in the system  $A(OH)_n - H_nX - H_2O$ . The logarithm of the concentration of A is represented versus pH (Figure 1.6). When equilibrium is obtained between a solution and an excess of solute, the solution becomes saturated and is represented with the line shown, which is the saturation line. If the concentration of the solute rises or decreases around this equilibrium point for each pH, the solution will become supersaturated in the compound in the first case, and will be undersaturated in the second case. In the supersaturated region, the compound will have an excess of ions in solutions and will precipitate, whereas in the undersaturation zone, the compound will dissolve in order to maintain the thermodynamic equilibrium.

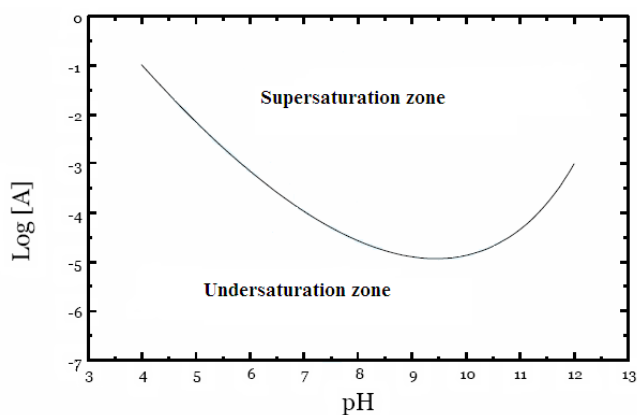


Figure 1.6. Solubility diagram for a theoretical system  $A(OH)_n - H_nX - H_2O$ .<sup>59,61</sup>

The same interpretation can be given for a system  $\text{Ca}(\text{OH})_2 - \text{H}_3\text{PO}_4 - \text{H}_2\text{O}$  which can be shown in Figure 1.7. The diagram can be represented as a function of the calcium concentration or phosphorous, but it is easier to visualize in the calcium case. The equilibrium solubilities are shown for the most common CaP: tetracalcium phosphate (TTCP), Dicalcium phosphate dihydrate (DCPD), Dicalcium phosphate anhydrous (DCP), octacalcium phosphate (OCP),  $\alpha$ -tricalcium phosphate ( $\alpha$ -TCP),  $\beta$ -tricalcium phosphate ( $\beta$ -TCP) and hydroxyapatite (HA). As can be observed, a negative slope can be observed in the neutral and acid zone, which means that the solubility increases as the pH decreases. In general, for a given pH, the lowest line will correspond to the most stable and less soluble compound. It is because of these diagrams that it can be concluded that for a pH higher than 4.2 and at 37°C, the most stable compound is HA, and that below this pH, the most stable compound is DCP. It can also be seen, that at pH lower than 8.5, the most soluble compound is TetCP, and at pH values higher than 8.5, the most soluble compound is DCPD.

It can then be concluded that, when a CaP is introduced in water, it will dissolve and precipitate in a CaP that is more stable at that temperature and pH. This is the basis of the calcium phosphate cements (CPC), being able to hydrolyze and evolve into a more stable system, which is usually HA, that is the mineral phase of bone.

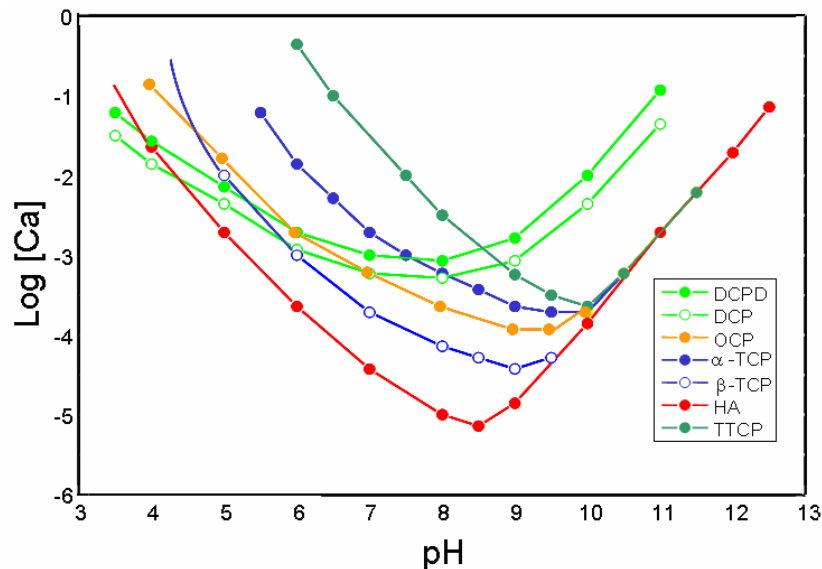


Figure 1.7. Solubility diagram for the system  $\text{Ca}(\text{OH})_2 - \text{H}_3\text{PO}_4 - \text{H}_2\text{O}^{60,60}$ .

## 1.4.2. Calcium phosphate cements

Calcium phosphate cements are blends of calcium phosphate powders and aqueous solution, which in many cases may be distilled water or an accelerant solution (e.g. sodium hydrogenphosphate). Once these two components are mixed together, a viscous and moldable paste is obtained, which sets to form a firm mass within minutes. Once the paste has become stiff enough, it can be placed into a defect, as bone substitute for the damaged part of the bone, where it hardens *in situ*. The amount of liquid and powder that will be mixed will determine the properties of the paste, as well as the properties of the final solid body. The paste may be injected into the defect, where it can intimately adapt to the bone cavity. The schematic phases of a CPC are shown in Figure 1.8:

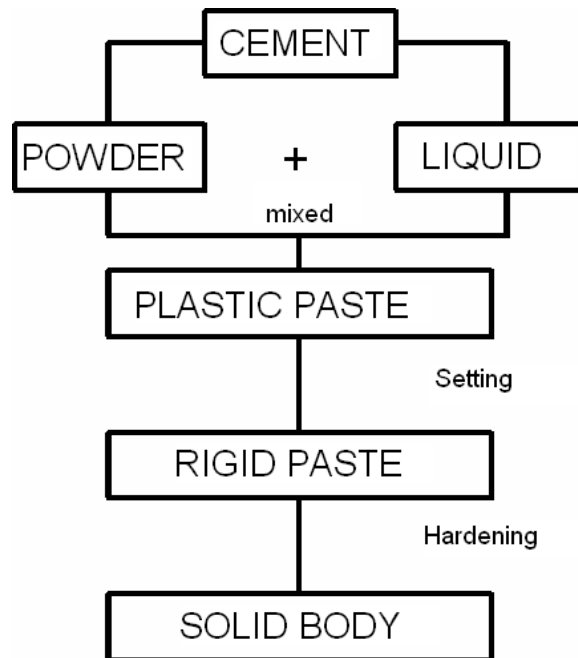


Figure 1.8. Scheme of the CPC preparation. Initially the powder and the liquid are mixed to form a paste, which upon the setting forms a rigid paste to finally lead to a solid body after the hardening.

They are considered as osteoconductive, which describes the ability of the material to have bone growing on its surface, and may in some cases, be osteoinductive. Another important feature is that CPC are osteotransductive, meaning that CPC are replaced by new bone tissue<sup>61-63</sup>. They possess sufficient compressive strength, are non cytotoxic, presenting

chemical and X-ray diffraction patterns similar to those of bone<sup>64</sup>. The main advantages and disadvantages of CPC are presented in Table 1.6.

Advantages	Disadvantages
<ol style="list-style-type: none"> <li>1. Self-setting ability <i>in vivo</i></li> <li>2. Good injectability that allows cement implantation by minimally invasive surgical techniques</li> <li>3. Good osteoconductivity and occasional osteoinductivity</li> <li>4. Can be replaced by newly formed bone after a period of time</li> <li>5. Moldability</li> <li>6. Excellent biocompatibility and bioactivity</li> <li>7. No toxicity</li> <li>8. Low cost</li> <li>9. Ease of preparation and handling</li> <li>10. Setting at body temperature</li> <li>11. Form chemical bonds to the host bone</li> <li>12. Clinically safe materials in their powder components</li> <li>13. Can be used to deliver antibiotics, anti-inflammatory drugs, growth factors, etc. at local sites</li> </ol>	<ol style="list-style-type: none"> <li>1. Mechanical weakness</li> <li>2. Can be washed out from surgical defect if excess of blood</li> <li>3. Lack of macroporosity</li> <li>4. The <i>in vivo</i> biodegradation may be slower than the growth rate of newly forming bone</li> </ol>

Table 1.6. Advantages and disadvantages of the use of CPC<sup>65</sup>.

The first monolithic calcium phosphate ceramic, at room or body temperature, was put forward by LeGeros *et al*<sup>66</sup> and Brown and Chow<sup>67,68</sup>. The first formulation consisted of the equimolar mixture of TTCP and dicalcium phosphate (DCPA or DCPD) which was mixed with water at a L/P ratio of 0.25 ml/g, obtaining a hardened CDHA after 30 minutes<sup>67,68</sup>. Several years after, more than 15 combinations of calcium phosphates were established as possible powders for CPC<sup>69-71</sup>. Depending on the pH value of a cement paste, only two end products may exist: poorly precipitated HA or CDHA (pH > 4.2) and brushite (pH < 4.2). That is why two main CPCs are known: apatite cements and brushite cements.

The first reaction that takes place in any CPC is the initial dissolution, which will depend on the chemical composition and the solution pH as was previously seen. The dissolved reactants form a supersaturated microenvironment respect the final products. It is their relative stability that will lead to the formation of one of the end products or the other. So basically, the mixing of the dry powder with an aqueous solution induces various chemical transformations, where crystals of the initial calcium orthophosphates rapidly dissolve and

precipitate into CDHA crystals or DCPD. During the second phase, which is the precipitation, the newly formed crystals grow and form a web of intermingling microneedles or microplatelets of the final products, providing the initial mechanical properties.

### 1.4.3. Collagen

Collagen is a French neologism from the 19<sup>th</sup> century that was meant to designate the constituent of connective tissues that produced glue (from the Greek,  $\chi\omicron\lambda\lambda\alpha$ , glue, and  $\gamma\epsilon\upsilon\omicron\varsigma$ , birth). In 1983, the Oxford dictionary defined collagen as “that constituent of connective tissue which yields gelatin on boiling”. That is because, most of the work was done on heat-denatured collagen.

Collagen is a fibrous protein found in all multicellular animals. Collagen is basically secreted by cells into the extracellular matrix. It is the main component of bones and skin, being the most abundant protein in mammals with a 25% contribution of the total protein mass in the body. The main structure of collagen is composed of three polipeptidic chains (alpha chains), which are bounded together forming a coil (Figure 1.9). Its triple helical structure is obtainable due to its different chains conformations. The alpha chains are unique in the sense that they repeat a determined structure in order to form the hierarchized structure. The chains are rich in proline, lysine and glycine. Proline and lysine may also be found in its hydroxylated form, which are hydroxyproline and hydroxylysine. Glycine is found every three aminoacids in order to be able to have its small side chain (Hydrogen) facing into the inner part of the helix. Proline is able to stabilize the helix form in each alpha chain. Each polypeptide forms a left-handed helix in which every third residue comes into the center of the superhelix, shifted by  $30^\circ$  from the preceding central residue of the same chain. This results in the formation of a right-handed superhelix. The repeating structure of collagen is then Gly – Xaa – Yaa, in which Xaa and Yaa can be any aminoacid, but are frequently proline and hydroxyproline. A posttranslational process allows for the maturation of the translation product into the fibrillar materials with high tensile strength, characteristic of collagen-rich tissues<sup>72</sup>. The basic collagen molecule has a length of 3000 Å and 15 Å of width, presenting a molecular weight of 300 kDa<sup>73,74</sup>.

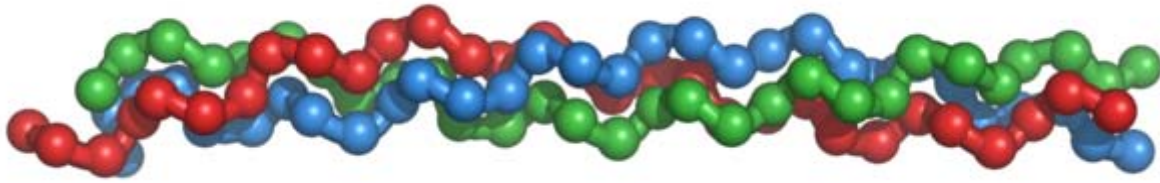


Figure 1.9. Tropocollagen molecule in which each of the different colors represents  $\alpha$  different a chain<sup>75</sup>.

It is important to highlight that collagen is the general term for the proteins of the ECM that present the triple helical structure, but that doesn't mean that all the proteins with this triple helical structure are identical. In fact, at the end of the 1960's, cartilage was studied, and it was seen to contain collagen with a primary structure different to that found in skin, tendons and bone, which had been previously studied (type I collagen). This new collagen was called type II and the molecules were shown to be homotrimers. Further on, another similar molecule was found and was named collagen type III. Type III collagen was isolated from tissues that also contained collagen I molecules, which was afterwards shown that, the two types of molecules could form heterotypic fibrils<sup>76</sup>. This created confusion since new collagen types started to appear. At present time, over 25 different types of alpha chains have been identified, which are codified by different genes. Although the combination of these different alpha chains could lead to thousands of collagen types, only around 20 types of collagen have been identified. The most important collagen types are type I, II, III, V and XI, but our interest will be focused in collagen type I, due to the fact that it is the collagen type present in bone and the most abundant collagen type. In the case of type I collagen, the composition is two  $\alpha 1$  and one  $\alpha 2$  chains. That is why a general definition of collagen had to be found in which all different types of collagens could be included: it is considered as a structural protein of the ECM which contains one or more domains having the conformation of a triple helix.

The characteristics of collagen as biomaterial and the way it interacts with the body, significantly differs from other polymers since it presents cell recognition domains and higher biocompatibility, therefore its use is widely extended<sup>77</sup>. Compared to other natural polymers, it presents biodegradability, weak antigenicity and superior biocompatibility. One of the main advantages of collagen is that it can self-assemble forming fibers and

bundles, making collagen stronger and more stable. The main advantages and some drawbacks for using collagen are summarized in Table 1.7.

Advantages	Disadvantages
Available in abundance and easily purified from living organism. Non-antigenic. Biodegradable and bioresorbable.  Non-toxic and biocompatible.  Synergic with bioactive components. High tensile strength.  Hemostatic: promotes blood coagulation. Different forms. Biodegradability can be regulated by cross-linking. Easily modifiable to produce materials as desired using its functional groups. Compatible with synthetic polymers.	High cost of pure type I collagen.  Variability of isolated collagen. Hydrophilicity which leads to swelling and more rapid release. Variability in enzymatic degradation rate as compared with hydrolytic degradation. Complex handling properties. Side effects, such as bovine spongiform encephalopathy.

Table 1.7. Advantages and disadvantages of using collagen as biomaterial<sup>78</sup>.

In the field of bone regeneration, collagen has been used, although due to its low mechanical properties it has been usually combined with other materials such as HA, which in addition can make the material osteoinductive under certain environments<sup>79,80</sup>. Nevertheless, it is not the only way collagen can be made osteoinductive, since it has also been used in some occasions as drug carrier (e.g. BMP-2) in order to induce bone cell differentiation<sup>81</sup>.

In order to reproduce the function needed, it is important to recreate the bone ECM structure. The structure of the ECM is basically composed of collagen, and that is why, many efforts have been put on developing systems which are able to recreate the appropriate bone ECM micro-architecture. That is why, collagen gels are used to create tissue equivalents. The properties of this gel will depend on the organization of the collagen fibrils in the network, which at the same time is a response of external stimuli, such as mechanical stimuli. These fibril gels create a 3D network on which cells can be seeded, which may promote *in vivo* like cellular activity that is completely different from those observed in 2D<sup>82</sup>.



#### 1.4.4. Calcium phosphate/collagen composites for bone regeneration

There are many studies in which collagen has been mixed with hydroxyapatite. These composites may present advantages over the different components individually. An accelerated osteogenesis was observed in a study in which collagen/HA scaffolds were implanted in Wistar rats in 5 mm calvariae defects and were shown to increase osteogenesis already after 28 days<sup>80</sup>. Other collagen/HA composite material has also shown better osteoconductive properties and calcification production identical to that of bone matrix<sup>83,84</sup>, presenting biocompatibility both, in animals and humans, as was observed in commercially available composites (Biostite and Bio-Oss)<sup>83,85</sup>. Mehlisch in the 90s, implanted a material composed of a collagen matrix with HA particles for ridge augmentation for 1 year and reported a high biocompatibility<sup>86</sup>. Besides the enhanced biological behavior, the composite mechanically may also behave in a better way than its components by themselves. The ductile properties of collagen may help increasing the low fracture toughness of ceramics. On the other hand, the addition of a ceramic in collagen has also been reported to have an increased resistance to three dimensional swelling compared to collagen as observed in a collagen calcium phosphate composite in the form of multilayer sheets obtained using enzymatic mineralization<sup>87</sup>. They have been also shown to improve its mechanical wet properties<sup>88</sup>.

Compared to other scaffolds, there is evidence of the biological advantage of collagen compared to artificial polymeric scaffolds, demonstrated in cartilage regeneration<sup>89</sup>, as well as a better cell adhesion to collagen surfaces rather than PLLA or PGA implants<sup>90</sup>. Some polymeric scaffolds can take up to two years to degrade (e.g. Poly(hydroxybutyrate) (PHB), Poly(hydroxyvalerate) (PHV))<sup>91</sup>, while some collagen hydroxyapatite composites have a more reasonable degradation rate between 2 months and 1 year<sup>92</sup>. On the other hand, when comparing hydroxyapatite/collagen composite scaffolds to other ceramic scaffolds, they perform well compared to HA or TCP<sup>89</sup>. The addition of collagen to the ceramic structure can provide improvements from a surgical point of view: shape control, spatial adaptation,

increased particle and defect wall adhesion and the capability to favor clot formation and stabilization<sup>85</sup>.

A synthetic bone graft substitute of type I bovine collagen, hydroxyapatite and tricalcium phosphate (Collagraft Bone graft matrix Strip) was used successfully in animal and human applications for long bone fractures<sup>93</sup>. It was approved by FDA in 1994 as a substitute for autogenous bone grafts for treating acute long bone fractures and traumatic defects when used with bone marrow and internal or external fixation. It was reported as a highly compatible and well incorporated in spinal fusion<sup>93</sup>. However, Muschler *et al*<sup>94</sup> reported the use of Collagraft in a canine spinal fusion model stabilized with acrylic bone cement and cerclage wire. They reported poor results, mainly attributed to poor stabilization of the spine through cement and cerclage wire fixation.

Nowadays, some biomaterials composed of hydroxyapatite and collagen may be found in the literature. The processes by which these are obtained differ among them and this leads to different final properties. The intention of the following paragraphs is to give an overview of the different techniques that are being used and that have been used for the preparation of hydroxyapatite and collagen composites.

#### *a) Soaking of collagen sponges*

The method consists on the immersion of a collagen porous matrix in a phosphate containing solution, mainly SBF or PBS, in order for the HA to precipitate. The HA crystals are able to precipitate on and throughout the collagen matrix. The collagen is usually lyophilized in order to obtain a porous sponge like morphology. The majority of these scaffolds are based on the method described by Kokubo<sup>95</sup>. When the fluid in which the collagen sponge is located becomes supersaturated in calcium and phosphates ions, such as when placed in SBF solution, HA precipitates on top of it<sup>96,97</sup>. It is considered as a fast and easy method to obtain a collagen HA scaffold. In this approach, the first experiments were done with SBF or PBS as mentioned, but since then, new solutions have arisen in order to also obtain HA which may affect the final properties of the HA<sup>98</sup>. In general, it is difficult to control the amount of HA that is incorporated into the scaffolds.

An upgrade of this principle consists on placing the collagen sponge in water and make calcium and phosphate solutions pass through the sponge drop by drop. Collagen has a solid form, making a calcium phosphate solution diffuse into the fibrils<sup>88</sup>. It is reported that in this way, the orientation of the collagen fibers can be controlled<sup>99</sup>. Furthermore, by controlling the solutions used and the speed at which the solutions are added, a gradient collagen scaffold with calcium rich areas and calcium depleted areas can be obtained<sup>100</sup>.

An even more interesting approach that was taken in a previous work was to create sponges with the soaking method and then incorporating cells arising from bone fragments. This sponges were then able to be coiled, obtaining scaffolds colonized with cells even in the inside of the scaffold<sup>101</sup>.

The use of a sponge is not always necessary. In another example, microbeads of collagen were prepared, and in order to stabilize the structure, these were crosslinked with glutaraldehyde and placed in PBS for the precipitation of the HA<sup>102</sup>.

Nevertheless, even though the majority of scaffolds are obtained having a collagen scaffold onto which the HA is precipitated, the opposite can also be found, in which a porous HA scaffold can be made, being impregnated afterwards with a collagen solution<sup>103</sup>.

#### *b) Simultaneous precipitation of calcium phosphate/collagen solutions*

Many other works relay on the principle of a simultaneous precipitation of collagen and HA. The condition for the stable formation of HA is alkaline, and collagen fibrillogenesis occurs at around body temperature and pH. That is why, for the fibrillogenesis of collagen to occur *in vitro*, it requires certain conditions of physiological saline with a precise pH and temperature<sup>104,105</sup>.

In order to obtain this simultaneous precipitation, the process is generally done through a simultaneous titration system. There are several ways through which this co-precipitation can be obtained. The system can be formed by a phosphate containing solution and collagen solution<sup>106</sup>, or a calcium containing and collagen solution<sup>104</sup>. This way, both the

collagen and the HA will precipitate at the same time. That is why the system is called co-precipitation or simultaneous precipitation.

It has been demonstrated that the c-axis of HA crystals can be induced to grow along the direction of collagen fibrils, if the right conditions of mineralization are met, in which the temperature is maintained at 40°C and the pH around 8-9<sup>107</sup>. The system by which it is prepared is similar to that shown in Figure 1.10. The way in which the experiment was carried out, was having 2 l of 99.6 mM Ca(OH)<sub>2</sub> aqueous suspension and another tank with 2 l of 59.7 mM H<sub>3</sub>PO<sub>4</sub> aqueous solution with 5 grams of atelocollagen. Both solutions were added drop by drop in a central tank, which initially contained 1 l of water. These concentrations were established in order to obtain a final weight ratio of HA/col of 80/20. The temperature was controlled in a water bath, and so was the pH by the simultaneous titration of Ca<sup>2+</sup> and PO<sub>4</sub><sup>3-</sup> solutions<sup>106,107</sup>. The solutions concentration is usually controlled so that the final ratio of HA/col is between 80/20 and 60/40 (wt/wt)<sup>107-110</sup>.

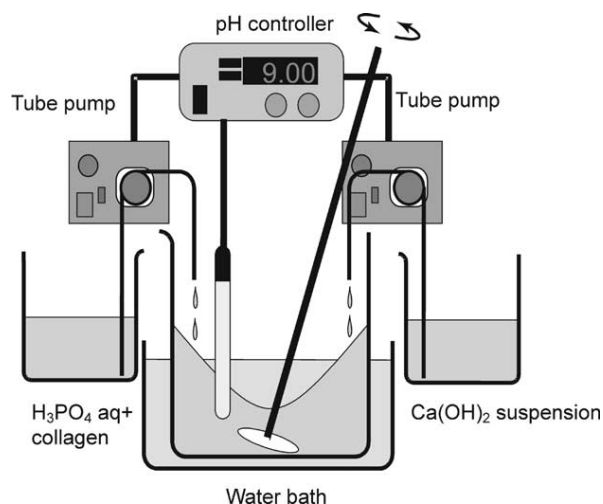


Figure 1.10. Representation of the system used to prepare scaffolds through a co-precipitation of collagen with calcium and phosphate ions<sup>107</sup>.

The results showed the fabrication of collagen fibers of 20 μm in length and having the c-axes of HA crystals aligned along the elongation direction of the HA/col fibers, which is similar to the structure found in bone<sup>111</sup>. The driving force for the surface interaction between HA and collagen was probably an interfacial interaction between these molecules, because HA formation on Langmuir-Blodgett monolayers indicates that HA nanocrystals

formed on carboxyl-terminated monolayer, but not formed on amino-terminated monolayer<sup>112</sup>. Red shifts were observed with FTIR when comparing the collagen spectra with those of the composites. Those shifts are related with a decrease in bonding energy of the C-O bond and is basically assumed to be caused by the interaction with  $\text{Ca}^{2+}$  ions. This method has been resembled by other authors by using similar protocols in which the collagen and the HA precipitate at the same time<sup>113</sup>.

#### *c) Solid freeform fabrication*

The use of solid freeform fabrication for collagen/HA scaffolds has not been directly applied to collagen slurries, but rather, moulds made of polymeric materials have been prepared with the solid freeform fabrication technique, onto which the collagen/HA slurries were then poured. Briefly, collagen slurries containing 70% wt of HA were mixed and blended. These slurries were then poured into the moulds fabricated through solid freeform fabrication of biocompatible materials (BioBuild and BioSupport). The moulds with the slurries were then frozen and after the complete freezing, these were immersed in ethanol for the complete dissolution of the moulds. The materials were then left drying in order to obtain the macroporous scaffolds. It is important to highlight that the morphology and porosity of the scaffolds completely depends on the solid freeform fabricated mould<sup>114-116</sup>.

#### *d) Freeze-dried collagen and HA slurries*

This method is also called the phase separation method or simply freeze-drying process. It is based on the freeze-drying of collagen:HA slurries to obtain macroporous scaffolds. The techniques described up to now usually had the collagen as the matrix of the material. With the present technique, materials with higher content of HA can be obtained. This means that in the case in which the amount of collagen is high, and therefore, becomes the continuous phase, the material obtained will be a highly porous material with HA deposits. In the case in which the amount of HA is high, the material obtained will be a ceramic with some collagen, not presenting, in general, macroporosity. The ratios of HA and collagen can be perfectly controlled by controlling the amount of HA incorporated<sup>81,117-120</sup>. In the previously described methods, since HA arises from precipitation, the amount of HA is more difficult to control and is generally between 80:20 or 60:40 wt ratios of HA:collagen.

With the present technique, most of the works present a higher range of HA:collagen weight ratios, ranging from 1:99 to 2:1<sup>81,119</sup>. Higher ranges have also been covered up to a 8:1 weight ratio of HA:collagen content in collagen scaffolds<sup>120</sup>. TenHuisen also obtained a composite with a higher ratio of HA in the composite, being HA the matrix of the material, achieving up to a 22:1 HA:collagen weight ratio<sup>121</sup>.

*e) Calcium phosphate cements with collagen*

There have been few works in which collagen has been combined with a CPC. An apatitic CPC composed of TTCP/DCP was studied in combination with collagen at a L/P ratio of 0.29 ml/g, adding collagen in its liquid and its powder phase<sup>122</sup>. The results showed that the incorporation of the collagen in the powder phase gave poor results in terms of setting time. Lower setting times were found when collagen was incorporated in the liquid phase, although the optimum results were found when the liquid phase was composed of collagen and an accelerant solution (e.g. sodium hydrogenphosphate). There was an increase in the setting time and a linear decrease in the diametral tensile strength when collagen was present in more than 1% in the liquid phase. When the accelerant solution was present, there was an improvement in workability and handling<sup>122</sup>. More recent works describe the addition of collagen (3% wt) in the liquid phase in a brushitic cement composed of MCP and  $\beta$ -TCP<sup>123</sup> at a L/P ratio of 0.29 ml/g and also reported an improvement in cement handling. Furthermore, collagen was found to accelerate the setting reaction and maintain the compressive strength similar to that of the cement without collagen. The most important claim was the excellent cohesion properties and high cellular adhesion<sup>123</sup>. An even more recent work reports a 10 fold increase in the work of fracture of an apatitic CPC composed of TTCP and DPA containing 5% collagen solution in its liquid phase for different L/P (e.g. 0.29, 0.33 and 0.4 ml/g)<sup>124</sup>. Furthermore, the presence of collagen doubled the initial cellular attachment in the composite at a L/P ratio of 0.29 ml/g for collagen concentrations of 2.5 and 5% wt<sup>124</sup>. Recent work also describes the hydrolysis of a collagen and  $\alpha$ -TCP paste in water<sup>125</sup>. Two different methods for the mixing were applied: simple mixing or milling the mixture, using 5% and 20% weight collagen ratios respect to HA. It was shown that in the case of having the non-milled composite, the diametral tensile strength decreased compared to HA alone, whereas it remained similar in the case of the milled case. The

diametral tensile strength was higher in the case of the milled composite compared to the non-milled composite and is attributed to the better dispersion of small collagen fibers in the composite<sup>125</sup>.

## 1.5. Cell interactions with biomaterials

The adhesion of cells to biomaterials is affected by the characteristics of the materials surface, which includes the chemistry, topography, surface energy, etc. All these parameters play an important role in the subsequent capacity of the cells to proliferate and differentiate, as well as to attach, adhere and spread on the initial stages. The behavior of the cells in the first stages of culture, will rule the posterior behavior of cells on the biomaterial.

There are several mechanisms by which cells are able to communicate among them<sup>126</sup> and with the surface of the ECM<sup>127</sup> (or to the surface of a material in which proteins have been deposited), which will determine the way in which the cells will behave. There is a high specificity between the ligands and the adhesive molecules. The ligands may be in the surface of the material or in neighboring cells. There are four families of adhesion molecules: selectins, immunoglobulin superfamily, cadherins and integrins. Only cadherins and integrins have been described in osteoblastic cells. Integrins are the adhesion molecules that deal with cell substrate adhesion, while cadherins control cell to cell adhesions. We will only briefly describe the integrins since these are the only ones that will actually be discussed during the thesis. Integrins consist of transmembrane heterodimers formed by the union of  $\alpha$  and  $\beta$  subunits. Each of the subunits presents a large extracellular domain, transmembrane domain and a short cytoplasmatic domain. These heterodimers are the ones that will send the information found outside the cells, inside, meaning that it will control the adhesion, spreading, proliferation, differentiation and even the apoptosis of the cell<sup>128-130</sup>.

The linking between the integrin receptors and the substratum of the material are the so called focal contacts. These focal contacts are closed junctions where the distance between the substrate surface and the cell membrane is between 10 – 15 nm. A focal contact occurs

essentially in cells with low motility and is promoted *in vitro* by ECM proteins, like fibronectin and vitronectin. These focal contacts and the subsequent architecture of the cytoskeleton will determine the mobility and the strength of the adhesion. In this context, if the architecture of the cytoskeleton is in the shape of long bundles, presenting finger like protrusions, they are called filopodia. If they are assembled in the form of a mesh and the structure of the protrusions is sheet like, they are called lamellipodia. It can be said that cells with a low motility present strong focal adhesions, whereas the ones with a high motility, form less adhesive structures.

It will be the surface characteristics of the material, as well as the capacity to attract proteins to its surface, that will determine the cell morphology. Cells will initially attach, adhere and finally spread. In the case of having a calcium phosphate cement, the ability to adsorb proteins on its surface will arise from the surface energy of the CDHA formed and from the high specific surface area, among other parameters, to attach proteins. Cells will be able to interact with the adsorbed proteins. The hypothesis is that by adding collagen on the structure of the CPC, there will be an increase of the chance for the cells to find a binding domain on the surface, through which cells will adhere.

### **1.5.1. Collagen-integrins interaction**

Integrins is a term which was first applied in 1987 to emphasize the role of these receptors in integrating the extracellular matrix outside the cell with the actin containing cytoskeleton inside the cell. The signals they convert travel two directions: from outside the cell, inside, and the other way round as well. They transduce information from the ECM to the cell and reveal the status of the cell to the ECM. This allows cells to make rapid and flexible responses.

Integrins are the largest family of cell adhesion receptors<sup>131</sup>. Integrin type receptors are composed of one  $\alpha$  and one  $\beta$  subunit. They are transmembrane proteins and are not covalently linked together. Integrin  $\alpha$ , has 5 subunits, only presenting 4 of them in vertebrates<sup>132</sup>. The largest subgroup on vertebrates is formed by  $\alpha$  subunits that have a special ligand binding inserted domain, named  $\alpha$ I domain. There are four integrins



containing  $\alpha$ I domain (subunits  $\alpha 1$ ,  $\alpha 2$ ,  $\alpha 10$  and  $\alpha 11$ ) for the collagen receptor integrins. These types of units have associated a  $\beta 1$  heterodimer. The most important and well known are  $\alpha 1\beta 1$  and  $\alpha 2\beta 1$ . Integrin  $\alpha 1\beta 1$  is expressed in many MSC and seems to be important for the action of many inflammatory cells. Integrin  $\alpha 2\beta 1$  is abundant on many epithelial cells types and platelets and is also expressed in MSC. These two integrins may have opposite effects on many signaling pathways<sup>133-135</sup>.

It is also well known that, depending on the type of collagen, the integrins also have different affinities (Figure 1.11). In other words, the type of integrin interaction may depend on the type of collagen. In this sense,  $\alpha 2$  and  $\alpha 11$ , have a higher affinity for the fibril forming collagens, such as types I, II and III, whereas,  $\alpha 1$  and  $\alpha 10$  have higher affinity for basement membrane (type IV) and beaded filament (VI) collagens. At the same time, the response that is given from the outside to the inside of the cell will also depend on the type of integrin that is being activated. In the case of  $\alpha 1$ , the proliferation is increased, whereas the collagen synthesis is decreased, whereas for  $\alpha 2$ , collagen synthesis is increased and so is the collagenase synthesis increased. In the case of  $\alpha 10$  and  $\alpha 11$  the effects are unknown.

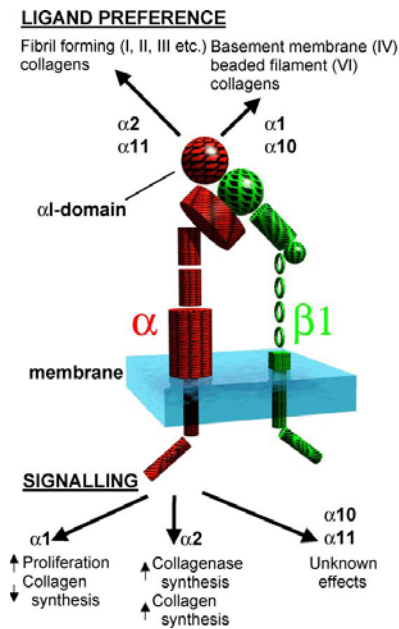


Figure 1.11. Representation of integrins involved in the collagen interaction with cells<sup>132</sup>.

## 1.5.2. Recognition sites in triple helical and denatured collagen

Receptor binding sites in collagens may be divided into at least 4 categories.

- Specific domains inside the triple helical areas that can be recognized by cell receptors. They represent highly specific binding. A good example is the GFOGER motif. These have high affinity for  $\alpha 2\beta 1$  integrin<sup>136,137</sup>.
- Relatively common sequences in the triple helix, such as GPO.
- Cryptic binding sites in collagens that can be recognized by receptors only after denaturation of the collagen. In this group, it can be found the well known RGD sequence, which is mainly recognized by other receptors such as VN, FN and Fgn type integrins. Actually, after heat denaturation (gelatin) of collagen,  $\alpha 5\beta 1$  and  $\alpha V$  integrins can bind to it.
- Specific receptor binding in non-collagenous domains, such as NC1 domain.

It is quite interesting to note, that the mechanism by which cells adhere to collagen is completely RGD-independent, since the RGD sequence in collagen is completely hidden in its native conformation. That is, cells adhere to collagen through  $\alpha 1\beta 1$ ,  $\alpha 2\beta 1$ ,  $\alpha 10\beta 1$  and  $\alpha 11\beta 1$  integrins which are RGD independent<sup>138,139</sup>, whereas an RGD dependent mechanism would be the adhesion of denatured collagen, such as gelatin, through integrins  $\alpha 5\beta 1$  and  $\alpha V\beta 3$ <sup>138,140,141</sup>.

## 1.6. References

1. Hesiod's Theogony poem 8<sup>th</sup> century BC.
2. Virchow R. Die Cellularpathologie in ihrer Begründung auf physiologische Gewebelehre. Hirschwald, Berlin (1858).
3. Loeb L. Ueber die Entstehung von Bindegewebe, Leukocyten und roten Blutkörperchen aus Epithel und über eine Methode, isolierte Gewebsteile zu züchten. Stern, Chicago (1987).
4. Ljunggren CA. Von der Fähigkeit des Hautepithels, ausserhalb des Organismus sein Leben zu behalten, mit Berücksichtigung der Transplantation. *Deutsche Zeitschrift für Mund-, Kiefer- und Gesichtschirurgie* **47**, 608-615 (1898).
5. Harrison RG. The outgrowth of the nerve fiber as a mode of protoplasmic extension. *Journal of Experimental Zoology* **9**, 787-846 (1910).
6. Green WT Jr. Behavior of rabbit chondrocytes during tissue culture and subsequent allografting. *Clinical and Orthopedic Related Research* **124**, 237-250 (1977).
7. Langer R & Vacanti JP. Tissue engineering. *Science* **260**, 920 (1993).
8. Dorozhkin SV. Calcium orthophosphates. *Journal of Materials Science: Materials in Medicine* **42**, 1061-1095 (2007).
9. Aubin JE & Triffitt JT. Principles of bone biology. Bilezikian JP, Raisz LG & Rodan GA (eds.), pp. 59 (1996).
10. Mullender MG, Huiskes R, Versleyen H & Buma P. Osteocyte density and histomorphometric parameters in cancellous bone of the proximal femur in five mammalian species. *Journal of Orthopedic Research* **14**, 972-979 (1996).

11. Väänänen K & Zhao H. Principles of bone biology. Bilezikian JP, Raisz LG & Rodan GA (eds.), pp. 127 (1996).
12. Bilezikian JP, Raisz CG & Rodan GA. Principles of bone biology. Academic Press, San Diego (2001).
13. Rho JY, Kuhn-Spearing L & Zioupos P. Mechanical properties and the hierarchical structure of bone. *Medical and Engineering and Physics* **20**, 92-102 (1998).
14. Adler CP. Bone diseases. pp. 1-30, Springer-Verlag, New York (2000).
15. Keller TS, Mao Z & Spengler DM. Young's modulus, bending strength, and tissue physical properties of human compact bone. *Journal of Orthopaedic Research* **8**, 592-603 (1990).
16. Carter DR & Hayes W. The compressive behavior of bone as a two-phase porous structure. *Journal of Bone and Joint Surgery - American Volume* **59A**, 954-962 (1977).
17. Carter DR, Schwab GH & Spengler DM. Tensile fracture of cancellous bone. *Acta Othopedic Scandinavian* **51**, 733-741 (1980).
18. Hadjidakis DJ & Androulakis II. Bone remodeling. *Annals New York Academy of Sciences* **1092**, 385-396 (2006).
19. Meyer U & Wiesmann HP. Bone and cartilage engineering. Springer, Heidelberg (2006).
20. Wolff J. The law of bone remodeling. Springer, New York (1986).
21. Cutter CS & Mehrara BJ. Bone grafts and substitutes. *Journal of Long Term Effects on Medical Implants* **16**, 249-260 (2006).
22. Cypher TJ & Grossman JP. Biological principles of bone graft healing. *Journal of Foot and Ankle Surgery* **35**, 413-417 (1996).

23. Constantino PD & Freidman CD. Synthetic bone graft substitutes. *Otolaryngologic Clinics of North America Journal* **27**, 1037-1073 (1994).
24. Arrington ED, Smith WJ, Chambers HG, Bucknell AL & Davino NA. Complications of iliac crest bone graft harvesting. *Clinical Orthopaedics and Related Research* **329**, 300-309 (1996).
25. Dodd CAF, Fergusson CM, Freedman L, Houghton GR & Thomas D. Allograft versus autograft bone in scoliosis surgery. *The Journal of Bone and Joint Surgery (Br)* **70-B**, 431-434 (1988).
26. Summers BN & Eisenstein SM. Donor site pain from the ilium: a complication of lumbar spine fusion. *Journal of Bone and Joint Surgery - British Volume* **71-B**, 677-680 (1989).
27. Younger EM & Chapman MW. Morbidity at bone graft donor sites. *Journal of Orthopaedic Trauma* **3**, 192-195 (1989).
28. Sandhu HS, Grewal HS & Parvataneni H. Bone grafting for spinal fusion. *Orthopedic Clinics of North America* **30**, 685-698 (1999).
29. Banwart JC, Asher MA & Hassanein RS. Iliac crest bone graft harvest donor site morbidity: a statistical evaluation. *Spine* **20**, 1055-1060 (1995).
30. Ross N, Tacconi L & Miles JB. Heterotopic bone formation causing recurrent donor site pain following iliac crest bone harvesting. *British Journal of Neurosurgery* **14**, 476-479 (2000).
31. Seiler JG & Johnson J. Iliac crest autogenous bone grafting: donor site complications. *Journal of South Orthopedics Association* **9**, 91-97 (2000).
32. Skaggs DL, Samuelson MA, Hale JM, Kay RM & Tolo VT. Complications of posterior iliac crest bone grafting in spine surgery in children. *Spine* **25**, 2400-2402 (2000).

33. Carter G. Harvesting and implanting allograft bone. *AORN journal* **70**, 660-670 (1999).
34. Boyce T, Edwards J & Scarborough N. Allograft bone: the influence of processing on safety and performance. *Orthopedic Clinics of North America* **30**, 571-581 (1999).
35. Bonfiglio M & Jeter WS. Immunological responses to bone. *Clinical Orthopaedics* **18**, 19-27 (1972).
36. Bos GD, Goldberg VM & Zika JM. Immune responses of rats to frozen bone allografts. *Journal of Bone and Joint Surgery - American Volume* **65-A**, 239-246 (1983).
37. Damien C & Parsons R. Bone graft and bone graft substitutes: a review of current technology and applications. *Journal of Applied Biomaterials* **2**, 187-208 (1991).
38. Hollinger JO & Brekke J. Role of bone substitutes. *Clinical Orthopaedics* **324**, 55-65 (1996).
39. Keating JF & McQueen MM. Substitutes for autologous bone graft in orthopaedic trauma. *Journal of Bone and Joint Surgery - British Volume* **83**, 3-8 (2001).
40. Palmer SH, Gibbons CL & Athanasou NA. The pathology of bone allograft. *Journal of Bone and Joint Surgery - British Volume* **81**, 333-335 (1999).
41. Pelker RR & Friedlaender GE. Biomechanical aspects of bone autografts and allografts. *Orthopedic Clinics of North America* **18**, 235-239 (1987).
42. Friedlaender GE, Strong DM, Tomford W & Mankin HJ. Long-term follow-up of patients with osteochondral allografts. A correlation between immunologic responses and clinical outcome. *Orthopedic Clinics of North America* **30**, 583-588 (1999).

43. Conrad EU *et al.* Transmission of the hepatitis-C virus by tissue transplantation. *Journal of Bone and Joint Surgery - American Volume* **77-A**, 214-224 (1995).
44. Simonds RJ, Holmberg SD & Hurwitz RL. Transmission of human immunodeficiency virus type I from a seronegative organ and tissue donor. *New England Journal of Medicine* **326**, 726-732 (1992).
45. Tomford WW. Transmission of disease through transplantation of musculo-skeletal allografts. *Journal of Bone and Joint Surgery - American Volume* **77**, 1742-1754 (1995).
46. Callan DP & Rohrer MD. Use of bovine-derived hydroxyapatite in the treatment of edentulous ridge defects: a human clinical and histologic case report. *Journal of Periodontology* **64**, 575-582 (1993).
47. Misch CE & Dietsch F. Bone grafting materials in implant dentistry. *Implant Dentistry* **2**, 158-167 (1993).
48. Moore WR, Graves SE & Bain GI. Synthetic bone graft substitutes. *ANZ Journal of Surgery* **71**, 354-361 (2001).
49. Albrektsson T & Johansson C. Osteoinduction, osteoconduction and osseointegration. *European and Spine Journal* **10**, S96-S101 (2001).
50. Shalak R & Fox C. Tissue Engineering. 26-2-1988. Conference Proceeding. New York, Alan Liss.
51. George JHS. Engineering of fibrous scaffolds for use in regenerative medicine. (Thesis) 2009.
52. Hench LL & Polak JM. Third generation biomedical materials. *Science* **295**, 1014 (2002).

53. Spine JD. Tissue engineering and reparative medicine. *Annals New York Academy of Sciences* **961**, 1-9 (2002).
54. Vallet-Regi M & Gonzalez-Calbet JM. Calcium phosphates as substitution of bone tissues. *Progress in Solid State Chemistry* **32**, 1-31 (2004).
55. Albee FH & Morrison HF. Studies in bone growth - Triple calcium phosphates as a stimulus osteogenesis. *Annals of Surgery* **71**, 32-39 (1920).
56. Ray RD, Degge J, Gloyd P & Mooney G. Bone regeneration - an experimental study of bone grafting materials. *Journal of Bone and Joint Surgery - American Volume* **34A**, 638-647 (1952).
57. Driessens FCM & Verbeeck RMH. *Biomaterials*. CRC Press, Florida (1990).
58. Driessens F & Verbeeck R. Implant materials in biofunction. *Advances in biomaterials*. de Putter C, de Lange GL, de Groot K & Lee AJC (eds.), pp. 105-111 Elsevier, Amsterdam, 1998.
59. Van Wazer JR & Gilchrist R. Phosphorous and its compounds. *Science* **129**, 1271-1272 (1985).
60. Chow LC. Development of self-setting calcium phosphate cements. *Journal of the Ceramic Society of Japan. International Edition* **99**, 927-936 (1992).
61. Driessens FC, Planell JA, Boltong MG, Khairoun I & Ginebra MP. Osteotransductive bone cements. *Proceedings of the Institution of Mechanical Engineers, part H: Journal of Engineering in Medicine* **212**, 427-435 (1998).
62. Frankenburg EP *et al.* Biomechanical and histological evaluation of a calcium phosphate cement. *The Journal of Bone and Joint Surgery* **80**, 1112-1124 (1998).
63. Frayssinet P, Gineste L, Conte P, Fages J & Rouquet N. Short-term implantation effects of a DCPD-based calcium phosphate cement. *Biomaterials* **19**, 971-977 (1998).



64. Ginebra MP. Orthopaedic bone cements. Deb S (ed.), pp. 206-230 CRC Press Woodhead Publishing limited, Cambridge, 2008.
65. Dorozhkin SV. Calcium orthophosphate cements for biomedical application. *Journal of Materials Science* **43**, 3028-3057 (2008).
66. LeGeros RZ, Chohayeb A & Shulman A. Apatitic calcium phosphates: possible dental restorative materials. *Journal of Dental Research* **61**, 343-347 (1982).
67. Brown WE & Chow LC. A new calcium phosphate setting cement. *Journal of Dental Research* **62**, 672-679 (1983).
68. Brown W & Chow L. Dental restorative cement pastes. Patent-4518430 (1985).
69. Driessens FC, Boltong MG & Bermudez O. Formulation and setting times of some calcium orthophosphate cements: a pilot study. *Journal of Materials Science: Materials in Medicine* **4**, 503-508 (1993).
70. Chow LC, Markovic M & Takagi S. Cements research progress. LJ Struble (ed.), pp. 215-238 American Ceramic Society, Watersville, OH,1998.
71. Driessens FCM *et al.* Effective formulations for the precipitation of calcium phosphate bone cements. *Journal of Materials Science: Materials in Medicine* **5**, 164-170 (1994).
72. Ramachandran GN & Reddi AH. Biochemistry of collagen. Plenum, New York (1976).
73. Traub W & Piez KA. Advances in protein chemistry. CB Anfinsen, JT Edsalla & FM Richards (eds.), pp. 245 Academic Press, New York,1971.
74. Nimni ME & Harkness RD. Collagen Biochemistry, vol I. ME Nimni (ed.), pp. 1-79 CRC Press, Boca Raton,1988.

75. Kramer RZ, Bella J, Mayville P, Brodsky B & Berman HM. Sequence dependent conformational variations of collagen triple-helical structure. *Nature Structural Biology* **6**, 454-457 (1999).
76. Mayne R & Burgenson RE. Structure and function of collagen types. Academic, Orlando, Florida (1987).
77. McPherson JM, Sawamura S & Amstron R. An examination of the biological response to injectable, glutaraldehyde cross-linked collagen implants. *Journal of Biomedical Materials Research* **20**, 93-107 (1986).
78. Lee CH, Singla A & Lee Y. Biomedical applications of collagen. *International Journal of Pharmaceutics* **221**, 1-22 (2001).
79. Takaoka K, Nakahara H & Yoshikawa H. Ectopic bone induction on and in porous hydroxyapatite combined with collagen and bone morphogenetic protein. *Clinical Orthopaedics* **234**, 250-254 (1988).
80. Gleeson JP, Plunkett NA & O'Brien FJ. Addition of hydroxyapatite improves stiffness, interconnectivity and osteogenic potential of a highly porous collagen-based scaffold for bone tissue regeneration. *European Cells and Materials* **20**, 218-230 (2010).
81. Murata M *et al.* Bone augmentation by recombinant human BMP-2 and collagen on adult rat parietal bone. *International Journal of Oral Maxillofacial Surgery* **28**, 232-237 (1999).
82. Pedersen JA & Swartz MA. Mechanobiology in the third dimension. *Annals of Biomedical Engineering* **33**, 1469-1490 (2005).
83. Serre CM, Papillard M, Chavassieux P & Boivin G. *In vitro* induction of a calcifying matrix by biomaterials constituted of collagen and/or hydroxyapatite: an ultrastructural comparison of three types of biomaterials. *Biomaterials* **14**, 97-106 (1993).

84. Wang RZ *et al.* Synthesis of nanophase hydroxyapatite collagen composite. *Journal of Materials Science Letters* **14**, 490-492 (1995).
85. Scabbia A & Trombelli L. A comparative study on the use of a HA/collagen/chondroitin sulphate biomaterial (Biostite®) and a bovine-derived HA xenograft (Bio-Oss®) in the treatment of deep intraosseous defects. *Journal of Clinical Periodontology* **31**, 348-355 (2004).
86. Mehlisch DR, Leider AS & Roberts WE. Histologic evaluation of the bone/graft interface after mandibular augmentation with hydroxylapatite/purified fibrillar collagen composite implants. *Oral Surgery, Oral Medicine, Oral Pathology, Oral Radiology, and Endodontology* **70**, 685-692 (1990).
87. Yamauchi K, Goda T, Takeuchi N, Einaga H & Tanabe T. Preparation of collagen/calcium phosphate multilayer sheet using enzymatic mineralization. *Biomaterials* **25**, 5481-5489 (2004).
88. Lawson AC & Czernuszka JT. Collagen-calcium phosphate composites. *Proceedings of the Institution of Mechanical Engineers, part H: Journal of Engineering in Medicine* **212**, 413-425 (1998).
89. Wang X *et al.* Tissue engineering of biphasic cartilage constructs using various biodegradable scaffolds: an in vitro study. *Biomaterials* **25**, 3681-3688 (2004).
90. El-Amin SF *et al.* Extracellular matrix production by human osteoblasts cultured on biodegradable polymers applicable for tissue engineering. *Biomaterials* **24**, 1213-1221 (2003).
91. Kohn J, Abramson S & Langer R. Biomaterials Science. Ratner BD, Hoffman AS, Schoen FJ & Lemons JE (eds.), pp. 115-127 Elsevier, San Diego, 2004.
92. Johnson KD *et al.* Porous ceramics as bone graft substitutes in long bone defects: a biomechanical, histological, and radiographic analysis. *Journal of Orthopaedic Research* **14**, 351-369 (1996).

93. Walsh WR *et al.* Mechanical and histologic evaluation of Collagraft in an ovine lumbar fusion model. *Clinical Orthopaedics and Related Research* **375**, 258-266 (2000).
94. Muschler GF *et al.* Evaluation of collagen ceramic composite graft materials in a spinal fusion model. *Clinical orthopaedics and Related Research* **328**, 250-260 (1996).
95. Kokubo T, Kushitani H, Sakka S, Kitsugi T & Yamamuro T. Solutions able to reproduce in vivo surface-structure changes in bioactive glass-ceramic A-W. *Journal of Biomedical Materials Research* **24**, 721-734 (1990).
96. Lickorish D, Ramshaw JAM, Werkmeister JA, Glattauer V & Howlett CR. Collagen-hydroxyapatite composite prepared by biomimetic process. *Journal of Biomedical Materials Research* **68A**, 19-27 (2004).
97. Zhang LJ *et al.* Hydroxyapatite/collagen composite materials formation in simulated body fluid environment. *Materials Letters* **58**, 719-722 (2004).
98. Goes JC *et al.* Apatite coating on anionic and native collagen films by an alternate soaking process. *Acta Biomaterialia* **3**, 773-778 (2007).
99. Iijima M, Moriwaki Y & Kuboki Y. Oriented growth of octacalcium phosphate on and inside the collagenous matrix in vitro. *Connective Tissue Research* **32**, 519-524 (1996).
100. Chaozong L, Zhiwu H & Czernuszka JT. Gradient collagen/nanohydroxyapatite composite scaffold: Development and characterization. *Acta Biomaterialia* **5**, 661-669 (2009).
101. Du C, Cui FZ, Zhu XD & de Groot K. Three-dimensional nano-HAp/collagen matrix loading with osteogenic cells in organ culture. *Journal of Biomedical Materials Research* **44**, 407-415 (1999).

102. Tsai SW, Hsu FY & Chen PL. Beads of collagen-hydroxyapatite composites prepared by a biomimetic process and the effects of their surface texture on cellular behavior in MG63 osteoblast-like cells. *Acta Biomaterialia* **4**, 1332-1341 (2008).
103. Teixeira S, Fernandes MH, Ferraz MP & Monteiro FJ. Proliferation and mineralization of bone marrow cells cultured on macroporous hydroxyapatite scaffolds functionalized with collagen type I for bone tissue regeneration. *Journal of Biomedical Materials Research* **95A**, 1-8 (2009).
104. Jens-Hilmar B, Michael M, Angelika T & Wolfgang P. Biomimetic mineralization of collagen by combined fibril assembly and calcium phosphate formation. *Chemistry of Materials* **11**, 2694-2701 (1999).
105. Zhang W, Liao SS & Cui FZ. Hierarchical self-assembly of nano-fibrils in mineralized collagen. *Chemical Materials* **15**, 3221-3226 (2003).
106. Kikuchi M *et al.* Biomimetic synthesis of bone-like nanocomposites using the self-organization mechanism of hydroxyapatite and collagen. *Composites Science and Technology* **64**, 819-825 (2004).
107. Kikuchi M, Itoh S, Ichinose S, Shinomiya K & Tanaka J. Self-organization mechanism in a bone-like hydroxyapatite/collagen nanocomposite synthesized in vitro and its biological reaction in vivo. *Biomaterials* **22**, 1705-1711 (2001).
108. Yoshida T, Kikuchi M, Koyama Y & Takakuda K. Osteogenic activity of MG-63 cells on bone-like hydroxyapatite/collagen nanocomposite sponges. *Journal of Materials Science: Materials in Medicine* **21**, 1263-1272 (2010).
109. Toh S *et al.* Development of an artificial vertebral body using a novel biomaterial, hydroxyapatite/collagen composite. *Biomaterials* **23**, 3919-3926 (2002).
110. Song JH, Kim HE & Kim HW. Collagen-Apatite nanocomposite membranes for guided bone regeneration. *Journal of Biomedical Materials Research: Applied Biomaterials* **83B**, 248-257 (2007).

111. Sasaki N & Sudoh Y. X-ray pole figure analysis of apatite crystals and collagen molecules in bone. *Calcified Tissue International* **60**, 361-367 (1997).
112. Sato K, Kumagai Y & Tanaka J. Apatite formation on organic monolayers in simulated body environment. *Journal of Biomedical Materials Research* **50**, 16-20 (2000).
113. Zhai Y, Cui FZ & Wang Y. Formation of nano-hydroxyapatite on recombinant human-like collagen fibrils. *Current Applied Physics* **5**, 429-432 (2005).
114. Sachlos E, Gotoro D & Czernuszka JT. Collagen scaffolds reinforced with biomimetic composite nano-sized carbonate-substituted hydroxyapatite crystals and shaped by rapid prototyping to contain internal microchannels. *Tissue Engineering* **12**, 2479-2487 (2006).
115. Sachlos E, Reis N, Ainsley C, Derby B & Czernuszka JT. Novel collagen scaffolds with predefined internal morphology made by solid freeform fabrication. *Biomaterials* **24**, 1487-1497 (2003).
116. Wahl DA, Sachlos E, Liu C & Czernuszka JT. Controlling the processing of collagen-hydroxyapatite scaffolds for bone tissue engineering. *Journal of Materials Science: Materials in Medicine* **18**, 201-209 (2007).
117. Roveri N *et al.* Biologically inspired growth of hydroxyapatite nanocrystals inside self-assembled collagen fibers. *Materials Science and Engineering C* **23**, 441-446 (2003).
118. Sionkowska A & Kozłowska J. Characterization of collagen/hydroxyapatite composite sponges as a potential bone substitute. *International Journal of Biological Macromolecules* **47**, 483-487 (2010).
119. Jones GL *et al.* Primary human osteoblast culture on 3D porous collagen-hydroxyapatite scaffolds. *Journal of Biomedical Materials Research* **94A**, 1244-1250 (2010).

120. Liu L, Zhang L, Ren B, Wang F & Zhang Q. Preparation and characterization of collagen-hydroxyapatite composite used for bone tissue engineering scaffold. *Artificial cells, Blood Substitutes and Biotechnology* **31**, 435-448 (2003).
121. TenHuisen KS, Martin RI, Klimkiewicz M & Brown PW. Formation and properties of a synthetic bone composite: hydroxyapatite-collagen. *Journal of Biomedical Materials Research* **29**, 803-810 (1995).
122. Miyamoto Y *et al.* Basic properties of calcium phosphate cement containing atelocollagen in its liquid or powder phases. *Biomaterials* **19**, 707-715 (1998).
123. Tamimi F *et al.* Brushite-collagen composites for bone regeneration. *Acta Biomaterialia* **4**, 1315-1321 (2008).
124. Moreau JL, Weir MD & Xu HH. Self-setting collagen-calcium phosphate bone cement: mechanical and cellular properties. *Journal of Biomedical Materials Research* **91A**, 605-613 (2009).
125. Touny AH, Bhaduri S & Brown PW. Formation of calcium deficient HAp/collagen composites by hydrolysis of  $\alpha$ -TCP. *Journal of Materials Science: Materials in Medicine* **21**, 2533-2541 (2010).
126. Edelman GM. Cell adhesion molecules. *Science* **219**, 450-457 (1983).
127. Ruoslahti E & Pierschbacher MD. Arg-Gly-Asp: A versatile cell recognition signal. *Cell* **44**, 517-518 (1986).
128. Hughes D, Salter D, Dedhar S & Simpson R. Integrin expression in human bone. *Journal of Bone Mineral Research* **8**, 527-533 (1993).
129. Saito T, Albelda S & Brighton C. Identification of integrin receptors on cultured human bone cells. *Journal of Orthopaedic Research* **12**, 384-394 (1994).

130. Schneider G & Burridge K. Formation of focal adhesion by osteoblasts adhering to different substrata. *Experimental Cell Research* **21**, 4264-4269 (1994).
131. Hynes RO. Integrins: bidirectional, allosteric signaling machines. *Cell* **110**, 673-687 (2002).
132. Huhtala M, Heino J, Casciari D, de Lucie A & Johnson MS. Integrin evolution: insights from ascidian and teleost fish genomes. *Matrix Biology* **24**, 83-95 (2005).
133. Riikonen T *et al.*  $\alpha 2\beta 1$  integrin is a positive regulator of collagenase (MMP-1) and collagen  $\alpha 1(I)$  gene expression. *Journal of Biological Chemistry* **270**, 13548-13552 (1995).
134. Ivaska J *et al.* Integrin  $\alpha 2\beta 1$  mediates isoform specific activation of p38 and upregulation of collagen gene transcription by a mechanism involving the  $\alpha 2$  cytoplasmatic tail. *Journal of Cell Biology* **147**, 401-416 (1999).
135. Ivaska J *et al.* Integrin  $\alpha 2\beta 1$  promotes activation of protein phosphatase 2A and dephosphorylation of Akt and GSK3 $\beta$ . *Molecular and Cellular Biology* **22**, 1352-1359 (2002).
136. Knight CG *et al.* The collagen-binding A-domains of integrin  $\alpha 1\beta 1$  and  $\alpha 2\beta 1$  recognize the same specific amino acid sequence, GFOGER, in native (triple-helical) collagens. *Journal of Biological Chemistry* **275**, 35-40 (2000).
137. Knight CG *et al.* Identification in collagen type I of an integrin  $\alpha 2\beta 1$ -binding site containing an essential GER sequence. *Journal of Biological Chemistry* **273**, 33287-33294 (1998).
138. Gullberg D *et al.* Analysis of alpha 1 beta 1, alpha 2 beta 1 and alpha 3 beta 1 integrins in cell-collagen interactions: identification of conformation dependent alpha 1 beta 1 binding sites in collagen type I. *EMBO journal* **11**, 3865-3873 (1992).

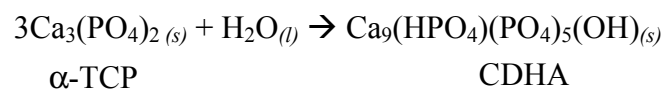


139. White DJ, Puranen S, Johnson MS & Heino J. The collagen receptor subfamily of the integrins. *International Journal of Cell Biology* **36**, 1405-1410 (2004).
140. Yamamoto M, Yamato M, Aoyagi M & Yamamoto K. Identification of integrins involved in cell adhesion to native and denatured type I collagens and the phenotypic transition of rabbit arterial smooth muscle cells. *Experimental Cell Research* **219**, 249-256 (1995).
141. Davis GE. Affinity of integrins for damaged extracellular matrix: alpha V beta 3 binds to denatured collagen type I through RGD sites. *Biochemical and Biophysical Research Communications* **182**, 1025-1031 (1992).

# Chapter 2: Calcium Phosphate Cement-Collagen for Bone Regeneration

## 2.1. Introduction

In chapter 1 it has already been mentioned that new bone substitutes must be found with similar properties to that of bone at a physico-chemical level, mechanical and biological level. The thesis is centered on a calcium phosphate cement (CPC) based on  $\alpha$ -tricalcium phosphate ( $\alpha$ -TCP) which is combined with collagen. Alpha tricalcium phosphate hydrolyses into calcium deficient hydroxyapatite (CDHA) through the reaction:



Collagen has already been described as an interesting biomaterial, especially from a biological point of view that may enhance the limited biological properties that CPCs may have in some cases. The combination of collagen and hydroxyapatite has been widely studied, since it tries to mimic the structure of bone. Most of the approaches are based on the formation of collagen sponges, on to where calcium phosphates precipitate<sup>1-3</sup>. A simultaneous precipitation of collagen and HA may also take place, forming mineralized collagen scaffolds<sup>4-6</sup>. These types of scaffolds are pre-forms that can further be implanted, but cannot be moulded or injected into a cavity.

Therefore, the combination of the collagen with an injectable and mouldable CPC, was thought as a system to improve the biological performance of a CPC. Nevertheless, first of all it was important to characterize the physicochemical properties of the CPC in order to understand the effect of adding collagen in its formulation.

Two of the main parameters that play a key role in the kinetics and setting reaction of CPC are the specific surface area of the starting powder and the particles size distribution<sup>7-9</sup>. This may be controlled by adjusting milling protocols of the  $\alpha$ -TCP in order to obtain different final properties. Therefore, in the present work, two different types of powders will be used. Moreover, collagen will be incorporated in the liquid phase of the CPC. Collagen may be extracted from many different animals or tissues, which results in different properties<sup>10,11</sup>. For example, collagens extracted from tendons are usually more insoluble than from other tissues<sup>12</sup>. In the present study, bovine pericardium collagen was used, which was completely soluble in acid medium. One of the approaches taken to be able to change the CPC features was to modify the liquid phase. In order to do so, three types of collagen solutions were used: the collagen solubilized in acid, the fibrillation or self-assembled collagen and the crosslinked collagen. The fibrillation was done by controlling the ionic strength, the pH and the temperature of the solution, obtaining a gel like collagen<sup>13-21</sup>. This fibrillised morphology was envisaged as a process to obtain a collagen similar to that found in the ECM.

Few are the works in which collagen is mixed with a calcium phosphate cement<sup>22-24</sup>. The approximations taken in the several works in which CPC is mixed with collagen, only take into account solubilized collagen or lyophilized collagen as a powder that can be mixed with the CPC powder. One of the novelties of the present work focuses on

applying the different treatments to collagen, obtaining different collagen states similar to those of the extracellular matrix. The effect of the different collagen treatments on the setting reaction of the CPC, as well as on the physico-chemical, morphological and mechanical properties of the CPC, were analyzed.

## 2.2. Objectives

The objective of this chapter was to prepare a CPC based on  $\alpha$ -TCP combined with collagen. The collagen was processed in order to obtain solubilized collagen, fibrillised collagen and crosslinked collagen. The different types of collagen were combined with the CPC, and the setting reaction, as well as the physical-chemical, mechanical and morphological properties of the composite CPC were characterized.

## 2.3. Materials and methods

### 2.3.1. Powder phase

#### 2.3.1.1. *Synthesis and preparation*

The powder phase of the cement was composed of  $\alpha$ -tricalcium phosphate ( $\alpha$ - $\text{Ca}_3(\text{PO}_4)_2$ ,  $\alpha$ -TCP). In order to fabricate  $\alpha$ -TCP, first of all, it must be taken into account that TCP has three allotropic phases, which are  $\alpha'$ ,  $\alpha$  and  $\beta$ . The  $\beta$  phase is stable at room temperatures and up to 1180°C, whereas the  $\alpha$  phase is stable at temperatures higher than 1180°C.

The powder phase of the CPC was obtained by sintering at 1400°C for 15 hours (Hobersal CNR-58) a mixture of calcium carbonate ( $\text{CaCO}_3$ , Sigma-Aldrich C4830) and calcium hydrogen phosphate ( $\text{CaHPO}_4$ , Sigma-Aldrich C7263). The two components were weighted in the appropriate molar ratios according to equation:



The final mixture weighted 175 grams (131,589 g of  $\text{CaHPO}_4$  and 48,399g of  $\text{CaCO}_3$ ). It was homogenized for 15 minutes with an overhead homogenizer (Whip Mix) and

introduced into a Platinum-Rhodium crucible. A sintering process was performed in a furnace (Hobersal CNR-58) following six steps (see Figure 2.1.):

- 1- Heating up to 300°C, for 1.45 hours at 2.5°C/min speed.
- 2- Carbon dioxide and water elimination at 300°C for 2 hours.
- 3- Heating up to 1100°C for 5 hours and 30 minutes at a 2.5°C/min speed.
- 4- Stabilization for 2 hours at 1100°C, allowing the transformation of  $\beta$ -TCP into  $\alpha$ -TCP.
- 5- Heating up to 1400°C for 2 hours at a 2.5°C/min speed.
- 6- Stabilization for 2 hours at 1400°C in order to make sure of the complete transformation into  $\alpha$ -TCP.

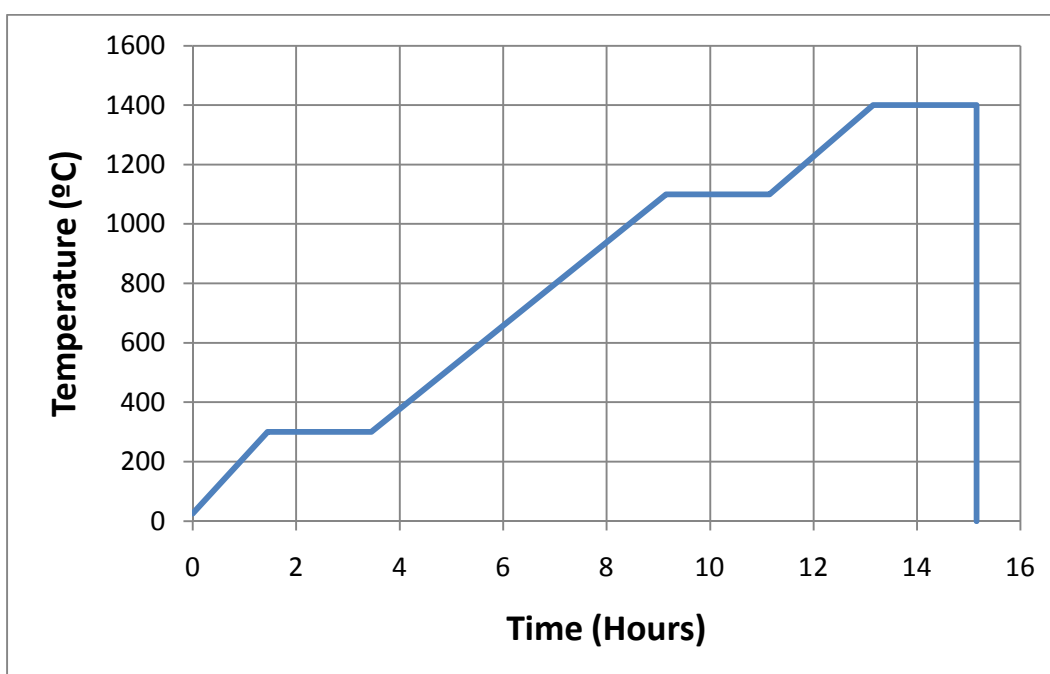
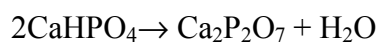
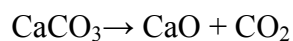
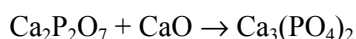


Figure 2.1. Heating ramp for the preparation of the  $\alpha$ -TCP powder.

During the initial heating up to 300°C, carbon dioxide and water were eliminated. The carbon dioxide was eliminated from the calcium carbonate and the water was eliminated from 2 molecules of calcium hydrogenphosphate, obtaining calcium oxide and calcium pyrophosphate:



Once the calcium pyrophosphate and the calcium oxide were obtained, the increase in temperature to 1100°C, and subsequent sintering and diffusion of these two molecules, produced TCP. Since depending on the temperature,  $\alpha$  or  $\beta$  could be obtained, in order to make sure of the complete conversion of  $\beta$  to  $\alpha$  TCP, the temperature was maintained at 1400°C for 2 hours. The reaction was as follows:



Once the sintering process finished, an air quench was done, in which the crucible was extracted and the block contained inside was crushed with a hammer into small pieces and air-cooled, in order to retain the  $\alpha$ -phase of the TCP.

The milling of the  $\alpha$ -TCP is an important step in the CPC fabrication process and is a critical point that determines the final properties of the different CPCs. Since CPC depends on many variables, maintaining as many variables as possible constant is a must. That is why, having a size distribution of the particles in a constant and same range every time the milling was done was necessary, in order to avoid changing the hydrolysis reaction kinetics of the different  $\alpha$ -TCP particles.

In this thesis, two main particle size distributions were used, one of them named as coarse, and the other one named as fine. The protocols for obtaining these two particle sizes were standardized, and after different studies regarding the effects of the milling time, the amount of balls used, the size of the balls and the rotation speed, two main protocols were obtained.

The milling was done in a planetary mill (Pulverisette 6, Fritsch GmbH) using an agatha recipient in both cases. For the coarse cement, 10 big balls (BB) (30 mm in diameter) were introduced in the recipient with 145 grams of  $\alpha$ -TCP and milled at 450 rpm for 15 minutes. For the fine powder, 145 grams of  $\alpha$ -TCP were milled, first with 10 BB at 450 rpm for 60 minutes, followed by a milling for 30 minutes with 100 small balls (sb) (10 mm in diameter) at 450 rpm.

The reaction of the CPC takes place in two steps, as previously mentioned in chapter 1; the first one consisting of dissolution of the  $\alpha$ -TCP and the second being the subsequent precipitation in a more stable phase, namely CDHA. In order to favor the latter one and

accelerate the process, a nucleating agent consisting of PHA (Alco ref. 1.02143) was added to enhance the precipitation of the CDHA. The reason was that the seed acts as an initial nucleating agent on top of which CDHA starts to precipitate. The effect of the seed is associated with the heterogeneous nucleation of the set cement. In order to do so, a 2% wt of PHA was introduced in the CPC powder, according to previous works<sup>7</sup>.

### *2.3.1.2. Characterization of the powder*

The specific surface area (SSA) of the powder was measured by nitrogen adsorption following the BET theory (Micromeritics, ASAP 2020).

The analysis of the particle size distribution was done by Laser diffraction, based on the optical principle according to which the small particles disperse the light in a determined and symmetric pattern. The intensity and the angle at which the light is dispersed is proportional to the particle volume as long as the material is opaque (refraction index = 1). The analysis were done in a LS 13 320 (Beckman Coulter).

Two main types of analysis can be done: in humid and in dry state. In the humid case, the particles are dispersed in alcohol, whereas in the dry state, the samples are measured under vacuum. The humid system is more accurate and has a better detection limit (between 2 nm and 40 nm), than the dry system (between 2 nm and 400 nm). It also has to be mentioned that the amount of powder needed in the dry state is in the order of magnitude of grams, whereas in the humid, the amount of sample needed is in the range of micrograms (three orders of magnitude less).

In order to obtain the particle size distribution of the initial TCP powders, the humid method was chosen. In order to do so, a tip of a spatula with the powder was introduced in alcohol, subjected to ultrasounds for 5 minutes to deagglomerate the powder particles and then introduced in the particle counter.

The phases present in the CPC powder were assessed by X-ray diffraction (XRD). The diffractogram was obtained with a Philips MRD diffractometer controlled by computer with a Nickel filter for the copper  $K_{\alpha}$  irradiation and a graphite monochromator. The working conditions were a potential of 40 KV and intensity of 30 mA. The range covered was between 4 and 40° of  $2\theta$ .

The diffractograms showed the peaks obtained for the diffraction and these were identified and compared with the crystallographic data of  $\alpha$ -TCP (JCPDS-29-359) and  $\beta$ -TCP (JCPDS-9-169). Since the adsorption coefficient in both cases was the same, the relative amounts of the two allotropic phases was obtained through the ratio of intensities of the highest peaks.

### 2.3.2. Liquid phase

The liquid phase was either a collagen solution or, in the control cements, accelerant solution (2.5% Na<sub>2</sub>HPO<sub>4</sub>) or 50 mM acetic acid.

#### 2.3.2.1. Preparation of collagen solutions

Collagen was introduced as the liquid phase of the CPC. Collagen was extracted from calf pericardium, which was a process done by the group at Clínica de Hierro in Madrid, leaded by Eduardo Jorge-Herrero. The process by which the collagen was processed is briefly described. The pericardium from young calves was obtained from slaughterhouses and transported to the lab in a 0.9% saline solution. The tissue was afterwards cleaned to remove any remnants of fat. Collagen was then isolated by enzymatic digestion with porcine pepsin (EC 3.4.23.1), 2100 U/mg, in a proportion of 1 mg per gram of tissue in a formic acid solution with a final concentration of 0.5 N, introducing 10 ml per gram of tissue. After 20 hours of agitation at 4°C, the tissue was centrifuged for 1 hour at 5000 x g in a Beckman L-70 centrifuge. The supernatant was precipitated with solid NaCl to reach a final concentration of 2.5 M, followed by 20 h of agitation at 4°C. Subsequently, the samples were centrifuged for 1 hour at 23000 x g. The precipitate was redissolved in 0.5 N acetic acid and dialyzed against 0.1N acetic acid. Once dialyzed, the samples were lyophilized. Previous to the mixture with the CPC powder, three different pre-treatments were applied to the collagen.

Solubilized collagen was named for the collagen that was completely dissolved in the solvent, which was a 50 mM acetic acid solution. In general, unless otherwise mentioned, the concentration used was 10 mg/ml.

The fibrillisation is a process in which the different collagen molecules are associated, obtaining a fibrillised or self-assembled structure. The formation of collagen fibers



involves the precipitation of the protein in an ordered form and was done by controlling the environmental conditions, such as pH, temperature and ionic strength.

The process applied consisted on the initial solubilization in 50 mM acetic acid and the addition of a 0.3 M sodium hydrogenphosphate stock solution to obtain a final concentration of sodium hydrogenphosphate in the collagen solution of 20 mM. The solution was kept during 20-30 minutes at 37°C, and was afterwards stabilized at pH 7.4 with the addition of NaOH 1 M. This method was a recompilation and modification of previous works reported in the literature<sup>14,20,21</sup>. The obtained collagen was fibrillised collagen.

Finally, a third method was used, in which the solubilized collagen was afterwards cross-linked adding 1% vol Glutaraldehyde solution (GA, Sigma-Aldrich G400-4) in order to obtain a 0.2% vol GA in the collagen slurry. That means that when preparing 1 ml of solubilized collagen, 2 µl of the 1% GA solution were added.

### *2.3.2.2. Collagen characterization*

In order to compare the different collagen treatments, samples were prepared at a concentration of 10 mg/ml and were afterwards lyophilized (Cryodos Telstar) for 24 hours. The specimens were characterized by scanning electron microscopy (SEM, JEOL JSM-840) and scanning differential calorimetry (DSC 2920, TA Instruments).

In order to prepare samples for SEM observation, after lyophilizing, samples were sputtered with gold in order to cover the surfaces of the collagen to make it conductive.

Differential scanning calorimetry (DSC) is a thermoanalytical technique in which the difference in the amount of heat released by the study sample and a control can be measured against temperature. The main objective of DSC was to observe the denaturation temperature that involves an energy change. A scan over a range of temperatures was done. DSC was applied to each of the lyophilized materials and done at a heating speed of 10°C/min from 25°C to 150°C (n=3). Negative values of heat evolution indicate exothermic process, whereas positive values indicate endothermic process.

### 2.3.3. Characterization of the setting reaction and cohesion

In the CPC preparation, the powder was added to the liquid phase, which was the collagen solution. The optimum L/P ratio was adjusted depending on the workability, ability to inject and the setting time. The L/P used in this chapter was maintained constant to 0.45 ml/g, unless otherwise specified.

Three variables were studied: collagen concentration (10 and 50 mg/ml), initial powder size (coarse and fine) and collagen treatment (fibrillised or non-fibrillised, as well as cross-linked collagen in some cases). From now on, the samples will be named as a function of the concentration (10 or 50), with the designation of the initial particle size (C or F) and if it is fibrillised or not (F or blank). The samples studied and the codes used are displayed in Table 2.1.

Code	Particle size	Collagen concentration (mg/ml)	Collagen treatment
<i>CTRLC</i>	Coarse	0	N.A.
<i>COLC10</i>	Coarse	10	Solubilized
<i>COLC10F</i>	Coarse	10	Fibrillised
<i>COLC50</i>	Coarse	50	Solubilized
<i>COLC50F</i>	Coarse	50	Fibrillised
<i>CTRLF</i>	Fine	0	N.A.
<i>COLF10</i>	Fine	10	Solubilized
<i>COLF10F</i>	Fine	10	Fibrillised
<i>COLF50</i>	Fine	50	Solubilized
<i>COLF50F</i>	Fine	50	Fibrillised

*Table 2.1. Samples studied and codes used for this chapter. The three main variables studied were the particle size (Coarse/Fine), the collagen concentration (0, 10 and 50 mg/ml) and the collagen treatment (Solubilized/Fibrillised).*

#### 2.3.3.1. Setting and cohesion times

The setting time of a CPC is the time upon which the cement starts to harden and cannot be molded anymore. When the powder is mixed with the liquid, a plastic and moldable paste is obtained. As time evolves, the paste loses its plasticity and mouldability, but increases its strength. The initial time in which a moldable paste loses its plasticity is called setting time.

The setting time can be monitored through different methods and can take into account several properties of the CPC. It can be tracked through viscosity measurements, through the heat released in the reaction or the dissolution of the reagents, among others.

The Gilmore needles are considered the easiest and fastest way to control the setting time. The protocol is described in the ASTM Standard C266-99. It is based on the resistance to the indentation of a needle on the cement. The system consists of two needles: a thick needle that has a weight of 113.4 g and a thin needle that has a weight of 453.6 g. The initial and final setting time are defined as, the time from the mixing of powder and liquid, after which the light and heavy needle did not leave any mark on the cement surface, respectively.

In order to prepare the reagents to measure the setting time, the collagen was weighted, at a concentration of 10 mg/ml with a L/P ratio of 0.45. The corresponding amount of powder was weighted and mixed with the collagen solution. Once the mixing was completed, the paste was introduced in brass cylinders, 5 mm in height and 10 mm in diameter.

The materials studied all had the same initial powder, being fine powder granulometry in this case, presenting different liquid solutions. The different solutions were the external control, which was an accelerant solution composed of 2.5%  $\text{Na}_2\text{HPO}_4$  and the internal control, which was 50 mM acetic acid solution. The collagen was mixed in the form of solubilized collagen, fibrillised collagen and crosslinked collagen. Another liquid phase used was a 0.2% GA solution.

Once implanted, a CPC is going to be surrounded by the body plasma and it has to be able to stay as a whole. The cohesion time is defined as the minimum time that takes place since the initial contact of the liquid phase with the solid phase, so that the immersed paste in a liquid is maintained and does not disintegrate.

In order to observe if the samples had cohesion after 2 minutes of preparation, the CPCs were mixed, being introduced afterwards in a water bath at 37°C. The CPC prepared presented as liquid phase acetic acid, soluble collagen and fibrillised collagen.

### 2.3.3.2. *Differential Scanning Calorimetry*

Differential scanning calorimetry monitored at 37°C was done in order to observe the energy evolution during the initial setting time. Between 50 and 100 mg of the composite were introduced in the lit, closing with the tap, without encapsulating the sample to avoid pressing the sample and pushing the water out of the capsule. In the space designated for the control in the DSC, another lit with tap was placed. The voltage needed to maintain the experimental samples and the control at the same temperature was recorded with time. The voltages were then converted to heat evolution using thermoelectric calibration constant and normalizing by the weight (W/g). The effect of collagen concentration was observed in these DSC, comparing CPC with a 10 mg/ml (COLF10) and a 50 mg/ml (COLF50) collagen concentration, with a cement containing acetic acid (CTRLF) in its liquid phase (n=3).

Since the mixing of the liquid phase and the powder phase were done outside the DSC, the initial minutes of setting were not observed. Furthermore, since the lit was not encapsulated in order to avoid extrusion of the liquid when encapsulating, there also existed a chance that part of the liquid evaporated. According to literature, some authors covered the CPC only with parafilm, but did not cover the samples with a tap<sup>25-28</sup>. In those works, no effect was attributed to water evaporation.

### 2.3.3.3. *pH evolution*

The pH evolution was determined of two slurries with a high L/P ratio. The L/P ratio was maintained high in order to allow the pH-meter to take the measurements. The liquid and the powder were mixed in a beaker and stirred by means of magnetical agitation. The pH-meter was then introduced in the beaker and the pH value was taken every 5 seconds. Soluble collagen was mixed with  $\alpha$ -TCP at L/P ratios of 14.29 and 33.33 ml/g for 1 hour with a collagen concentration of 5 mg/ml (n=3). These values of L/P ratios were taken from previous literature work in order to be able to compare the results<sup>29</sup>. Acetic acid and water were mixed at the same L/P ratios and were used as controls (n=3).

## 2.3.4. Calcium phosphate cement properties

### 2.3.4.1. Collagen liberation during setting

Bradford spectrophotometric analysis was done in order to determine the amount of collagen released from the CPC. For that purpose, the cement with collagen was soaked in distilled water in order to control the amount of collagen that was released from the cements during the 7 day setting reaction. The cements were prepared mixing the fine powder with two different collagen concentrations of the solubilized collagen, 10 and 50 mg/ml. The samples studied were COLF10 and COLF50, as well as the same samples with crosslinked collagen (COLF10-GA and COLF50-GA). The reason to compare the solubilized collagen with the crosslinked solubilized collagen was to observe if the collagen would dissolve and would be released to the water without the crosslinking with GA. The crosslinked collagen was used as a control since it is known that with the GA crosslinking, collagen is stable and does not dissolve when put in contact with an aqueous solution.

The amount of sample studied was, approximately, 0.5 grams of cement paste, meaning that the amount of collagen was 0.2 ml. That means that there were 2 mg of collagen in the whole sample in the 10 mg/ml concentration collagen CPC and 10 mg of collagen for the 50 mg/ml CPC. The samples were then introduced in two different amounts of distilled water: 1 ml and 12 ml. All the water was removed for analysis and replaced after 1, 2, 3, 4, 5, and 6 hours and then every day, up to 7 days, doing the experiment in triplicates.

The Bradford protein assay was used and it is a method to determine the total protein concentration. The concentration interval in which the spectrophotometric response is linear respect to the protein concentration is the range between 1.25 and 25  $\mu\text{g/ml}$ . 100  $\mu\text{l}$  of the supernatant were collected and mixed with 100  $\mu\text{l}$  of the Bradford reagent. It is based on the binding of the dye Coomassie to the protein. In the studied range of assay, the dependence is linear between the amount of protein present and the amount of protein linked to the dye. The assay is colorimetric, which means that the increase in color intensity increases with the protein concentration. The protein concentration was

then determined by comparison with standard protein of bovine serum albumin solutions, measured at an absorbance of 595 nm.

In order to verify and corroborate the results, a nanodrop spectrophotometer (NanoDrop 8000 Spectrophotometer, Thermo Scientific), which consists of a spectrophotometer of high accuracy that only needs 1-2  $\mu\text{l}$  of sample to do the measurement, was used. This technique is useful, accurate and fast for determining nucleic acids and proteins. The different solutions were measured without any dilution.

#### *2.3.4.2. Collagen distribution*

The distribution of the collagen in the cement was evaluated by fluorescence technique using (3-(4-carboxybenzoyl)quinoline-2-carboxaldehyde) (CBQCA) as fluorescent agent. This reagent has the ability to link to amino groups. A 48 well plate was used and several pieces of the set cement, which was set in water for 7 days, were introduced in them ( $n=3$ ). A total volume of 600  $\mu\text{l}$  was introduced in each well, containing a 1 mM solution of CBQCA (previously dissolved in acetone) and 2 mM in KCN. The samples were left reacting for 90 minutes and rinsed afterwards three times in distilled water for 15 minutes. Samples were observed by means of confocal microscopy (Leica TCS-SPE), soaking them in distilled water and leaving them immersed in water during the observation in order to avoid the interference of salts. Fluorescence images at 488 nm and reflexion images were taken for each sample. Since CPC may present some autofluorescence, a CPC without collagen was used to measure the background fluorescence. Afterwards, samples were analyzed in the same conditions, making any signal of fluorescence arise from the collagen molecule. The studied samples were CTRLF, COLF10, COLF10F, COLF50 and COLF50F.

#### *2.3.4.3. Scanning electron microscopy (SEM)*

The samples were freeze-dried to eliminate water, in order to facilitate gold sputtering of the samples. Once the samples were coated, the samples were observed in a SEM (JEOL JSM-840).

#### 2.3.4.4. *Fourier Transformed Infrared Spectroscopy*

The material analyzed consisted of the CPC with the different collagen treatments, in order to see the differences with a collagen concentration of 10 mg/ml and 50 mg/ml (COLF10, COLF10F, COLF50, COLF50F and CTRLF) (n=3).

The methodology consisted on crashing the composite, to obtain a fine powder that was then mixed at a ratio of 1:100 with potassium bromide (KBr). Potassium bromide is transparent to the IR and does not interfere with the measure. Both of the powders were homogeneously mixed and introduced in a device on top of which a load of 1000 kg.cm<sup>-2</sup> was applied. The result was a semitransparent disk with which the measurement was done. The disk was afterwards placed in the spectrophotometer (FTIR Bomem MB-120) and the measurement was done. The spectrums were done 30 times and an average spectrum was obtained. A blank with no sample was obtained in order to have the base line.

In order to observe better the possible interactions of HA and collagen, a 70:30 wt% CPC:collagen in weight composite was prepared with soluble collagen (n=3) in order to increase the amount of collagen in the composite. The collagen was prepared at a concentration of 50 mg/ml, and in order to maintain the ratio 70:30 %wt, a L/P ratio of 8.62 ml/g was used. In this case, in which the proportion of collagen was higher, the samples had sponge-like morphology, making difficult crashing the samples. Therefore, random parts of the composite were cut and placed in a diamond cell and observed with an IR Microscope Plan Spectra Tech attached to the previous FTIR, Bomem MB-120.

#### 2.3.4.5. *X-Ray diffraction*

X-Ray diffraction was carried out in order to determine the phase evolution from the initial stages until the end product was obtained. In this case, the process applied was the same as in section 2.3.1.2, but the comparison was done between the JCPDS cards of  $\alpha$ -TCP and HA (JCPDS-9-432).

Fine CPC composed of acetic acid (CTRLF), solubilized collagen (COLF10) and fibrillised collagen (COLF10F) as the liquid phase were prepared and left setting for 1, 2, 4, 8, 16, 24, 48, 72, 96, 120, 168, 240 and 336 hours (n=1). The amount of  $\alpha$ -TCP

that had reacted at time  $t$  was determined through the reaction conversion with the formula:

$$w_t = \frac{I_t M_{\text{CDHA}}}{I_0 M_{\alpha\text{-TCP}} - I_t (M_{\alpha\text{-TCP}} - M_{\text{CDHA}})}$$

Where  $w_t$  is the fraction of  $\alpha$ -TCP at time  $t$ ,  $I_t$  is the intensity of the peak  $30.74^\circ$  at time  $t$ ,  $M_{\text{CDHA}}$  is the adsorption coefficient of the CDHA, which is  $84.97 \text{ cm}^2/\text{g}$ ,  $I_0$  is the intensity of the peak at time zero and  $M_{\alpha\text{-TCP}}$  is the adsorption coefficient of  $\alpha$ -TCP, which is  $86.43 \text{ cm}^2/\text{g}$ . The standard deviation was taken as the square root of the intensity<sup>30</sup>.

#### 2.3.4.6. Helium pycnometry

The skeletal density of a material can be calculated by introducing a determined amount of sample and measuring the volume it occupies using a Helium pycnometer (AccuPyc 1330). The pycnometer is based in two cells: the calibrated sample cell ( $V_{\text{cell}}$ ), in which the sample is introduced and the calibrated expansion cell ( $V_{\text{exp}}$ ). The first assumption is that  $V_{\text{cell}}$  and  $V_{\text{exp}}$  are at ambient pressure ( $P_a$ ) and ambient temperature ( $T_a$ ) and that the valve that communicates both of the cells is closed.  $V_{\text{cell}}$  is then charged up to an elevated pressure ( $P_g$ ).

Since this technique is non-destructive, a total of three cylinders ( $\varnothing=6 \text{ mm}$  and  $h=12 \text{ mm}$ ) before being used for the mercury intrusion porosimetry, were weighted and then introduced in the chamber. The process was repeated three times with different cylinders.

#### 2.3.4.7. Mercury intrusion porosimetry

Mercury intrusion porosimetry (MIP, Micromeritics, Autopore IV) was used to measure total porosity of the samples, as well as to obtain a pore size distribution of the sample represented as  $dV/d\log D$  respect pore entrance diameter ( $D$ ). Three different variables were studied: initial powder particle size, collagen concentration and fibrillation of collagen ( $n=1$ ).



### 2.3.4.8. *Injectability*

Injectability can be defined as the ability a paste has to be extruded through a syringe. It was measured by the weight percentage of the cement paste that was injected from a standard syringe, by a force of 100 N. A L/P ratio of 0.45 ml/g was used. Before the mixture of the two components, a 5 ml syringe with a 2 mm opening was weighted ( $W_e$ ). The paste was then introduced in the syringe and weighted again ( $W_f$ ). The syringe was then placed in the mechanical compression instrument (MTS Bionix 858), at an advancing speed of 15 mm/min until a 100 N force was obtained. At the end of the assay, the syringe was weighted ( $W_a$ ). The injectability (I) was defined as:

$$I = \frac{(W_f - W_a)}{(W_f - W_e)} \times 100$$

The assay was done for a minimum of three samples and all the samples were injected 2 minutes after mixing the powder and the liquid. The samples studied were CTRLF, COLF10 and COLF10F (n=3).

### 2.3.4.9. *Mechanical properties*

Cylinders were prepared introducing the slurries into Teflon cylinder moulds of 12 mm height and 6 mm diameter and left reacting for seven days in Ringer's solution. The CPC cylinders were then extracted from the Teflon mould and tested. A standard number of ten cylinders were prepared for each composition and used for compression testing in Universal Testing Machine (Adamel Lhomargy DY 34) at a crosshead speed of 1 mm/min. The force was axially applied. The samples analyzed were CTRLF, COLF10, COLF10F, COLF50, COLF50F, CTRLC, COLC10, COLC10F, COLC50 and COLC50F.

A representation of the force applied versus the displacement was recorded. These units were given as force, in Newtons, and the displacement, in mm. The force was then transformed into stress, by dividing the force by the area and the displacement was transformed into strain, by subtracting the initial length of the material and dividing by the initial length, obtaining a dimensionless value. Calculating the stress in compression gives a negative value, since the initial value is bigger than the final value. Absolute

values were then used. The test finished when the samples broke, obtaining a value for the maximum strength applied.

$$\sigma = \frac{F}{S}$$
$$\varepsilon = \frac{l_f - l_o}{l_o}$$

The tension applied was then represented versus the strain, obtaining the  $\sigma$  vs  $\varepsilon$  curve. The slope of the initial linear displacement corresponds to the Young modulus.

#### *2.3.4.10. Statistical analysis*

Statistical analysis was carried out with significance of 5%. One way analysis of variance (ANOVA) with Fisher post-hoc test was conducted. The data are expressed as mean  $\pm$  standard deviation.

## **2.4. Results**

### **2.4.1. Powder phase**

#### *2.4.1.1. Thermal treatment*

After the sintering for 15 hours, the quenching was done fractioning the TCP block. XRD of the powder confirmed the production of  $\alpha$ -TCP. The diffractogram shown in Figure 2.2 shows the characterized diffractogram with the identified peaks corresponding to  $\alpha$ -TCP and shows the presence of small amounts of  $\beta$ -TCP (< 4%).

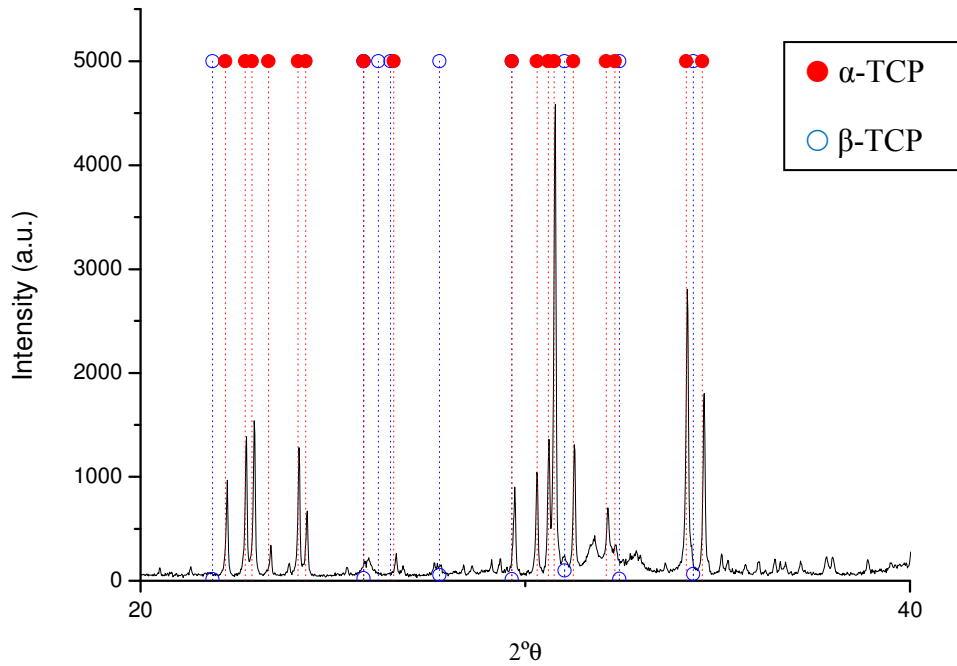


Figure 2.2. X-Ray diffractogram of the obtained  $\alpha$ -TCP powder after heat treatment. The indexation of the peaks identifies  $\alpha$ -TCP as the main phase of the powder, having less than 4% of  $\beta$ -TCP.

#### 2.4.1.2. Particle size distribution

The specific surface area of the coarse  $\alpha$ -TCP powder was  $1.228 \pm 0.008 \text{ m}^2/\text{g}$ , having a median of  $5.186 \pm 0.572 \text{ }\mu\text{m}$ . The specific surface area of the fine  $\alpha$ -TCP powder had a value around two times that of the coarse  $\alpha$ -TCP, having a value of  $2.347 \pm 0.005 \text{ m}^2/\text{g}$ . The median particle size was  $2.41 \pm 0.048 \text{ }\mu\text{m}$ . The particle size distributions for coarse and fine  $\alpha$ -TCP are shown in Figure 2.3.

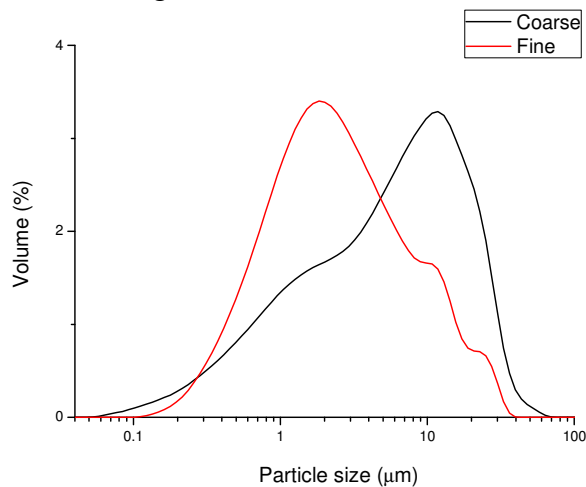


Figure 2.3. Particle size distribution for the coarse and the fine  $\alpha$ -TCP powder. The median for the coarse  $\alpha$ -TCP was found at a value of  $5.186 \pm 0.572 \text{ }\mu\text{m}$ , whereas for fine  $\alpha$ -TCP, the peak was found at  $2.41 \pm 0.048 \text{ }\mu\text{m}$ .

## 2.4.2. Liquid phase

When collagen was solubilized in acetic acid, the viscosity of the solution was higher than water. The viscosity increased even more when the collagen was fibrillised. A gel block was formed. When the crosslinking was done, bundles and aggregations of collagen fibres were formed.

The SEM images of the lyophilized collagen solutions after the different treatments are shown in Figure 2.4. The morphology of the solubilized collagen was homogenous, showing membrane morphology throughout the whole sample (Figure 2.4.a), whereas for the fibrillised collagen, a more fibrous structure was observed (Figure 2.4.b). A more anisotropic structure was formed which combined the membrane morphology previously observed with a more elongated and fibrous structure. The morphology of the crosslinked collagen was similar to that of the solubilized collagen, although presenting a higher number of interconnecting fibres (Figure 2.4.c).

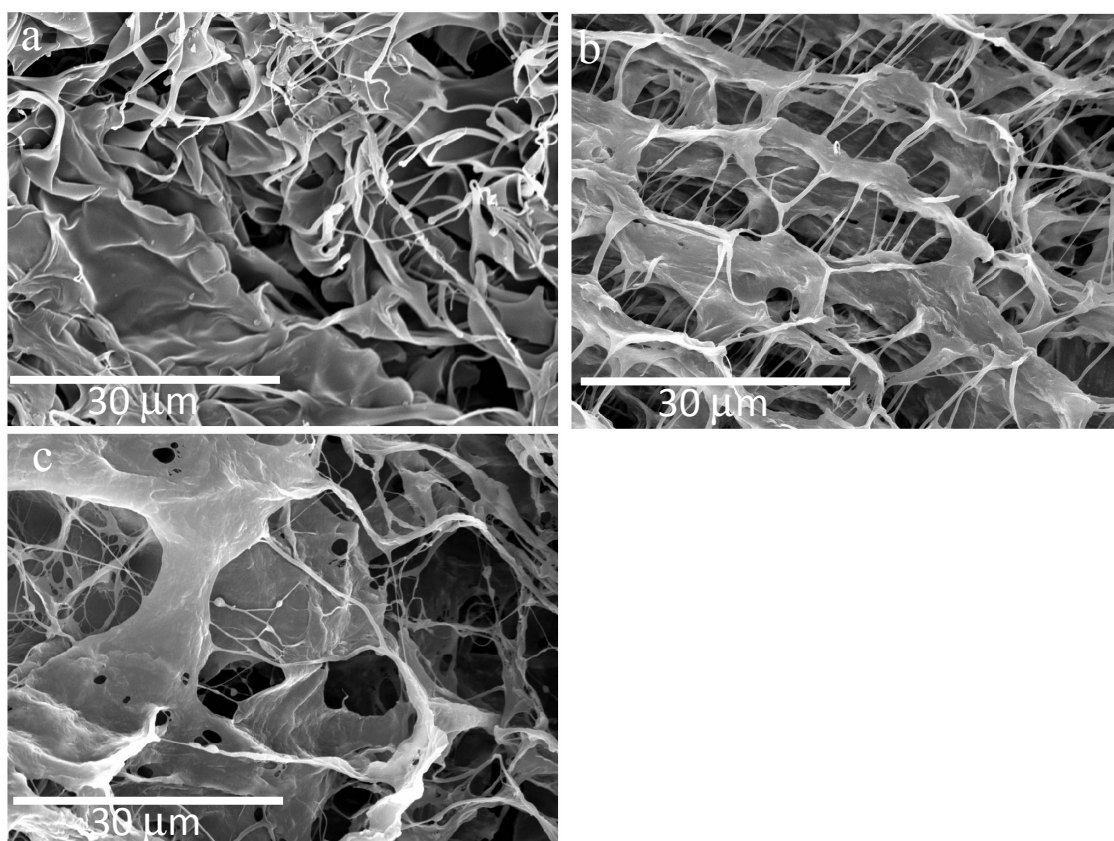


Figure 2.4. SEM micrographs for the lyophilized collagen solutions after the three different treatments: a) solubilized: presenting a homogenous membrane structure, b) fibrillised: presenting a heterogeneous structure which combined the previous membrane structure with a more fibrous structure and c) crosslinked: presenting fibres heterogeneously distributed.

The thermal analysis by DSC showed an exothermic peak in the three types of collagen solutions which refer to the denaturation temperature of collagen. The negative values for the heat evolution were indicative of an exothermic process. A displacement of the peak was observed when comparing solubilized collagen and fibrillised collagen (Figure 2.5). The solubilized collagen presented a peak at  $70\pm 2^\circ\text{C}$ , whereas for the fibrillised collagen it appeared at  $89\pm 2^\circ\text{C}$ . Crosslinked collagen showed the peak at  $85\pm 2^\circ\text{C}$ . DSC results were indicative of an effective fibrillisation of collagen but no difference was observed between the fibrillised and crosslinked collagen. The increase in the denaturation temperature was similar for fibrillised and crosslinked collagen compared to the solubilized collagen.

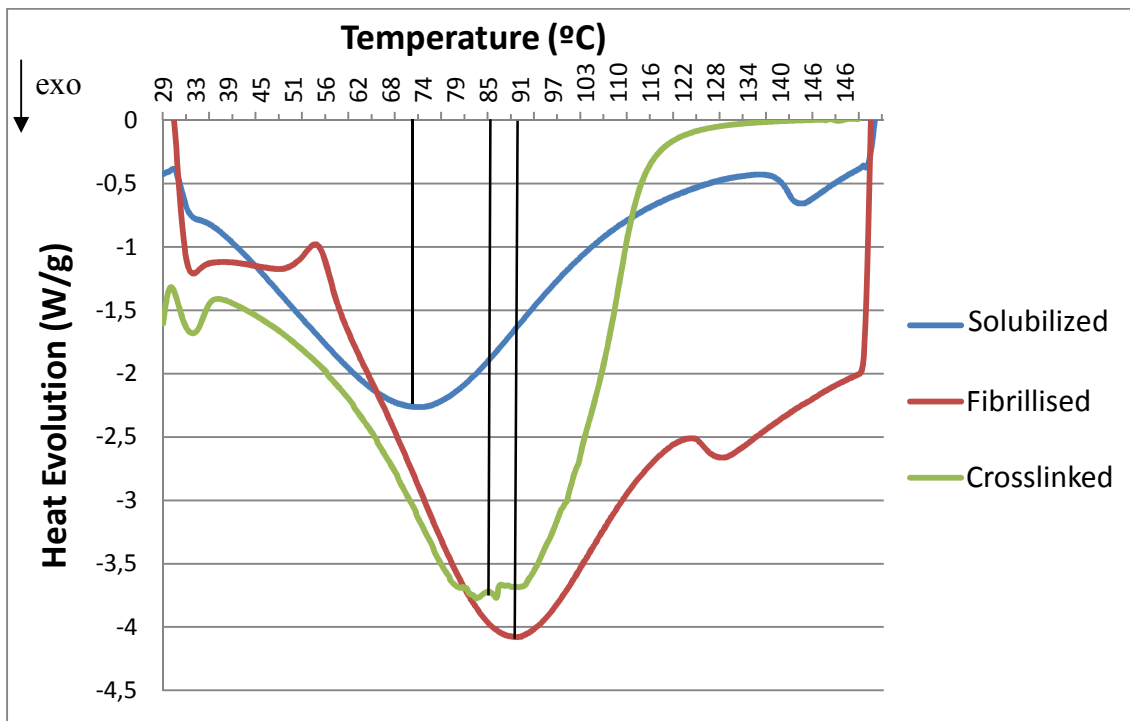


Figure 2.5. DSC of the different collagen treatments, in which the different peaks indicate the denaturation temperature. The solubilized collagen presented a peak at  $70\pm 2^\circ\text{C}$ . This value was increased when the collagen was crosslinked ( $85\pm 2^\circ\text{C}$ ) and fibrillised ( $89\pm 2^\circ\text{C}$ ).

### 2.4.3. Characterization of the setting reaction

A high L/P ratio of 0.45 ml/g was used when mixing the powder with collagen solutions due to their high viscosity. When the powder was mixed with the collagen solutions, the viscosity of the paste was higher than for the acetic acid used as a control, but still had a workable consistency. When the collagen was fibrillised, the behaviour was similar to

that of solubilized collagen. When the crosslinker was added, although bundles of collagen appeared, making the mixing already heterogeneous in the initial stages, the CPC was still workable.

### 2.4.3.1. Setting and cohesion times

Setting times of the cements prepared with the different collagen solutions and also with 2.5 wt% Na<sub>2</sub>HPO<sub>4</sub> (accelerant solution) or 50 mM acetic acid, that served as control CPCs, were measured with the Gillmore needles and the results are shown in Table 2.2. The standard deviation is taken as  $\pm 1$  minute.

	<b>t<sub>0</sub> (min)</b>	<b>t<sub>f</sub> (min)</b>
2.5 wt% Na <sub>2</sub> HPO <sub>4</sub> solution	6	15
50 mM acetic acid solution	15	40
Solubilized collagen	13	35
Fibrilised collagen	12	32
Crosslinked collagen	5,5	27
GA	20	-

Table 2.2. Setting times for cements prepared with 10 mg/ml collagen concentration for the different collagen treatments and cement at L/P ratio of 0.45 ml/g. Standard deviation is  $\pm 1$  minute for all series.

The incorporation of acetic acid in the CPC clearly increased the setting times to 15 minutes compared to the 6 minutes obtained with accelerant solution. When collagen was added, the values were similar to those of the acetic acid, meaning that the main responsible for the increase in the setting time was the acidic character of the solution. No big differences were observed when comparing the fibrillised (12 min) and solubilized collagen (13 min). Nevertheless, the setting times were similar to those of the accelerant solution when glutaraldehyde was added into the collagen solution (5.5 min). When GA was used without collagen, the values were much higher than in the presence of collagen (20 min).

The CTRLF, COLC10 and COLC10F samples presented cohesion after immersing them in the water bath. The cohesion times was proven to be less than 2 minutes.

### 2.4.3.2. Differential scanning calorimetry

Figure 2.6 shows the heat evolution for the control cement with acetic acid and for the collagen-containing cements with 10 or 50 mg/ml. Exothermy, revealed by the negative

values of the heat evolution, was observed until 600 min. At this point no more heat evolution was detected indicating that water had completely reacted or evaporated. In order to assess the phase obtained, DRX was done. The samples consisted of 75%  $\alpha$ -TCP and 25% CDHA, indicating that the transformation was not complete.

The rate of heat evolution shows that as the collagen concentration was increased in the CPC, at the initial times, there was less heat evolution, meaning that there was a higher release of energy for the cement without collagen. After 200 minutes approximately, the heat evolution for the CTRLF was reduced, obtaining similar values for the different samples. After 400 minutes of reaction, the collagen containing samples released higher heat compared to the CTRLF. The results do show differences, but as mentioned in materials in methods, it also has to be taken into account that water evaporation can also play a role in the heat evolution.

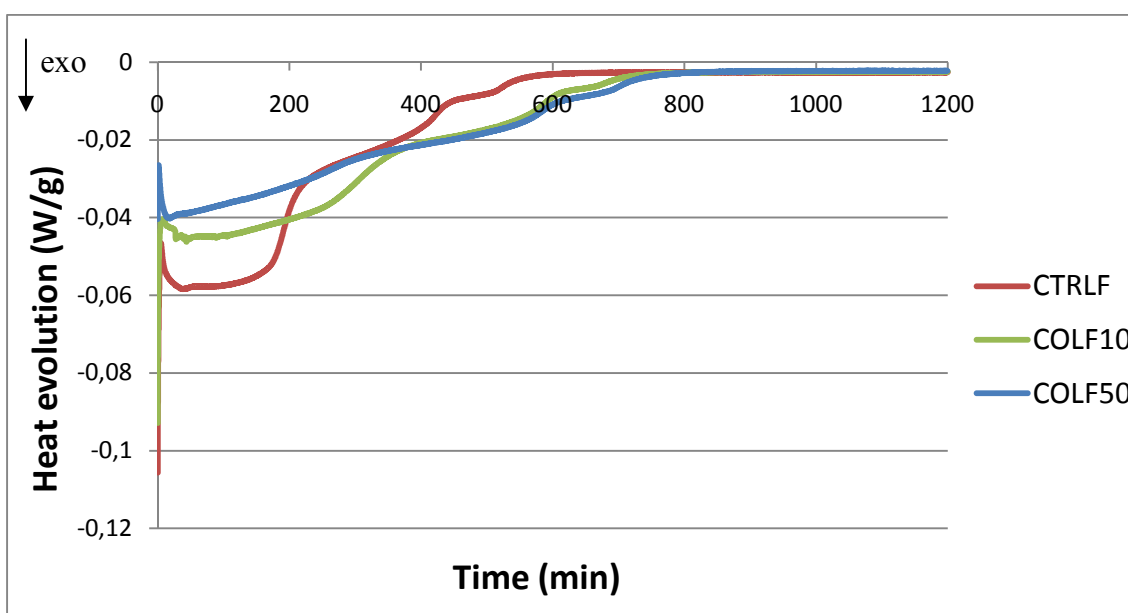


Figure 2.6. Heat evolution for the setting reaction of the CPC mixed with collagen (10 mg/ml and 50 mg/ml) and acetic acid at a L/P ratio of 0.45 ml/g.

In order to observe better the initial reaction time, the graph in Figure 2.6 was represented in logarithmic scale (Figure 2.7.). In this graph it can be seen that the reaction takes place slower initially as the collagen concentration is increased.

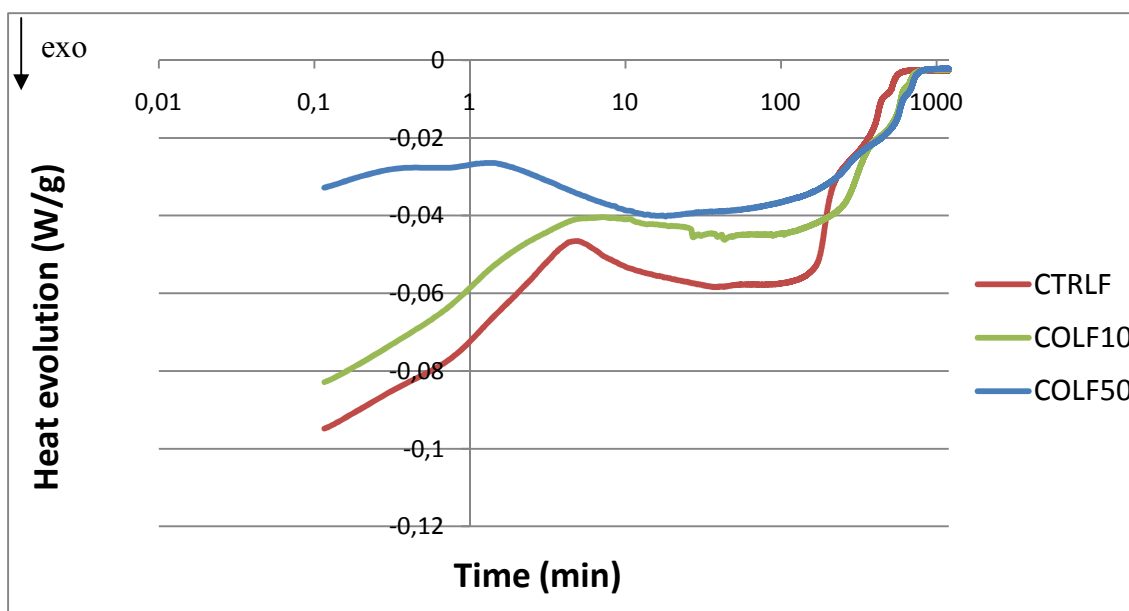


Figure 2.7. Heat evolution in logarithmic scale for the setting reaction of the CPC mixed with collagen (10 mg/ml and 50 mg/ml) and acetic acid at a L/P ratio of 0.45 ml/g.

### 2.4.3.3. pH evolution

Figure 2.11 shows the pH evolution when mixing the fine CPC powder with different solutions as liquid phase (water, 50 mM acetic acid or 10 mg/ml collagen solution in 50 mM acetic acid). The increase of the pH was similar when having water, acetic acid or the collagen solution (Figure 2.8). Nevertheless, compared to water solution, there was a delay in the dissolution kinetics. The pH plateau was achieved earlier in the water containing cements than in the collagen or acetic acid containing cements. When the L/P ratio was decreased, the acetic acid and the collagen containing mixtures continued having a delay in the dissolution kinetics. Furthermore, there was also a slight delay in the dissolution kinetics in the collagen containing samples compared to the acetic acid containing samples (Figure 2.9.). This can be observed since the collagen and acetic acid curves do not completely overlap at low times.



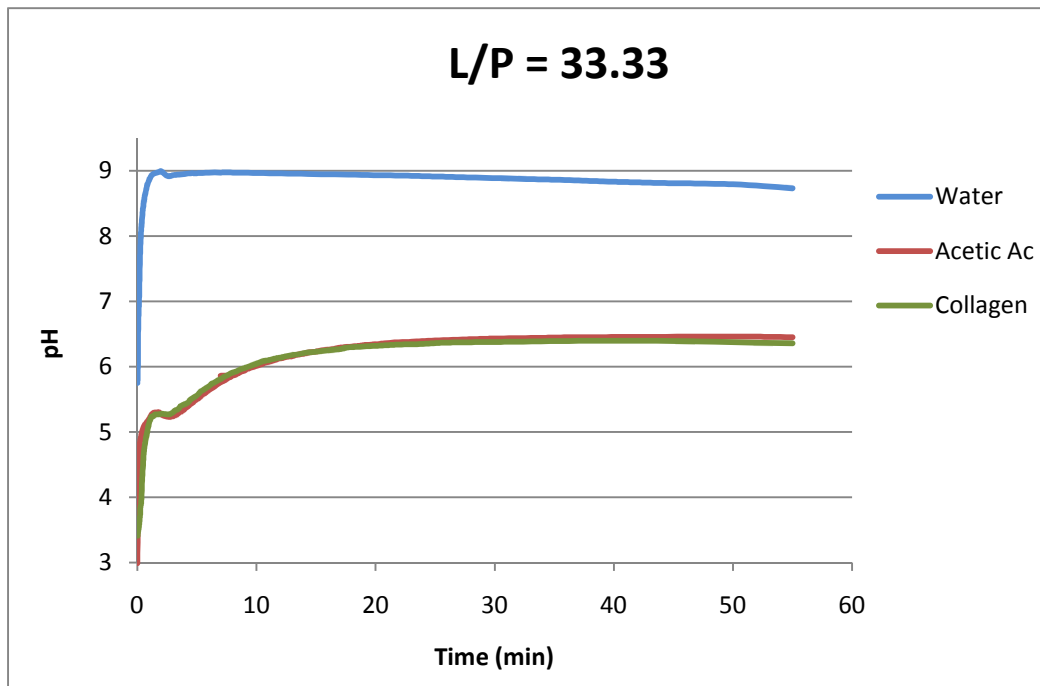


Figure 2.8. pH curve for different cement formulations containing water, 50 mM acetic acid solution or 5 mg/ml collagen solution in 50 mM acetic acid as the liquid phase of the CPC, at a L/P ratio of 33.33 ml/g.

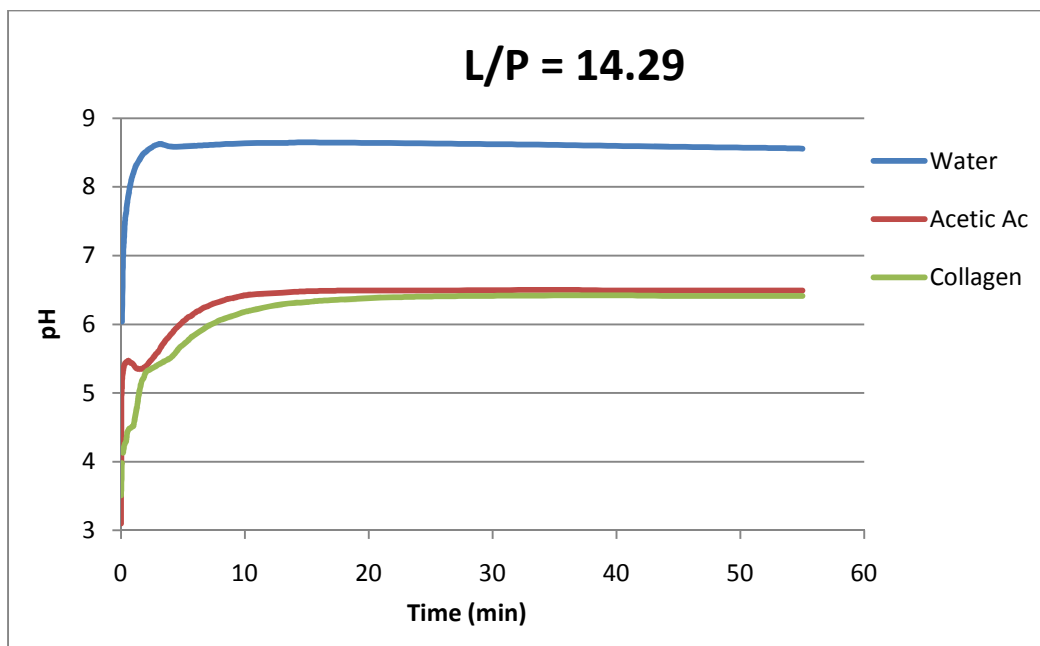


Figure 2.9. pH curve for different cement formulations containing water, 50 mM acetic acid solution or 5 mg/ml collagen solution in 50 mM acetic acid as the liquid phase of the CPC, at a L/P ratio of 14.29 ml/g.

## 2.4.4. Calcium phosphate cement properties

### 2.4.4.1. Collagen release during the setting reaction

The amount of collagen released from the samples was analyzed for up to 7 days. Collagen is known to be soluble in acidic conditions and is not supposed to be soluble in neutral pH. However, in order to know if collagen was being dissolved during the soaking period in water, where the cements were immersed while the setting reaction was taking place, Bradford analysis was done.

No change in the coloration of the solution was observed, neither with the cross-linked nor the non-crosslinked collagen for the different time points, meaning that the amount of collagen released in the medium at the different time points, if any, was very low, below the detection limit.

From these results, it can be concluded that the amount of collagen dissolved was lower than 1.25  $\mu\text{g/ml}$  in the different amounts of water, both for the crosslinked and the non-crosslinked specimens for the different time points, which would represent less than a 0.025% of collagen dissolved to the medium when having a 10 mg/ml collagen concentration in the 1 ml sample. In the 10 mg/ml collagen CPC immersed in 12 ml, the release was lower than 0.3% collagen. Furthermore, for the 50 mg/ml solution immersed in the 1 ml and 12 ml, the maximums released were lower than 0.005% and 0.06% respectively. From these results, it was concluded that collagen crosslinking was not necessary.

The same result was obtained from the Nanodrop spectrophotometer, in which the concentration of the protein detected didn't differ from the blank. The different values oscillated around 0. The detection limit of the spectrophotometer was 0.0025 mg/ml.

### 2.4.4.2. Collagen distribution

CPC presented autofluorescence when observed under confocal microscopy. Therefore, the intensity that was observed for the CTRLF was subtracted for all other samples. The first samples analyzed were the samples COLF10 and COLF50 (Figure 2.10). The image in the left corresponds to the reflection image and the image in the right

corresponds to the image taken with the exciting laser beam. For COLF10 (Figure 2.10b), the intensity was lower compared to COLF50 (Figure 2.10d). In both cases, the distribution was shown to be homogenous; the only thing that varied was the intensity, which was dependent on the concentration.

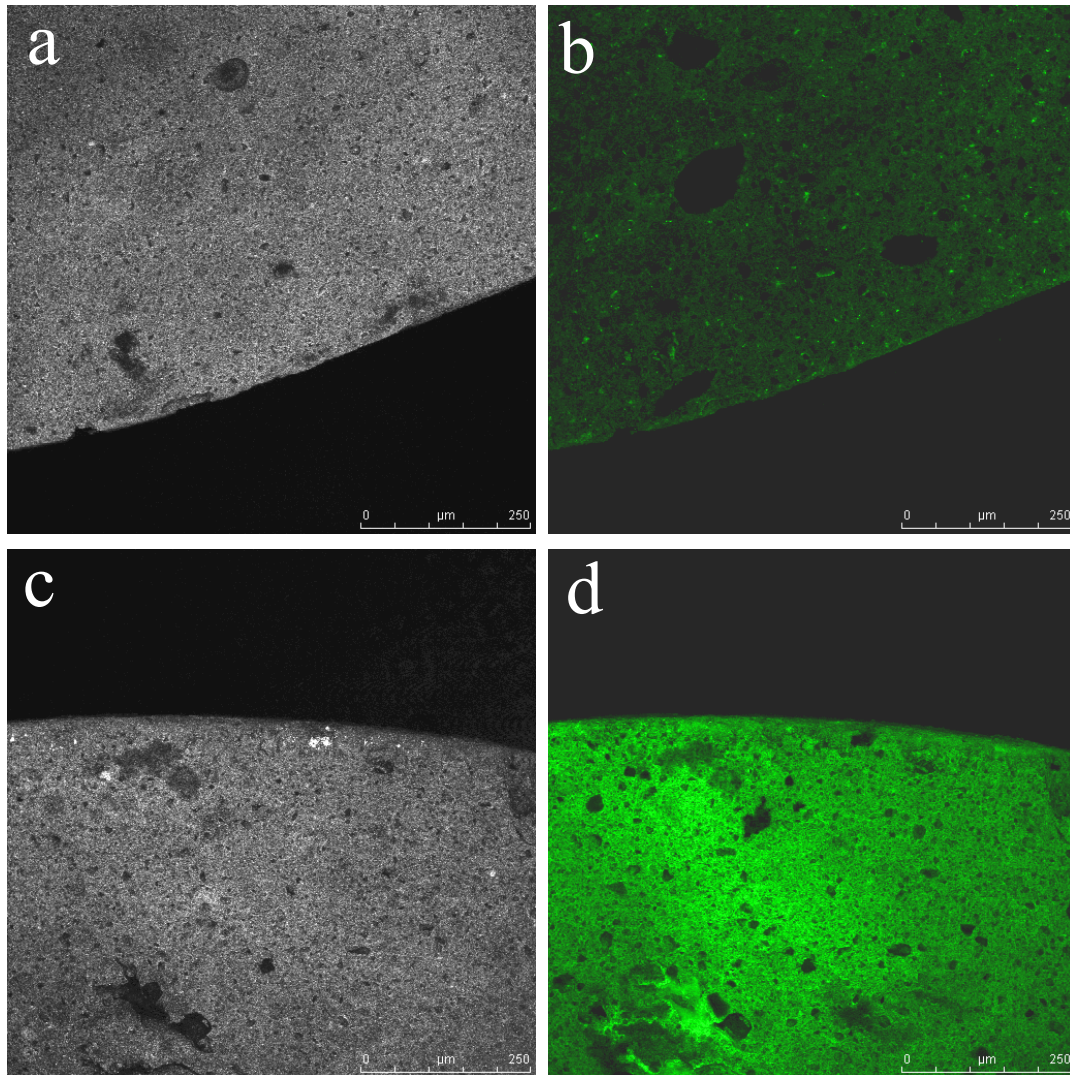


*Figure 2.10. Distribution of collagen in a cement with L/P of 0.45 ml/g with solubilized collagen at two different concentrations after 7 day immersion in water: 10 mg/ml (a,b) and 50 mg/ml (c,d). a) corresponds to the optical image of the studied area of the cement for the 10 mg/ml solubilized collagen, b) corresponds to the fluorescence image of the studied area of the cement for the 10 mg/ml solubilized collagen, c) corresponds to the optical image of the studied area of the cement for the 50 mg/ml solubilized collagen, d) corresponds to the fluorescence image of the studied area of the cement for the 50 mg/ml solubilized collagen.*

Regarding the fibrillised collagen, the structure was completely different (Figure 2.11). There were areas in which the collagen was present, and parts of the CPC in which no collagen was present at all. When collagen was fibrillised, a non-homogenous

distribution was observed, although an increase of the intensity in the areas in which collagen was present, compared to the COLF10 and COLF50, was observed.

The difference when comparing low concentration with a high concentration was the higher amount of gaps that the COLF10F left (Figure 2.11b). For COLF50F, collagen appeared almost in the totality of the sample (Figure 2.11d.), whereas for COLF10F, collagen only appeared in some parts. The intensity was higher in both cases compared to the same concentrations with the solubilized collagen.

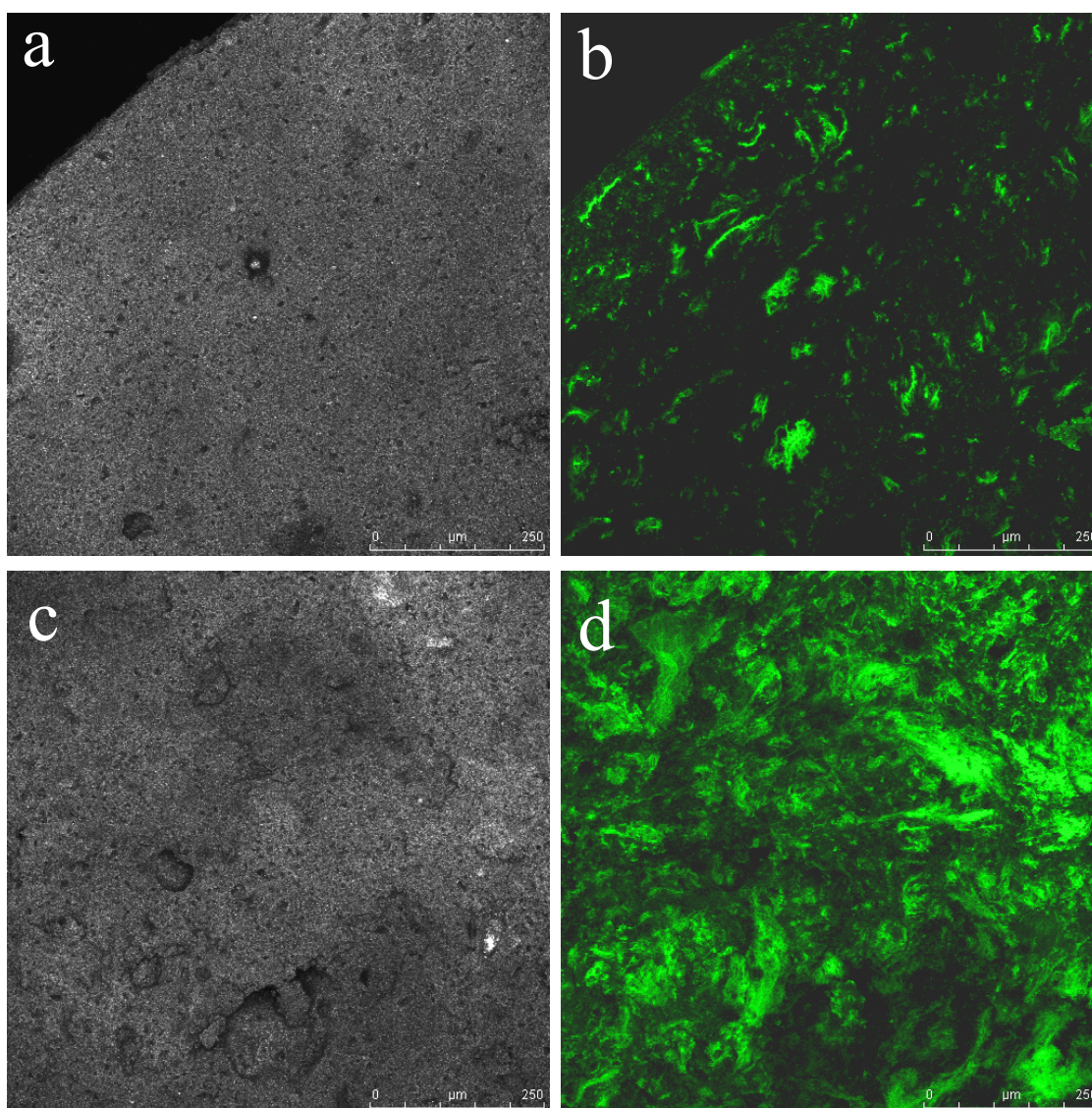


Figure 2.11. Distribution of collagen in a cement with L/P of 0.45 ml/g with fibrillised collagen at two different concentrations after 7 day immersion in water: 10 mg/ml (a,b) and 50 mg/ml (c,d). a) corresponds to the optical image of the studied area of the cement for the 10 mg/ml fibrillised collagen, b) corresponds to the fluorescence image of the studied area of the cement for the 10 mg/ml fibrillised collagen, c) corresponds to the optical image of the studied area of the cement for the 50 mg/ml fibrillised collagen, d) corresponds to the fluorescence image of the studied area of the cement for the 50 mg/ml fibrillised collagen.

In summary, the collagen distribution was homogenous for soluble collagen, whereas it tended to be heterogeneous for fibrillised collagen. As the amount of collagen was increased, the intensity also increased for the soluble collagen, and not so much for the fibrillised collagen.

#### *2.4.4.3. Scanning electron microscopy*

As can be seen in Figure 2.12a, the fracture surface images of CTRLF revealed that HA crystals were aggregated surrounding the original  $\alpha$ -TCP particles. Typical Hadley cells were observed, showing an empty thick shell of hydration products inside which a  $\alpha$ -TCP grain had fully reacted. At higher magnifications, it was seen that the structure consisted of a network of small HA crystals, combined with some bigger crystals (Figure 2.12b). Regarding COLF10, the morphology was similar to that of CTRLF (Figure 2.12c and d). The presence of the collagen was not detected with this type of technique.

In contrast, the collagen was observed in the samples containing fibrillised collagen (Figure 2.12e and f). In this case, the collagen was observed as bundles of collagen fibers arranged on top of the CPC crystals. These fibers were only observed in some parts of the CPC composite. The morphology was similar between the fibrillised collagen and crosslinked collagen with GA (Figure 2.12g and h).

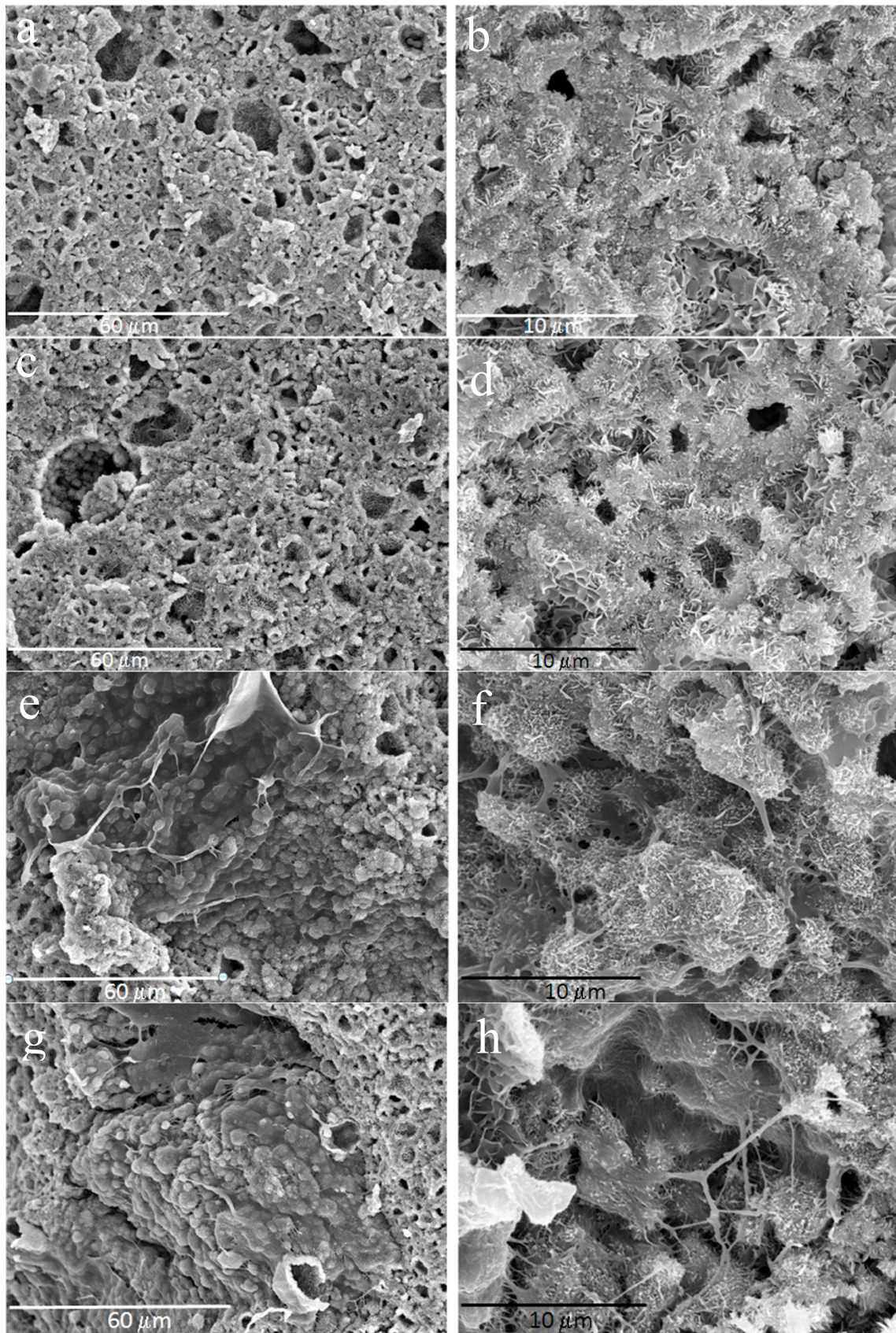


Figure 2.12. SEM micrographs for the different CPC materials at two different magnifications for a L/P ratio of 0.45 ml/g after 7 day immersion in Ringer solution: a) and b) CTRLF, c) and d) COLF10, e) and f) COLF10F, g) and h) COLF10 crosslinked with GA.

#### 2.4.4.4. Fourier Transformed Infrared Spectroscopy

Figure 2.13 shows the results for the fine CPC for the two different concentrations and the two different collagen treatments (solubilized and fibrillised) after 7 days of setting in Ringer's solution at 37°C. Attention should be focused on the amide I region, which is located in the 1658  $\text{cm}^{-1}$  zone. This gives information on the C=O bond of the carboxylic acid in the collagen and the possible interaction with the calcium phosphate. As can be seen, the information given by Figure 2.13 is quite limited in this respect, since a very small band appears in this area and no shifts can be observed. This band also appears in the CTRLF, meaning that the band arises from the CPC and not from the collagen. The main band observed is the phosphate band at 1026  $\text{cm}^{-1}$ , which corresponds to the stretching of the  $\text{PO}_4^{3-}$  group in the HA.

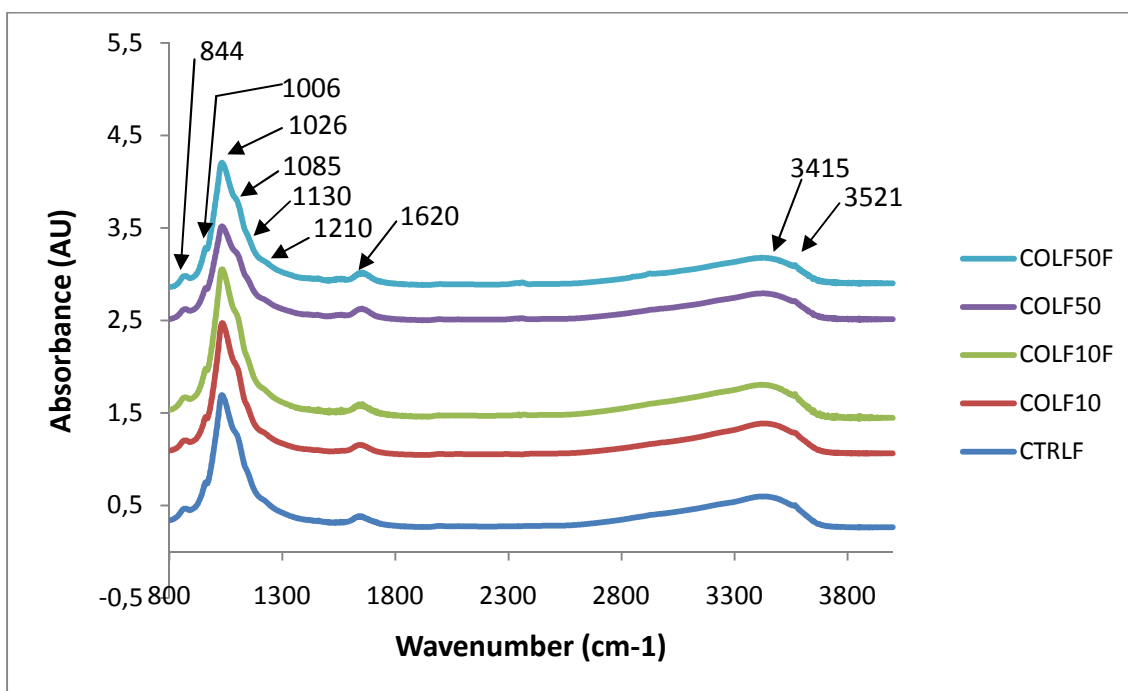


Figure 2.13. FTIR spectrum for the different materials at L/P ratio of 0.45 ml/g after 7 day immersion in Ringer solution for: CTRLF, COLF10, COLF10F, COLF50 and COLF50F.

The assignment of the different bands represented in Figure 2.13 is summarized in Table 2.3.

Wavenumber (cm-1)	Vibration
3521	OH stretching
3415	Water-adsorbed deformation
1620	OH water-adsorbed bending
1210	$\delta_{OH}$ mode of $HPO_4^{2-}$ hydrogen-bonded
1130	$\nu_3$ vibration component of $HPO_4^{2-}$ groups
1085	$\nu_3$ (PO4)
1026	$\nu_3$ (PO4)
1006	$\nu_1$ (PO4)
844	$\nu_3$ P-O(H) deformation of $HPO_4^{2-}$ groups

Table 2.3. Main FTIR bands observed for the CPC at a L/P ratio of 0.45 ml/g after 7 day immersion in Ringers solution. The same bands were observed for all the studied materials: CTRLF, COLF10, COLF10F, COLF50 and COLF50F.

In order to verify what kind of interaction appeared between the collagen and the cement, and taking into account that the amount of collagen used in the prepared cements were too low for IR detection, the amount of collagen was increased. A CPC containing a 50 mg/ml collagen solution at a L/P ratio of 8.62 ml/g, which corresponded to a 70/30 % w/w composite of cement/collagen was prepared. Figure 2.14 shows the main bands observed in it with the corresponding assignation.

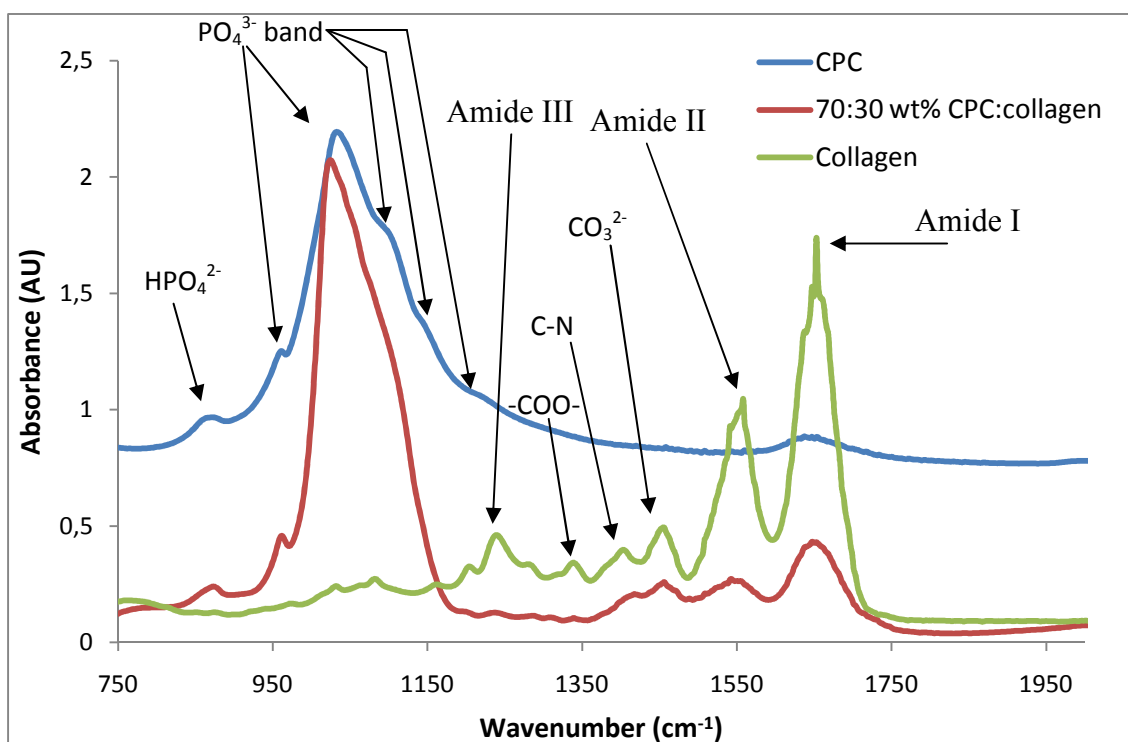


Figure 2.14. FTIR spectrum of the a composite prepared in the ratio in weight 30:70 of collagen:CPC after 7 days in aqueous solution, compared to the CPC for 7 days in aqueous solution and collagen.



In this case, the main shifts observed were in the phosphate band, which did not exist in collagen, which appeared at  $1031\text{ cm}^{-1}$  for calcium phosphate and changed to  $1024\text{ cm}^{-1}$  for the composite material (Figure 2.15). There are two other bands which also correspond to the phosphate group that appeared at  $961\text{ cm}^{-1}$  for the CDHA and the composite, and another band at  $1111\text{ cm}^{-1}$ , that also had the same value for the composite. The shoulder at  $1145\text{ cm}^{-1}$  only appeared on the CPC. The other band present that appeared at  $872\text{ cm}^{-1}$  corresponded to the presence of the hydrogenphosphate group.

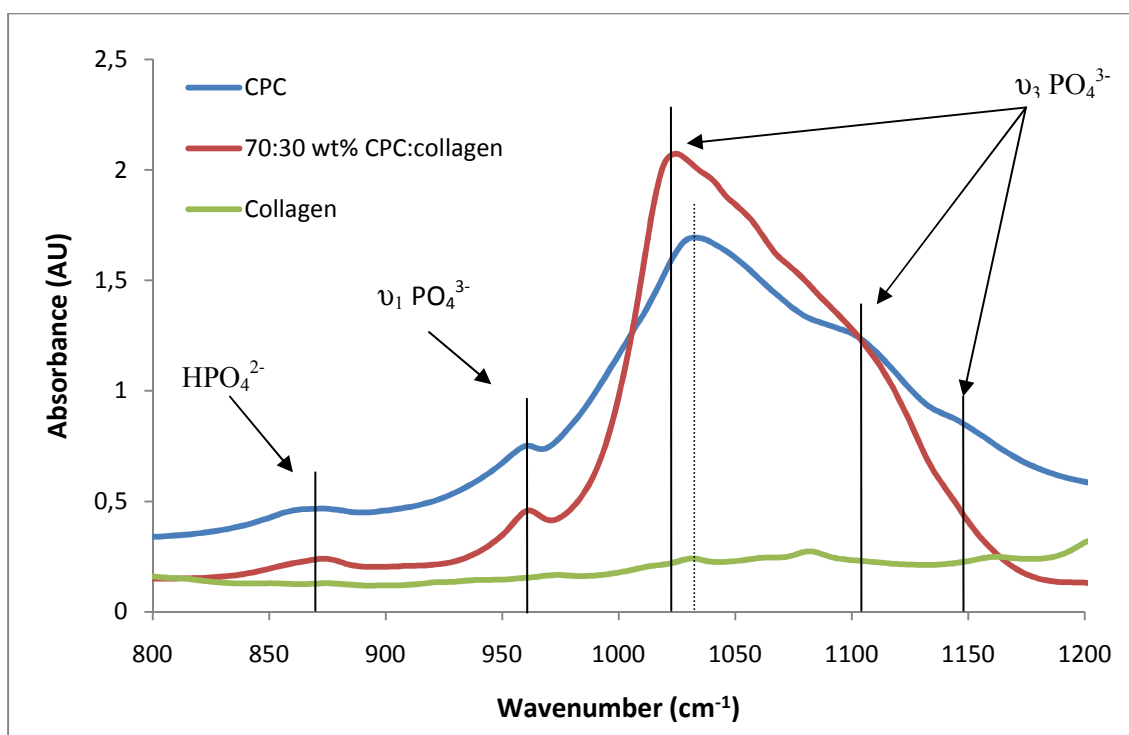


Figure 2.15. FTIR spectrum of the CPC, composite material made of 70:30 %wt CPC:collagen and collagen. The L/P ratio used for the CPC was 8.62 ml/g and was then left in water for 7 days for the complete transformation into CDHA. The presented area corresponds to the phosphate modes of vibration. Only one shift appears which corresponds to the phosphate mode of vibration 3. The dotted line indicates the presence of a shift.

The assignment of the different bands observed in Figure 2.15 is shown in Table 2.4.

CDHA band ( $\text{cm}^{-1}$ )	Composite band ( $\text{cm}^{-1}$ )	Assignment
1145	-	$\nu_3$ vibration component of $\text{HPO}_4^{2-}$ groups
1111	1111	$\nu_3$ (PO4)
1031	1024	$\nu_3$ (PO4)
961	961	$\nu_1$ (PO4)
872	872	$\nu_3$ P-O(H) deformation of $\text{HPO}_4^{2-}$ groups

Table 2.4. FTIR bands and assignation of the phosphate zone of the composite material made of 70:30 %wt CPC:collagen and the CPC. The L/P ratio used was 8.62 ml/g and the samples were then left in water for 7 days for the complete transformation into CDHA.

In the amide region, collagen showed several bands. The first two bands observed in collagen appeared at  $1238\text{ cm}^{-1}$  and  $1334\text{ cm}^{-1}$  that corresponded to the amide III and to a carboxylic mode of vibration respectively (Figure 2.16). These bands did not appear on the composite. Collagen then showed a band at  $1404\text{ cm}^{-1}$ , which appeared at the same wavelength for the composite material that corresponded to the C-N bending mode of vibration. The presence of carbonates was shown with the band at  $1148\text{ cm}^{-1}$  for collagen and the composite. There were two bands that did show a shift in the wavelength, which were the amide II and the amide I. The wavelengths values had a red shift, meaning that the wavelengths values were decreased. Regarding the amide II, the red shift went from  $1558\text{ cm}^{-1}$  for collagen, to  $1551\text{ cm}^{-1}$  in the composite. The amide I band also showed a shift from  $1653\text{ cm}^{-1}$  to  $1647\text{ cm}^{-1}$ . Amide I is the band with the most important information, since it is the COO stretching band and determines the possible interaction with the calcium phosphate.

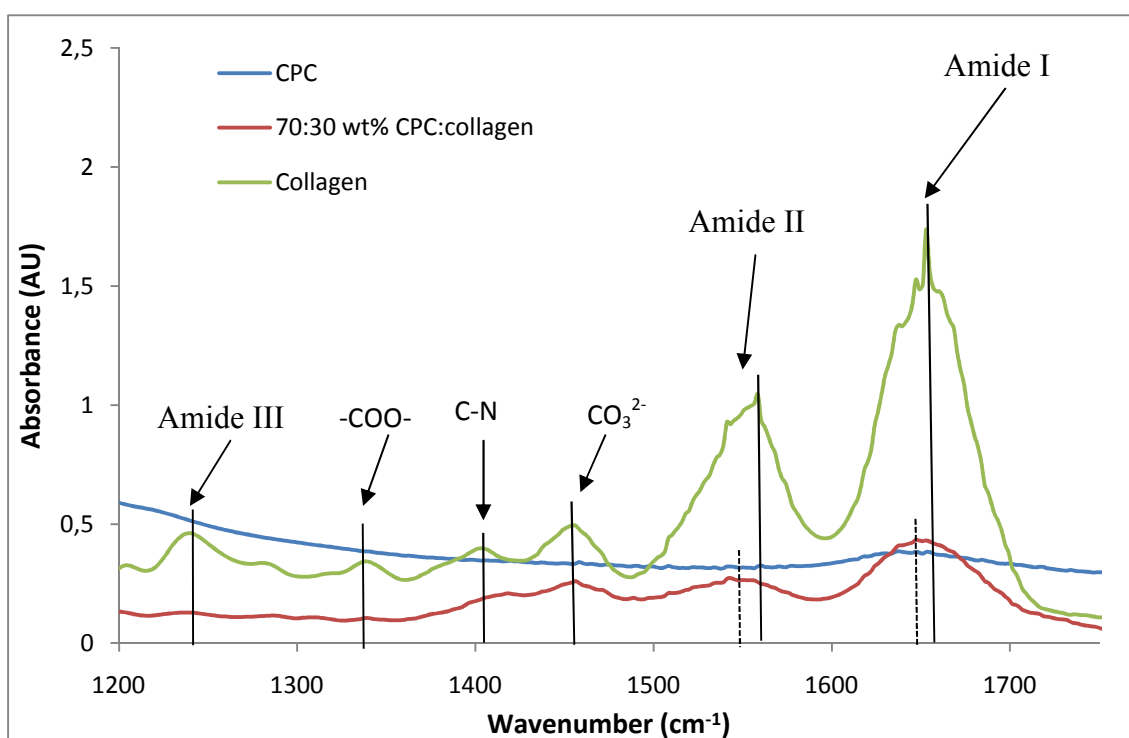


Figure 2.16. FTIR spectrum of the CPC, composite made of 70:30 %wt CPC:collagen and collagen. The L/P ratio used for the CPC was 8.62 ml/g and the CPC was then left in water for 7 days for the complete transformation into CDHA. The amide region is shown in this figure. Two main shifts appear at  $1558$  and  $1653\text{ cm}^{-1}$ , corresponding to the amide II and amide I. The dotted lines indicate the presence of a shift.

The assignment of the different bands observed in Figure 2.16 is shown in Table 2.5.

Collagen (cm <sup>-1</sup> )	Composite (cm <sup>-1</sup> )	Assignment
1653	1647	Amide I (C=O bend)
1558	1551	Amide II (N-H stretch, C-N bend)
1448	1448	CO <sub>3</sub> <sup>2-</sup>
1404	-	C-N bend
1334	-	Antisymmetric stretching -COO-
1238	-	Amide III (C-N bend, N-H stretch)

Table 2.5. FTIR bands and assignment of the amide zone of the composite material made of 70:30 %wt CPC:collagen and the collagen. The L/P ratio used for the CPC was 8.62 ml/g and the samples were then left in water for 7 days for the complete transformation into CDHA.

#### 2.4.4.5. X-Ray diffraction

X-Ray diffraction was used in order to analyse the evolution of the phases present in the CPC during the reaction. The results showed the same crystalline phase, CDHA both for cements with and without collagen. The process was monitored as was mentioned before and the results are shown in Figures 2.17, 2.18 and 2.19 for the CTRLF, COLF10 and COLF10F, respectively. It is shown in all three cases that, as time goes on, the peaks for  $\alpha$ -TCP disappear, giving rise to the HA peaks.

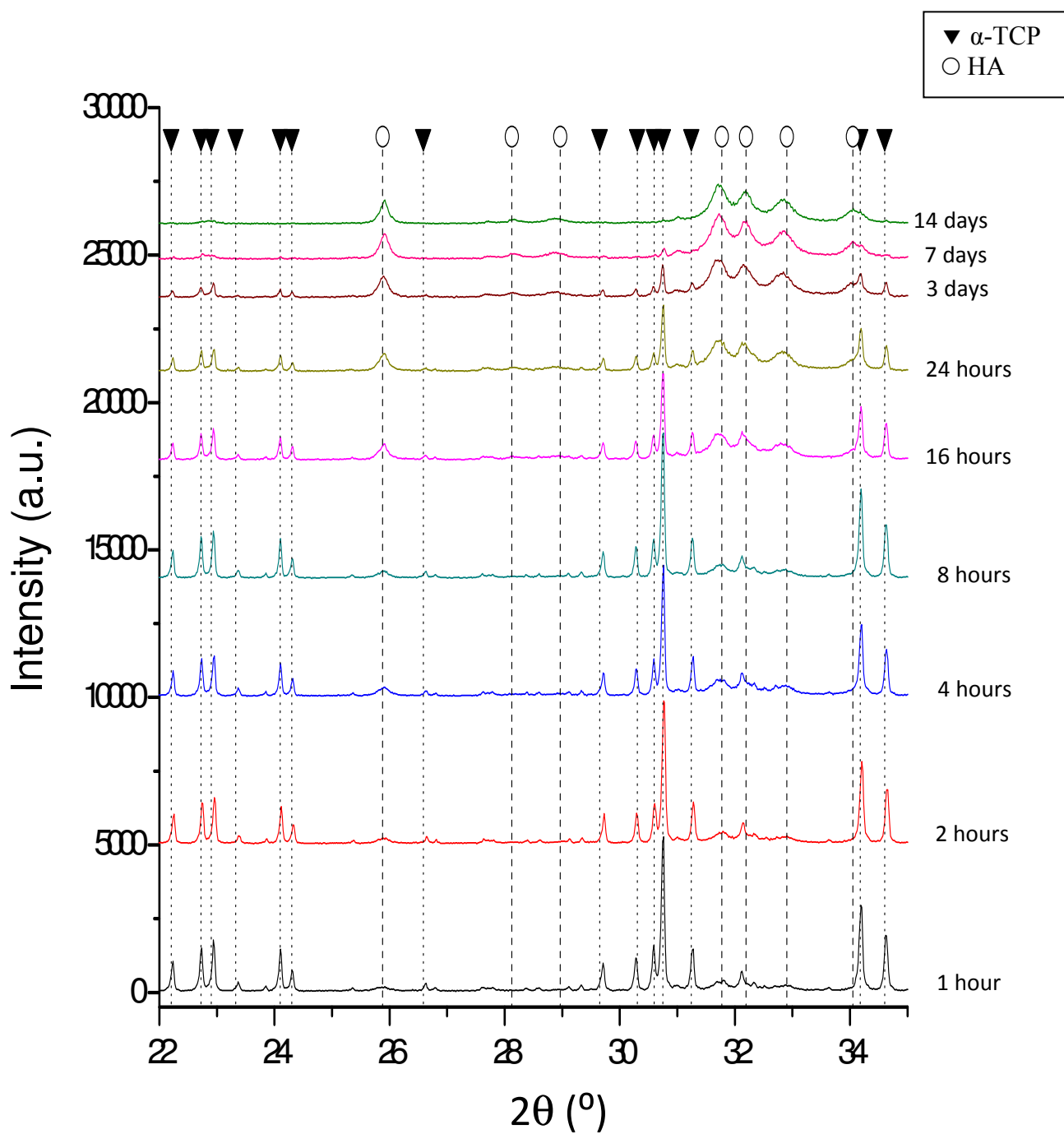


Figure 2.17. Phase evolution during the setting of the  $\alpha$ -TCP for 14 days in water monitored by XRD for CTRLF at a L/P ratio of 0.45 ml/g.

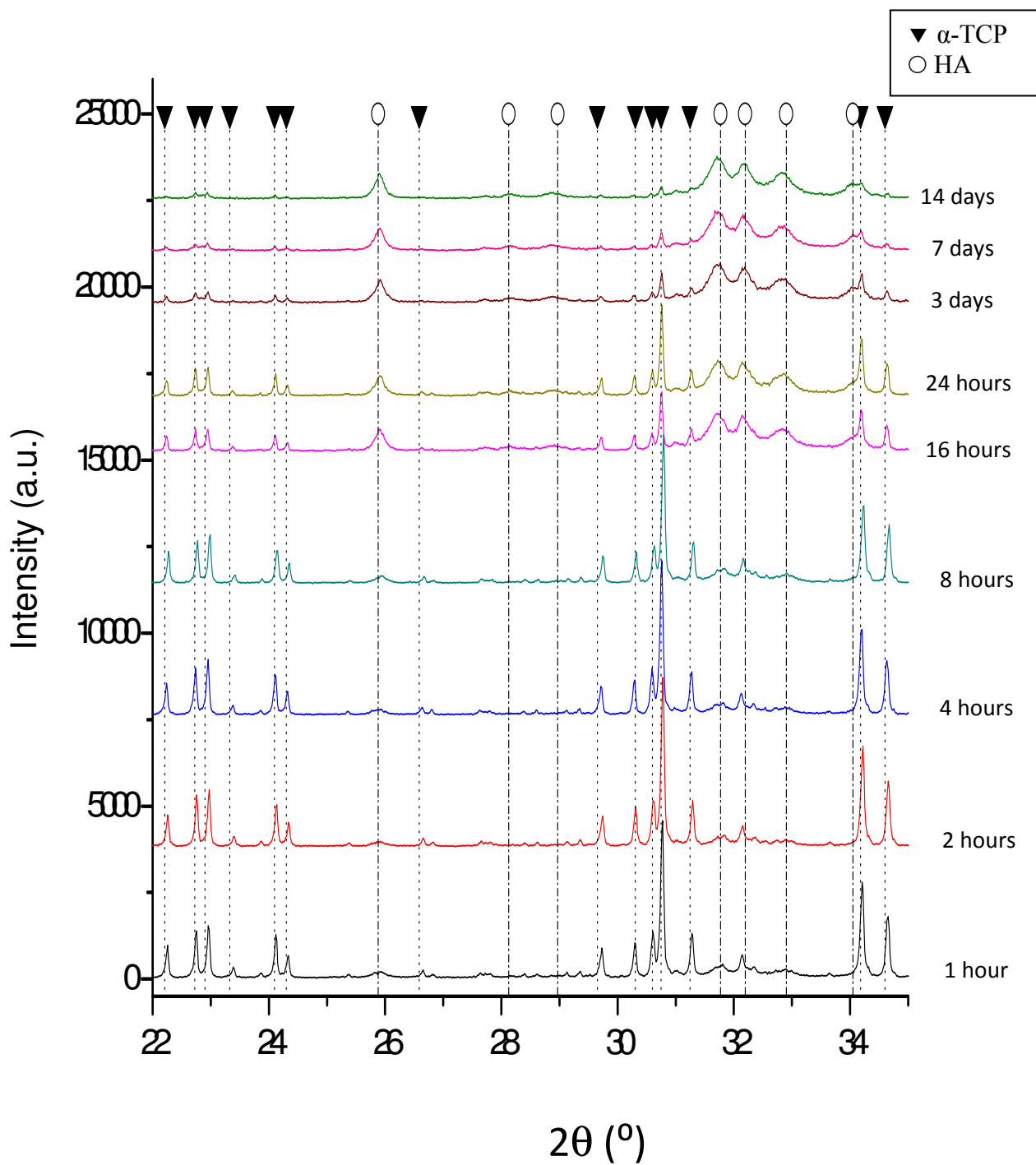


Figure 2.18. Phase evolution during the setting of the  $\alpha$ -TCP for 14 days in water monitored by XRD for COLF10 at a L/P ratio of 0.45 ml/g.

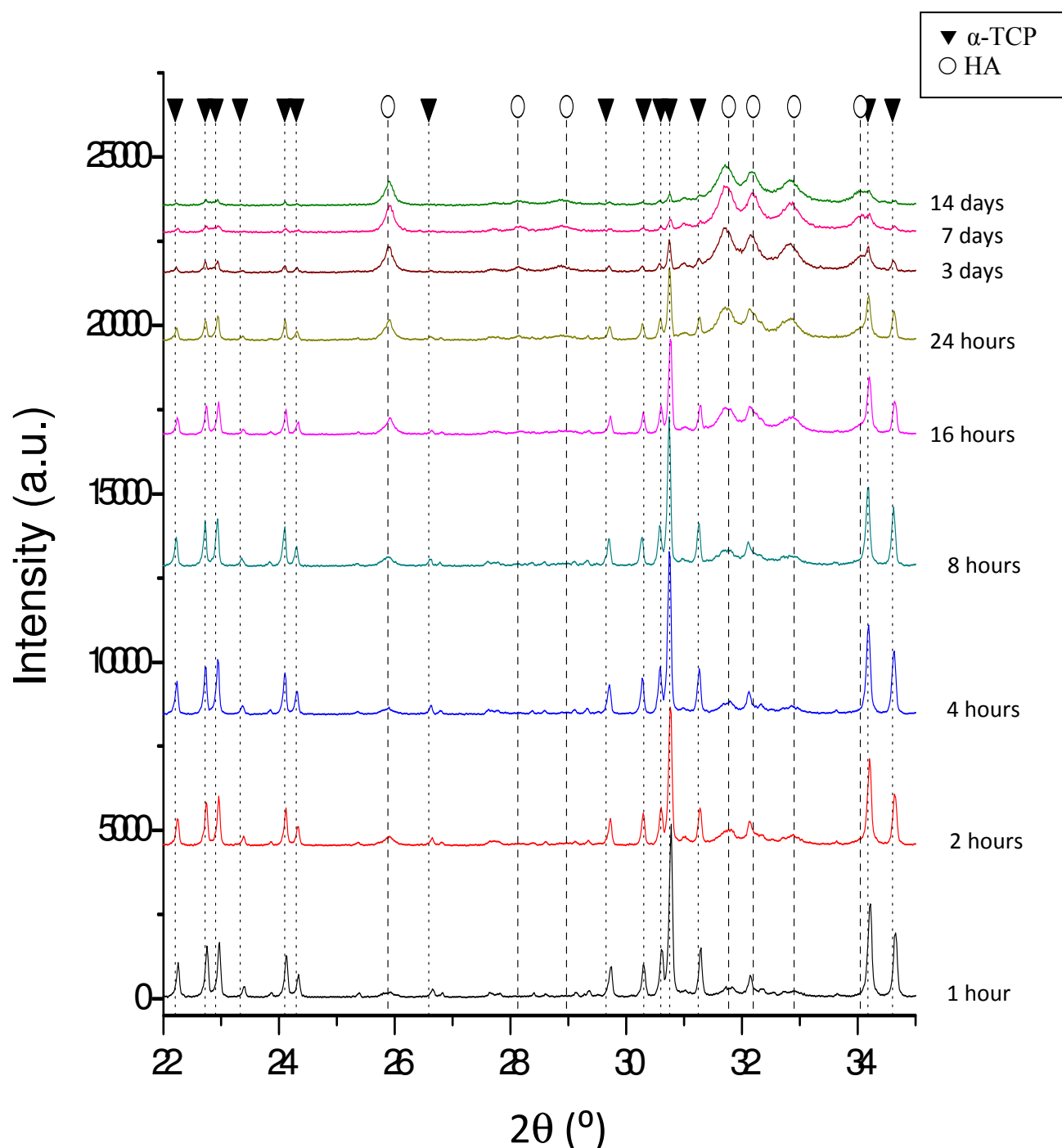


Figure 2.19. Phase evolution during the setting of the  $\alpha$ -TCP for 14 days in water monitored by XRD for COLF10F at a L/P ratio of 0.45 ml/g.

Figure 2.20 shows the kinetics of the transformation reaction. It is seen that the three different materials have similar kinetics. After 3 days, almost all the CPC had transformed into CDHA. The end product was the same in all cases. Nevertheless, after 14 days, the amount of  $\alpha$ -TCP reacted was 96% for CTRLF, 92% for COLF10 and 93% for COLF10F.

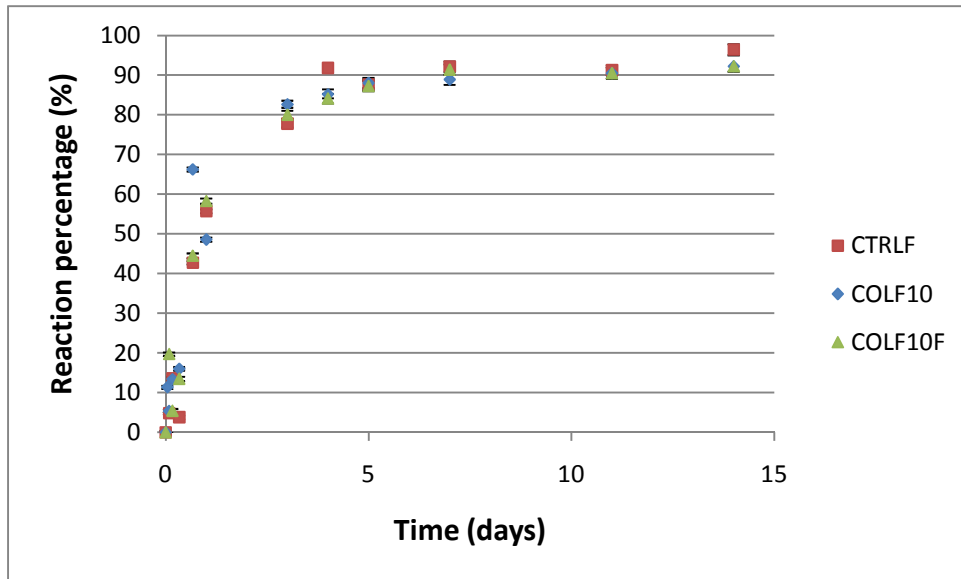


Figure 2.20. Percentage of reaction as a function of time obtained from the DRX analysis for the CTRLF, COLF10 and COLF10F at a L/P ratio of 0.45 ml/g.

The graphic was transformed into logarithmic scale as is shown in Figure 2.21. The reaction kinetics was similar for the three series studied.

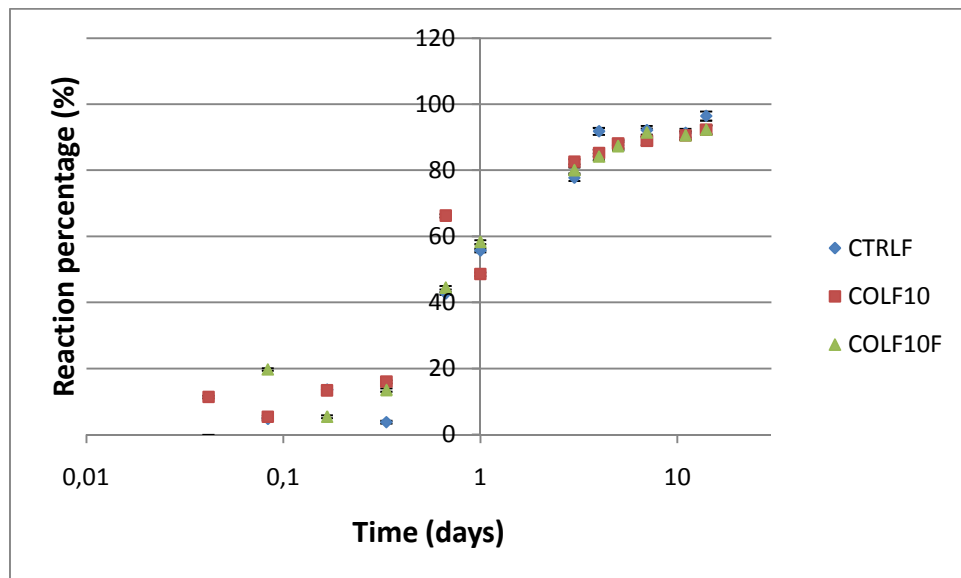


Figure 2.21. Logarithmic representation of the percentage of reaction as a function of time obtained from the DRX analysis for CTRLF, COLF10 and COLF10F at a L/P ratio of 0.45 ml/g.

#### 2.4.4.6. Helium pycnometry

The skeletal density of the different samples measured by Helium pycnometer is shown in Figure 2.22. It is observed that, as expected, the density decreased when collagen was

incorporated. The values decreased from  $2.86 \text{ g/cm}^3$  for the CTRLF, to  $2.84 \text{ g/cm}^3$  for the 10 ml/mg collagen containing CPC and up to  $2.80 \text{ g/cm}^3$  for the 50 ml/mg collagen-containing CPC. The relationship was inversely proportional to the concentration, meaning that as the collagen concentration increased, the density decreased. There were no significant differences when comparing the fibrillised collagen samples and the non-fibrillised collagen samples.

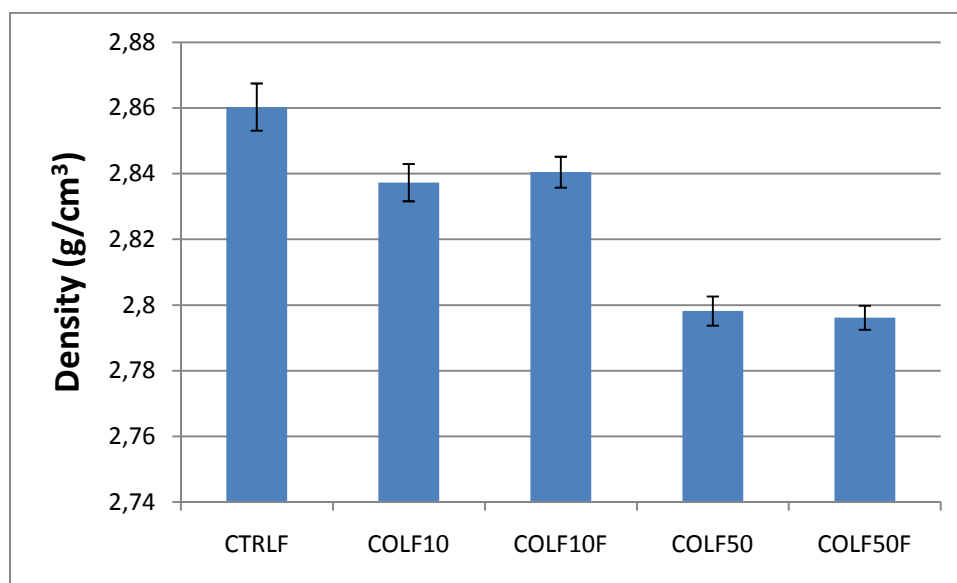


Figure 2.22. Skeletal density for the CPC with fine initial particle size with and without collagen for a L/P ratio of 0.45 ml/g.

#### 2.4.4.7. Porosimetry

The total porosity of the samples and the pore size range measured by MIP are shown in Table 2.6. The porosities for the different samples were shown to range between 41% and 48%. The measured pore size ranged between  $0.006 \mu\text{m}$  for the lowest limit, since it is the limit of detection of the porosimeter, and  $4.7 \mu\text{m}$ . Nevertheless, the peak of the different pore size distributions was in the same order of magnitude for the different samples.



	POROSITY (%)	RANGE ( $\mu\text{m}$ )	Main peak ( $\mu\text{m}$ )	Secondary peak ( $\mu\text{m}$ )
CTRLC	41,2	0,006-1,312	0.021	0.0770
COLC10	41,1	0,006-1,412	0.095	-
COLC10F	47,3	0,006-2,664	0.032	0.730
COLC50	43,9	0,006-0,121	0.040	-
COLC50F	43,6	0,006-3,142	0.095	-
CTRLF	42,9	0,006-0,121	0.017	-
COLF10	43,1	0,006-0,520	0.017	-
COLF10F	44,1	0,006-0,329	0.021	-
COLF50	41,2	0,006-0,095	0.014	-
COLF50F	48,0	0,006-4,707	0.026	0.403

Table 2.6. Values for the total porosity, pore size range and highest volume pore sizes for the materials composed of CPC with and without collagen as the liquid phase of the CPC for a L/P ratio of 0.45 ml/g.

The information shown in Table 2.6 was extracted from Figure 2.23 to Figure 2.28 that represent the entrance pore size distribution for the different samples.

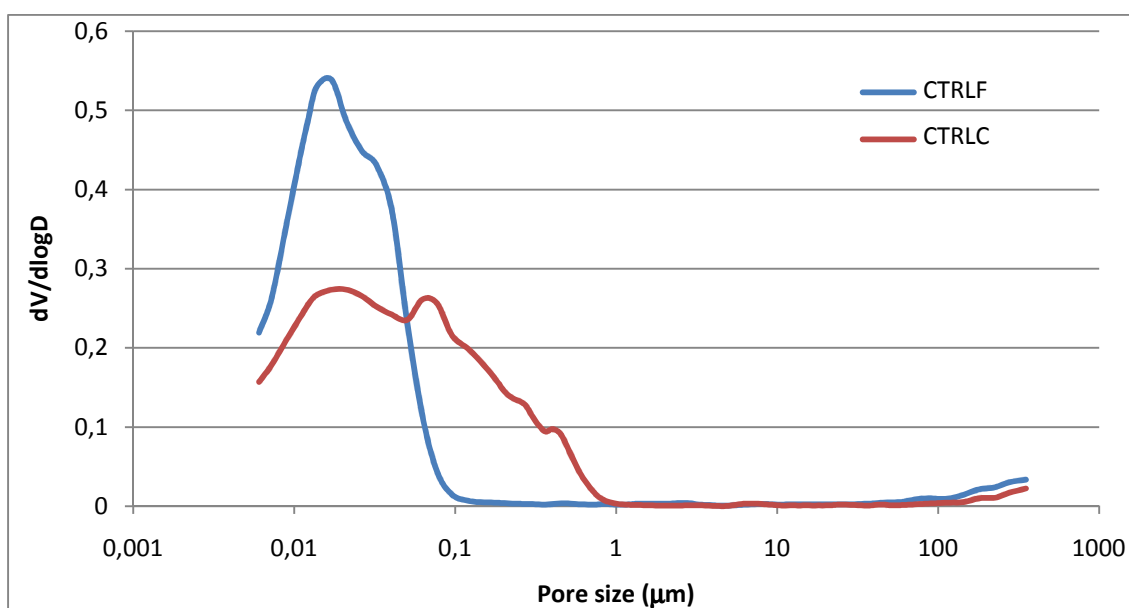


Figure 2.23. Pore size distribution for CTRLF and CTRLC for a L/P ratio of 0.45 ml/g using 50 mM acetic acid as liquid phase.

It can be seen that the coarse CPC had a pore size distribution between 0.006  $\mu\text{m}$  and 1  $\mu\text{m}$ , whereas the fine CPC had a narrower pore size distribution which ranged between 0.006  $\mu\text{m}$  and 0.1  $\mu\text{m}$  (Figure 2.23). The total porosity of the samples was similar, with a value of 41% for the CTRLC and 43% for the CTRLF.

The pore size distribution of the samples containing solubilized collagen is shown in Figure 2.24. In the COLF10 and COLC10 samples, the results were very similar to those for their respective controls (Figure 2.24a). When the collagen was incorporated in higher concentrations (COLF50 and COLC50), there was a small shift to lower pore sizes in both cases (Figure 2.24b). The peak became narrower, and for the COLC50, the pore size was reduced to 0.1  $\mu\text{m}$ .

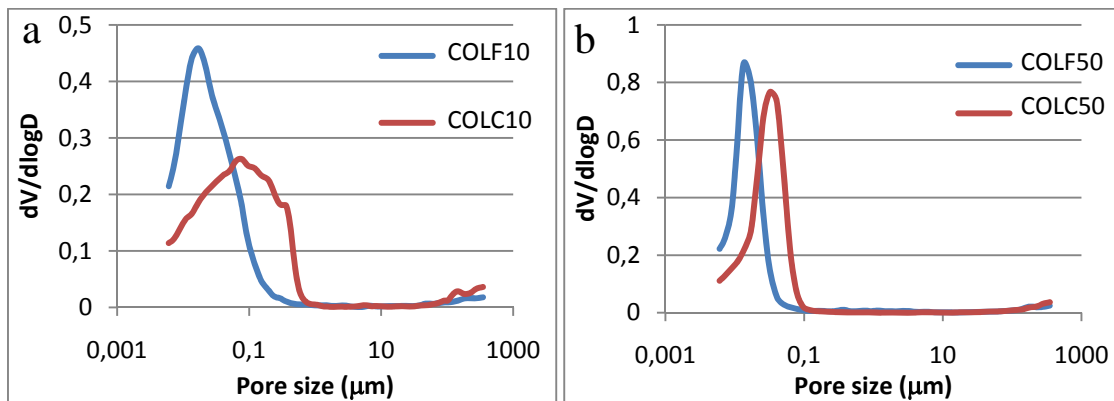


Figure 2.24. Pore size distribution comparing the two different CPC initial particle size distributions in the presence of collagen: COLF and COLC for two different concentrations at a L/P ratio of 0.45 ml/g: a) 10 mg/ml and b) 50 mg/ml.

The results for the samples containing fibrillised collagen are shown in Figure 2.25. For the low concentration (COLF10F and COLC10F), the pore size distribution was similar to the control (CTRLF and CTRLC) and for COLC10F, there were a higher number of pores in the submicron range, which was associated with a slight increase in the total porosity (47% for COLC10F and 41% for CTRLC) (Figure 2.25.a). As observed in Figure 2.25b, when the collagen was incorporated in higher concentrations, COLC50F had similar pore size distribution and porosity to the CTRLC, whereas COLF50F had a higher total porosity (48%) than the CTRLF (43%) associated with an increase in the micron sized pores volume.

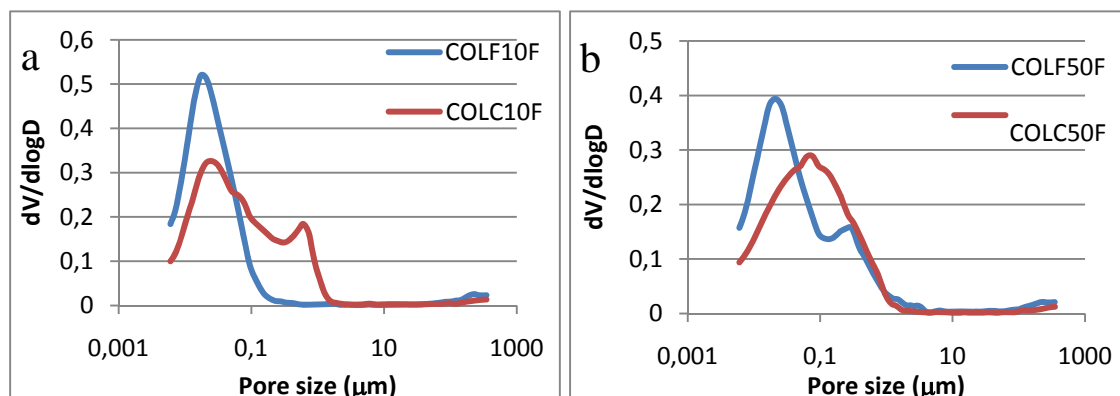


Figure 2.25. Pore size distribution comparing the two different CPC initial particle size distributions in the presence of fibrillised collagen: COLF and COLC for two different concentrations at a L/P ratio of 0.45 ml/g: a) 10 mg/ml and b) 50 mg/ml.

The comparison between the solubilized and the fibrillised collagen in the samples with 10 mg/ml and 50 mg/ml can be found in Figure 2.26. The curves for the coarse CPC were very similar among them (Figure 2.26a), as well as the curves for the fine CPC (Figure 2.26b), which were also very similar among them. That means that there is no direct effect of the presence of soluble collagen or fibrillised collagen at low collagen concentrations on the pore size distribution.

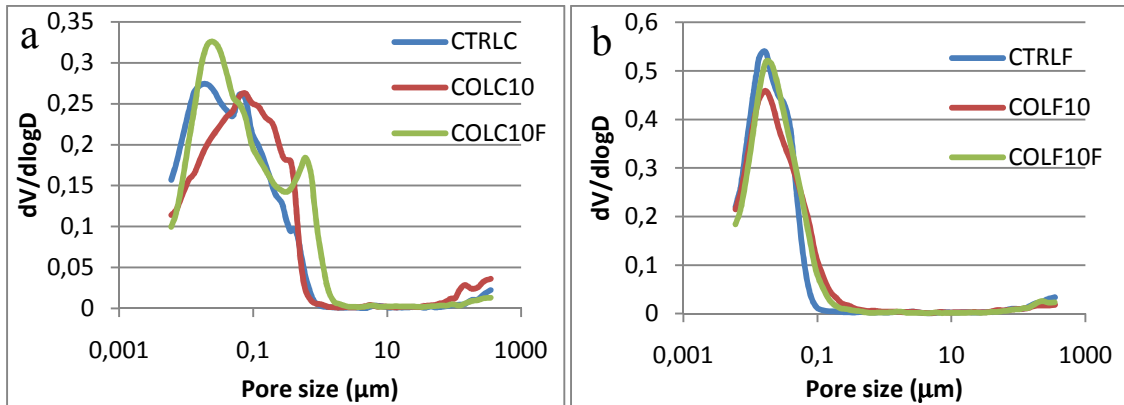


Figure 2.26. Pore size distribution comparing the soluble collagen and the fibrillised collagen composite with the control at 10 mg/ml for at a L/P ratio of 0.45 ml/g: a) coarse and b) fine.

In order to see the effect at higher concentrations of collagen, the same parameters were compared with the high collagen concentration, 50 mg/ml (Figure 2.27.). Regarding coarse CPC, the COLC50F and the CTRLC were very similar, whereas the COLC50 had a much narrower distribution. Regarding the fine CPC, CTRLF and COLF50 had similar distributions, whereas the COLF50F was the one with a broader distribution.

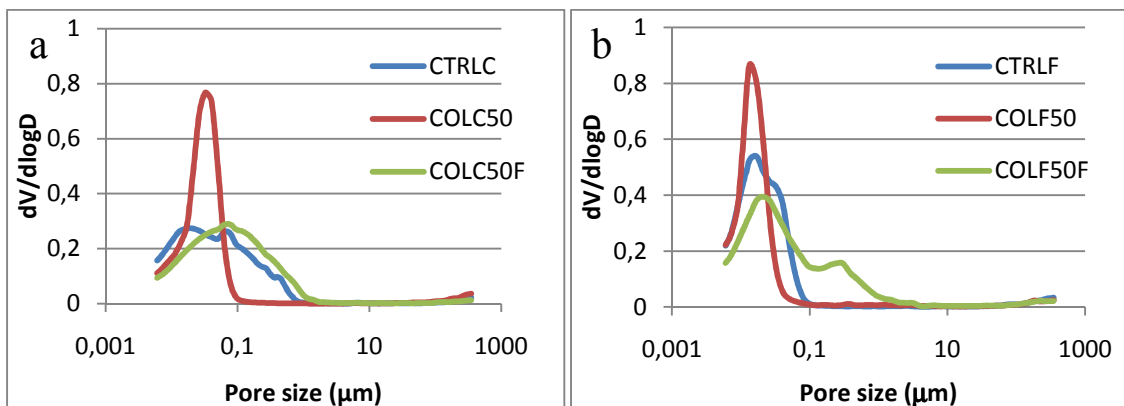


Figure 2.27. Pore size distribution comparing the soluble collagen and the fibrillised collagen composite with the control at 50 mg/ml for at a L/P ratio of 0.45 ml/g: a) coarse and b) fine.

Finally, in order to compare different concentrations, the samples with the two concentrations were compared among them with their respective controls (Figure 2.28.). For the coarse CPC, as was previously seen, the 10 mg/ml had no effect on the pore size distribution, whereas the 50 mg/ml reduced the peak to 0.1  $\mu\text{m}$ . Regarding fine CPC, COLF10 did have a small increase in the pore size distribution compared to CTRLF, whereas COLF50 decreased the pore size distribution compared to CTRLF.

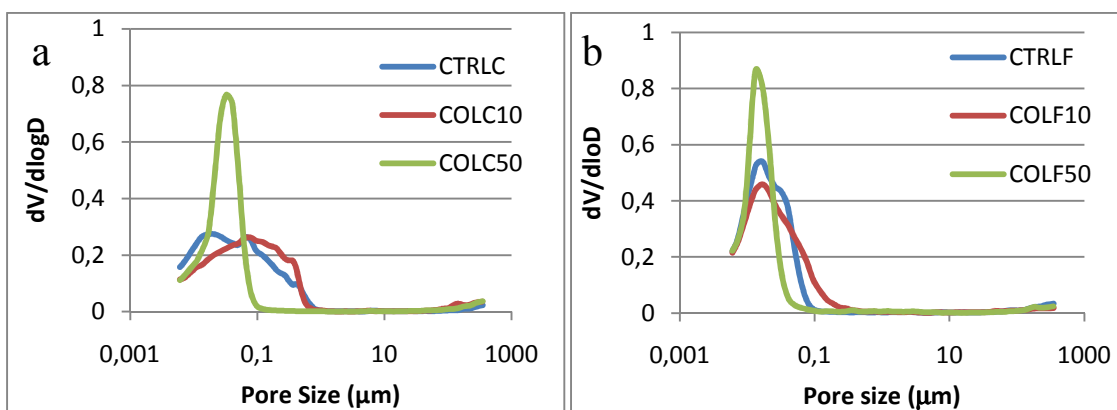


Figure 2.28. Pore size distribution comparing the two collagen concentrations (10 and 50 mg/ml) with the control for a determined initial CPC particle size for a L/P ratio of 0.45 ml/g, being a) coarse and b) fine.

#### 2.4.4.8. Injectability

Figure 2.29 shows the injectability of the control cement and the collagen-containing cements. For the CTRLF, 50% of the paste was injected, whereas for COLF10 and COLF10F, 96% and 65% of the paste were injected, respectively.

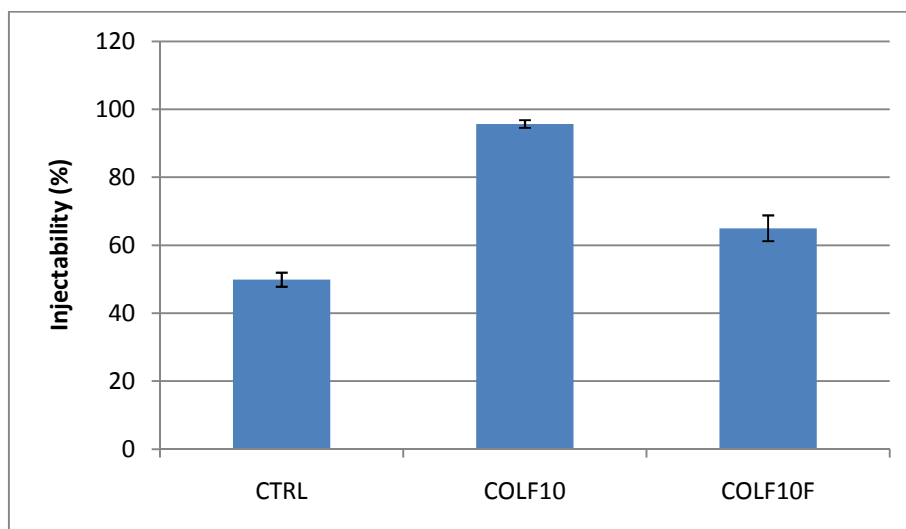


Figure 2.29. Percentage of injectability for CTRLF, COLF10 and COLF10F for L/P ratio of 0.45 ml/g.

The force diagram is shown in Figure 2.30. Regarding CTRLF, it was seen that the force started increasing as the piston slowly advanced. Every time the piston advanced, the force increased and it was more difficult to inject the paste. A different behavior was observed for the soluble and fibrillised collagen (COLF10), in which the force increased up to 20 N, and at that force, a plateau was reached. The plateau was maintained until the force started to increase in the case of the COLF10F, not being able to inject all the paste. However, for COLF10, the force remained constant at the 20 N value until all the paste was completely injected. The force increased to 100 N when the piston reached the end of the syringe.

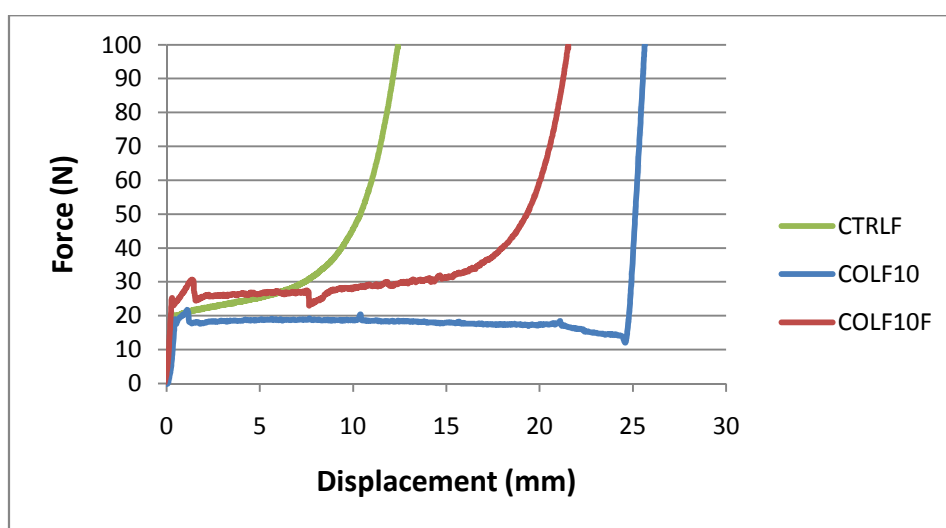


Figure 2.30. Force diagram for the injected materials CTRLF, COLF10 and COLF10F for L/P ratio of 0.45 ml/g.

Figure 2.31 shows the initial yield force needed to start injecting the paste. It can be seen that the CTRLF and the COLF10 had similar values, being  $21.5 \pm 1.5$  N and  $20.6 \pm 1.7$  N respectively. The yield force for COLF10F was higher,  $25.1 \pm 0.5$  N. Furthermore, it is also interesting to note that in both of the cases in which collagen was present, once the paste started to be injected, the force started to increase. Afterwards, a considerable decrease in the force (5 N at the most) was observed, being able to inject the paste at the same force as the initial value. This decrease in the force was not found for the CTRLF.

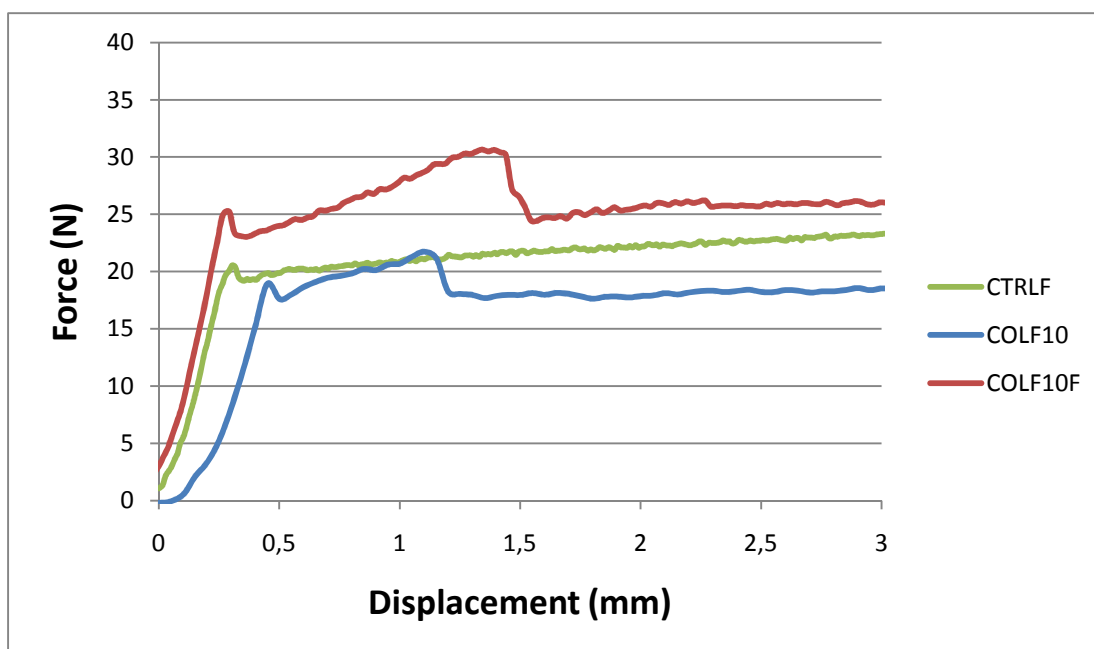


Figure 2.31. Force diagram for the injected materials CTRLF, COLF10 and COLF10F at short displacements for L/P ratio of 0.45 ml/g.

#### 2.4.4.9. Mechanical properties

The compressive strength for the coarse and fine CPC with collagen is shown in Figure 2.32. When the collagen concentration was low (e.g. 10 mg/ml), the compressive strength of the CPC did not significantly vary. Nevertheless, when higher concentrations of collagen were incorporated in the CPC (50 mg/ml), the compressive strength of the CPC diminished. Compared to control, the samples with a concentration of 50 mg/ml of collagen presented half the compressive strength of the control material.

When collagen was incorporated as fibrillised collagen, the samples presented lower values compared to those of the solubilized collagen, except for the COLF10F, in which an increase was observed, although it was not statistically significant. Significant differences were found between COLC10 and COLC10F. In general, the values obtained with the coarse CPC were lower than those with fine CPC, being the differences statistically significant for the samples CTRL, COL10F and COL50.

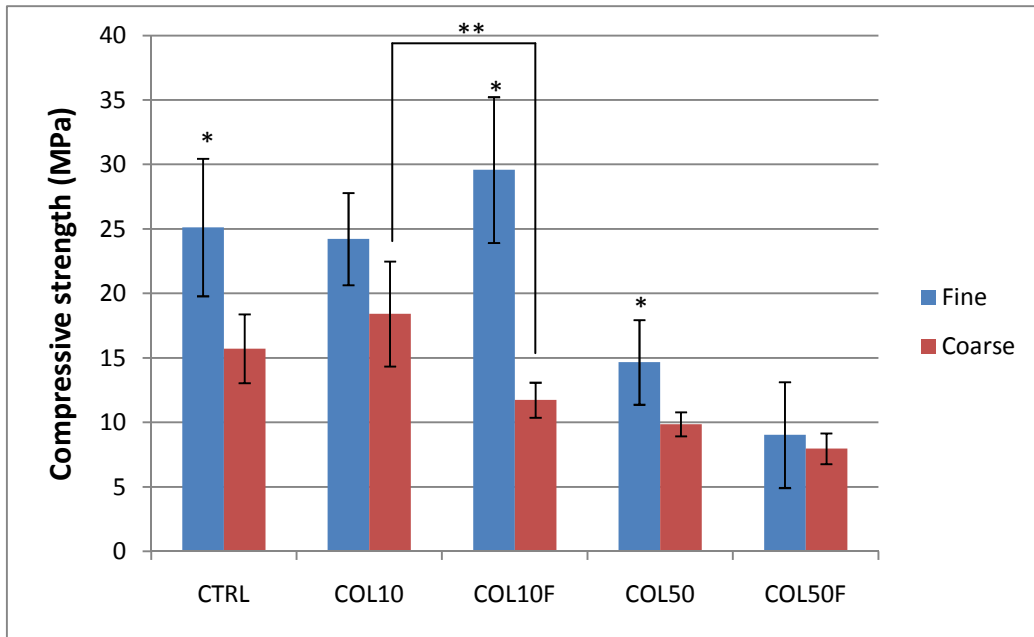


Figure 2.32. Maximum strength for the CPC with fine and coarse initial particle size prepared at a L/P ratio of 0.45 ml/g using acetic acid, solubilized collagen and fibrillised collagen as liquid phase of the CPC after 7 day reaction in water.\*denotes significant differences between coarse and fine CPC. \*\*denotes significant difference between the fibrillised and solubilized collagen for coarse CPC for a concentration of 10 ml/mg.

Representative stress-strain curves for the different fine CPC series are shown in Figure 2.33. These curves were used to calculate the compressive strength, as well as the strain the materials presented. It is shown that the slopes of the different curves are similar to CTRLF, except for the COLF50F and COLF10F. It can be seen that the strain before breaking is higher for the fibrillised collagen composites (COLF10F and COLF50F).

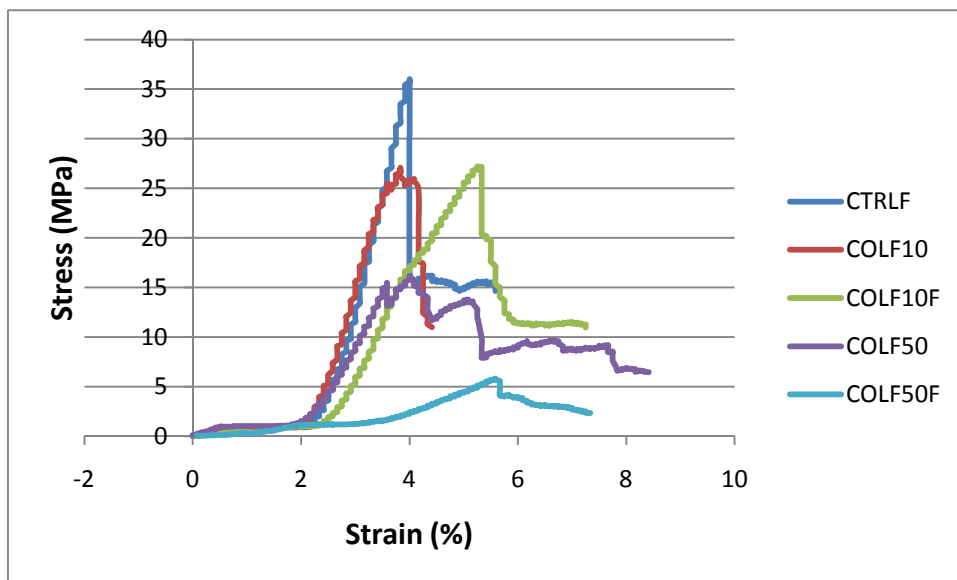


Figure 2.33. Stress-strain curves for the fine series CPC at a L/P ratio of 0.45 ml/g after 7 days setting in water.

## 2.5. Discussion

### 2.5.1. Collagen processing

One of the objectives of the study was to characterize the effect of different collagen pre-treatments previous to the mixture with the CPC powder. That is why it was important to initially characterize the fibrillised collagen and the crosslinked collagen, compared to the solubilized collagen. The assembly of collagen molecules into fibrils is an entropy-driven process, similar to that occurring in other protein self-assembly systems, such as microtubules, actin filaments and flagella. These processes are driven by the loss of solvent molecules from the surface protein molecules and results in assemblies with a circular cross-section, which minimize the surface area/volume ratio of the final assembly.<sup>19</sup> The resulting molecule is rod-like and self-assembles spontaneously to form fibrils, in the process named as fibrillogenesis<sup>31,32</sup>. The length and diameter of the fibrils will depend upon the conditions involved in the growth.

The kinetics of fibrillogenesis has been previously studied. Gross was one of the first scientists to focus in collagen fibrillogenesis and made a first analysis on precipitation of collagen fibrils from neutral salts and measured the increase in opacity of the system as time evolved<sup>13,33</sup>. The rate of precipitation varied with temperature and ionic strength, obtaining considerable changes in the fibrils size. The variation of rate of precipitation with ionic strength and pH indicated that it was controlled to some extent by electrostatic interactions between the soluble collagen particles.<sup>14</sup> Collagen self-assembly involved a phase transition with no change in molecular conformation<sup>15</sup>.

Under typical assembly conditions, which are those used in this study, which is a temperature between 31-38°C and pH around 7, it has been reported that the intensity of scattered light measured by light scattering technique and by turbidimetric methods has a sigmoideal shape, with an initial lag phase<sup>14,34</sup>. The images shown by AFM in the work by Goh *et al* showed that at the beginning monomers, dimers and short oligomers were present. Once the lag phase concluded, the microfibrils proliferated and were present until the termination of assembly<sup>21</sup>.



The process of fibrillation was assessed in this study by DSC. It was observed that the denaturation temperature was 70°C for the solubilized collagen, 85°C for the crosslinked collagen and 89°C for the fibrillised collagen (Figure 2.5). The denaturation temperature for collagen depends on the collagen source<sup>35</sup>. Parameters such as type of animal and tissue of origin play a key role on the final denaturation temperature, which range between 50 and 80°C<sup>35</sup>, although in some animals these values can drop even more, like in the case of fishes, where the denaturation temperature is usually around 30°C<sup>36,37</sup>.

Concerning pericardium collagen, which was the collagen used in the present work, the denaturation temperatures were found to be around 70°C for samples from sheep origin<sup>38</sup>. A study that used bovine pericardium collagen, which has the same animal origin as in the present study, reported a denaturation temperature of 70°C<sup>39</sup>. This value matches exactly our values found for the solubilized collagen sample.

In order to increase the denaturation temperature, which is directly related with higher mechanical properties and less degradation susceptibility, the collagen was crosslinked<sup>40</sup>. The method used to cross-link may affect the final denaturation temperature<sup>41-43</sup>. Most of the works use GA or a mixture of 1-Ethyl-3-(3-dimethylaminopropyl)carbodiimide hydrochloride (EDC) and *N*-hydroxysulfo succinimide (NHS) for crosslinking or as controls to compare with new crosslinking methods, since they are considered the most efficient crosslinkers and present significant increase in denaturation temperature<sup>44</sup>. In general, the temperatures that have been reported for crosslinked pericardium collagen are similar to those presented in the present work. For instance, a temperature raise from 70°C for the soluble collagen to 83°C for the collagen crosslinked with Hexamethylene diisocyanate (HMDC) for bovine pericardium derived collagen was reported<sup>39</sup>. In two other works, the values raised up to 85°C for the crosslinked pericardium collagen<sup>45,46</sup>. In another study, the crosslinking process was optimized for the NHS:EDC molecule and it was seen that the highest denaturation temperature that was obtained for bovine pericardium collagen was 86.9°C<sup>43</sup>. Therefore, these values match very close the 85°C found for our crosslinked collagen.

Regarding the fibrillised collagen, up to our knowledge, no works have been reported on bovine pericardium collagen. Fibril formation involves the aggregation and alignment of collagen molecules<sup>17,18</sup>, which, according to previous reports, improves

thermal stability<sup>47,48</sup>. Similar works regarding other types of collagen have reported an increase in the denaturation temperature when the collagen was gelified or self-assembled. Some of the works reveal big increase in the denaturation temperature, although in those cases, the denaturation temperature of the untreated collagen was rather low<sup>49,50</sup>. Bae *et al* revealed an increase of the denaturation temperature of gelified stingray collagen up to 44.3°C<sup>50</sup> compared to the untreated stingray collagen of 33.2°C<sup>37</sup>. Our results suggest that the self-assembly of the soluble collagen led to similar denaturation temperature to those of cross-linked collagen.

It was also seen by SEM that the morphologies were different depending on the treatment (Figure 2.4). The solubilized collagen presented a homogenous membrane structure whereas the fibrillised collagen presented a different structure, presenting an ordered fibre structure. Crosslinked collagen presented similar structure to the solubilized collagen, with the combination of the membrane and some fibres. The morphologies for the solubilized collagen and crosslinked were observed to be similar to previous works done on the characterization of collagen<sup>3</sup>. The fibrillised collagen was not studied in this previous work.

Therefore, it can be concluded that the addition of Na<sub>2</sub>HPO<sub>4</sub> at a final 20 mM concentration, which increased the ionic strength and raised the pH to a 7.2 value, led to a self-assembly of collagen molecules (Figure 2.34) by the process of fibrillation through the entropy-driven process<sup>51</sup>. The fibrillation increased the size of collagen fibres, and binded the different triple helix molecules<sup>52</sup>. Fibrillation and crosslinking was then associated with an increase in the crystallinity of the material which was shown by the increase of the denaturation temperature as shown by DSC<sup>42,53</sup>.

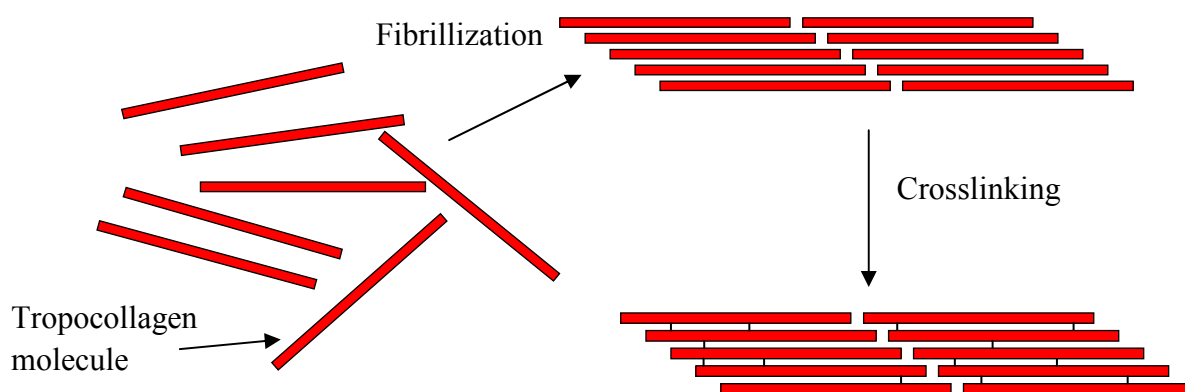


Figure 2.34. Schematic representation of the different collagen conformations. Each of the red bars represents a triple helix of the collagen molecule. a) Solubilized collagen b) Fibrillised collagen and c) Crosslinked collagen.

## 2.5.2. Setting reaction

When the collagen solution was mixed with the powder, the paste obtained had a high viscosity. It was actually the fact that collagen solution initially had a higher viscosity than water, which made the mixing with the CPC slightly more difficult and therefore higher L/P ratios were needed, being 0.45 ml/g the lowest one in which a workable paste was obtained (with water or accelerant solution the lowest L/P ratio may range between 0.32 and 0.35 ml/g). The liquid to powder ratio determines the final properties of the CPC, as well as the rheological properties of the CPC paste. This affects the different properties that have been studied and therefore, the optimum L/P ratio has to be optimized depending on the application in each case. In general, as the L/P ratio increases, the mechanical properties decrease, due to an increase in porosity. On the other hand, a low amount of liquid leads to a poor workability of the paste and difficulties the formation of a slurry and subsequent dissolution of the reagents.

The maximum collagen concentration, above which the slurry was not workable for a L/P ratio of 0.45 ml/g was a collagen concentration of 50 mg/ml. Tamimi *et al* reported a maximum workable concentration of 30 mg/ml<sup>22</sup> using a brushite CPC with a L/P ratio of 0.28 ml/g. Knepper-Nicolai *et al* reported that an apatitic cement (Biocement D) was mixed at a L/P ratio of 0.42 ml/g with a 25 mg/ml collagen solution<sup>54</sup>. Moreau *et al* used three different L/P ratios ranging from 0.28 to 0.4 ml/g with collagen concentrations up to 75 mg/ml, although the lowest L/P ratio did not result in a workable paste for the higher collagen concentration<sup>24</sup>.

One of the requirements that CPC must fulfil is to form a paste with cohesion when immersed in aqueous solution. It is important that the CPC maintains its integrity once it is placed in contact with body fluids. What we found was that all CPC formulations presented cohesion after 2 minutes, both in the presence and absence of collagen. Therefore, it was not necessary to incorporate any additives to enhance cohesion. Indeed, polymeric materials such as chitosan<sup>55</sup>, alginate<sup>56,57</sup>, gelatine<sup>58,59</sup> or even collagen<sup>23</sup>, have been combined with CPC and have increased the anti-washout and handling properties of the CPC, since the gel is able to entrap the CPC particles.

In order to observe when the CPC started to harden, or if the setting reaction was being delayed, Gilmore needles were used. The setting times were similar when comparing

the different CPC prepared with acetic acid, with collagen and with fibrillised collagen (Table 2.2). Nevertheless, the values were increased respect to the accelerant solution ( $\text{Na}_2\text{HPO}_4$ ). Similar results were found for a TTCP CPC, in which the values of setting time measured by the same method increased up to 30 minutes in the presence of collagen<sup>23</sup>. In another study, it was found that acetic acid reduced the setting time of a CPC composed of TTCP<sup>60</sup> and this was attributed to the lower pH compared to water.

In order to further characterize the initial setting reaction, DSC was applied for soluble collagen mixed with the CPC at different concentrations: 10 and 50 mg/ml (Figure 2.6 and Figure 2.7). It was interesting to observe that the heat evolution was lower in the CPC in which the collagen was present, and depended on the collagen concentration, being lower for the higher collagen concentration. In general, this method was more objective and sensitive than the Gillmore needles, but one of the main drawbacks was that the first 2-3 minutes of the reaction could not be monitored due to the sample preparation and equipment set-up<sup>61</sup>. Furthermore, water evaporation may also play a role in the heat evolution in our case. Previous works hasn't taken into account the water evaporation and have observed similar heat evolutions patterns as in the present work. Nevertheless, the equipments are different and can make sure that water evaporation does not take place since the calorimeter were designed to observe the setting reaction of a cement<sup>25-28</sup>. In our case, the DSC was not specifically designed for cements, but can still be used to measure the setting reaction, although the results have to be analyzed carefully.

Previous works done on DSC with similar composites showed that the effect of adding collagen or gelatine in the composite delayed the setting reaction in agreement with the results obtained in the present work. When gelatine was mixed with gypsum, there was a retardation in mineralization as gelatine concentration was increased<sup>26</sup>. It was also found that in collagen and gelatine matrixes, the onset of HA formation was higher compared to aqueous medium<sup>62</sup> and was attributed to the steric blockage of the HA inside the gels. This same effect was attributed to proteoglycans, which are known to inhibit HA formation<sup>63,64</sup>. Boskey showed that, collagen solutions do not promote calcium phosphate formation within calcium and phosphate solutions<sup>65</sup>. In agreement with this explanation, it was found that collagen itself was not an hydroxyapatite nucleator<sup>66</sup> and that it inhibits the HA formation<sup>62</sup>.

On the other hand, several studies have demonstrated the ability of collagen to nucleate and grow HA crystals<sup>67-69</sup>. This ability has been attributed to the carboxylic groups of collagen<sup>22,70,71</sup>. Furthermore, TenHuisen demonstrated that in a TTCP cement, the presence of gelatine did not alter the time for the HA formation unless the concentration was increased, having an increase in viscosity associated<sup>28</sup>, whereas the presence of collagen actually accelerated the HA formation, verified with DSC<sup>72</sup>. When TTCP and DCP were mixed with collagen, completion of the reaction to form HA was accelerated from 4.5-5 hours when mixed with water, to 2.5-3 hours when mixed with collagen solutions<sup>72</sup>.

Another important observation was that the same limitations of the equipment did not allow to show the complete transformation into CDHA. In our results, it was shown by XRD that the amount of CDHA formed after the DSC experiment was around 25%. Nevertheless, in previous studies it was also seen that the growth of the product resulted in a decrease in the rate of reaction as the process became dependent on diffusion<sup>25</sup>. As it is well known, the mechanism by which these types of CPC react, the process is initially controlled by surface area, until sufficient HA is formed to become controlled by diffusion<sup>73;74</sup>. This may explain the incomplete reaction of the  $\alpha$ -TCP together with the limitations of the DSC employed. Once the reaction became controlled by diffusion or that all the liquid had evaporated due to the equipment, no more changes were observed in the DSC. Other works have been able to show heat evolution for a longer period of time and is probably due to the higher amounts of CPC present, and therefore, to higher amounts of water that may react.

The pH evolution during the initial stages of the setting reactions were measured in order to observe the ion release (Figure 2.8 and 2.9). There was an increase in the pH when the reaction started to take place regardless if the liquid phase was water, acetic acid solution or collagen solution. After the  $\alpha$ -TCP powder was mixed with the liquid, calcium and phosphate were dissociated and found in solution. The phosphate groups were then protonated due to the presence of water, forming hydrogenphosphate and increasing the pH, since the amount of protons in solutions was being reduced<sup>7,9,74,75</sup>. A delay was found in the pH shift for both of the L/P ratios in the presence of the acetic acid solution and collagen solution compared to water. In both cases the pH was lower due to the presence of acetic acid. Since the acetic ion has a highly electronegative

oxygen in solution, the protons could be attracted both to the acetic ions and to the phosphate groups. Therefore, in the presence of the acetic acid, the pH increase took place slower. The pH was then stabilized in all cases when the phosphate groups had been protonated.

It is also worth highlighting that the lower pH obtained for the CPC containing acetic acid or collagen solutions compared to the water containing CPC was also expected to give a higher solubility according to Figure 1.7, since the solubility according to the phase diagram is higher. However, this lower pH may also decrease the precipitation reaction of the CDHA since the solubility of the HA is increased. Therefore, the net effect is that the dissolution-precipitation reaction should not be affected by the pH.

For high L/P ratios (33.33 ml/g), the pH raise of the CPC in the presence of collagen was observed to be as fast as the acetic solution (Figure 2.8), whereas at low L/P ratio (14.29 ml/g), the pH raise was slightly delayed when collagen was present (Figure 2.9). This was probably due to the higher viscosity of the slurry, which made the mixing slower and delayed the ion diffusion respect to the acetic acid solution. The effect of lower diffusion rates and the higher viscosity of a polymeric solution, being gelatin, was also previously observed by TenHuisen *et al* for hydroxyapatite gelatine composites<sup>28</sup>. A previous work in which gelatine and  $\alpha$ -TCP were mixed at the same L/P ratios as in the present study, similar pH results were observed<sup>30</sup>. Nevertheless, their results showed a higher increase in the final pH for the lower L/P ratio that was attributed to an intermediate phase, which was OCP<sup>30</sup>.

The delay in the pH raise with a collagen concentration of 5 mg/ml was already observed for a L/P = 14.29 ml/g, which was the more extreme conditions that could be used to be quantified with the pHmeter. It was not possible to measure the pH evolution for higher collagen concentrations, since the viscosity was too high. Similar situation happened when the L/P ratio was decreased too much, making a slurry in which the pH wasn't able to be measured.

As conclusion, the slower pH evolution found in the collagen containing CPC at a L/P of 14.29 ml/g can be ascribed to the high viscosity of the collagen solution. When cement was mixed with water, the wetting of the powder was instantaneous after mixing. With collagen, the mixing of the slurry was not as fast. Once the collagen was

completely mixed with the powder, the ion diffusion throughout the collagen network was somehow hindered. Hunter suggested that, the diffusion in the gels was slow due to the structuring of solvent molecules inside the gel<sup>76</sup>. In other studies, it was said that the diffusion was not possible, arriving to the conclusion that hydroxyapatite was not even formed due to the presence of collagen in a TTCP CPC with a 3% collagen solution<sup>23</sup>.

### **2.5.3. Collagen release and collagen distribution**

The collagen release during the setting of the CPC was measured for up to 7 days, which is the time needed for the transformation into CDHA. It was observed with the Bradford study and the quantification with Nanodrop that no collagen was released at any time point.

In the CPC with 10 mg/ml collagen concentration, if all the collagen was released into the medium, the maximum concentration of the collagen in the supernatant solution would have been 5 mg/ml (when the samples were immersed in 1 ml of water) and 0.41 mg/ml (when the samples were immersed in 12 ml of water), and for the CPC containing 50 mg/ml collagen concentration, 25 mg/ml (when the samples were immersed in 1 ml of water) and 2.08 mg/ml (when the samples were immersed in 12 ml of water). These values are high enough for any of the two techniques to detect the presence of collagen. Since no collagen was detected in the presence and in the absence of the crosslinker, and knowing that the detection limit for the Bradford was 1.25 µg/ml and 2.5 µg/ml for the Nanodrop, it was concluded that less than 0.0025% ( $1.25 \mu\text{g}/5000 \mu\text{g} * 100$ ) of the collagen was dissolved for the COLF10 immersed in 1 ml of water.

These results were further confirmed through the confocal microscopy observation of the CPC with a fluorescent marker (CBQCA) (Figure 2.10 and 2.11). The results confirmed that after the setting, collagen was present in the CPC. Since the CPC was immersed in water for 7 days for the setting, this result confirmed that the collagen was not susceptible to washout and that it was trapped in the CPC structure. For the samples containing solubilized collagen, the distribution was totally homogenous (Figure 2.10). This was probably because the collagen was in the form of monomers dispersed throughout the CPC and probably found between the crystal network. When the collagen concentration was increased, the fluorescence intensity increased, still having a homogenous distribution (Figure 2.10). Regarding the samples with fibrillised collagen,

the samples were observed to be heterogeneous (Figure 2.11). The collagen bundled-up together by means of fibrillisation, making interconnections between the different collagen monomers. The light was brighter than for the solubilized collagen, because there was higher amount of collagen concentrated in certain points. Furthermore, the images also revealed that, even though the pH rises to near neutral pH when the setting reaction takes place as observed in Figure 2.8 and 2.9, and it is known that this is near the pH at which fibrillisation takes place, the collagen was still maintained as solubilized and did not fibrillise.

Therefore, it was concluded that no collagen was released and that the crosslinking was not necessary. There are two reasons that explain this behavior. The first one is that the calcium phosphate is found as the matrix of the material, having the collagen between the ceramic particles. Therefore, the collagen is entrapped between the compact structures formed by the CDHA. Furthermore, since CDHA presents high amount of  $\text{Ca}^{2+}$ , and collagen presents high amount of carboxylic groups, it is possible to have a chemical interaction between the two chemical groups. Similar results have been found for CPC, in which it was observed that the presence of collagen made a compact structure which did not allow for collagen to be released<sup>22</sup>. In general, CPC with collagen don't incorporate crosslinkers, although no published data demonstrates the reason why it is not necessary<sup>22,24,77</sup>.

#### 2.5.4. Microstructure

The microstructure formed for the CPC in the presence of collagen was very similar to that of the control CPC (Figure 2.12 a-d). At low magnification, Hadley shells are visible in the structure for the CTRLF and COLF10, which are formed when  $\alpha$ -TCP is brought in contact with water, dissolving and followed by the precipitation of CDHA surrounding the  $\alpha$ -TCP powder, giving rise to shell-like structure (Figure 2.12 a,c). At higher magnification it was seen that the structure was conformed of an entangled network of the CDHA crystals (Figure 2.12 b). The same structure was found in the presence of solubilized collagen (Figure 2.12d). Tamimi *et al* observed similar microstructure both in the presence and absence of the collagen to the results observed in the present study<sup>22</sup>. They attributed this observation to an homogenous distribution of the collagen, and since the collagen was in the form of small molecules, it was not



detectable by SEM<sup>22</sup>. This is in agreement with the fluorescence results found in the present work, in which collagen was found to be distributed homogeneously. The presence of collagen was detected by SEM when the collagen was fibrillised and crosslinked (Figure 2.12 e-h), presented as bundles or membranes covering the CDHA crystals. This happened because the aggregation of the small monomers into bigger sized collagen molecules in the form of bundles, which were detectable with SEM. Moreau *et al* used a TTCP CPC with collagen in the form of fibers, which were clearly detectable by SEM<sup>24</sup>, and attributed this observation to the aggregation of different collagen molecules to form a braided structure.

### 2.5.5. Phase evolution and CPC-collagen interaction

The XRD diffractograms confirmed that the presence of collagen did not alter the setting reaction of the CPC and that CDHA was formed as the final product of the setting reaction (Figure 2.17, 2.18 and 2.19). It was also seen that the kinetics of the CDHA formation were similar in the presence of acetic acid, solubilized collagen and fibrillised collagen (Figure 2.20 and 2.21). Although in the setting reaction studies (pH evolution, DSC and Gilmore needles) a small delay was observed at very short times (during the first minutes of reaction) this does not contradict the XRD study where the first value of the kinetic study is 1 hour. In previous studies it was shown that collagen hindered the transformation of the CPC into HA also at short times<sup>23</sup>. Therefore, it can be concluded that a small delay is found only during the initial minutes of reaction, but after 1 hour, the conversion of the  $\alpha$ -TCP into CDHA takes place at a similar rate in the presence and absence of collagen.

The collagen molecule has about 1000 residues per chain, in which about 20 % of these residues have a side chain of COOH or NH<sub>2</sub>. When collagen is mixed with a calcium phosphate, the dissolution of the calcium phosphate will lead to the liberation of Ca<sup>2+</sup> and PO<sub>4</sub><sup>3-</sup> ions to the medium which will be able to interact with the COO<sup>-</sup> and NH<sub>3</sub><sup>+</sup> groups of the collagen molecules. These interactions, mainly electrostatic, have been previously studied by FTIR and have appeared as shifts in wavenumber when calcium and phosphate solutions were mixed with collagen solutions<sup>78</sup>.

The interaction between the collagen and CPC for the samples with L/P ratio of 0.45 ml/g containing 10 mg/ml or 50 mg/ml solution showed no significant bands in the

amide region (Figure 2.13). Therefore, a composite with higher content of collagen was fabricated. It was seen in the results that there were two main regions in which a shift was detected for the 70:30 wt% composite (Figure 2.14): the amide I ( $\sim 1650\text{ cm}^{-1}$ ) and amide II ( $\sim 1550\text{ cm}^{-1}$ ) region corresponding to collagen, and the  $\nu_3\text{ PO}_4^{3-}$  mode of vibration ( $\sim 1030\text{ cm}^{-1}$ ) region corresponding to the CDHA.

Regarding the phosphate groups, the most predominant band corresponded to the  $1041\text{ cm}^{-1}$  band for the CDHA which shifted to  $1031\text{ cm}^{-1}$  for the composite material (Figure 2.15, Table 2.4). A possible explanation was the interaction between the  $\text{NH}_3^+$  groups and the  $\text{PO}_4^{3-}$  groups, weakening the bond and creating the shift. Nevertheless, this shift has not been previously discussed in the literature by other authors and therefore it is difficult to speculate about the rationale behind.

The most relevant bands appeared in the amide region, and more specifically, the amide I region (Figure 2.16, Table 2.5). The amide I corresponds to the bending of the bond between carbon and oxygen of the carboxylic group ( $\text{C}=\text{O}$ ). It was seen that there was a shift from  $1653\text{ cm}^{-1}$  for collagen to  $1647\text{ cm}^{-1}$  for the composite (Figure 2.16). The observed shift was  $6\text{ cm}^{-1}$ . The possible interaction present here was between the calcium atoms and the carboxylic group. These shifts have been previously discussed and will therefore be taken into consideration.

The interaction in separate of collagen and  $\text{Ca}^{2+}$  ions and phosphate ions can be monitored and were indeed studied in previous works. An experimental study was done in which recombinant human like collagen (RHLC) was mixed with several solutions<sup>79</sup>. A comparison between RHLC, RHLC with Ca ions, RHLC with phosphate ions and RHLC with calcium phosphate was done in order to see which of the ions had the biggest effect in the IR shifts. The positions of RHLC and RHLC with phosphate ions were almost the same, revealing that there was no obvious interaction between RHLC and phosphate ions. When RHLC and RHLC with Ca ions were compared, there were some differences. Two concentrations of Ca ions were introduced, for the lower concentration, amide I, appeared at  $1639\text{ cm}^{-1}$ , while for the higher concentration, the amide I appeared at  $1633\text{ cm}^{-1}$ . The amide I in pure RHLC was observed at  $1662\text{ cm}^{-1}$ <sup>79</sup>. When the RHLC was combined with the calcium phosphate, a similar shift appeared as the one observed when RHLC was mixed with the calcium ions, decreasing from  $1662$

$\text{cm}^{-1}$  for collagen to  $1653 \text{ cm}^{-1}$  for the composite. From these results, it can be seen that, in the mineralization of the RHLC, there is no interaction with phosphates. The red shift observed in the amide I was attributed to the weakening of the C=O bond in the peptide chain because of the formation of new chelate bonds between calcium ions and C=O bonds. This is thought to be quite reasonable since the fact that the oxygen from the carbonyl has a nonbonding pair of electrons which can chelate metal atoms<sup>79</sup>. This theory has been supported by other authors<sup>4,68,79-81,92</sup>. This was also demonstrated by a decrease in the carboxylic group bond order (from 1.76 to 1.51), meaning that the free electrons in the oxygen were able to chelate calcium ions<sup>68</sup>.

Table 2.7 reports the values given by other authors for the wavenumbers shift in the amide I region when a calcium phosphate is incorporated in the structure of collagen. The explanation given by the different authors on the shift is the chelation of the calcium ions with the carboxylic groups of the collagen as previously explained. As can be seen in Table 2.7, the shifts are in the range of  $3 \text{ cm}^{-1}$  to  $14 \text{ cm}^{-1}$ . The range found in the present study falls within this range ( $6 \text{ cm}^{-1}$ ). This shift can therefore be assigned to the interaction of the collagen and the CDHA. This shift and the fact of having an electrostatic binding between the collagen and the CDHA, may also be related with the fluorescent images (Figure 2.10 and 2.11). It is possible that besides the physical interaction of the collagen and the CDHA which retains the collagen in the CDHA network, there may also be a physical-chemical interaction which enhances the retention of the collagen in the structure as was shown by fluorescence.

Material	Amide I shift (collagen to collagen/CaP)	Author
<i>Mineralization on PHBV/collagen composite</i>	1659 to 1656 (3 $\text{cm}^{-1}$ )	Jingjun W <sup>79</sup>
<i>Collagen mineralization</i>	1657 to 1651 (6 $\text{cm}^{-1}$ )	Zhang W <sup>80</sup>
<i>Simultaneous precipitation of collagen</i>	Shift (no value given)	Keeney M <sup>81</sup>
<i>Mineralization of recombinant human like collagen</i>	1662 to 1653 (9 $\text{cm}^{-1}$ )	Wang Y <sup>92</sup>
<i>Collagen mineralization in SBF</i>	1663 to 1649 (14 $\text{cm}^{-1}$ )	Zhang LJ <sup>75</sup>
<i>CPC with collagen</i>	1653 to 1647 (6 $\text{cm}^{-1}$ )	Present study

Table 2.7. Wavenumber appeared in the literature when comparing collagen and a composite composed of hydroxyapatite and collagen.

## 2.5.6. Density and porosity

The skeletal density of composite CPC decreased as the collagen concentration was increased (Figure 2.22). Even though the presence of collagen was low, the skeletal

density decreased and this was because the collagen has a lower density than the calcium phosphate, making the material decrease its density. This skeletal density is an intrinsic property of the material. The extrinsic parameter that relates directly with the morphology of the material is the porosity. The total porosity was measured with the mercury intrusion porosimeter.

The effect of three variables in the porosity of CPC were studied, being the initial particle size distribution of the powder, the presence of solubilized collagen and fibrillised collagen and the collagen concentration. The initial particle size of the cement powder, being coarse and fine, influenced the pore size range, which were higher for the coarse cements, although presented similar values of total porosity (Table 2.6). The particle size distribution was considered as the parameter that changed the most the pore sizes. Solubilized collagen was not shown to affect significantly the porosities nor the pore size distributions for the low (10 mg/ml) and high (50 mg/ml) collagen concentrations. Similar trend was observed for the fibrillised collagen at low collagen concentrations, although at higher concentrations, the presence of fibrillised collagen increased the pore size distribution to higher pore sizes. This was probably due to the fact that, as was seen in the collagen distribution observed by fluorescence, the collagen was heterogeneously dispersed, forming bundles. Once these bundles were dried, they could leave a void in which the mercury could easily penetrate and that was why these higher pore sizes were observed.

It is known that porosity has high significance in the field of drug delivery systems. In fact, several studies proved the efficiency of the CPC as drug delivery vehicle<sup>82</sup>. The main difference of the CPC with other materials, is that the drug can be mixed with the liquid or the solid<sup>83</sup>, or can be incorporated by adsorption in the set cement<sup>84</sup>. In both of the cases, one of the most important parameters is the pore size and its pore size distribution<sup>85,86</sup>.

In a previous study, it was shown the importance of the nano and microporosity in the CPC<sup>87</sup>. The influence of the initial liquid to powder ratio, as well as the influence of the initial particle size of the CPC, had huge relevance in the field of protein adsorption and the ability for proteins to penetrate inside the matrix. It was seen that as the L/P ratio was increased, the amount of protein that was able to penetrate was increased, but this penetration was also depended on the initial particle size. Since the different particle

sizes created two well defined microstructures, the lower the specific surface area, the higher the porosity, and therefore, a higher protein penetration.

### 2.5.7. Injectability

When performing an *in vivo* or a clinical application, one of the first parameter that surgeons will deal with is the injectability. One of the main complains surgeons have, is that CPC are poorly injectable<sup>88-91</sup>. Some CPC are not injectable due to the high force that must be applied for the injection or that because not all the paste can be extruded.

Our results revealed that the presence of collagen increased the injectability of the CPC, from 50% to 96% for the CTRLF and COLF10 samples respectively (Figure 2.29). Nevertheless, the presence of fibrillised collagen did not show the same efficiency for the CPC extrusion. The increase in injection was only up to 65%. Furthermore, the presence of fibrillised collagen showed an increase in the force needed to start injection respect to the CPC with solubilized collagen and the CTRLF (Figure 2.30). This can be adscribed to the presence of an initial paste composed of CPC and collagen bundles. Solubilized collagen did enhance the injectability, but the presence of the bundles decreased the ability to be injected. Furthermore, both CPC with collagen in the liquid phase presented a slight increase in the force needed to start injecting the paste (Figure 2.31). This can be attributed to the higher viscosity of the paste.

It is known that the ability of a CPC to be injected can be enhanced by the increase in the L/P ratio, the use of round particles, the addition of citrate ions and the use of viscous polymer solutions<sup>91</sup>. The presence of polymers combined with the CPC have been shown to enhance the injectability<sup>92-95</sup>. The main reason for the enhanced injectability is the lubricating effect that the polymer has on the different cement particles<sup>91,96,97</sup>. The presence of a polymer between the different grains may reduce the friction between the different grains and therefore increase the injectability<sup>96,97</sup>. This was thought as the main reason for an increased injectability observed in the CPC combined with collagen.

One of the most important problems in the ability to inject a CPC is the phase separation or the filter-pressing effect. When a CPC is injected, a certain pressure is applied to the syringe and this pressure is directly applied to the cement paste. Since the

paste has to pass through a small cannula at the end, there can be the filter pressing<sup>91</sup>. This occurs when a phase separation takes place, meaning that when the injection is produced, the liquid is extruded, whereas most of the powder remains in the syringe<sup>91,98,99</sup>. That means that the L/P ratio inside the syringe can be controlled, but once it is injected, the L/P ratio of the extruded paste can be different from the initial one. If the paste is able to be injected completely, the phase separation is less likely to happen. In the case in which not all the paste is injected, the force will start to increase, and therefore, the phase separation will take place. The incorporation of collagen or other polymers in general, may reduce the phase separation effect, and therefore the injectability may be increased<sup>91</sup>. Although the incorporation of collagen was not designed to increase this feature, the results showed that it did enhance the injectability.

## 2.5.8. Mechanical properties

The results for the compressive strength showed that for the low concentration (10 mg/ml) collagen containing CPC, the compressive strength was similar to that of the control (Figure 2.32). Nevertheless, a clear decrease of the mechanical properties was found when the collagen concentration was increased, both for fine and coarse CPC. The decreased values for the CPC containing the higher concentrations of collagen cannot be attributed to an increase in the total porosity of the samples, since it was previously shown to be similar (Table 2.6). The results are in agreement with previous works that reported that for similar collagen concentrations incorporated in the CPC, the effect on the compressive strength was non-existing<sup>22</sup>, although when the collagen concentration was increased, the compressive strength was reduced<sup>23</sup>. The presence of fibrillised collagen slightly decreased the mechanical properties compared to the solubilized collagen containing samples. Nevertheless, it is worth highlighting that the presence of the fibrillised collagen, especially for the COLF50F, there was an increase in the strain, although it presented a lower compressive strength, leading non-catastrophic failures compared to the brittle failure of the CTRLF (Figure 2.33). This was also previously seen when a CPC was combined with collagen fibers<sup>24</sup>. The enhanced mechanical properties in that case were attributed to the presence of HA on the collagen fibres which were able to resist crack propagation.

Lower values of compressive strength were found for the coarse than for the fine CPC. This cannot be attributed to the porosities since they present similar total porosities (Table 2.6.). However, it was previously reported that for the same inorganic CPC, the mechanical properties for coarse and fine were not statistically different<sup>9</sup>.

## **2.6. Conclusions**

The results have shown that collagen containing CPC can be obtained by dissolving collagen in the liquid phase of a CPC. Different collagen treatments were applied in order to observe the effect of collagen morphology on the properties of the CPC. Collagen was shown to be a retarder of the hydrolysis of the  $\alpha$ -TCP into CDHA at the initial reaction times. The main principle underlying this delay was the presence of the acetic acid and the higher viscosity of the collagen solution. Nevertheless, already after 1 hour, there were no differences in the kinetics of the transformation into CDHA in the presence of collagen and that the final product was not altered.

An important finding was that the collagen was not released during the 7 day setting reaction in water. This was further confirmed by the observation of collagen with a fluorescent marker in the set CPC. The distribution was shown to be homogenous for the solubilized collagen and heterogeneous for the fibrillised collagen. It was also seen that the presence of collagen, increased the injectability and that it did not influence the mechanical properties at low collagen concentrations, whereas at higher collagen concentrations there was a decrease in the mechanical properties.

## 2.7. References

1. Du C, Cui FZ, Zhu XD & de Groot K. Three-dimensional nano-HAp/collagen matrix loading with osteogenic cells in organ culture. *Journal of Biomedical Materials Research* **44**, 407-415 (1999).
2. Lickorish D, Ramshaw JAM, Werkmeister JA, Glattauer V & Howlett CR. Collagen-hydroxyapatite composite prepared by biomimetic process. *Journal of Biomedical Materials Research* **68A**, 19-27 (2004).
3. Zou C *et al.* Preparation and characterization of porous [beta]-tricalcium phosphate/collagen composites with an integrated structure. *Biomaterials* **26**, 5276-5284 (2005).
4. Kikuchi M, Itoh S, Ichinose S, Shinomiya K & Tanaka J. Self-organization mechanism in a bone-like hydroxyapatite/collagen nanocomposite synthesized in vitro and its biological reaction in vivo. *Biomaterials* **22**, 1705-1711 (2001).
5. Myun CC, Ikoma T, Kikuchi M & Tanaka T. Preparation of a porous hydroxyapatite/collagen nanocomposite using glutaraldehyde as a crosslinkage agent. *Journal of Materials Science Letters* **20**, 1199-1201 (2001).
6. Kikuchi M *et al.* Biomimetic synthesis of bone-like nanocomposites using the self-organization mechanism of hydroxyapatite and collagen. *Composites Science and Technology* **64**, 819-825 (2004).
7. Ginebra MP *et al.* Setting reaction and hardening of an apatitic calcium phosphate cement. *Journal of Dental Research* **76**, 905-912 (1997).
8. Ginebra MP, Fernandez E, Driessens FCM, Boltong MG & Planell JA. Influence of the particle size of the powder phase in the setting and hardening behaviour of a calcium phosphate cement. *Bioceramics* **10**, 481 (1997).
9. Ginebra MP, Driessens FCM & Planell JA. Effect of the particle size on the micro and nanostructural features of a calcium phosphate cement: a kinetic analysis. *Biomaterials* **25**, 3453-3462 (2004).



10. Angele P et al. Influence of different collagen species on physico-chemical properties of crosslinked collagen matrices. *Biomaterials* **25**, 2831-2841 (2004).
11. Quereshi S et al. Extraction and partial characterization of collagen from different animal skins. *Recent Research in Science and Technology* **2**, 28-31 (2010).
12. Seteven FS & Thomas H. Preparation of insoluble collagen from human cartilage. *Biochemical Journal* **135**, 245-247 (1973).
13. Bensusan HB & Hoyt BL. The effect of various parameters on the rate of formation of fibers from collagen solutions. *Journal of the American Chemical Society* **80**, 719-724 (1958).
14. Wood GC & Keech MK. The formation of fibrils from collagen solutions. 1. The effect of experimental conditions: kinetic and electron-microscope studies. *Biochemical Journal* **75**, 588 (1960).
15. Cassel JM. The kinetics of the heat precipitation of collagen. *Journal of American Leather Chemists Association* **51**, 556-557 (1962).
16. Hayashi T & Nagai Y. Effect of pH on the stability of collagen molecule in solution. *Journal of Biochemistry* **73**, 999-1006 (1972).
17. Piez KA. Structure and assembly of the native collagen fibril. *Connective Tissue research* **10**, 25-36 (1982).
18. Veis A. Collagen fibrillogenesis. *Connective Tissue Rresearch* **10**, 11-24 (1982).
19. Kadler KE, Holmes DF, Trotter JA & Chapman JA. Collagen fibril formation. Review article. *Biochemistry Journal* **316**, 1-11 (1996).
20. Delorenzi NJ, Sculsky G & Gatti CA. Effect of monovalent anions on type I collagen fibrillogenesis in vitro. *International Journal of Biological Macromolecules* **19**, 15-20 (1996).
21. Goh MC et al. Fibril formation in collagen. *Physica A* **239**, 95-102 (1997).

22. Tamimi, F. *et al.* Brushite-collagen composites for bone regeneration. *Acta Biomaterialia* **4**, 1315-1321 (2008).
23. Miyamoto Y *et al.* Basic properties of calcium phosphate cement containing atelocollagen in its liquid or powder phases. *Biomaterials* **19**, 707-715 (1998).
24. Moreau JL, Weir MD & Xu HH. Self-setting collagen-calcium phosphate bone cement: mechanical and cellular properties. *Journal of Biomedical Materials Research* **91A**, 605-613 (2009).
25. Brown PW & Fulmer M. Kinetics of hydroxyapatite formation at low temperature. *Journal of the American Ceramic Society* **74**, 934-940 (1991).
26. TenHuisen K & Brown PW. Microstructural development and formation kinetics in a mineralizing system for bone: Calcium sulfate-gelatin. *Biomimetics* **1**, 131-150 (1992).
27. Fulmer MT & Brown PW. Effects of temperature on the formation of hydroxyapatite. *Journal of Materials Research* **8**, 1687 (1993).
28. TenHuisen KS & Brown PW. The formation of hydroxyapatite-gelatin composites at 38°C. *Journal of Biomedical Materials Research* **28**, 27-33 (1994).
29. Panzavolta S *et al.* Porous composite scaffolds based on gelatin and partially hydrolyzed [alpha]-tricalcium phosphate. *Acta Biomaterialia* **5**, 636-643 (2009).
30. Cullity BD. Elements of X-Ray Diffraction. Addison-Wesley Publishing Company Inc, (1978).
31. Peng H *et al.* In vitro degradation and release profiles for electrospun polymeric fibers containing paracetamol. *Colloids and Surfaces B: Biointerfaces* **66**, 206-212 (2008).
32. Prockop DJ, Kivirikko KI, Tuderman L & Guzman NA. The biosynthesis of collagen and its disorders. *The New England Journal of Medicine* **301**, 13-23 (1979).

33. Gross J. The behavior of collagen units as a model in morphogenesis. *Journal of Biophysical and Biochemical Cytology* **2**, 261 (1956).
34. Fletcher GC. Dynamic light scattering from collagen solutions. I. Translational diffusion coefficient and aggregation effects. *Biopolymers* **15**, 2201-2217 (1976).
35. McClain PE & Wiley ER. Differential scanning calorimeter studies of the thermal transitions of collagen. *The Journal of Biological Chemistry* **247**, 692-697 (1972).
36. Burjanadze TV. New analysis of the phylogenetic change of collagen thermostability. *Biopolymers* **53**, 523-528 (2000).
37. Bae I *et al.* Biochemical properties of acid-soluble collagens extracted from the skins of underutilised fishes. *Food Chemistry* **108**, 49-54 (2008).
38. Naimark WA *et al.* Thermomechanical analysis of collagen crosslinking in the developing lamb pericardium. *Biorheology* **35**, 1-16 (1998).
39. Naimark WA, Pereira CA, Tsang K & Lee JM. HMDC crosslinking of bovine pericardial tissue: a potential role of the solvent environment in the design of bioprosthetic materials. *Journal of Materials Science: Materials in Medicine* **6**, 235-241 (1995).
40. Bigi A, Cojazzi G, Panzavolta S, Rubini K & Roveri N. Mechanical and thermal properties of gelatin films at different degrees of glutaraldehyde crosslinking. *Biomaterials* **22**, 763-768 (2001).
41. Duan X & Sheardown H. Crosslinking of collagen with dendrimers. *Journal of Biomedical Materials Research* **75A**, 510-518 (2005).
42. Orban JM *et al.* Crosslinking of collagen gels by transglutaminase. *Journal of Biomedical Materials Research* **68A**, 756-762 (2004).
43. Lee JM, Edwards HHL, Pereira CA & Samii SI. Crosslinking of tissue-derived biomaterials in 1-ethyl-3-(3-dimethylaminopropyl)-carbodiimide (EDC). *Journal of Materials Science: Materials in Medicine* **7**, 531-541 (1996).

44. Rault I, Frei V & Herbage D. Evaluation of different chemical methods for cross-linking collagen gel, films and sponges. *Journal of Materials Science: Materials in Medicine* **7**, 215-221 (1996).
45. Lee JM, Pereira CA, Abdulla D, Naimark WA & Crawford I. A multi-sample denaturation temperature tester for collagenous materials. *Medical Engineering Physics* **17**, 115-121 (1995).
46. Petite H, Rault I, Huc A, Menasche P & Herbage D. Use of acyl azide method for cross-linking collagen-rich tissues such as pericardium. *Journal of Biomedical Materials Research* **24**, 179-187 (1990).
47. Nomura Y, Toki S, Ishii Y & Shirai K. The physicochemical property of shark type I collagen gel and membrane. *Journal of Agricultural Food Chemistry* **48**, 2028-2032 (2000).
48. Nomura Y, Yamano M & Shirai K. Renaturation of  $\alpha 1$  chains from shark skin collagen type I. *Journal of Food Science* **60**, 1233-1236 (1995).
49. Yunoki S, Nagai N, Suzuki T & Munekata M. Novel biomaterial from reinforced salmon collagen gel prepared by fibril formation and cross-linking. *Journal of Bioscience and Bioengineering* **98**, 40-47 (2004).
50. Bae I *et al.* Characteristics of a self-assembled fibrillar gel prepared from red stingray collagen. *Fish Science* **75**, 765-770 (2009).
51. Komsa-Penkova R, Koynova R, Kostov G & Tenchov BG. Thermal stability of calf skin collagen type I in salt solutions. *Biochimica et Biophysica Acta* **1297**, 171-181 (1996).
52. Prockop DJ & Fertala A. Inhibition of the self-assembly of collagen I into fibrils with synthetic peptides. Demonstration that assembly is driven by specific binding sites on the monomers. *Journal of Biological Chemistry* **273**, 15598-15604 (1998).

53. Barbani N, Giusti P, Lazzeri L, Polacco G & Pizzirani G. Bioartificial materials based on collagen: 1. Collagen cross-linking with gaseous glutaraldehyde. *Journal of Biomaterials Science. Polymer Edition* **7**, 461-469 (1995).
54. Knepper-Nicolai B *et al.* Influence of osteocalcin and collagen I on the mechanical and biological properties of Biocement D. *Biomolecular Engineering* **19**, 227-231 (2002).
55. Zhang Y & Xu HHK. Effects of synergistic reinforcement and absorbable fiber strength on hydroxyapatite bone cement. *Journal of Biomedical Materials Research* **75A**, 832-840 (2005).
56. Ishikawa K *et al.* Non-decay type fast-setting calcium phosphate cement: Hydroxyapatite putty containing an increased amount of sodium alginate. *Journal of Biomedical Materials Research* **36**, 393-399 (1997).
57. Tajima S, Nishimoto N, Kishi Y, Matsuya S & Ishikawa K. Effects of Added Sodium Alginate on Mechanical Strength of Apatite Cement. *Dental Materials Journal* **23**, 329-334 (2004).
58. Wang X, Chen L, Xiang H & Ye J. Influence of anti-washout agents on the rheological properties and injectability of a calcium phosphate cement. *Journal of Biomedical Materials Research* **81B**, 410-418 (2007).
59. Shie MY, Chen DCH, Wang CY, Chiang TY & Ding SJ. Immersion behavior of gelatin-containing calcium phosphate cement. *Acta Biomaterialia* **4**, 646-655 (2008).
60. TenHuisen KS & Brown PW. The effects of citric and acetic acid on the formation of calcium-deficient hydroxyapatite at 38°C. *Journal of Materials Science: Materials in Medicine* **5**, 291-298 (1994).
61. Hofmann MP, Nazhat SN, Gbureck U & Barralet JE. Real-time monitoring of the setting reaction of brushite-forming cement using isothermal differential scanning calorimetry. *Journal of Biomedical Materials Research B* **79B**, 360-364 (2006).

62. Blumenthal NC, Cosma V & Gomes E. Regulation of Hydroxyapatite formation by gelatin and type I collagen gels. *Calcified Tissue International* **48**, 440-442 (1991).
63. Blumenthal NC, Posner AS, Silverman LD & Rosenberg LC. Effect of proteoglycans on in vitro hydroxyapatite formation. *Calcified Tissue International* **27**, 75 (1979).
64. Chen CC, Boskey AL & Rosenberg LC. The inhibitory effect of cartilage proteoglycans on hydroxyapatite growth. *Calcified Tissue International* **36**, 285 (1984).
65. Boskey AL. Hydroxyapatite formation in a dynamic collagen gel system: effects of type I collagen, lipids and proteoglycans. *Journal of Physical Chemistry* **93**, 1628-1633 (1989).
66. Termine JD *et al.* Osteonectin, a bone-specific protein linking mineral to collagen. *Cell* **26**, 99-105 (1981).
67. Roveri N *et al.* Biologically inspired growth of hydroxyapatite nanocrystals inside self-assembled collagen fibers. *Materials Science and Engineering C* **23**, 441-446 (2003).
68. Rhee SH & Lee JD. Nucleation of hydroxyapatite crystal through chemical interaction with collagen. *Journal of the American ceramic society* **83**, 2890-2892 (2000).
69. Sato K, Kumagai Y & Tanaka J. Apatite formation on organic monolayers in simulated body environment. *Journal of Biomedical Materials Research* **50**, 16-20 (2000).
70. Giriya EK, Yokogawa Y & Nagata F. Influence of carboxyl groups present in the mineralizing medium in the biomimetic precipitation of apatite on collagen. *Key Engineering Materials* **254-256**, 399-402 (2004).
71. Zhang LJ *et al.* Hydroxyapatite/collagen composite materials formation in simulated body fluid environment. *Materials Letters* **58**, 719-722 (2004).

72. TenHuisen KS, Martin RI, Klimkiewicz M & Brown PW. Formation and properties of a synthetic bone composite: Hydroxyapatite-collagen. *Journal of Biomedical Materials Research* **29**, 803-810 (1995).
73. Brown PW. Effects of particle size distribution on the kinetics of hydration of tricalcium silicate. *Journal of the American Ceramic Society* **72**, 1829-1832 (1989).
74. Ginebra MP, Fernandez E, Driessens FCM & Planell JA. Modeling of the hydrolysis of  $\alpha$ -tricalcium phosphate. *Journal of the American Ceramic Society* **82**, 2808-2812 (1999).
75. Durucan C & Brown PW. Reactivity of  $\alpha$ -tricalcium phosphate. *Journal of Materials Science* **37**, 963-969 (2002).
76. Maquet J, Theveneau H, Djabourov M & Papon P. <sup>1</sup>H n.m.r. study of gelatin gels. *International Journal of Biological Macromolecules* **6**, 162-163 (1984).
77. Touny AH, Bhaduri S & Brown PW. Formation of calcium deficient HAp/collagen composites by hydrolysis of  $\alpha$ -TCP. *Journal of Materials Science: Materials in Medicine* **21**, 2533-2541 (2010).
78. Wang Y *et al.* Investigations of the initial stage of recombinant human-like collagen mineralization. *Materials Science and Engineering: C* **26**, 635-638 (2006).
79. Yingjun W, Gang W, Xiaofen C, Jiandong Y & Kun W. Rapid calcification on solution blending of homogenous PHBV/collagen composite. *Journal of Applied Polymer Science* **112**, 963-970 (2009).
80. Zhang W, Huang ZL, Liao SS & Cui FZ. Nucleation Sites of Calcium Phosphate Crystals during Collagen Mineralization. *Journal of the American Ceramic Society* **86**, 1052-1054 (2003).
81. Keeney M, Collin E & Pandit A. Multi-channeled collagen-calcium phosphate scaffolds: their physical properties and human cell response. *Tissue Engineering: Part C* **15**, 265-273 (2009).

82. Slosarczyk A, Szymure-Oleksiak J & Mycek M. The kinetics of pentoxifylline release from drug loaded hydroxyapatite implants. *Biomaterials* **21**, 1215-1221 (2000).
83. Bohner M *et al.* Gentamicin-loaded hydraulic calcium phosphate bone cement as antibiotic delivery system. *Journal of Pharmaceutical Sciences* **86**, 565-572 (1997).
84. Nihouannen DL, Hacking SA, Gbureck U, Komarova SV & Barralet JE. The use of RANKL-coated brushite cement to stimulate bone remodeling. *Biomaterials* **29**, 3253-3259 (2008).
85. Mathiowitz E. Encyclopedia of controlled drug delivery. John Wiley and Sons, New York (1999).
86. Ratner BD, Hoffman AS, Schoen FJ & Lemons JE. Biomaterials Science. An introduction to Materials in Medicine. Academic Press, San Diego (2004).
87. Espanol M *et al.* Intrinsic porosity of calcium phosphate cements and its significance for drug delivery and tissue engineering applications. *Acta Biomaterialia* **5**, 2752-2762 (2009).
88. Ishikawa K. Effects of spherical tetracalcium phosphate on injectability and basic properties of apatitic cement. *Key Engineering Materials* **204-242**, 369-372 (2003).
89. Bohner M & Baroud G. Injectability of calcium phosphate pastes. *Biomaterials* **26**, 1553-1563 (2005).
90. Leroux L, Hatim Z, Freche M & Lacout JL. Effects of various adjuvants (lactic acid, glycerol and chitosan) in the injectability of a calcium phosphate cement. *Bone* **25**, S31-S34 (1999).
91. Khairoun I, Boltong MG, Driessens FCM & Planell JA. Some factors controlling the injectability of calcium phosphate bone cements. *Journal of Materials Science: Materials in Medicine* **9**, 425-428 (1998).



92. Andrianjatovo H & Lemaitre J. Effects of polysaccharides on the cement properties in the monocalcium phosphate/ $\beta$ -tricalcium phosphate systems. *Innovation in Technology, Biology and Medicine* **16S**, 140-147 (1995).
93. Belkoff SM, Mathis JM, Jasper LE & Deramond H. An ex vivo biomechanical evaluation of a hydroxyapatite cement for use with vertebroplasty. *Spine* **26**, 1542-1546 (2001).
94. Borzacchiello A, Sanginario V, Ambrosio L, Ginebra MP & Planell JA. Characterization of an injectable hydrogel composite for orthopedic applications. Proceedings of the Second International Conference on New Biomedical Materials. 2003. Cardiff, UK. 4-6-2003.
95. Ginebra MP *et al.* Mechanical and rheological improvement of a calcium phosphate cement by the addition of a polymeric drug. *Journal of Biomedical Materials Research* **57**, 113-118 (2001).
96. Lombois H, Halary JL, Van Damme H & Colombet P. Adsorption, lubrication et interaction de contact dans les pâtes denses polymère-ciment. Proceedings of the 38ème colloque annuel du groupe français de rhéologie . 2003. Brest, France.
97. Mansoutre S, Colombet P & Van Damme H. Water retention and granular rheological behavior of fresh C<sub>3S</sub> paste as a function of concentration. *Cement concrete research* **29**, 1441-1453 (1999).
98. Khairoun I, Driessens FCM, Boltong MG, Planell JA & Wenz R. Addition of cohesion promoters to calcium phosphate cements. *Biomaterials* **20**, 393-398 (1999).
99. Habib M, Baroud G, Gitzhofer F & Bohner M. Mechanisms underlying the limited injectability of hydraulic calcium phosphate paste. *Acta Biomaterialia* **4**, 1471 (2008)

# Chapter 3: Cell Response to Injectable CPC/Collagen Composites

## 3.1. Introduction

The previous chapter focused on the preparation and characterization of the collagen CPC composites. The final goal of these materials is to be able to enhance the biological performance. Hydroxyapatite and collagen have been combined, mainly as macroporous tissue engineering scaffolds. Hydroxyapatite is known to be a biocompatible biomaterial *in vitro* as well as *in vivo*, with an osteoconductive potential<sup>1-3</sup>. Therefore it has been combined with collagen by several methods as described in chapter 1. However, in the collagen scaffolds, the matrix is composed of collagen, onto which small amounts of HA precipitate<sup>4-7</sup>. In the present chapter, the matrix of the material is the calcium

phosphate, and the effect of collagen on the *in vitro* biological performance is studied in this chapter.

In previous works in which collagen was mixed with a CPC, the biological aspects were not deeply studied<sup>8-11</sup>. The main effect that was reported in the previous works was the ability of the collagen to increase the initial adhesion on the CPC material. The effect of collagen on cell proliferation and differentiation on CPC based materials has not been previously studied. The concentration of the collagen solution incorporated in the CPC was 10 mg/ml, since higher collagen concentrations have reported no difference at early cell attachment on other CPC<sup>11</sup>.

## 3.2. Objectives

The objective of this chapter was to study the *in vitro* cell response to injectable calcium phosphate cement –collagen composite material. The effect of collagen addition, as well as the pre-treatment of the collagen to form solubilized or fibrillised collagen was investigated. The study was aimed at analyzing the initial adhesion of osteoblastic cells SaOs-2 on the material, as well as to observe the proliferation and differentiation after 1, 7 and 14 days.

## 3.3. Materials and methods

### 3.3.1. Materials

The study was done on 15 mm diameter disks. The disks were prepared by moulding the CPC paste in Teflon moulds of 15 mm in diameter and 2 mm in height. After 3 hours, the disks were unmolded and left reacting in Ringer's for 7 days in order to ensure the transformation of the  $\alpha$ -TCP into CDHA. The L/P used was 0.45 ml/g. The liquid phase of the CPC was a 50 mM acetic acid solution for the control and two different 10 mg/ml collagen solutions: solubilized and fibrillised.

The materials were coded using 4 letters. The first three letters corresponded to COL, which identified the samples as containing collagen, followed by C, meaning the initial particle size of the CPC, which was coarse in this case, followed by a number referring to the concentration of the collagen solution. Finally, the presence of and F at the end

indicated that the collagen had been fibrillised. The materials studied were then: COLC10, COLC10F and CTRLC. The CTRLC was CPC composed of coarse cement with acetic acid solution was coded as. The tissue culture plastic (empty well) was also used as control, being coded as TCPS. The materials were sterilized by immersion for 1 hour in 70% ethanol.

### **3.3.2. Cells**

Human osteoblast-like Saos-2 cells were used as cell model. The cells were maintained in McCoy medium (Sigma, M8403) supplemented with 0.75% of L-glutamine (GIBCO 25030), 1% penicillin/streptomycin (GIBCO 15140), 2 % of sodium pyruvate (GIBCO 11360) and 15 % of fetal bovine serum (GIBCO 10270-106) in a humidified atmosphere of 5% CO<sub>2</sub> in air. The culture medium was exchanged every second day. Upon confluence the cells were detached with a minimum amount of trypsin-EDTA (Gibco) that was inactivated with FBS after 5 minutes. The cells were then re-cultured or used for experiments.

Saos-2 cells were harvested from nearly confluent flasks as described above and seeded in 24 well plates. Afterwards, 1.5 ml of complete medium was added, changed after 24 hours and then changed every 48 hours.

### **3.3.3. Cell behavior on CPC/collagen composites**

#### *3.3.3.1 Initial adhesion*

In order to verify the effect of the presence of collagen in the CPC in terms of initial cell attachment, an initial adhesion assay was performed. 15 mm diameter disks were prepared as previously described. COLC10, COLC10F, CTRLC and TCPS samples were studied. The materials were left overnight in contact with serum free medium to wet the samples. On the next day, the cells were seeded on the materials at a concentration of 1.000.000 cells/well and were left in contact with the material for 4 hours. The samples were then removed and placed in another well plate and the number of cells attached to the material was quantified. The viability of the cells was estimated spectrophotometrically with the LDH assay and the cell morphology was assessed by fluorescence microscopy after FDA staining.

### 3.3.3.2 Cell proliferation and cell differentiation

For the same materials used in the initial adhesion test, 100.000 cells were seeded per well, which represented approximately 14.000 cell/cm<sup>2</sup>. Proliferation, performed with an LDH kit, differentiation, measured by the quantification of ALP activity, as well as FDA and SEM images after 1, 7 and 14 days were taken.

## 3.3.4. Characterization

### 3.3.4.1. Proliferation

Relative cell numbers were evaluated at 1, 7, and 14 days by the lactate dehydrogenase (LDH) assay. The LDH activity was then determined spectrophotometrically with a commercially available LDH kit (Roche, Germany) in a plate reader (Power WaveX, Bio-Tek Instruments, USA; 490 nm). For that purpose, at each time point, the samples were washed twice with PBS and lysed by freeze-thawing, following at least two repeating cycles in the culture plate. The lysates were then transferred into eppendorfs. The lysates were centrifuged at 1500 rpm for 10 min to remove cell debris. Aliquots of the samples were placed on 96 well plates to obtain a final sample volume of 100 µl, after the corresponding dilution. Afterwards, 100 µl of the reaction mixture was placed on the wells, with the previously added sample. The reaction mixture was composed of the mixture of the catalyst, which is a mixture of Diaphorase/NAD<sup>+</sup>, and the dye solution, which is composed of Iodotetrazolium chloride and sodium lactate (Figure 3.1). The mixture of the reaction mixture and the samples aliquots, were left reacting for 30 minutes, after which 50 µl of a stop solution, composed of 1M HCl, was placed in each well in order to stop the reaction. A calibration curve with decreasing concentrations of cells was created to express results in cell number.

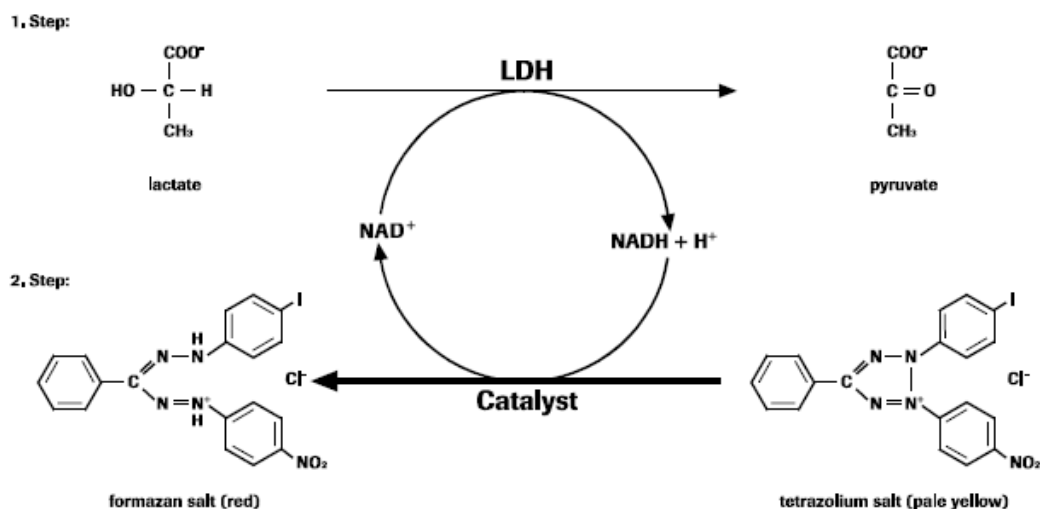


Figure 3.1. Diagram of LDH oxidation of lactate into pyruvate through the reduction of  $\text{NAD}^+$  to  $\text{NADH}$ . The reaction in step 2 shows how the tetrazolium salt is reduced to a formazan salt which has the red coloration of the end product which is done through the help of the catalyst and the oxidation of the  $\text{NADH}$  to  $\text{NAD}^+$  (From LDH kit Roche).

### 3.3.4.2. Differentiation

The retention of osteoblastic phenotype was evaluated by measuring alkaline phosphatase activity. No osteogenic medium was used. A colorimetric method, based on the conversion of p-nitrophenyl phosphate into p-nitrophenol in the presence of alkaline phosphatase, was used. The lysates obtained in the previous section were mixed with 2-Amino-2-methyl-1-propanol buffer (Sigma Diagnostics Inc A9226.) and phosphatase substrate solution (Sigma, 4 mg/ml P5994), and incubated for 30 minutes at  $37^\circ\text{C}$ . The reaction was stopped with 0.05 M NaOH and the production of p-nitrophenol was determined by measuring the absorbance at 405 nm. The values were calibrated to a standard curve, prepared from known concentrations of p-nitrophenol (Sigma N7660), and the results for alkaline phosphatase activity were normalized to the number of cells on each sample.

### 3.3.4.3. Fluorescein Diacetate staining

To follow the overall morphology of adhering living cells, fluorescence images were obtained after the fluorescein diacetate staining (FDA, Invitrogen F1303) (Figure 3.2.), to obtain control on cell viability. At given time of incubation, the living cells were labeled with fluorescein diacetate (FDA), by adding  $10\ \mu\text{l/ml}$  from a stock of 1 mg/ml

FDA in acetone to the medium. Under these conditions, the vital cells converted FDA in a fluorescent analogue via their esterases. The dye was then removed and rinsed three times with water and observed with PBS at 37°C. Representative pictures of the adhered cells were then taken with a fluorescent microscope (Nikon, Eclipse E600) using the green channel.

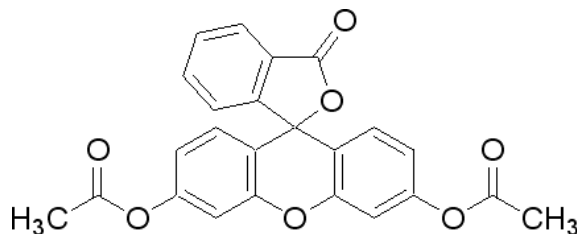


Figure 3.2. Representation of the Fluorescein Diacetate molecule.

#### 3.3.4.4. Scanning Electron Microscopy

Cell morphology was further characterized by means of SEM. For that purpose, the samples were washed in 0.1M Phosphate buffer, pH 7.4, and cells were fixed with a 2.5% glutaraldehyde (Sigma-Aldrich G400-4) solution in PBS, washed and maintained in 0.1M phosphate buffer. Osmium tetroxide (Sigma-Aldrich 201013) was added after fixation, and graded ethanol solutions were used to dehydrate the samples (50, 70, 90, 96 and 100% ethanol). Finally hexamethyldisilazane (HDMS, Fluka 52620) was used for complete dehydration of the samples, being air-dried afterwards.

#### 3.3.5. Statistical analysis

Statistical analysis was carried out with significance of 5%. One way analysis of variance (ANOVA) with Fisher post-hoc test was conducted. The data are expressed as mean  $\pm$  standard deviation.

### 3.4. Results

#### 3.4.1. Initial cell adhesion

The fluorescent images after FDA staining for the different materials showed the initial attachment after 4 hours in serum-free medium (Figure 3.3). In general, cells appeared

to be rounded, although some cells were starting to expand. There were some differences between the different materials concerning the amount of the cells observed. In CTRLC (Figure 3.3.a and b) and COLC10F (Figure 3.3.e and f), the number of cells present was similar. However, for the COLC10 (Figure 3.3.c and d), there were a higher number of cells compared to the other two substrates.

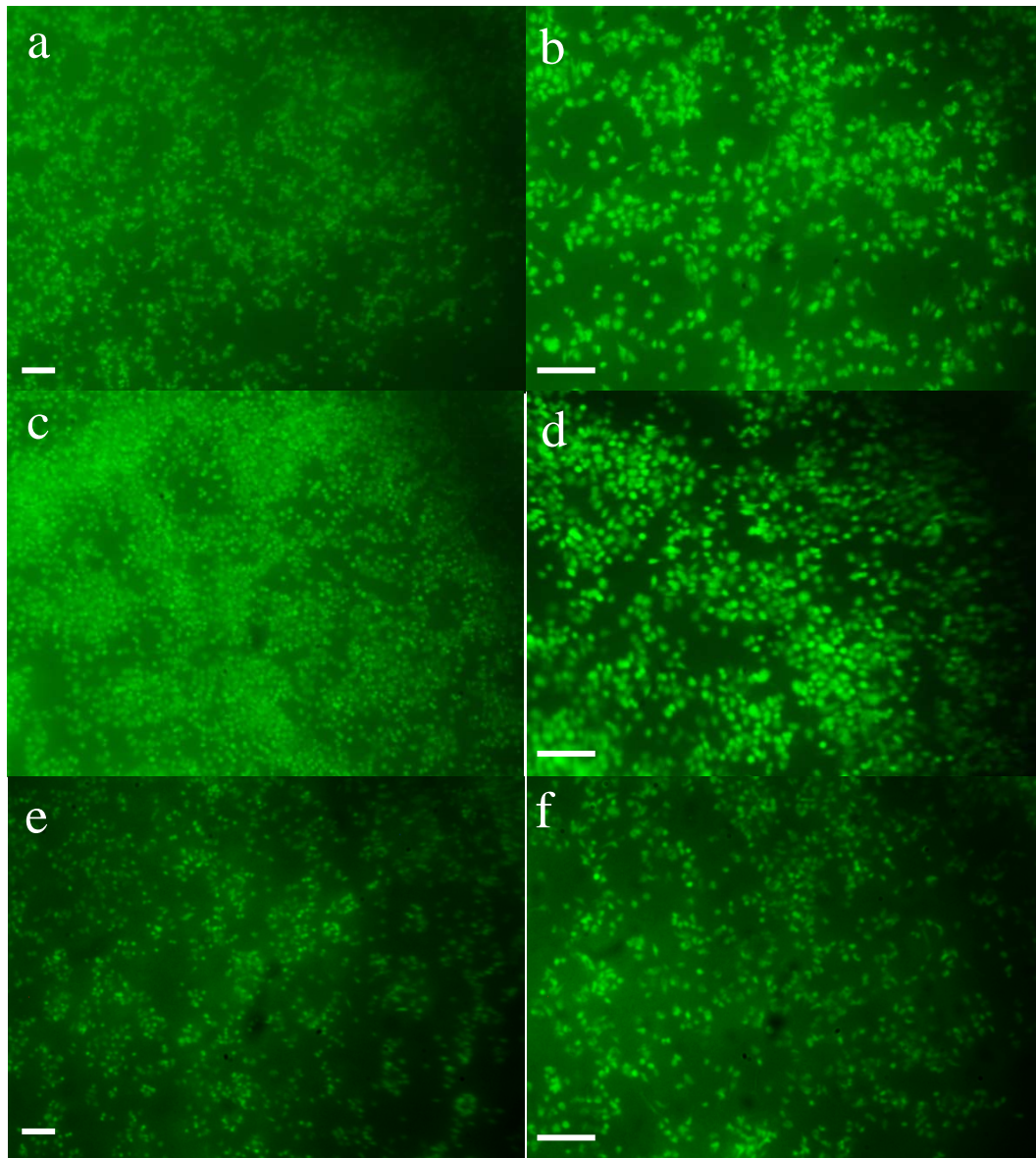


Figure 3.3. Initial adhesion of Saos-2 cells after 4 hours on the different materials at two different magnifications. a) and b) CTRLC, c) and d) COLC10, e) and f) COLC10F. Scale bar = 100  $\mu\text{m}$ .

Figure 3.4 shows the number of cells that attached to different CPC materials and the TCPS measured by LDH. TCPS presented the highest value of cells attached, although only 300.000 cells out of the 1.000.000 initially seeded attached, which represented a



30% of cell attachment. On the other hand, the amount of cells that attached to the CTRLC was 100.000, representing a 10% of the cells initially attached. These values were further increased in the presence of collagen for the samples COLC10 and COLC10F, arriving to values close to those of TCPS, being 25% and 15% respectively of cell attachment.

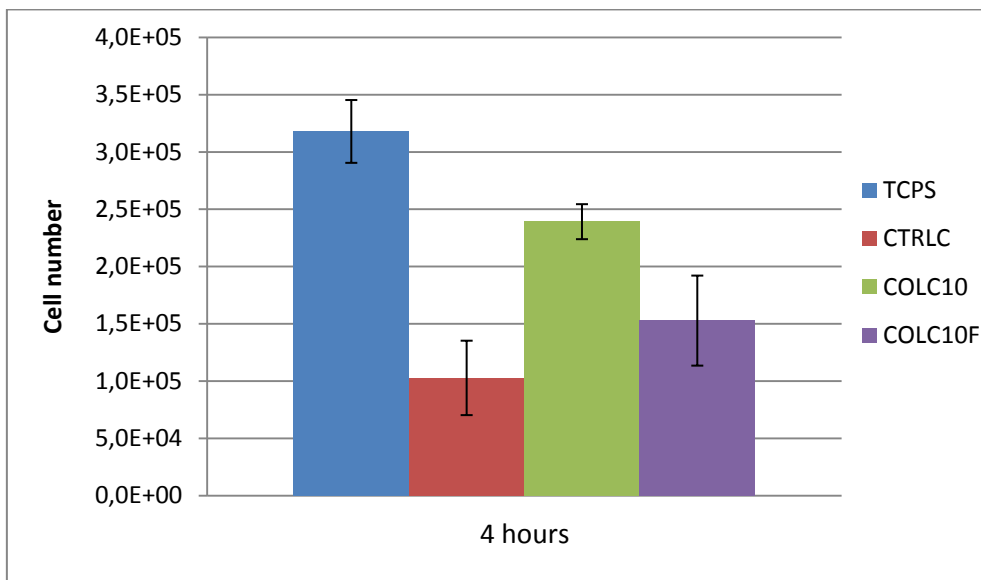


Figure 3.4. Quantification of number of cells after 4 hours, representing the number of cells that have attached to the well and the number of cells extracted from the material.

### 3.4.2. Cell proliferation and cell differentiation

#### 3.4.2.1. Proliferation

The results for proliferation at 1, 7 and 14 days are shown in Figure 3.5. Initially, after 1 day the number of cells was low in the 4 cases, having a higher number in the TCPS. After 7 days, the number of cells on TCPS raised considerably, whereas it remained low for CTRLC and COLC10F. However, in COLC10 the number of cells was three times higher than for the CTRLC and COLC10F. Finally, after 14 days, the proliferation for COLC10 was higher than the CTRLC, and was also higher than the COLC10F. The CTRLC and the COLC10F samples seemed to behave in a similar way, not presenting significant differences among them.

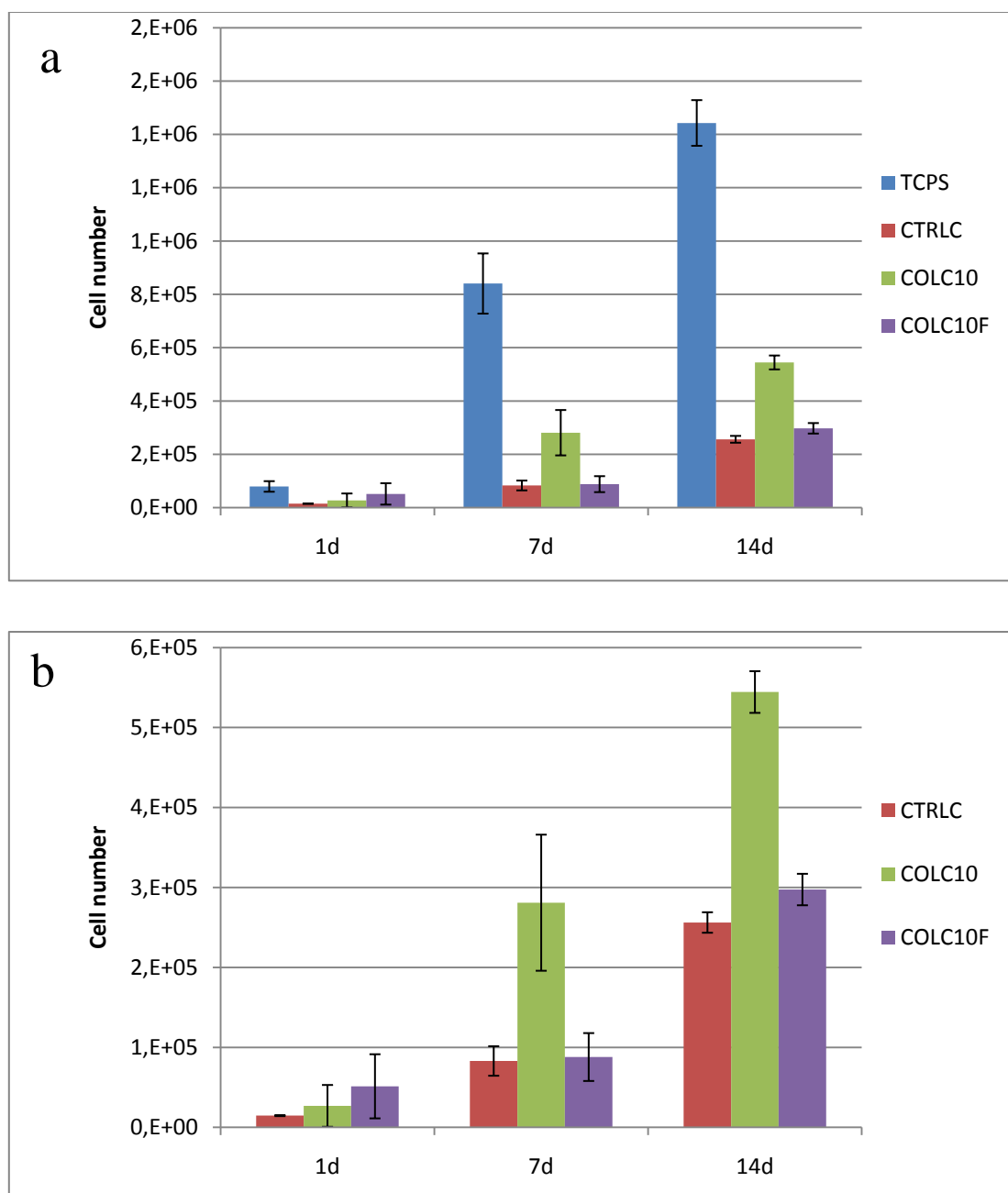


Figure 3.5. Number of cells measured by LDH after 14 days of culture for the a) TCPS, CTRLC, COLC10F and COLC10. In b) the cell number is only expressed for the CPC materials in order to observe more clear the differences among the CPC materials.

### 3.4.2.2. Differentiation

The results for differentiation at 1, 7 and 14 days measured by means of ALP activity are shown in Figure 3.6. The media did not present osteogenic factors. The first observation that can be made is that when the CPC was present, the ALP activity was significantly higher than that of the TCPS. Furthermore, there were two clear ALP evolution patterns. For the TCPS and CTRLC, the ALP values raised from 1 to 7 days,

obtaining its peak at 7 days, and decreasing afterwards at 14 days. However, for the collagen containing CPC, the maximum was achieved after 1 day, decreasing its value progressively after 7 and 14 days.

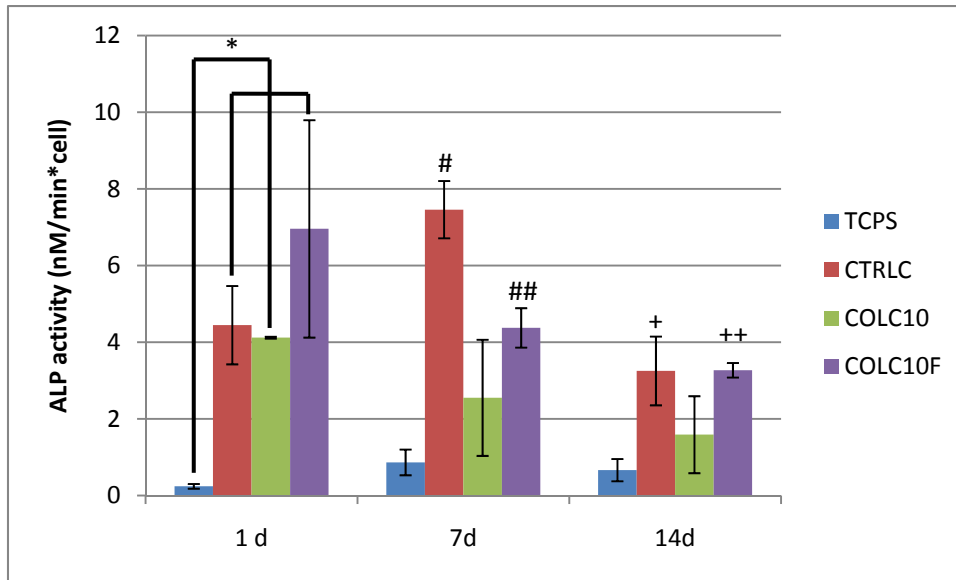


Figure 3.6. Alkaline phosphatase activity after 14 days of culture for the TCPS, CTRLC, COLC10F and COLC10. \* denotes significant differences between COLC10F and COLC10. \* denotes significant differences between TCPS and the rest of the materials at 1 day. # denotes significant differences between CTRLC and the rest of the materials. ## denotes significant differences between COLC10F and TCPS and CTRLC. + denotes significant differences between CTRLC and TCPS. ++ denotes significant differences between COLC10F and TCPS and COLC10.

### 3.4.2.3. Overall cell morphology

The cell morphology observed by SEM for 1, 7 and 14 days can be observed in Figures 3.7, 3.8 and 3.9. In general, the main difference that was observed was that, in COLC10F, cells were more elongated. That is, cells expanded their phyllopodia to find the best focal adhesion on the material. For CTRLC and COLC10, the cells were shown to have a more homogenous spread zone. In COLC10, cells were flat and expanded, whereas in the CTRLC, cells were smaller and more shrank. This behavior was found at 1, 7 and 14 days.

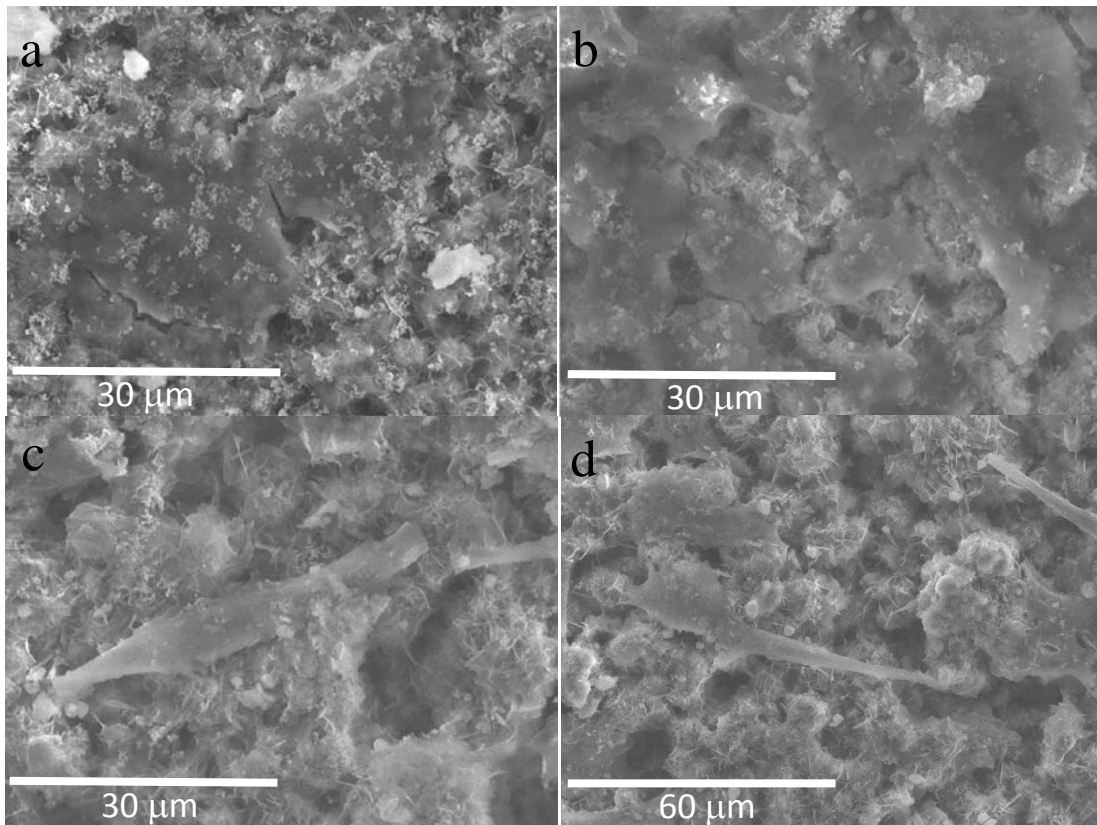


Figure 3.7. Cell morphology observed by SEM after 24 hours of culture for a) CTRLC, b) COLC10 and c) and d) COLC10F.

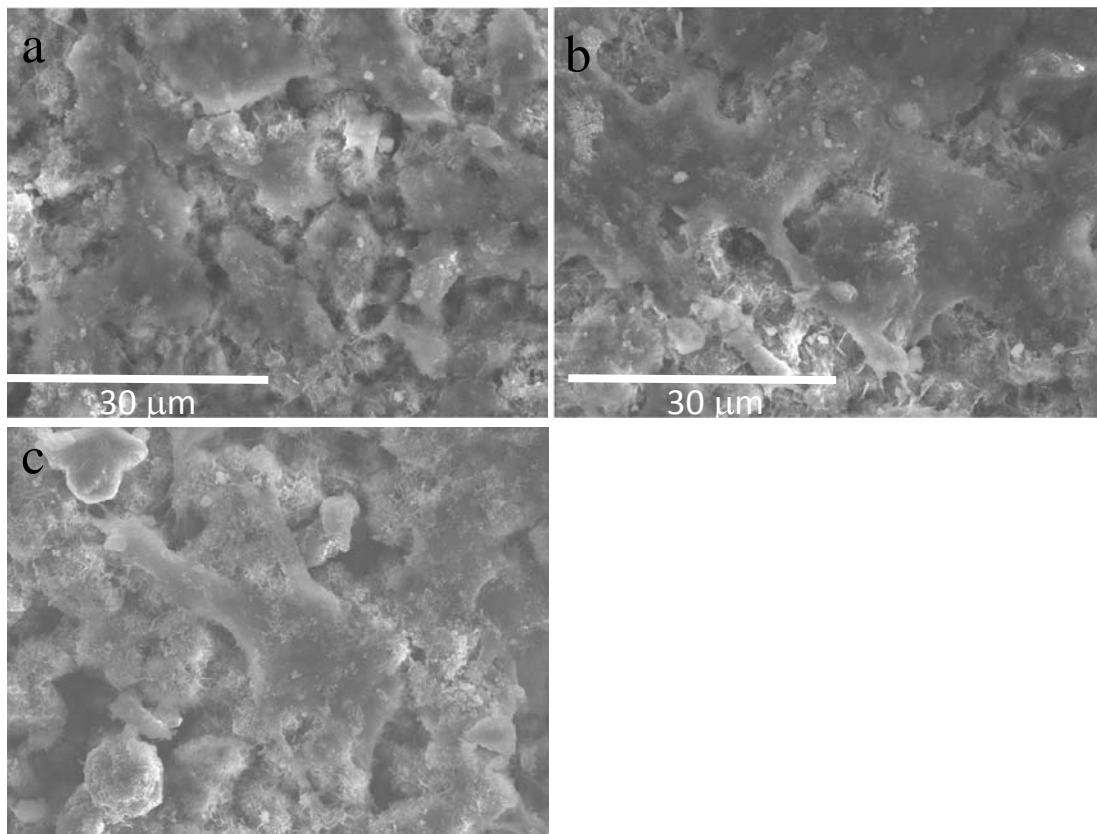


Figure 3.8. Cell morphology observed by SEM after 7 days of culture for a) CTRLC, b) COLC10 and c) COLC10F.

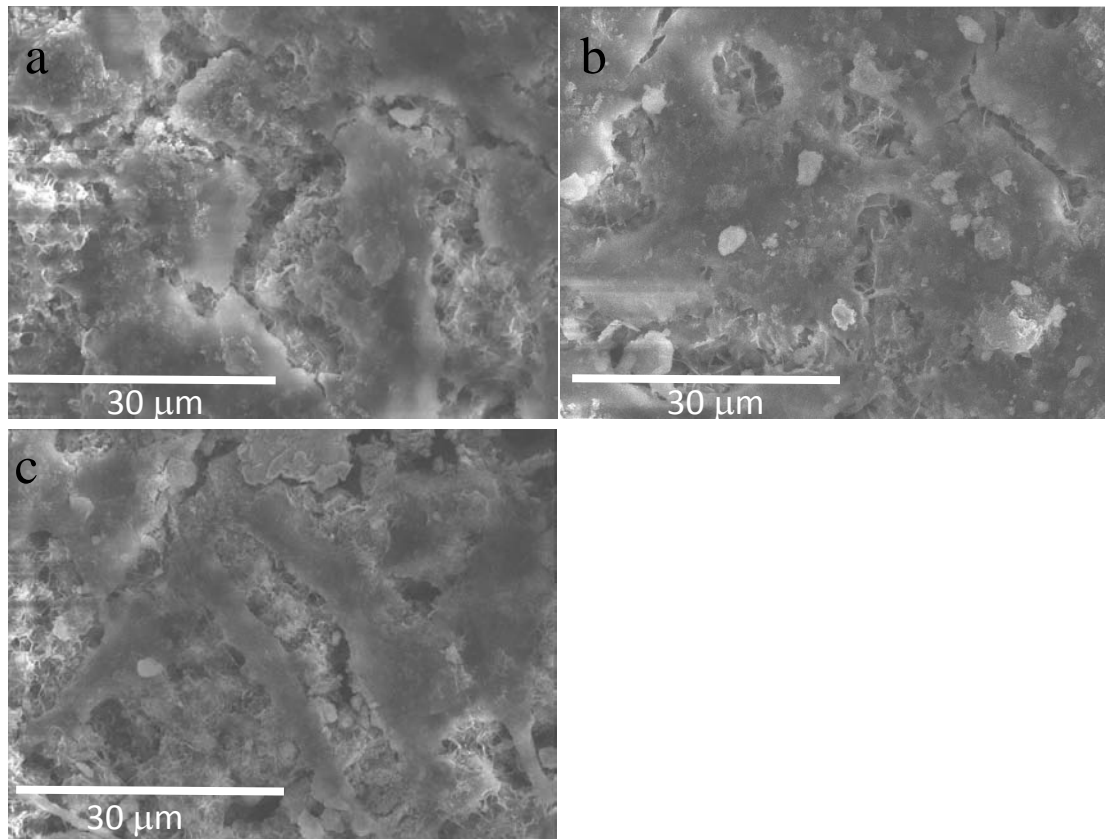


Figure 3.9. Cell morphology observed by SEM after 14 days of culture for a) CTRLC, b) COLC10 and c) COLC10F.

### 3.5. Discussion

The main objective of this chapter was to assess the enhancement of the biological properties of the CPC in the presence of collagen. It is known that collagen has the aminoacid sequences recognized by the integrins that enhance cell adhesion (e.g. GFOGER). If the integrins do not recognize any protein on the surface of the material or in any type of surface, the cells will have difficulties to attach.

In order to understand what happened in the initial stage of interaction material-cell, a cellular adhesion experiment was conducted. It is important to highlight, that in general, apatitic substrates have lower adhesion and proliferation than the TCPS, and similar results have previously been reported<sup>12-17</sup>. It was seen that only 10% of the cells initially seeded on the CTRLC attached to the material (Figure 3.4). Nevertheless, the incorporation of collagen in the CPC raised the cell adhesion values to 15% for the CPC containing fibrillised collagen and 25% for the CPC containing solubilized collagen.

These values were considered as a significant increase, especially if these are compared to the optimum material, which was the TCPS that had 30% of cell attachment. The results are in accordance with a previous work, in which a CPC was mixed with water and then collagen powder was aggregated, performing a small *in vitro* study, and what was observed was that the presence of collagen increased the number of attached cells on the substrates<sup>9</sup>. In that case, the amount of cells that initially attached was around 50%, whereas in our case it was around 25% for the solubilized collagen sample. Nevertheless, the ratio of adhered cells respect the CPC without the collagen in that study and in our study is constant, being the initial adhesion around 2.5 times higher in the presence of collagen compared to the CPC without collagen<sup>9</sup>. The increase in cell adhesion in the presence of collagen is due to the presence of the GFOGER aminoacid sequence, among others, that stimulate cell adhesion<sup>18</sup>.

The initial attachment pattern was then continued in the culture for 14 days, in which it was seen that the proliferation was the highest for the TCPS (Figure 3.5). TCPS, as in the case of the cell attachment experiment, continued presenting higher cell number than the CPC containing samples, which was an expected result as previously demonstrated for apatitic substrates<sup>12,14-16,17</sup>. However, the proliferation rates for the CPC containing materials behaved similar to those found previously in this type of CPC without collagen, in which the number of cells was low after 1 and 7 days<sup>12</sup>. Actually, in the previous study, they compared the effect on cell behavior of the two different initial particle size, showing a higher proliferation for a coarse and a higher differentiation for fine cements<sup>12</sup>. In our study, the coarse CPC was used in order to enhance the cellular proliferation.

The lower rates of proliferation in the apatitic substrates may be related with the presence of a crystal morphology in the surface<sup>19-21</sup>. This crystal morphology reduces and delays cell attachment, and consequently, cell proliferation. The same crystal morphology was found in the collagen containing CPC, however, the collagen increased the proliferation rates for the CPC, although the increase was only found for the solubilized collagen, whereas the fibrillised collagen behaved in a similar way to the CTRLC. Furthermore, it has also been previously reported that a material with similar inorganic phase, being  $\alpha$ -TCP, could be cytotoxic even when the transformation into CDHA had taken place<sup>22</sup>. It has also been studied that the liberation of CPC particles

into the medium smaller than 10  $\mu\text{m}$ , could inhibit cell proliferation<sup>23</sup>. However, collagen promoted cellular adhesion<sup>18</sup> and it also reduced the amount of CPC particles liberated to the medium, which were seen by simple visual inspection of the different wells. This last feature was also previously observed and was attributed to the higher cohesion CPC presented in the presence of collagen<sup>9</sup>.

Regarding the cell morphology observed by SEM, it was seen that the cell morphology presented a shrank morphology for the CPC not containing collagen (Figure 3.7, 3.8 and 3.9). In the collagen containing CPC, the cells presented higher protrusions, which was a similar behavior found in a previous work that combined HA with collagen, in which a better cell spreading was found for the composite<sup>24</sup>. It was also found that the cell morphology was found to be different depending on the collagen pre-treatment. The explanation for the different cell morphology depending on the collagen treatment could be related with the collagen distribution in the CPC matrix. In the presence of solubilized collagen, the collagen was distributed throughout the whole surface, having the aminoacids sequence present in the whole material. The integrins in the cell recognized this extracellular matrix and attached to the surface. In the samples with fibrillised collagen, the distribution was heterogeneous, presenting bundles of collagen in certain areas and no collagen in other areas. The average distance between the different collagen bundles was approximately 50  $\mu\text{m}$  as derived from the fluorescence images in chapter 2 (Figure 2.10 and 2.11). Cells would have a higher affinity to attach to the parts of the material in which the collagen sequences were present. That is why cells would move their phyllopodia into zones in which there was collagen. In other words, cells had to stretch much more their protrusions to find collagen in the surface, showing the elongated cell structure. The cell morphology observed by SEM is schematically represented in Figure 3.10, in which the green areas represent the collagen and the red color represents the cells. It can be seen that in the case of homogenous collagen distribution, cells spread their protrusions in all directions, whereas in the case of the heterogeneous collagen distribution, cells expand their phyllopodia to determined parts of the material in which the collagen is present.

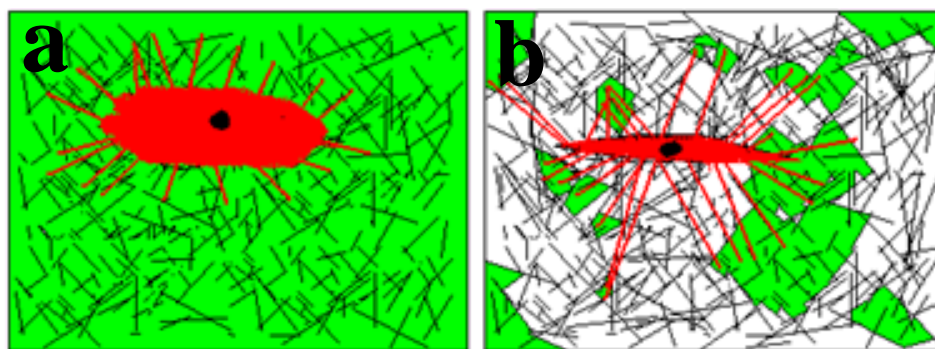


Figure 3.10. Schematic representation of cell attachment for the collagen CPC composites: a) COLC10, b) COLC10F. The white and black background represents the CDHA, whereas the green signal represents the collagen. a) Cells spread since cells are able to recognize the different adhesion motifs found in collagen, distributed homogeneously on the surface of the composite, through the integrins. b) Cells expanding their filopodia in order to find the adhesion motif of collagen, which is distributed heterogeneously on the fibrillated collagen CPC composite, therefore, presenting a more stretched cellular morphology.

The differentiation patterns analyzed by ALP activity clearly showed higher ALP values for the CPC samples compared to the TCPS (Figure 3.6). Regarding the cell differentiation, it was observed that the presence of the CPC significantly increased the differentiation compared to TCPS. This was also previously reported and was attributed to the crystal morphology of the CPC<sup>12</sup>. HA has been proved to have high differentiation activities<sup>25-28</sup> and was therefore the main effect for the higher ALP activity on the CPC substrates.

Nevertheless, it was interesting to note that the differentiation in the presence of collagen changed the pattern compared to the CTRLC. It was shown that in the presence of collagen, there was a high initial ALP activity and this one decreased with time. In the CTRLC, the peak of ALP was found at 7 days and then decreased. Therefore, the mechanism by which the cells interacted with the sample might have been different, obtaining an earlier differentiation in the presence of collagen compared to the CPC without collagen. A hypothesis is that the cell interaction with the CPC has a different integrin binding. For the CTRLC and TCPS, the binding is produced through an RGD-dependent mechanism via the  $\alpha 5 \beta 1$  integrin, whereas in the presence of collagen type I, the anchorage is through integrin  $\alpha 2 \beta 1$ , which is known to induce osteoblastic differentiation and can therefore serve as cell attachment and differentiation factor<sup>29-32</sup>. An increase in ALP values by the  $\alpha 2 \beta 1$  integrin present in collagen has been previously reported compared to TCPS<sup>33</sup>. Furthermore, composite materials comprising



collagen and calcium phosphate have also shown an increase in osteoblastic differentiation even at short times<sup>7</sup>. Therefore, although the main effect of the increased ALP values was the CPC itself and that the collagen barely had a significant effect on the differentiation values, it was important to highlight that the presence of collagen seemed to advance the differentiation pattern.

### **3.6. Conclusions**

The results have shown that the presence of collagen enhanced cell adhesion on CPC-based substrates by a factor of 2.5. Proliferation was also enhanced in the presence of collagen. Differentiation was high in the presence of the CPC compared to the control. Collagen changed the differentiation pattern, having the ALP peak after 1 day, whereas in the absence of collagen, the peak was found at 7 days. The form in which collagen was incorporated could also tailor the cell behavior, having a slightly higher ALP activity for the fibrillised collagen, compared to the solubilized collagen, in which the proliferation was enhanced.

### 3.7. References

1. Takechi M *et al.* Initial histological evaluation of anti-washout type fast-setting calcium phosphate cement following subcutaneous implantation. *Biomaterials* **19**, 2057-2063 (1998).
2. Miyamoto Y *et al.* Non-decay type fast-setting calcium phosphate cement: setting behavior in calf serum and its tissue response. *Biomaterials* **17**, 1429-1435 (1996).
3. Miyamoto Y *et al.* In vivo setting behavior of fast-setting calcium phosphate cement. *Biomaterials* **16**, 855-860 (1995).
4. Sionkowska A & Kozłowska J. Characterization of collagen/hydroxyapatite composite sponges as a potential bone substitute. *International Journal of Biological Macromolecules* **47**, 483-487 (2010).
5. Gleeson JP, Plunkett NA & O'Brien FJ. Addition of hydroxyapatite improves stiffness, interconnectivity and osteogenic potential of a highly porous collagen-based scaffold for bone tissue regeneration. *European Cells and Materials* **20**, 218-230 (2010).
6. Tsai SW, Hsu FY & Chen PL. Beads of collagen-nanohydroxyapatite composites prepared by a biomimetic process and the effects of their surface texture on cellular behavior in MG63 osteoblast-like cells. *Acta Biomaterialia* **4**, 1332-1341 (2008).
7. Dawson JI *et al.* Development of specific collagen scaffolds to support the osteogenic and chondrogenic differentiation of human bone marrow stromal cells. *Biomaterials* **29**, 3105-3116 (2008).
8. Miyamoto Y *et al.* Basic properties of calcium phosphate cement containing atelocollagen in its liquid or powder phases. *Biomaterials* **19**, 707-715 (1998).
9. Tamimi F. *et al.* Brushite-collagen composites for bone regeneration. *Acta Biomaterialia* **4**, 1315-1321 (2008).

10. Touny AH, Bhaduri S & Brown PW. Formation of calcium deficient HAp/collagen composites by hydrolysis of  $\alpha$ -TCP. *Journal of Materials Science: Materials in Medicine* **21**, 2533-2541 (2010).
11. Moreau JL, Weir MD & Xu HHK. Self-setting collagen-calcium phosphate bone cement: Mechanical and cellular properties. *Journal of Biomedical Materials Research* **91A**, 605-613 (2009).
12. Engel E *et al.* Discerning the role of topography and ion exchange in cell response of bioactive tissue engineering scaffolds. *Tissue Engineering* **14**, 1341 (2008).
13. Deligianni DD, Katsala ND, Koutsoukos PG & Missirlis YF. Effect of surface roughness of hydroxyapatite on human bone marrow cell adhesion, proliferation, differentiation and detachment strength. *Biomaterials* **22**, 87-96 (2001).
14. Knabe C *et al.* Evaluation of calcium phosphates and experimental calcium phosphate bone cements using osteogenic cultures. *Journal of Biomedical Materials Research* **52**, 498-508 (2000).
15. Link DP, van den Dolder J, Wolke JGC & Jansen JA. The cytocompatibility and early osteogenic characteristics of an injectable calcium phosphate cement. *Tissue Engineering* **13**, 493-500 (2007).
16. Yuasa T *et al.* Effects of apatite cements on proliferation and differentiation of human osteoblasts in vitro. *Biomaterials* **25**, 1159-1166 (2004).
17. Oreffo ROC, Driessens FCM, Planell JA & Triffitt JT. Growth and differentiation of human bone marrow osteoprogenitors on novel calcium phosphate cements. *Biomaterials* **19**, 1845-1854 (1998).
18. Heino J. The collagen family members as cell adhesion proteins. *Bioessays* **29**, 1001-1010 (2007).
19. Zhang W, Walboomers XF, Van Osch G, Van den Dolder J & Jansen JA. Hard tissue formation in a porous HA/TCP ceramic scaffold loaded with stromal cells

- derived from dental pulp and bone marrow. *Tissue Engineering* **14**, 285-294 (2008).
20. Bjerre L, Bünger C, Baatrup A, Kassem M & Mygind T. Flow perfusion culture of human mesenchymal stem cells on coralline hydroxyapatite scaffolds with various pore sizes. *Journal of Biomedical Materials Research* **97A**, 251-263 (2011).
  21. Liu Y *et al.* Influence of calcium phosphate crystals morphology on the adhesion, spreading and growth of bone derived cells. *Journal of Biomedical Materials Research* **90A**, 972-980 (2009).
  22. dos Santos LA *et al.*  $\alpha$ -Tricalcium phosphate cement: "in vitro" cytotoxicity. *Biomaterials* **23**, 2035-2042 (2002).
  23. Pioletti DP *et al.* The effects of calcium phosphate cement particles on osteoblast functions. *Biomaterials* **21**, 1103-1114 (2000).
  24. Zhu X *et al.* Characterization of nano hydroxyapatite/collagen surfaces and cellular behaviors. *Journal of Biomedical Materials Research* **79A**, 114-127 (2006).
  25. Turhani D *et al.* In vitro growth and differentiation of osteoblast-like cells on hydroxyapatite ceramic granule calcified from red algae. *Journal of Oral and Maxillofacial Surgery* **63**, 793-799 (2005).
  26. Ohgushi H, Dohi Y, Tamai S & Tabata S. Osteogenic differentiation of marrow stromal stem cells in porous hydroxyapatite ceramics. *Journal of Biomedical Materials Research* **27**, 1401-1407 (1993).
  27. Mygind T *et al.* Mesenchymal stem cell ingrowth and differentiation on coralline hydroxyapatite scaffolds. *Biomaterials* **28**, 1036-1047 (2007).
  28. Rosa AL, Beloti MM & Van Noort R. Osteoblastic differentiation of cultured rat bone marrow cells on hydroxyapatite with different surface topography. *Dental Materials* **19**, 768-772 (2003).

29. Mizuno M, Fujisawa R & Kuboki Y. Type I collagen-induced osteoblastic differentiation of bone-marrow cells mediated by collagen-alpha2beta1 integrin interaction. *Journal of Cell Physiology* **184**, 207-213 (2000).
30. Salaszyk RM, Williams WA, Boskey A, Batorsky A & Plopper GE. Adhesion to vitronectin and collagen I promotes osteogenic differentiation of human mesenchymal stem cells. *Journal of Biomedical Biotechnology* **2004**, 24-34 (2004).
31. Takeuchi Y *et al.* Differentiation and transforming growth factor-beta receptor down-regulation by collagen-alpha2beta1 integrin interaction is mediated by focal adhesion kinase and its downstream signals in murine osteoblastic cells. *Journal of Biological Chemistry* **272**, 29309-29316 (1997).
32. Carvalho RS, Kostenuik PJ, Salih E, Bumann A & Gerstenfeld LC. Selective adhesion of osteoblastic cells to different integrin ligands induces osteopontin gene expression. *Matrix Biology* **22**, 241-249 (2003).
33. Mizuno M & Kuboki Y. Osteoblast-related gene expression of bone marrow cells during the osteoblastic differentiation induced by type I collagen. *Journal of Biochemistry* **129**, 133-138 (2001).

# **Chapter 4: Cell Response to Collagen-Calcium Phosphate Cement Scaffolds Investigated for Nonviral Gene Delivery**

## **4.1. Introduction**

The present chapter is the result of the collaboration with the group of Tissue Engineering Laboratories led by Professor Myron Spector at the VA Boston Healthcare System, in association with the department of Materials science at MIT and Harvard Medical School. This work was developed in Boston during a PhD stay for 9 months.

The strategy taken in this chapter differs considerably from the previous chapters. The reason is that in the previous chapters, the combination of the calcium phosphate cement and the collagen formed a mouldable and injectable paste which was able to adapt to any shape and was able to set *in vivo*. In the present chapter, a tissue

engineering approach was taken, in which a mineralized collagen scaffold was fabricated. This pre-formed scaffold was neither injectable nor self-setting. Nevertheless, in this approach the mineralized collagen scaffold had a higher degree of macroporosity which allowed a higher cell penetration, important for bone tissue engineering applications.

In general, an ideal bone graft should present a 3D network that provides support volume and attachment sites to the cells, namely the extracellular matrix; growth factors, which may induce osteogenesis and vascularization; and the presence of cells with osteogenic potential<sup>1</sup>. The design of synthetic bone grafts should aim at the development of constructs able to develop the same functions described above, and therefore should cover not only the intrinsic properties of the material itself, but also include specific biological functionalities directed to its osteogenic potential.

The fabrication of three dimensional collagen scaffolds has been widely explored for the regeneration of several tissues<sup>2-5</sup>. Collagen scaffolds have proven to have good biological properties for tissue engineering, but presenting low stiffness. The incorporation of calcium phosphates into the scaffold can be used as a strategy not only to increase their stiffness, but also their osteoconductive potential<sup>6,7</sup>. There are three main routes used to obtain composite collagen/CaP scaffolds: i) soaking a collagen sponge in calcium phosphate containing solution<sup>8-14</sup>; ii) simultaneous precipitation of calcium phosphate solutions at neutral pH with collagen solutions<sup>15-23</sup> and iii) freeze drying of slurries composed of calcium phosphate and collagen<sup>24-28</sup>. In general, the first method is considered the fastest method to obtain mineralized collagen, although it is difficult to control the amount of calcium deposited. In the second method it was shown that it is possible to get the c-axes of HA crystals aligned along the direction of the collagen fibers, which is similar to the structure found in bone<sup>22</sup>. The third method allows controlling the ratios of the calcium phosphate incorporated in the collagen scaffold, being usually in the range of 0.15 to 8 HA:collagen wt ratio<sup>26-28</sup>.

The combination of three dimensional scaffolds with growth factors has proven to be an effective approach for the regeneration of bone, being able to make the scaffolds osteoinductive<sup>29</sup>. One of the main challenges is to be able to deliver the growth factor (such as bone morphogenetic proteins, BMPs) *in vivo* at a therapeutic level due to the short lives of the molecules and its high cost<sup>30</sup>. Gene therapy has appeared as an

alternative, in which the cells are able to produce a specific protein when a gene is properly transferred into the cells<sup>31</sup>.

In the gene therapy approach, two main mechanisms by which the cells are transfected can be found: viral and non-viral vehicles. Both systems have been employed to incorporate high doses of proteins for tissue engineering applications. Viral vectors are known to have higher transfection efficiency, although they present high immunogenicity, making non-viral transfection the most appropriate gene delivery vehicle for tissue engineering applications<sup>32</sup>.

Calcium phosphate (CaP) based approaches are an attractive option for non-viral plasmid DNA transfection into cultured cells<sup>33</sup>. They are usually based on the use of CaP as nanoparticles<sup>34-37</sup>. Their sizes are in the range of 300 nm and the mechanism by which the cells were transfected was by endocytosis of the nanoparticles<sup>37</sup>. Nevertheless, these nanoparticles are not viable scaffolds on top of which cells can be seeded. Therefore, the purpose of this work was to develop a collagen-hydroxyapatite (HA) scaffold for the non-viral delivery of the plasmid encoding the osteoinductive protein BMP-7. The intention was to provide a local and prolonged release of this growth factor by the cells seeded or migrating within the scaffold. As an innovative route, the collagen-HA scaffold was obtained by the combination of a calcium phosphate cement (CPC) in a collagen template. The CPC was composed of  $\alpha$ -tricalcium phosphate ( $\alpha$ -TCP), which upon hydrolysis, transforms into hydroxyapatite (HA), therefore leading to the precipitation of HA nanometric crystals within the collagen matrix.

## 4.2. Objectives

The specific aim of this study was to develop collagen/CPC scaffolds with different amounts of inorganic phase (13, 23 or 83% wt) and to evaluate their effect on cell behavior. Moreover, the delivery of the BMP-7 plasmid incorporated in the scaffolds into mesenchymal stem cells (MSCs) *in vitro* and the expression of the protein was also assessed when varying the amount of plasmid incorporated.



## 4.3. Materials and methods

### 4.3.1. Collagen preparation

A mixture of porcine collagen type I and type III, named as collagen type I/III (obtained from Geistlich Biomaterials, Wolhusen, Switzerland), was used. In order to solubilize the collagen, the collagen powder was introduced in a 10 mM HCl solution at a 1% wt concentration. The solution was then blended at 14,000 rpm in order to solubilize the collagen and maintained at 4°C through a refrigerating system. The collagen was blended for 6 hours for the complete dissolution of the powder.

### 4.3.2. Calcium phosphate cement powder

The powder phase of the composite was prepared as previously described in chapter 2, section 2.3.1 using the coarse CPC.

### 4.3.3. Preparation of the scaffolds

The  $\alpha$ -TCP powder was dispersed in 1 ml of distilled water. The  $\alpha$ -TCP suspension was then incorporated in the dissolved collagen. The collagen and the  $\alpha$ -TCP were mixed in the overhead blender at 6000 rpm for 1 hour at 4°C. The following samples were prepared: 13, 23 and 83 wt% HA (g HA/g composite); and the collagen without TCP (0% HA). After the fabrication process, the samples were immediately placed in the freeze-dryer (Virtis Advantage) and freeze dried for 20 hours at -40°C and 200 mTorr. Once the freeze-drying process was done, the samples were crosslinked with a dehydrothermal method at 105 °C and 30 mm Hg with vacuum for 24 hours. This treatment leads to the formation of covalent linkages among the polypeptide chains of the collagen fibers by slowly removing the water, resulting in an increase in the strength of the collagen<sup>38,39</sup>. The samples were then cut with a forensic punch to obtain 8 mm diameter and 2 mm thick samples. The scaffolds were then hydrated by immersion in graded alcohols: 100%, 96%, 90%, 70% and water. Further crosslinking was performed with 14 mM 1-ethyl-3-(3-dimethylaminopropyl) carbodiimide hydrochloride and 5.5 mM N-hydroxysuccinimide (EDAC; Sigma Chemical Co, St Louis, MO, USA) applied for 30 minutes at room temperature. The excess of crosslinking agent was washed out by rinsing in PBS. The scaffolds were subsequently immersed in water for 5 days for the complete reaction of the  $\alpha$ -TCP into HA.

#### 4.3.3.1. Scaffold characterization

In order to identify the mineral phase formed in the scaffold, the samples were digested in 500 µg/ml proteinase K solution dissolved in Tris-HCl overnight at 37 °C in order to degrade the collagen matrix. The crystals were then crushed in order to obtain a powder and were analyzed by X-Ray diffraction (XRD, Philips MRD) to confirm the presence of HA. Ni-filtered Cu K<sub>α</sub> radiation was used. The step-scanning was performed with an integration time of 50 s at intervals of 0.017° (2θ). Indexing of the peaks was carried out by means of Joint Committee on Powder Diffraction Standards (JCPDS) cards 29-359 for α-TCP and 9-432 for HA.

The different composite scaffolds were analyzed by scanning electron microscopy (SEM; FEI/Philips XL30 FEG ESEM) in order to observe the differences in the morphology of the samples. The specimens were coated with gold-palladium in order to increase the conductivity of the samples.

#### 4.3.4. Plasmid preparation

Multiplication of the pcBMP7 plasmid (Figure 4.1) (obtained from Stryker Biotech, Hopkinton, MA) was performed by heat-shock transformation into E.coli DH5α (DH5α—Invitrogen, Cat#18258-012) competent cells. Cells grew overnight in Lysogeny broth medium (LB medium, composed of 10g/l bacto tryptone (Becton, Dickinson and Company, Product # 211705), 5 g/l bacto yeast (Becton, Dickinson and Company, Product # 288620) and 10 g/l NaCl) containing ampicilin (VWR 80055-786). 50 µl of the cells were put in an eppendorf and kept on ice. The circular DNA (5 µl), which was resistant to ampicilin, was then added into the E. coli cells and mixed gently swirling the pipette tip. The mixture was then incubated for 30 minutes on ice and afterwards into a water bath at 42°C for 45 seconds (heat shock). Five hundred microliters of pre-warmed LB medium with no antibiotic were added and the tubes were incubated for 1 hour at 37°C and shaken at 225 rpm. Different volumes ranging between 20 and 200 µl of the resulted culture were spread on LB agar plates (same composition as LB medium with 15 g/l agar (VWR DF0445-17)) with ampicilin. Only the bacteria with the plasmid, and therefore having resistance to ampicilin, grow on the agar plate. The plates cultured were left overnight at 37°C.

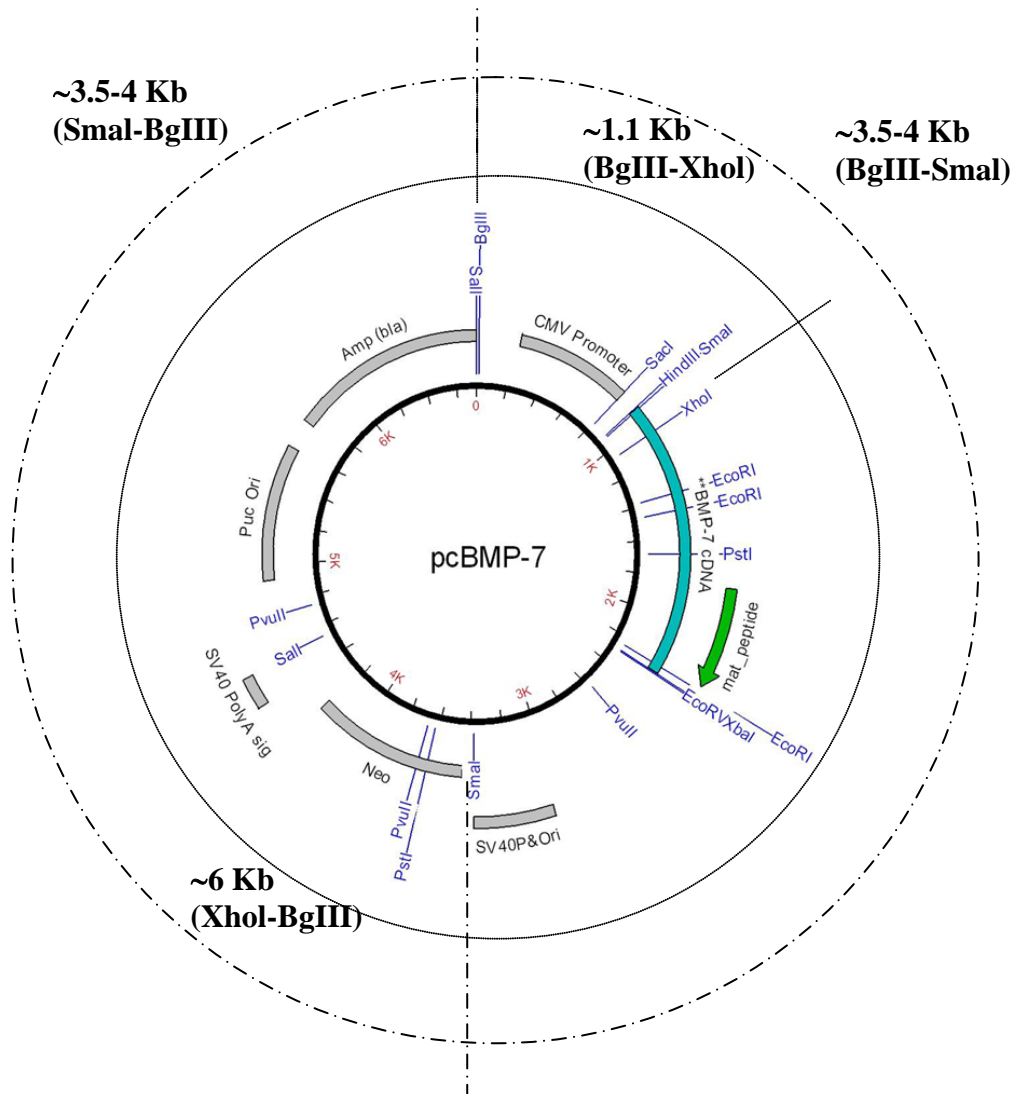


Figure 4.1. Map of the pcBMP7 plasmid incorporated in the scaffolds. The outer circles represent the fragments that are obtained after cutting the DNA with determined enzymes. The inner dotted circles corresponds to the DNA solution in contact with BgIII and XhoI, obtaining a fragment of approximately 1.1 Kb and another one of approximately 6 Kb. The outer circles represents the DNA solution in contact with the enzymes BgIII and SmaI, obtaining two different fragments of approximately 3.5-4 Kb.

Once the Petri dishes with the bacterial cells having the DNA incorporated proliferated, several colonies from the Petri dish were picked with a sterile stick and placed in a culture tube with 5 ml of LB medium with ampicillin (100 µg/ml). The tubes were spinned at 250 rpm in the warm room at 37°C for 6 to 8 hours. The content of the tube was afterwards introduced into a flask containing 1000 ml of LB medium with the ampicillin. It was left overnight, shaking at 260 rpm in the warm room at 37°C. A total of 4 liters were prepared in order to isolate the gene and obtain a high amount. It was then purified using QIAfilter plasmid Mega kit (Qiagen; Valencia, CA. Cat #12183).

The absorption ratio at 260 nm and 280 nm was used to determine the plasmid concentration and purity. The plasmid integrity was verified with polyacrylamide gel electrophoresis. Different DNA solutions were introduced in the wells. The DNA solutions were cut with specific enzymes. These enzymes cut the DNA according to the plasmid map in certain regions. The enzymes used were: XhoI in one case and SmaI on the other. The initial segment was cut with the BglIII enzyme in both cases. The specific regions where these enzymes cut the DNA and the resulting fragments are shown in Figure 4.1. Once the electrophoresis was applied, the different DNA segments were separated in the gel according to the different weights. The size of the pcBMP7 was 6.7 kb.

#### **4.3.5. MSC culture**

Mesenchymal stem cells isolated from goat marrow were used. Cells were thawed and expanded using low glucose DMEM supplemented with 1% Pen/Strep and 10% FBS (non-osteogenic medium) as the medium. When confluence was achieved, cells were trypsinized and counted with trypan blue. Cells were sub cultured in a tissue culture flask or seeded onto the scaffolds.

Twenty-four well plates were coated with 1% agarose solution in order to prevent cell attachment to the bottom of the dishes. Scaffolds were placed on top of the agarose coating. Cells were seeded on top of the scaffolds at a concentration of  $10^6$  cells per scaffold. Cells were left for a period of time to attach to the scaffolds, which were maintained wet, after which, 1 ml of expansion medium was added. After 24 hours, the expansion medium was replaced with osteogenic medium consisting of  $\alpha$ -MEM supplemented with 0.173  $\mu$ M L-ascorbic acid, 10mM  $\beta$  glycerophosphate and 100 nM Dexamethasone, as well as 1% penicillin/streptomycin (pen/strep) solution and 10% fetal bovine serum (FBS). The medium was changed every two days.

#### **4.3.6. *In vitro* behavior of scaffolds containing different HA content**

The effect of having different amounts of HA incorporated in the collagen scaffold was verified. The four types of scaffolds prepared were: Collagen scaffold, Collagen-13 % HA scaffold, Collagen-23 % HA scaffold and collagen-83% HA scaffold. Cell proliferation in the 4 groups of scaffolds was determined by measuring the DNA

content (n=6), and the differentiation by means of alkaline phosphatase (ALP) activity (n=6), after 1, 7 and 14 days. Cell morphology was assessed by SEM and histology at 7 and 14 days.

#### *4.3.6.1. Proliferation*

Cell proliferation was measured by means of the DNA picogreen assay at 1, 7 and 14 days. For that purpose, scaffolds were washed in PBS at each time and frozen without liquid. In order to measure the DNA, samples were freeze-dried overnight and digested afterwards in a 500 µg/ml proteinase K (Sigma, Cat# P-6556) solution dissolved in Tris-HCl at 60°C. The solution was prepared under sterile conditions and then 1 ml of solution was introduced in each of the wells for analysis. Samples were then vortexed before and after leaving the samples degrading overnight.

The assay was done using the Quant-iT PicoGreen dsDNA assay kit (Molecular Probes P7589). The method consisted in a fluorimetric assay measured in a 96-well plate (Black Isoplate, Wallac #1450-571) in a plate reader (Wallac) recording the excitation/emission at 485/535 nm. A standard Lambda solution was prepared in order to have the fluorescent value for different DNA concentrations.

#### *4.3.6.2. Differentiation*

The alkaline phosphatase activity was measured at 1, 7 and 14 days. The samples were washed twice in phosphate buffered saline (PBS), freezing the samples afterwards with PBS and a drop of Tween 20. The samples were then freeze-thawed three times in order to enhance cell lysis. Afterwards, samples were analyzed using the QuantiChrom Alkaline phosphatase assay kit (BioAssay Systems, DALP-250).

Briefly, in order to carry out the ALP determination, the working solution was initially prepared by mixing for each well, the following proportions: 200 µl of assay buffer, 5 µl of Mg acetate (final 5mM) and 2 µl of pNPP liquid substrate (10 mM). Two hundred µl of distilled water and 200 µl of Tartrazine Standard were introduced in a clear bottom 96 well plate. In other wells, 5 µl of each of the samples were introduced in the wells, as well as 195 µl of working solution, in order to obtain a final volume of 200 µl. The plate was read at OD<sub>405nm</sub> at time zero and read again 4 minutes after. The ALP activity in IU/l was then calculated as:

$$\text{ALP activity} = \frac{(OD_4 - OD_0) \cdot 1000 \cdot RV}{4 \cdot \epsilon \cdot l \cdot SV}$$

Where  $OD_4$  and  $OD_0$ , are the values of the sample at time 4 and time 0 minutes. The factor 1000 converts IU/ml to IU/l. RV was the total reaction volume (200  $\mu$ l). The number 4 was the time waited for the second reading. The absorbance factor  $\epsilon$ , was  $18.75 \text{ mM}^{-1} \cdot \text{cm}^{-1}$ ,  $l$  was the light path in cm and can be described as  $l = (OD_{\text{Tart}} - OD_{\text{H}_2\text{O}}) / (\epsilon \cdot C) = 1.321 \cdot \Delta OD$ . SV is the sample volume, being 5  $\mu$ l.

#### 4.3.6.3. Cell morphology

Cell-seeded scaffolds were washed twice in PBS, and then immersed in a 2.5% glutaraldehyde (Sigma-Aldrich G400-4) solution in PBS. The samples were then treated in a 1% solution of osmium tetroxide (Sigma-Aldrich 201013) in order to increase the electron-contrast of the samples. Graded ethanol solutions were used to dehydrate the samples (50, 70, 90, 96 and 100% ethanol).

Samples for histology were immediately fixed at the determined time points in 4% paraformaldehyde solution. Samples were then dehydrated overnight in a tissue processor (Leica TP 1020) containing graded alcohols (70%, 80%, 95% and 100%) and xylene, and left afterwards in paraffin. Samples were then embedded in paraffin (Thermo Shandon Histocentre 2) and solidified by cooling them. Paraffin blocks were then cut (6  $\mu$ m thick) using a microtome (Finesse Thermo Shandon) and placed on the slides.

In order to prepare samples for staining, cut sections that were placed on each of the slides were then warmed at 55°C to detach the paraffin from the slide (Slide warmer, Slide-Line). Samples were immediately introduced in xylene and then in graded alcohols (100%, 95%, 90% and 80%), and finally in water to completely remove the paraffin. Samples were then stained according to each of the established protocols. The sections were stained with Hematoxylyn and eosin, Masson's trichrome<sup>40</sup> and Von Kossa in order to visualize cell morphology, as well as the collagen scaffold<sup>41</sup>.

#### 4.3.7. Plasmid incorporation

In the second part of the study, the effect of incorporating the plasmid in the scaffold was determined for the collagen-83% HA construct. The amount of plasmid incorporated varied from 0 to 50  $\mu$ g. 20  $\mu$ l of the solution containing the appropriate

amount of plasmid were pipetted into the surface of the scaffold. The low amounts of plasmid incorporated were for safety reasons.

The amount of BMP-7 contained within the scaffolds after 1, 4 and 7 days (n=3) was determined by freeze-thawing them three times and physically breaking them down in order to release the BMP-7 produced. The amount of BMP-7 was measured by a sandwich ELISA kit for BMP-7 protein (DuoSet ELISA Development System human BMP-7 DY354). In order to also observe the effect of the plasmid on cell proliferation, a DNA assay was performed as previously described. The values for BMP-7 expression were represented as normalized values with respect to the amount of DNA obtained for the proliferation assay.

In order to make sure that in the case of the quantification of DNA, what was being read was because of the cells, an internal control was done. The previously described procedure was applied in a series of scaffolds without incorporating the cells in order to see if the DNA quantification technique would also quantify the DNA from the plasmid.

#### **4.3.8. Statistical analysis**

The cell experiments were performed using six replicates for each scaffold composition. Statistical analysis was carried out with significance of 5% or less. One-factor analysis of variance (ANOVA) with Fisher's post-hoc test was conducted. The data are expressed as mean value  $\pm$  standard error.

### **4.4. Results**

The collagen differed significantly from the collagen described in the other chapters. The main difference was that this collagen was less soluble. Therefore, the collagen had to be blended at higher rpm in order to solubilize and break the collagen fibers. The blending process was carried out for 6 hours. The viscosity of this collagen was much higher than the previous one, although the concentration was the same.

#### **4.4.1. Microstructure of the scaffolds**

As shown in Figure 4.2, the XRD patterns revealed that the transformation of the initial  $\alpha$ -TCP into HA was complete after 5 days immersion in water, being therefore HA the only mineral phase present in the scaffolds.

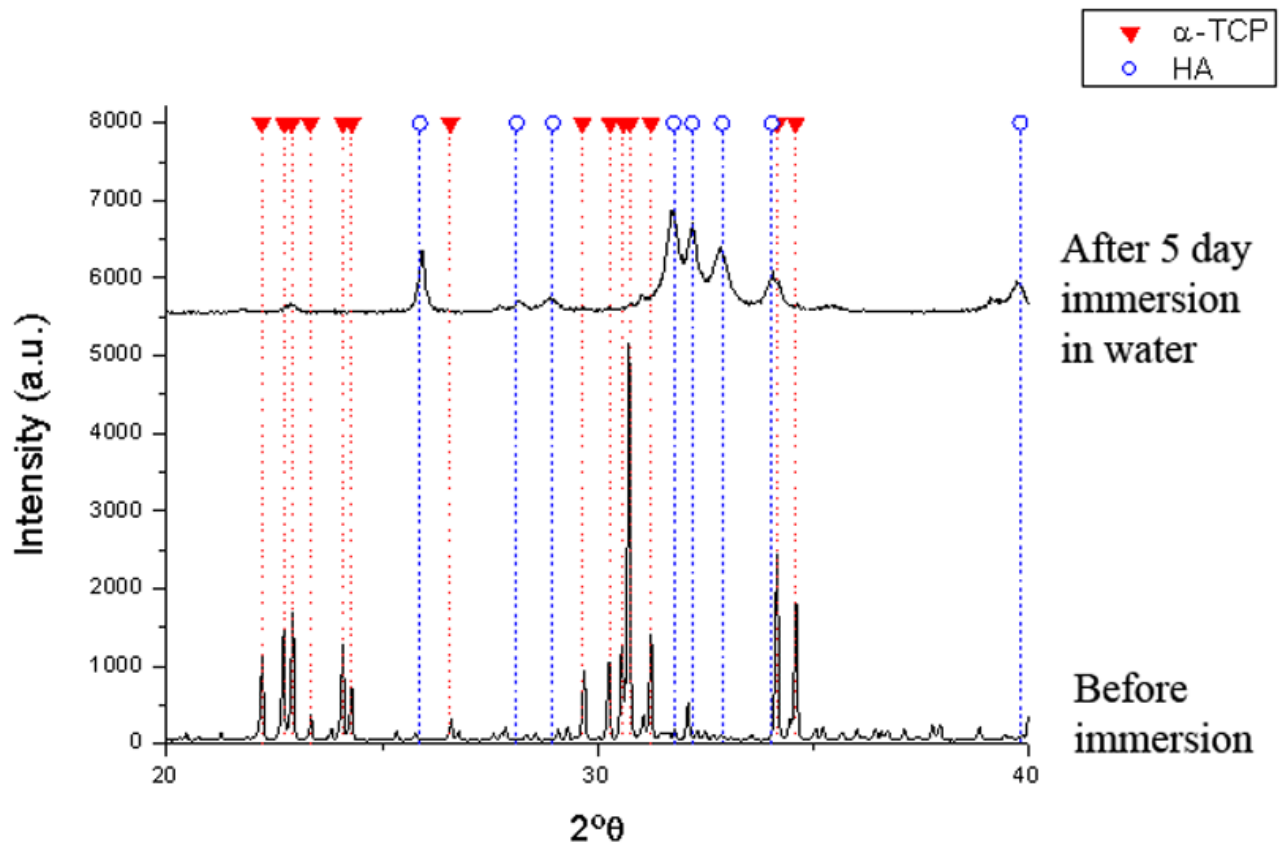


Figure 4.2. X-Ray diffraction patterns of 83% HA scaffold before (bottom) and after (top) 5 days immersion in water. Initially the scaffold contained only  $\alpha$ -TCP as a mineral phase, which completely hydrolysed to HA after 5 days.

Homogeneous slurries were obtained with the collagen type I/III and  $\alpha$ -TCP. It was important to stir the system for time enough so that the  $\alpha$ -TCP and the collagen would intimately mix, avoiding problems of heterogeneity. The microstructures of the collagen-13% and collagen-23% scaffolds were very similar (Figure 4.3a and b), demonstrating collagen fibers with some crystals incorporated into the matrix. The morphology of the scaffolds containing 83% HA was completely different (Figure 4.3c). In this case, the collagen fibers were completely covered by the HA crystals. The matrix of the collagen (Figure 4.3d) was seen as completely smooth with no particles dispersed



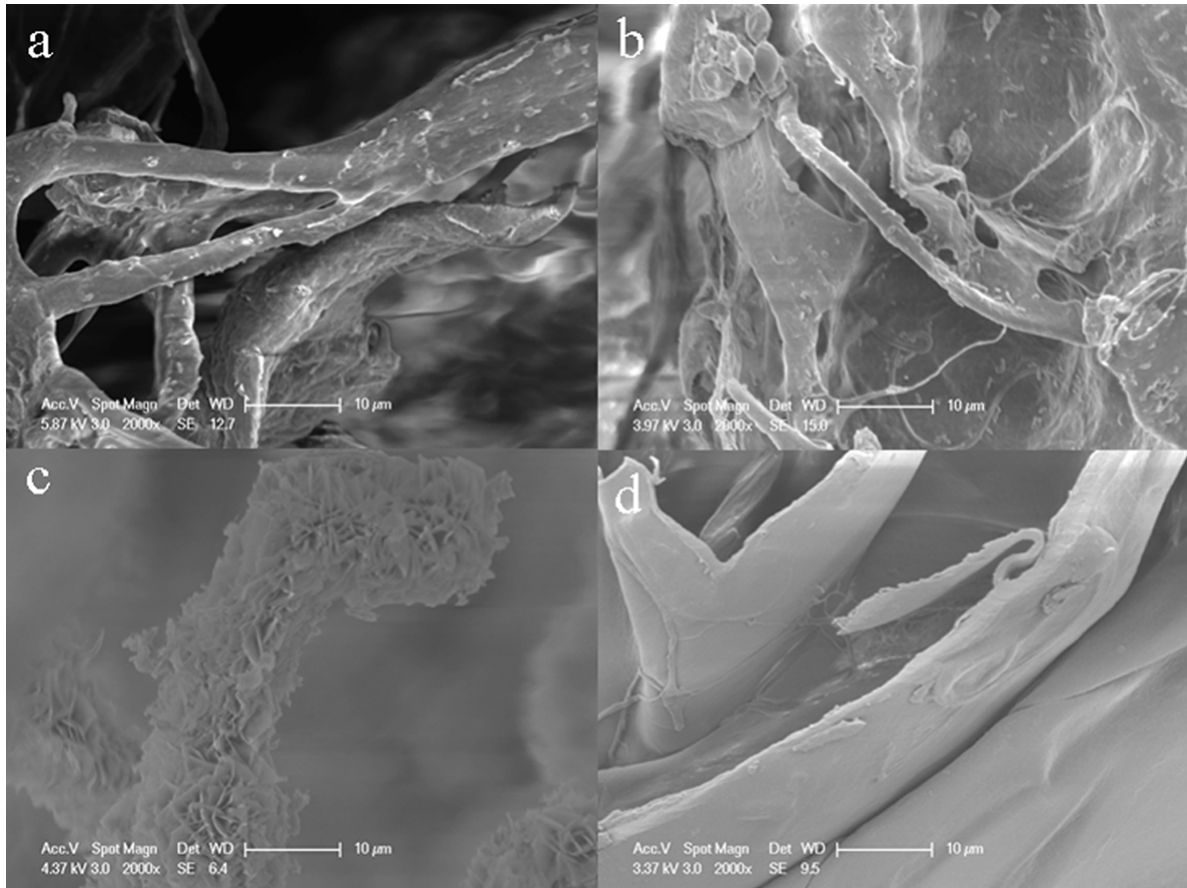


Figure 4.3. SEM images of collagens prepared with different % HA in wt a) 13%, b) 23%, c) 83% and d) 0%.

#### 4.4.2. Plasmid characterization

The electrophoresis obtained for the plasmid is shown in Figure 4.4. The different bands that appear in the electrophoresis gel correspond to the fragments that were cut with the different enzymes. Bands 1, 2, 5 and 6 correspond to the control ladder. The values correspond to those observed in Figure 4.4b. In the case of lane 3, the presence of one band was observed at around 3.5-4 Kb. This band corresponds, to the plasmid cut with the enzymes *Sma*I and *Bg*III. It should be seen as two bands, but since the values are very similar, it can only be seen as one band. On the other hand, the bands that appear in lane 4, appear at 1.1 Kb, 6Kb and 7 Kb. These bands correspond exactly to the plasmid cut with the enzymes *Xho*I and *Bg*III, being the 7 Kb band the complete uncut plasmid. The bands correspond to the segments that were shown in Figure 4.1. This is then giving the information that the plasmid obtained corresponded to the map obtained for BMP7 plasmid.

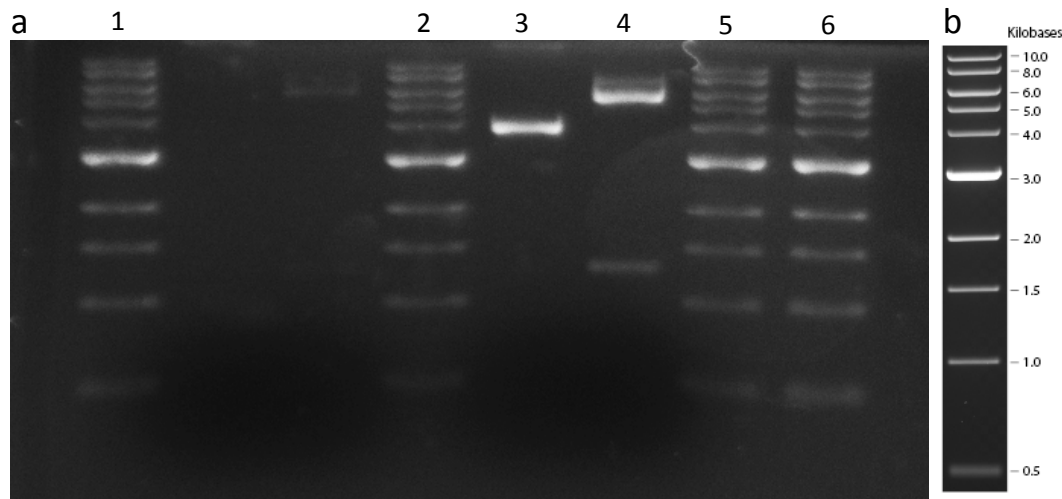


Figure 4.4. a) Electrophoresis gel for the plasmid cut with the mentioned enzymes *BglIII*, *SmaI* and *XhoI*. Lanes 1, 4, 7 and 8 correspond to the control ladder. Lane 5 corresponds to the plasmid cut with *SmaI* and *BglIII*. Band 6 corresponds to the plasmid cut with *XhoI* and *BglIII*. b) Ladder used in the electrophoresis that appears in lane 1, 4, 7 and 8 and corresponds to the values in kilobases.

### 4.4.3. Cell response to collagen scaffolds with different HA contents

The 1-day DNA content, reflecting the initial attachment of the mesenchymal stem cells to the scaffolds, was substantially lower for the collagen-83% HA scaffold compared to the 13% HA and 23% HA constructs, which were comparable (Figure 4.4a). The collagen scaffolds which did not contain HA, contained about 40% fewer cells than the 13 and 23% HA samples (Figure 4.4a).

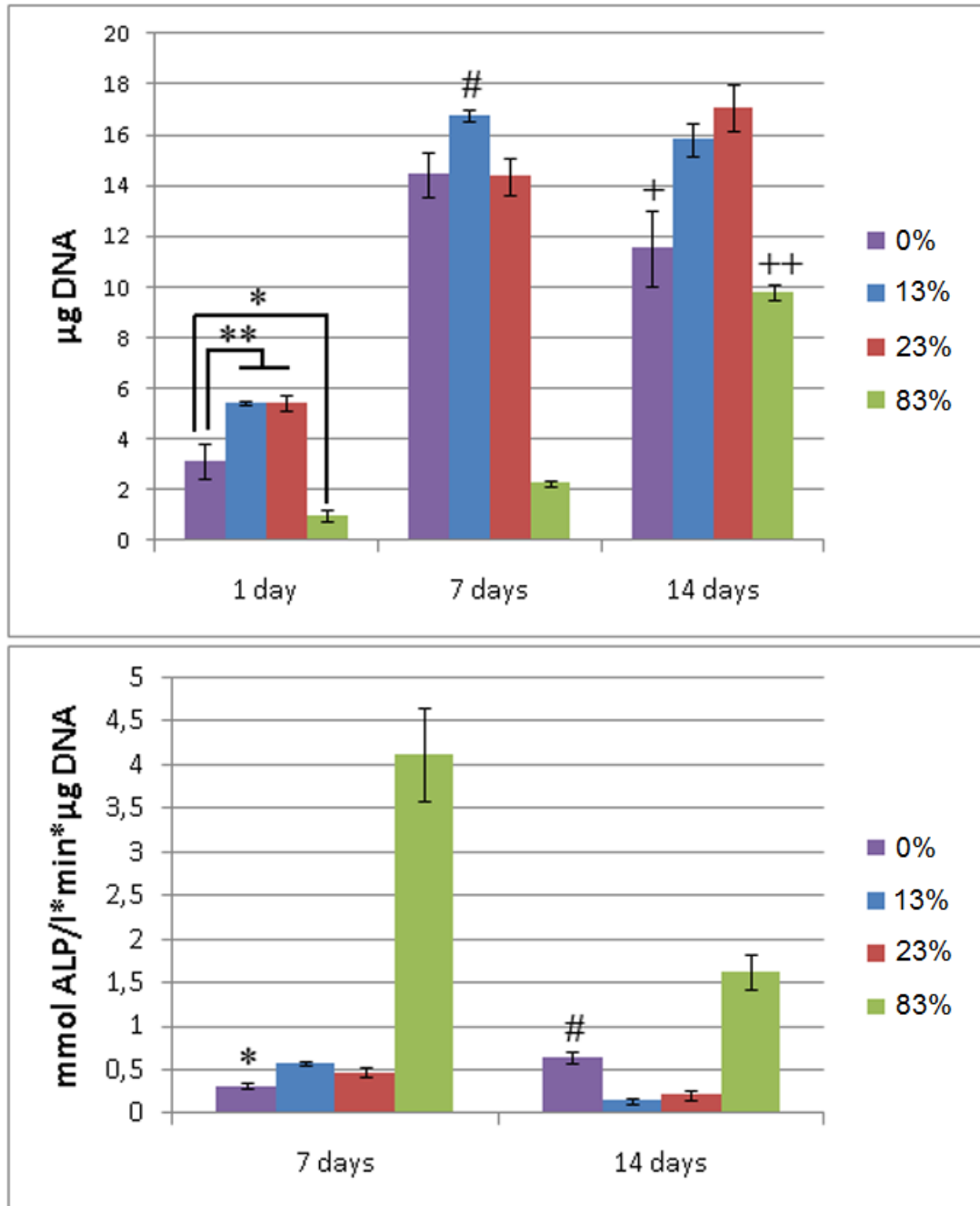


Figure 4.5. a) Cell proliferation measured by means of DNA quantification. \* indicates significant differences between 0% HA scaffolds and 83% scaffolds at 1 day. \*\* indicates significant differences between 0% HA and 13% and 23% HA scaffolds at 1 day. # indicates significant difference between 13% HA and the other scaffolds at 7 days. + indicates significant differences between 0% HA and 13% and 23% HA at 14 days and ++ indicates significant differences between the 13% and 23% HA scaffolds and the 83% HA scaffold ( $p < 0.05$ ). b) Alkaline phosphatase activity for the scaffolds with different amounts of HA incorporated. \* denotes significant differences between 0% HA and the other compositions at 7 days. # denotes significant differences between 0% HA and the other compositions

After 7 days, the amount of DNA in the collagen and 13 and 23% HA scaffolds increased dramatically compared to the 1-day values, indicating considerable cell proliferation (Figure 4.5a). While the number of cells in the 83% HA constructs

increased more than 2-fold compared to the 1-day measurements, the cell content was less than 13% of that in the other scaffold groups (Figure 4.5a). There were no significant differences in the DNA contents among the 0, 13 and 23% HA groups after 7 days.

No increase in cell proliferation was observed at 14 days for the scaffolds containing 0, 13 and 23% HA, compared to the 7-day results (Figure 4.5a). There was, however, almost a 5-fold increase in the number of cells in the collagen-83% HA scaffolds from 7 to 14 days (Figure 4.5a). There was no significant difference in cell number between the 13 and 23% HA scaffolds at 14 days, but the 13 and 23% HA scaffolds had significantly higher DNA contents than the 0% and 83% HA scaffolds.

After 7 days, the ALP activity, normalized to the number of cells in the scaffolds, was 7-fold higher for the 83% HA scaffolds compared to the constructs in the 3 other groups (Figure 4.5b). The ALP values for the 13 and 23% HA groups were comparable, and the collagen scaffold group displayed about 60% of their value (Figure 4.5b). Between the 7- and 14-day periods, the ALP content of the collagen scaffolds increased about 2-fold, while the values for the HA containing scaffolds all decreased. After 14 days the ALP/cell was higher for the collagen scaffolds compared to the 13 and 23% HA groups, but the highest ALP content was still found for the collagen-83% HA scaffolds.

Monolayers of cells were found on the walls of the 13 and 23% HA scaffolds after 7 and 14 days (Figure 4.6a and b). The cells were well spread, presenting filipodia extending throughout the scaffold. In the case of the 83% HA scaffolds, there were differences when comparing 7 and 14 days. After 7 days, there were few cells on the scaffold, with few contact points with the material, presenting an elongated shape (Figure 4.6c). After 14 days, a higher number of cells were observed on the scaffold, with a more spread morphology, presenting higher amounts of expanding filipodia. One of the main differences with the 13 and 23% HA scaffolds, was the presence of deposits on top of the cells, probably corresponding to extracellular matrix (Figure 4.6d).

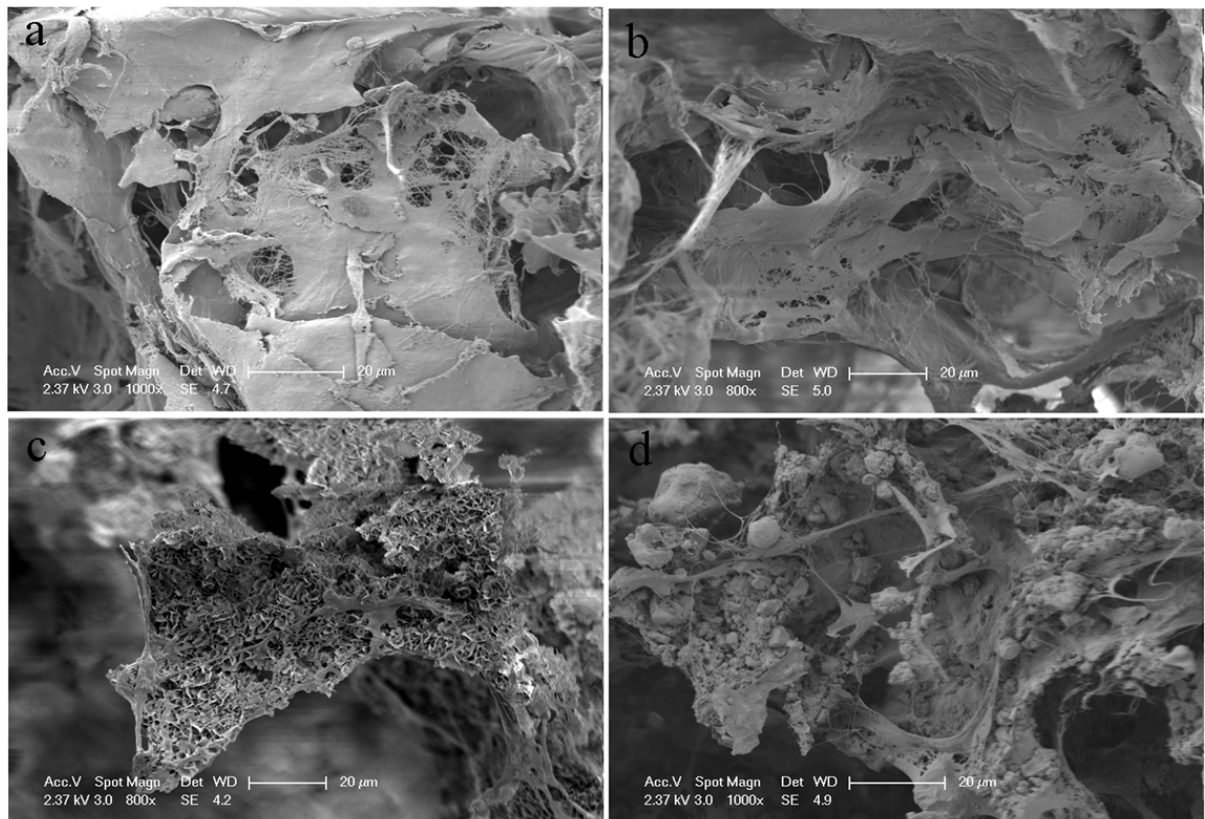


Figure 4.6 SEM images of the cell morphology on the different scaffolds for a) 13% HA (14 days), b) 23% HA (14 days), c) 83% HA (7 days) and d) 83% HA (14 days).

Similar trends were observed through the Masson's trichrome staining of the histological sections (Figure 4.7). Qualitatively, higher numbers of cells were observed in the 13 and 23% HA scaffolds (Figure 4.7 a and b), having in general an elongated morphology and creating an entangled cell network. In the case of the 83% HA, the number of cells was lower with fewer protrusions and filipodia (Figure 4.7c). In the case of the collagen scaffold alone (0% HA; Figure 4.7d), the cells tended to agglomerate in certain parts of the scaffold, and their morphology was similar to that found in the 13 and 23% HA scaffolds. Interestingly, according to the histological and SEM studies, the cells were able to penetrate throughout the whole thickness of the scaffold, in all the series studied. Of note was that the scaffold itself stained red, instead of blue, with the Masson trichrome stain, related to the state of strain in the collagen at the time of fixation. When collagen is in a relaxed state at the time of paraformaldehyde fixation, Masson trichrome stains the collagen blue; collagen that is under tension at the time of fixation is stained red<sup>42</sup>.

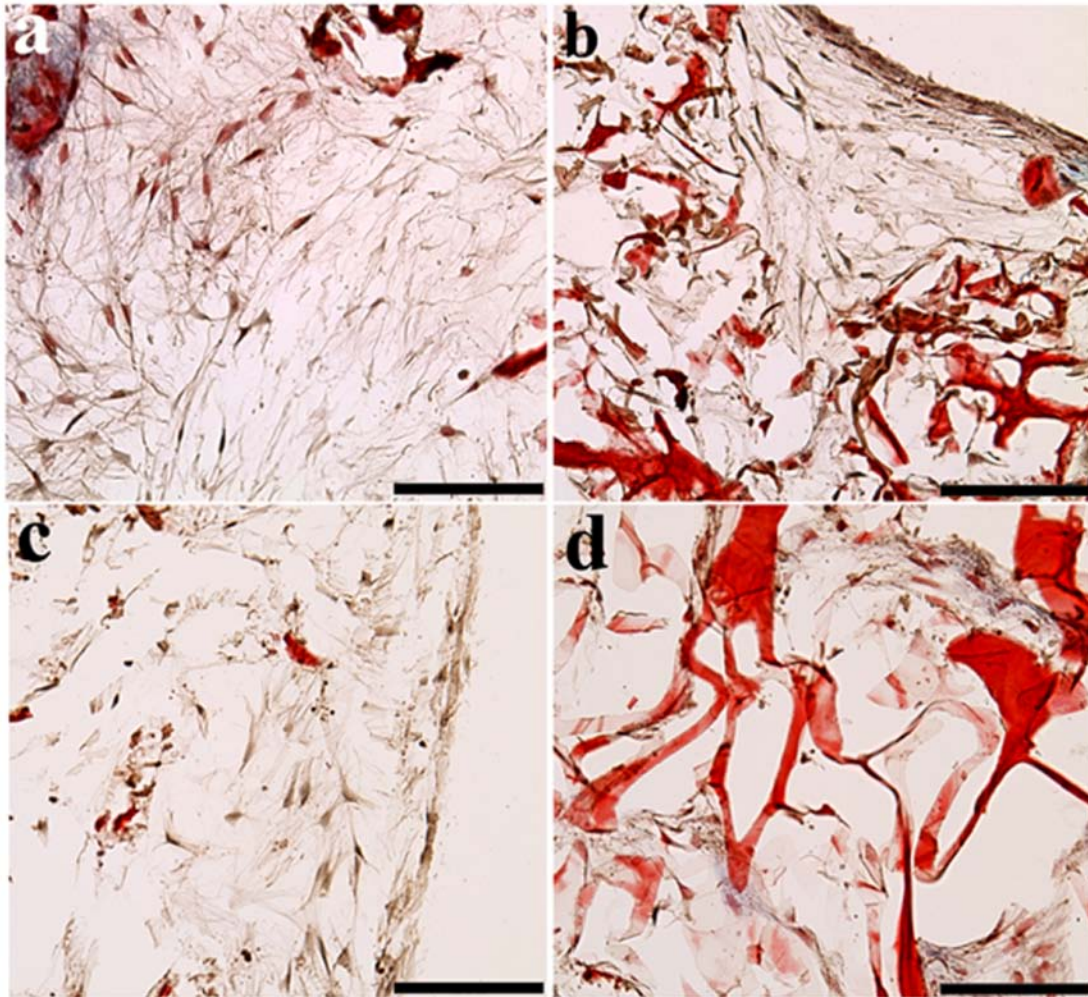


Figure 4.7 Histological sections of the different scaffolds stained with Masson's trichrome, being a) 13% HA, b) 23% HA, c) 83% HA and d) 0% HA. Scale bar = 100  $\mu$ m.

The Von Kossa stain is shown in Figure 4.8. The brown/black deposits observed corresponds to the calcium deposits. As can be observed, there is a higher content of calcium in the 83% HA scaffolds. In the 13 and 23% HA scaffolds, only some deposits can be observed. In all the cases, the calcium deposits arise from the calcium phosphate cement incorporated in the scaffold. In the collagen scaffolds, no calcium deposits can be observed. The cells can be observed in pink, whereas the collagen was observed as light pink.

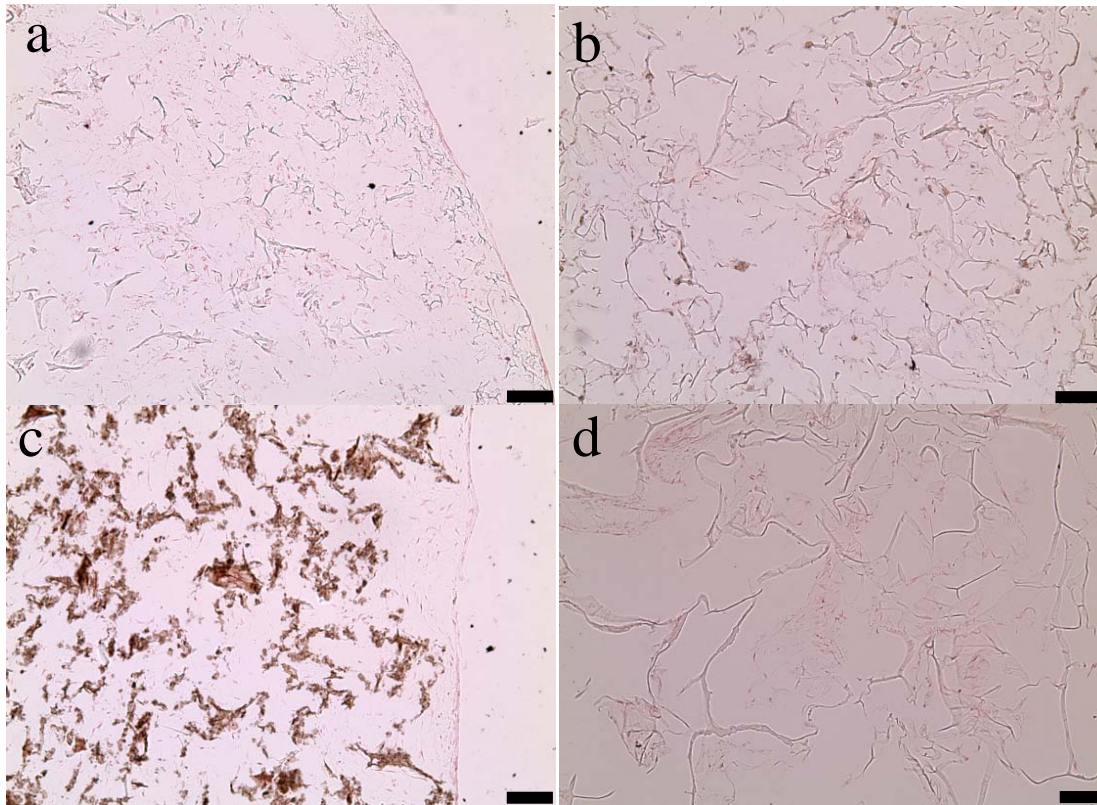


Figure 4.8. Histological sections of the different scaffolds stained with Von Kossa, being a) 13% HA, b) 23% HA, c) 83% HA and d) 0% HA. Scale bar = 100  $\mu$ m.

#### 4.4.4. BMP-7 expression

In this part of the study, the plasmid encoding BMP-7 was incorporated in the 83% HA scaffolds, using different plasmid loadings. First, it was assessed that the plasmid did not interfere with the DNA technique used to quantify cell proliferation. This was done by incorporating the plasmid in the scaffolds without seeding cells and afterwards applying the procedure of DNA quantification, and no signal was obtained.

As shown in Figure 4.9, cell proliferation was higher in the cases in which the plasmid was present. In all cases the trend shown was that the higher doses of plasmid increased the amount of cells. The increase in proliferation was dose dependent, except in the case of the 20  $\mu$ g and 50  $\mu$ g dose in which the proliferation was the same.

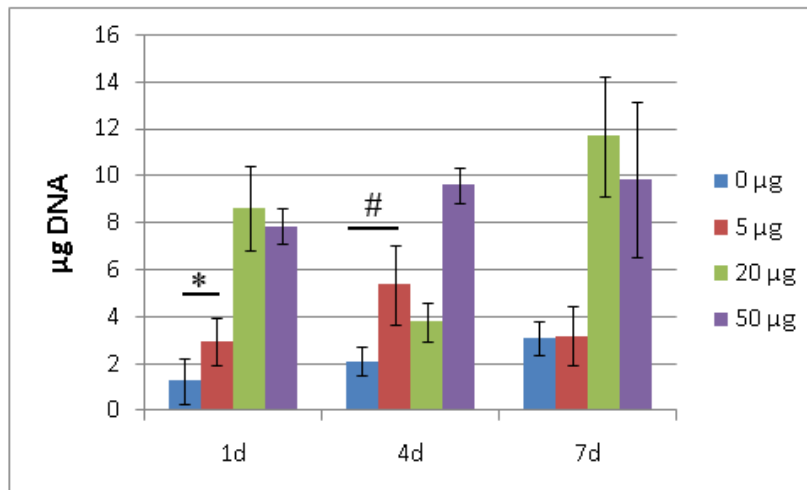


Figure 4.9. Proliferation measured by means of DNA quantification for scaffolds composed of 83% HA containing different amounts of plasmid: 0, 5, 20 and 50 µg. \*indicates significant differences between 0 and 5 µg of plasmid incorporated at 1 day. # indicates significant differences between 0 and 5 µg of plasmid incorporated at 4 days ( $p < 0.05$ ).

Regarding the expression of the BMP-7 protein, the highest levels of protein were found in the scaffolds after 1 day and, interestingly, the highest amount was found for 20 µg of incorporated plasmid (Figure 4.10). At 4 days, the highest BMP-7 content was obtained for the 5 µg dosed scaffolds. But after 14 days, the 20 µg dosed scaffolds yielded again the highest BMP-7 levels in the matrix (Figure 4.10). The BMP-7 accumulated in the scaffolds over the 7-day period was higher for the plasmid groups, compared to the non-transfected controls (0.264 ng of BMP-7 for the 20 µg group, compared to 0.139 ng of BMP-7 for the 0 µg group).

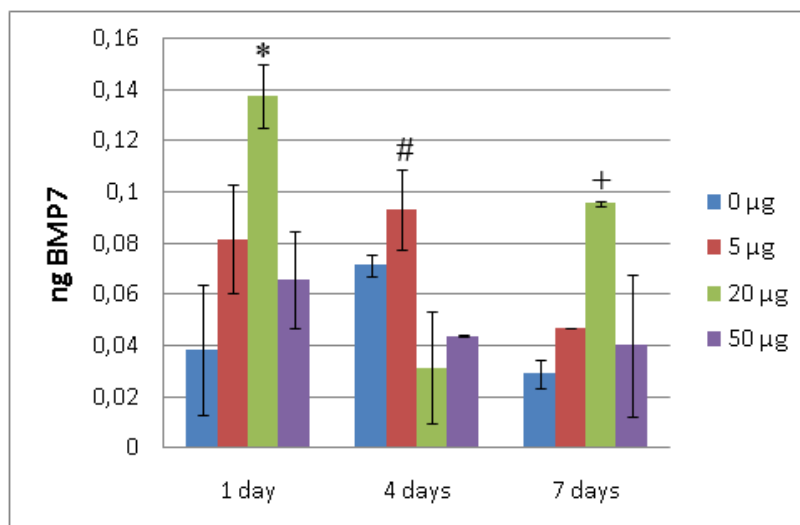


Figure 4.10. BMP7 expression for the 83% HA scaffolds with different amounts of plasmid incorporated during 7 days. \* denotes significant differences between the 20 µg plasmid loaded scaffolds and the other plasmid loadings at 1 day. # denotes significant differences between the 5 µg plasmid loaded scaffolds and the other plasmid loadings at 4 days. + denotes significant differences between the 20 µg plasmid loaded scaffolds and the other plasmid loadings at 7 days.



The values of the BMP-7 measured in the scaffolds were normalized by the DNA content of the specimens (Figure 4.11). After 1 and 4 days, the control scaffolds which were not supplemented with plasmid contained the highest amounts of BMP-7 normalized to DNA. By 7 days, however, the collagen-83% HA scaffold dosed with 5  $\mu\text{g}$  of plasmid had the highest amount of BMP-7 (Figure 4.11).

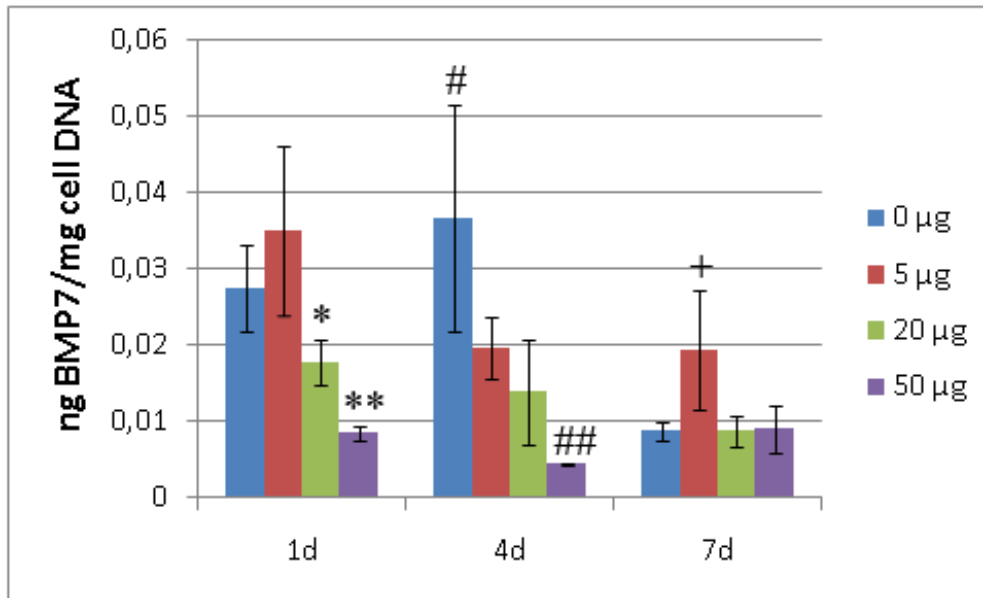


Figure 4.11. BMP7 expression normalized by the DNA content from cell proliferation for the 83% HA scaffolds with different amounts of plasmid incorporated during 7 days. \* denotes significant differences between the 20  $\mu\text{g}$  plasmid loaded scaffolds and the other plasmid loadings at 1 day. \*\* denotes significant differences between the 50  $\mu\text{g}$  plasmid loaded scaffolds and the other plasmid loadings at 1 day. # denotes significant differences between the 0  $\mu\text{g}$  plasmid loaded scaffolds and the other plasmid loadings at 4 days. ## denotes significant differences between the 50  $\mu\text{g}$  plasmid loaded scaffolds and the other plasmid loadings at 4 days. + denotes significant differences between the 5  $\mu\text{g}$  plasmid loaded scaffolds and the other plasmid loadings at 4 days.

## 4.5. Discussion

The present work allowed the development of macroporous collagen-HA scaffolds with different HA contents. Initially, the collagen/ $\alpha$ -TCP slurry was blended at 4°C, avoiding the formation of bundles due to collagen precipitation. The hydrolysis of  $\alpha$ -TCP has an increase of the pH associated which, near neutral pH, may induce the collagen precipitation. This would lead to a heterogeneous slurry, and therefore to heterogeneous scaffolds. By decreasing the temperature, the hydrolysis rate was reduced, which combined with the blending process, reduced the risk of bundle formation.

A recent study of collagen-glycosaminoglycan scaffolds<sup>43</sup> has shown that at the temperature used for the dehydrothermal treatment of the freeze-dried collagen/ $\alpha$ -TCP (105 °C), about 25 % of collagen is denatured. It will be interesting in future work to evaluate the degree of collagen denaturation in the collagen/ $\alpha$ -TCP, to determine if the calcium phosphate may play a protective role in reducing the collagen denaturation. One would not expect a reaction between the collagen and the calcium phosphate during the dehydrothermal treatment at 105°C. The calcium phosphate is not altered in any way at this temperature, being completely stable. It would also be of interest in future studies to investigate how the EDAC-crosslinked material is degraded *in vivo*, with respect to the ultimate clinical applications.

The characterization of the scaffolds by XRD showed the transformation of the mineral phase into HA (Figure 4.2). SEM observations revealed that at low amounts of incorporated HA, the HA precipitates were found in the fibers of the collagen and not in the voids (Figure 4.3a and b). At higher amounts of incorporated HA, the structure revealed a similar trend, observing HA completely covering the collagen fibers (Figure 4.3c). Once again, the HA was precipitating on top of these collagen fibers and the crystalline structure of the mineral phase corresponded to that previously seen in previous work in which the  $\alpha$ -TCP had been hydrolyzed<sup>44</sup>. An interesting fact is that the porous structure of the collagen network was maintained similar in all cases, being the main difference, the mineralization of the collagen fibers. Further physico-chemical characterization will be assessed for the different scaffolds (e.g., mechanical properties, FTIR, pore size distribution).

The proliferation of the mesenchymal stem cells and their differentiation to osteogenic cells were comparable for the collagen scaffold and the scaffolds containing 13 and 23% HA (Figure 4.5). The main difference was observed for the higher content (83%) of HA. In this case, the proliferation was significantly lower compared to the other types of scaffolds, owing in part to the fewer cells initially adhered to the scaffold. The main benefit of the higher amounts of HA, was the significant increase in ALP activity, suggesting the high efficiency of the HA to induce the differentiation of the MSC into osteoblasts. This observation was not seen in similar types of scaffolds, in which it was shown that the incorporation of different ratios of HA on the collagen scaffolds did not change the ALP activity<sup>45</sup>.

The lower proliferation of the 83% HA initially can be attributed to the fact that, when cells are seeded, collagen plays an important role in initial adhesion. In this case, the cells lack this benefit since they only enter in contact with the HA and not with the underlying collagen. Moreover, it has been previously reported that for a set CPC analogous to the one used in this work, the microstructure of the HA had a direct effect on cell proliferation and differentiation<sup>46</sup>. It was seen that, depending on the microstructure cell proliferation could be delayed. Although there were lower rates of proliferation in the scaffolds with the highest HA content, in cell differentiation was increased.

The SEM observation of the cell morphologies revealed the trend previously mentioned for proliferation and differentiation. Cell morphology was clearly different for the 13 and 23% HA scaffolds and the 83% HA scaffolds (Figure 4.6 and 4.7). In the first two cases, the cells presented a spread morphology creating a cell layer on the scaffold which was probably near confluence, as shown by the proliferation assay. In the case of the 83% HA, cells are only able to attach to the HA, and this adhesion is slower than in the case of collagen due to the absence of the cell adhesion motifs sequences present in collagen. This is revealed by the cell morphology observed for the 83% HA, where the cells presented elongated morphology with few contact points.

It is also worth highlighting that after 14 days, cells were able to proliferate, as was seen by the proliferation assay, and were shown to cover most of the scaffold surface, presenting expanded cells on the 83% HA scaffolds. The main difference was the presence of a higher extracellular matrix formation in the case of the 83% HA compared to the other two cases, which would be in agreement with the ALP results obtained. Future studies will address later time points in order to assess the biological behavior of the scaffolds at longer culture times.

In order to increase the osteoinduction ability of the scaffolds, BMP is widely used in the field of bone regeneration<sup>29,47,48</sup>. In the present work, the approach is different, since the BMP-7 was not incorporated into the scaffold, being expressed by the cells after transfection of a specific gene encoding the BMP-7 protein. The plasmid used in the present work has already been previously used *in vivo*, presenting promising results<sup>49</sup>. The BMP-7 has a higher affinity for HA, that is why the BMP-7 levels were measured directly on the scaffolds by breaking them<sup>50,51</sup>. Actually, the amount of BMP-7 was also measured in preliminary studies in the medium, but the values obtained were even

lower and therefore, the results were analyzed in the scaffold. The amount of BMP-7 produced was higher in the 20  $\mu\text{g}$  plasmid loading after 1 and 7 days and it was also found that the accumulated values in this case were 0.264 ng (Figure 4.9). Nevertheless, a surprising fact was that when the values of BMP7 were normalized by the cell content, it was seen that the amount of BMP7 per cell content was higher in the cases in which no plasmid was present (Figure 4.11). This also means that the combination of the scaffolds with the MSCs in the osteogenic media is expressing the BMP-7 protein. Therefore, the main effect of the plasmid was the increase on cell proliferation, not directly on protein expression (Figure 4.10). As mentioned in the results, it was discarded that the higher proliferation rates measured with the DNA kit could correspond to the signal coming from the gene DNA, since the incorporation of the gene without cells in the scaffold and the subsequent DNA reading gave no value.

The intention of the work was to incorporate a CaP in the collagen structure since CaP have been widely used for more than 30 years as gene delivery vehicles, having low efficiencies, but showing few problems of cytotoxicity. In these cases, the CaP have been used as nanoparticles<sup>34-37</sup>. These nanoparticles are usually in the range of 300 nm and the mechanism by which the cells are transfected is by endocytosis of the nanoparticles<sup>37</sup>. There are a large number of factors that affect the transfection efficiency, such as, time of contact between the material with the plasmid and the cells, the cell type used, the Ca/P ratio, as well as the morphology of the precipitate among others<sup>34,52,53</sup>.

The use of CaP in the form of nanoparticles is challenging for their use as tissue engineering scaffolds<sup>34-36</sup>. These nanoparticles have been combined with alginate hydrogels as an implantable device, but not combined with cells<sup>54</sup>. That is why the use of tissue engineering constructs incorporating HA was thought as a promising system to deliver the plasmid and to be able to combine them with cells. Unfortunately, the amount of protein was low and in some cases was comparable to the values in the absence of plasmid. This means that the plasmid might not have been incorporated inside the cells, although the possible mechanism by which the plasmid could have been incorporated was discussed.

In the case of having the HA in the collagen matrix, a continuous surface of HA crystals is created. Therefore, it was hypothesized that the plasmid could have been incorporated as naked DNA or as part of the crystals. Because HA may present

electrostatic charges, the gene is able to physically attach to the surface of the crystal. These crystals may be detached from the structure by manipulation (e.g. media changing) or degradation of the scaffold<sup>55</sup> or a CaP may be precipitated on the surface of the existing HA due to the supersaturation of calcium and phosphates in the medium. The size of these HA crystals are in the range of several hundreds of nanometers to several microns. That is why some HA may break and detach from the structure, being in the range of sizes which the cells are able to endocytosise.

It seems that even if the plasmid was able to enter the cells, the transfection was still low probably due to the aggressive environment found inside the cell cytoplasm<sup>56,57</sup>. The more protected the gene is, the higher the transfection efficiency will be, although it has been shown that the efficiencies are less than 2% even when the gene is protected with a CaP<sup>34</sup>.

## **4.6. Conclusions**

Collagen-CPC scaffolds may serve as macroporous scaffolds for MSC proliferation and differentiation. The scaffolds produced were shown to homogeneously distribute the HA on the collagen fibers. The different HA contents affected cell proliferation and differentiation. The use of the scaffolds as gene delivery vehicles for the production of BMP7 must be improved although significant levels of BMP7 were expressed, associated with an increase in cell proliferation.

## 4.7. References

1. Cancedda R, Giannoni P & Mastrogiacomo M. A tissue engineering approach to bone repair in large animal models and in clinical practice. *Biomaterials* **28**, 4240-4250 (2007).
2. Stone KR, Steadman JR, Rodkey WG & Li S. Regeneration of meniscal cartilage with use of a collagen scaffold. Analysis of preliminary data. *Journal of Bone and Joint Surgery American* **79**, 17770-17777 (1997).
3. Ahn S, Yoon H, Kim Y, Lee S & Chun W. Designed three dimensional collagen scaffolds for skin tissue regeneration. *Tissue Engineering C* **16**, 813-820 (2010).
4. Yu K, Takashi I & Yasuhiko T. Adipose tissue formation in collagen scaffolds with different biodegradabilities. *Journal of Biomaterials Science, Polymer Edition* **21**, 463-476 (2010).
5. Sumita Y, Honda MJ, Ohara T, Tsuchiya S, Sagara H, Kagami H & Ueda M. Performance of collagen sponge as a 3-D scaffold for tooth tissue engineering. *Biomaterials* **27**, 3238-3248 (2006).
6. Wahl DA, Sachlo E, Liu C & Czernuszka JT. Controlling the processing of collagen-hydroxyapatite scaffolds for bone tissue engineering. *Journal of Materials Science: Materials in Medicine* **18**, 201-209 (2007).
7. Yamauchi K, Goda T, Takuchi N, Einaga H & Tanabe T. Preparation of collagen/calcium phosphate multilayer sheet using enzymatic mineralization. *Biomaterials* **25**, 5481-5489 (2004).
8. Lickorish D, Ramshaw JAM, Werkmeister JA, Glattauer V & Howlett CR. Collagen-hydroxyapatite composite prepared by biomimetic process. *Journal of Biomedical Materials Research* **68A**, 19-27 (2004).
9. Zhang LJ *et al.* Hydroxyapatite/collagen composite materials formation in simulated body fluid environment. *Materials Letters* **58**, 719-722 (2004).

10. Goes JC *et al.* Apatite coating on anionic and native collagen films by an alternate soaking process. *Acta Biomaterialia* **3**, 773-778 (2007).
11. Lawson AC & Czernuszka JT. Collagen-calcium phosphate composites. *Proceedings of the Institution of Mechanical Engineers H* **212**, 413-425 (1998).
12. Iijima M, Moriwaki Y & Kuboki Y. Oriented growth of octacalcium phosphate on and inside the collagenous matrix in vitro. *Connective Tissue Research* **32**, 519-524 (1996).
13. Chaozong L, Zhiwu H & Czernuszka JT. Gradient collagen/nanohydroxyapatite composite scaffold: Development and characterization. *Acta Biomaterialia* **5**, 661-669 (2009).
14. Du C, Cui FZ, Zhu XD & de Groot K. Three-dimensional nano-HAp/collagen matrix loading with osteogenic cells in organ culture. *Journal of Biomedical Materials Research* **44**, 407-415 (1999).
15. Bradt JH, Mertig M, Teresiak A & Pompe W. Biomimetic mineralization of collagen by combined fibril assembly and calcium phosphate formation. *Chemistry of Materials* **11**, 2694-2701 (1999).
16. Zhang W, Liao SS & Cui FZ. Hierarchical self-assembly of nano-fibrils in mineralized collagen. *Chemical Materials* **15**, 3221-3226 (2003).
17. Kikuchi M *et al.* Biomimetic synthesis of bone-like nanocomposites using the self-organization mechanism of hydroxyapatite and collagen. *Composites Science and Technology* **64**, 819-825 (2004).
18. Kikuchi M, Itoh S, Ichinose S, Shinomiya K & Tanaka J. Self-organization mechanism in a bone-like hydroxyapatite/collagen nanocomposite synthesized in vitro and its biological reaction in vivo. *Biomaterials* **22**, 1705-1711 (2001).
19. Yoshida T, Kikuchi M, Koyama Y & Takakuda K. Osteogenic activity of MG-63 cells on bone-like hydroxyapatite/collagen nanocomposite sponges. *Journal of Materials Science: Materials in Medicine* **21**, 1263-1272 (2010).

20. Toh S *et al.* Development of an artificial vertebral body using a novel biomaterial, hydroxyapatite/collagen composite. *Biomaterials* **23**, 3919-3926 (2002).
21. Song JH, Kim HE & Kim HW. Collagen-Apatite nanocomposite membranes for guided bone regeneration. *Journal of Biomedical Materials Research: applied biomaterials* **83B**, 248-257 (2007).
22. Sasaki N & Sudoh Y. X-ray pole figure analysis of apatite crystals and collagen molecules in bone. *Calcified Tissue international* **60**, 361-367 (1997).
23. Zhai Y, Cui FZ & Wang Y. Formation of nano-hydroxyapatite on recombinant human-like collagen fibrils. *Current Applied Physics* **5**, 429-432 (2005).
24. Roveri N *et al.* Biologically inspired growth of hydroxyapatite nanocrystals inside self-assembled collagen fibers. *Materials Science and Engineering C* **23**, 441-446 (2003).
25. Sionkowska A & Kozłowska J. Characterization of collagen/hydroxyapatite composite sponges as a potential bone substitute. *International Journal of Biological Macromolecules* **47**, 483-487 (2010).
26. Gleeson JP, Plunkett NA & O'Brien FJ. Addition of hydroxyapatite improves stiffness, interconnectivity and osteogenic potential of a highly porous collagen-based scaffold for bone tissue regeneration. *European Cells and Materials* **20**, 218-230 (2010).
27. Jones GL *et al.* Primary human osteoblast culture on 3D porous collage-hydroxyapatite scaffolds. *Journal of Biomedical Materials Research* **94A**, 1244-1250 (2010).
28. Liu L, Zhang L, Ren B, Wang F & Zhang Q. Preparation and characterization of collagen-hydroxyapatite composite used for bone tissue engineering scaffold. *Artificial Cells, Blood Substitutes and Biotechnology* **31**, 435-448 (2003)



29. Takahashi Y, Yamamoto M & Tabata Y. Enhanced osteoinduction by controlled release of bone morphogenetic protein 2 from biodegradable sponge composed of gelatin and  $\beta$ -tricalcium phosphate. *Biomaterials* **26**, 4856-4865 (2005).
30. Wozney JM & Rosen V. Bone morphogenetic protein and bone morphogenetic protein gene family in bone formation and repair. *Clinical and Orthopedic Research* **346**, 26-37 (1998).
31. Azzam T & Domb AJ. Current developments in gene transfection agents. *Current Drug Delivery* **1**, 165-193 (2004).
32. Kofron MD & Laurencin CT. Bone tissue engineering by gene delivery. *Advanced Drug Delivery Reviews* **58**, 555-576 (2006).
33. Maitra A. Calcium phosphate nanoparticles: second-generation nonviral vectors in gene therapy. *Expert Reviews on Molecular Diagnosis* **5**, 893-905 (2005).
34. Sokolova VV, Radtke I, Heumann R & Epple M. Effective transfection of cells with multi-shell calcium phosphate-DNA nanoparticles. *Biomaterials* **27**, 3147-3153 (2006).
35. Bish S, Bhakta G, Mitra S & Maitra A. pDNA loaded calcium phosphate nanoparticles: highly efficient non-viral vector for gene delivery. *International Journal of Pharmaceutics* **288**, 157-168 (2005).
36. Roy I, Mitra S, Mitra A & Mozumdar S. Calcium phosphate nanoparticles as novel non-viral vectors for targeted gene delivery. *International Journal of Pharmaceutics* **250**, 25-33 (2003).
37. He Q, Mitchell AR, Johnson SL, Wagner-Bartak C, Morcol T & Bell SJD. Calcium phosphate nanoparticle adjuvant. *Clinical Diagnosis Laboratory Immunology* **7**, 899-903 (2000).
38. Weadock KS, Miller EJ, Bellincampi LD, Zawadsky JP & Dunn MG. Physical crosslinking of collagen fibers: comparison of ultraviolet irradiation and

- dehydrothermal treatment. *Journal of Biomedical Materials Research* **29**, 1373-1379 (1995).
39. Yannas IV. Collagen and gelatin in the solid state. *Journal of Macromolecules Science Reviews Macromolecules Chemistry* **C7**, 49-104 (1972).
  40. Masson P. Some histological methods. Trichrome stainings and their preliminary technique. *Journal of Techniques and Methods* **12**, 75-90 (1929).
  41. Bancroft J & Gamble M. Theory and practice of histological techniques. Sixth Edition. Churchill Livingstone-Elsevier. Philadelphia, USA (2008).
  42. Flint MH, Lyons MF, Meaney MF & Williams DE. The Masson staining of collagen — an explanation of an apparent paradox. *Histochemistry Journal* **7**, 529-546 (1975).
  43. Haugh GH, Jaasma MJ & O'Brien FJ. The effect of dehydrothermal treatment on the mechanical and structural properties of collagen-GAG scaffolds. *Journal of Biomedical Materials Research A* **89**, 363-369 (2009).
  44. Ginebra MP *et al.* Setting reaction and hardening of an apatitic calcium phosphate cement. *Journal Dental Research* **76**, 905-912 (1997).
  45. Jones GL *et al.* Primary human osteoblast culture on 3D porous collagen-hydroxyapatite scaffolds. *Journal of Biomedical Materials Research A* doi: 10.1002/jbm.a.32805 (2010).
  46. Engel E *et al.* Discerning the role of topography and ion exchange in cell response of bioactive tissue engineering scaffolds. *Tissue Engineering* **14**, 1341-1351 (2008).
  47. Laflamme C & Rouabhia M. Effect of BMP-2 and BMP-7 homodimers and a mixture of BMP-2/BMP-7 homodimers on osteoblast adhesion and growth following culture on a collagen scaffold. *Biomedical Materials* **3**, 1-10 (2008).
  48. Tsiridis E, Bhalla A, Ali Z, Gurav N, Heliotis M, Deb S & DiSilvio L. Enhancing the osteoinductive properties of hydroxyapatite by the addition of

- human mesenchymal stem cells, and recombinant human osteogenic protein-1 (BMP-7) in vitro. *Injury* **37**, S25-S32 (2006).
49. Bright C, Park YS, Sieber AN, Kostuik JP & Leong KW. In vivo evaluation of plasmid DNA encoding OP1 protein for spine fusion. *Spine* **31**, 2163-2172 (2006).
  50. Zhou H, Wu T, Dong X, Wang Q & Shen J. Adsorption mechanism of BMP-7 on hydroxyapatite (001) surfaces. *Biochemical and Biophysics Research Communications* **361**, 91-96 (2007).
  51. Boix T *et al.* Adsorption of recombinant human bone morphogenetic protein rhBMP-2 onto hydroxyapatite. *Journal of Inorganic Biochemistry* **99**, 1043-1050 (2005).
  52. Orrantia E & Chang PL. Intracellular distribution of DNA internalized through calcium phosphate precipitation. *Experimental Cell Research* **190**, 170-174 (1990).
  53. Olton D *et al.* Nanostructured calcium phosphates (NanoCaPs) for non-viral gene delivery: influence of the synthesis parameters on transfection efficiency. *Biomaterials* **28**, 1267-1279 (2007).
  54. Krebs MD, Salter E, Chen E, Kathleen AS & Alsberg E. Calcium phosphate-DNA nanoparticle gene delivery from alginate hydrogels induces *in vivo* osteogenesis. *Journal of Biomedical Materials Research* **92A**, 1131-1138 (2010).
  55. Keeney M, van den Beucken J, van der Kraan PM, Jansen JA & Pandit A. The ability of a collagen/calcium phosphate scaffold to act as its own vector for gene delivery and to promote bone formation via transfection with VEGF<sub>165</sub>. *Biomaterials* **31**, 2893-2902 (2010).
  56. Luo D & Saltzman WM. Synthetic delivery systems. *Nature Biotechnology* **18**, 33-37 (2000).
  57. Wiethoff CM & Middaugh CR. Barriers to nonviral gene delivery. *Journal of Pharmaceutics Science* **92**, 203-217 (2003).

# **Chapter 5: Porous Hydroxyapatite and Gelatin/Hydroxyapatite Microcarriers Obtained by Calcium Phosphate Cement Emulsion**

## **5.1. Introduction**

The present chapter and the following two chapters deal with the application of the CPC designed in Chapter 2 to a new processing route aimed at the fabrication of microscaffolds for bone tissue engineering. The urgent need of bone grafts has triggered the new area of bone tissue engineering, where the development of scaffolds to carry high amounts of viable and proliferating osteoprogenitor cells is a topic of extensive

research<sup>1</sup>. Microcarriers (MC), which can be defined as small beads where anchorage dependent cells grow in suspension<sup>2</sup>, are promising candidates for this application, as they provide significantly higher surface for cellular interaction<sup>2</sup>. First proposed by Van Wezel in 1967<sup>3</sup>, MC in cell culture constitute a system with a high specific surface (which depends on the sphericity) available for the cells to adhere, thus being able to grow in extremely high density (theoretically, up to 8 times more) in comparison to the conventional culture<sup>2</sup>. Moreover, they can also be used to encapsulate different biological moieties or drugs<sup>4</sup>. As scaffold for tissue engineering, MC have several advantages: (i) they can be made injectable, by simply immersing them in a suitable medium; (ii) as a suspension, they can adapt to the shape of any tissue defect; (iii) they can create a discontinuous liquid environment, assuring sufficient diffusion of nutrients and gases; and finally (iv) they ensure homogenous distribution of cells. As can be seen in Figure 5.1, the MC may behave, once implanted, as scaffold in which the cells may be homogeneously distributed, compared to the typical macroporous scaffolds, in which sometimes the cell penetration and diffusion may be decreased.

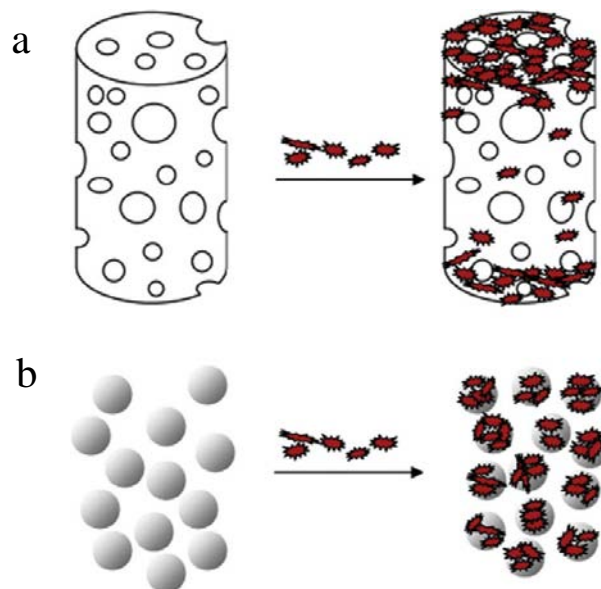


*Figure 5.1. The concept of using microcarriers as cell microcarriers or microscaffolds, with respect to its cell distribution showing: a) non-homogenous cell seeding on macroporous scaffold and b) homogenous cell seeding on microcarriers<sup>5</sup>.*

MC have been obtained from several materials, including polymers such as dextran, polylactic acid, chitosan, alginates or gelatine<sup>6-8</sup>, ceramics such as hydroxyapatite (HA), silica or bioactive glasses<sup>9,10</sup>, and composites<sup>11,12</sup>.

Calcium phosphate (CaP) based materials are being increasingly used as synthetic bone grafts. Together with their unlimited availability, these biomaterials have other advantages such as their bioactivity and osteoconductivity. However, they are not osteogenic, and in presence of these synthetic materials, bone regeneration can take a long time for the complete functional recovery. In order to enhance their efficiency as bone grafts, CaP can be combined with growth factors, such as bone morphogenetic proteins or they can also be associated with cells<sup>13-15</sup>.

CaP have been traditionally fabricated as dense or macroporous blocks, although granules are also widely used, since their resorption has been predicted to be faster<sup>15</sup>. Most granules used for bone regeneration applications have irregular shapes and submillimeter sizes. However, when they are intended to be associated with cells or with bioactive molecules, the control of the shape, size and textural properties of these particulate materials becomes crucial<sup>14,15</sup>. In this context, the development of porous calcium phosphate MC with tailored size and porosity represents a significant advance. The introduction of customized porosity, allows the incorporation of biological moieties or drugs and its controlled release. The round shape, in addition to enhance cell attachment<sup>2</sup>, is envisaged to minimize non-desirable inflammation reactions from the body. Moreover, a higher sphericity contributes to enhancing injectability, as compared to irregular granules.

Previous studies reported the fabrication of CaP MC, and more specifically hydroxyapatite (HA) MC by different routes. Generally, a two-step process was needed, consisting first, in the formation of the MC, for instance, by the dispersion of HA/polymer slurries in a hydrophobic medium, followed by a high temperature sintering stage<sup>4,9,17</sup>. Alternatively, HA-coatings were formed on glass<sup>17</sup> or carbon<sup>18</sup> MC. Composite MC containing HA were also prepared by combining an organic phase, such as sodium alginate<sup>20</sup>, gelatin<sup>12</sup> or collagen<sup>11</sup> with HA. In this approach, the stabilisation of the MC was obtained by the gellification or crosslinking of the organic phase, which encapsulated the HA particles.

In this work, a different strategy was used, based on the emulsion of a calcium phosphate cement paste (CPC) in oil. The CPC emulsion method was first proposed by Bohner<sup>5,10</sup>, and has been proved to be successful for the processing of macroporous ceramic scaffolds<sup>21</sup>. However, to our knowledge, no studies have been performed on its

application for the production of HA and composite MC. One of the main advantages of this approach is that, it should allow the preparation of HA MC at low temperature, without the need of a high temperature sintering step. The reason is that the CPC paste, which constitutes the hydraulic phase in the emulsion, has the ability to self-set through a dissolution-precipitation reaction, stabilising the CaP droplets<sup>22</sup>. This implies that, hydrated compounds can be formed as the MC constituents, with morphologies and compositions very similar to the CaP found in the mineralized tissues and with high specific surface. Furthermore, provided the intrinsic porosity of CPC in the micro/nanometric range, this route can allow the preparation of MC with a particular microtexture suitable for drug delivery applications<sup>23,24</sup>. An additional advantage of the proposed technique is that it allows the incorporation of water soluble polymers in the MC by dissolving them in the liquid phase of the CPC.

## **5.2. Objectives**

The objective of this chapter was the preparation of porous HA MC by the CPC emulsion technique, and the analysis of the effect of different processing parameters on their final properties. The incorporation of gelatin in the MC, with the aim of enhancing cell recognition<sup>25</sup>, was also explored. The *in vitro* cell response of the MC obtained was assessed by means of osteoblastic-like Saos-2 cell cultures.

## **5.3. Materials and methods**

### **5.3.1. Microcarriers preparation**

The powder phase of the CPC was composed of  $\alpha$ -TCP, obtained as described in chapter 2. For the inorganic MC, the powder was mixed with a x10 Phosphate Buffer Solution (PBS). The liquid to powder ratio was adjusted in order to obtain a fluid paste. Three millilitres of this paste were introduced into a beaker, which contained 300 ml of the oil and the emulsion was produced by means of mechanical stirring (Heidolph BDC 2002) (Figure 5.2). No emulsifying agent, which could compromise the biocompatibility of the MC, was added. Stirring was prolonged until CPC setting time was reached. MC were afterwards extracted adding a 0.01% surfactant solution (Triton X-100, Sigma-Aldrich 23,472-9) dissolved in Ringers (0.9% sodium chloride (Panreac

121659.1214) aqueous solution) into the oil emulsion. MC were then separated and cleaned with acetone. Once extracted, the MC were immersed in a Ringers solution for the  $\alpha$ -TCP hydrolysis to a CDHA to be completed.

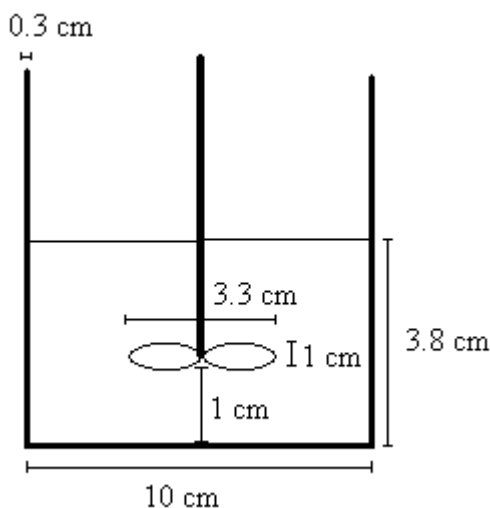


Figure 5.2. Schematic representation of the parameters that are controlled in the fabrication of the MC.

In the present work, the effect of different variables on the MC fabrication and properties was analyzed by means of a  $2^3$  factorial design. The studied variables included:

*a) Type of oil.* Oils with two different viscosities were used: sunflower oil (40 cP) and olive oil (80 cP). In a preliminary study, vaseline oil (200 cP) was also tested, but it was discarded because it was not possible to obtain a CPC emulsion;

*b) Initial powder size of the CPC.* It is known that, rheological properties and setting times of CPC pastes are strongly affected by the particle size distribution of the powder phase. Two different milling protocols for the CPC powder were established, leading to two particle size distributions, with a median particle size of  $5.18 \pm 0.25 \mu\text{m}$  for the coarse CPC and  $2.48 \pm 0.15 \mu\text{m}$  for the fine CPC. Since the viscosity of the paste varied with the particle size of the powder, the L/P ratio used for the emulsions was adjusted in each case to the minimum value at which a fluid paste could be obtained. According to this criterion, the L/P ratio was 0.7 ml/g for the coarse powder and 0.8 ml/g for the fine powder.



c) *Speed of rotation.* Two different rotation speeds, 600 and 900 rpm, were tested.

The MC were coded depending on the oil used as O (olive oil) or S (sunflower oil), followed by the particle size C (coarse) and F (fine), and the speed, 600 or 900 rpm. Thus, the different MC series were: OC600, OC900, OF600, OF900, SC600, SC900, SF600 and SF900.

Composite gelatine/HA MC were obtained by the addition of gelatine (Rousselot ref LB-B, Bloom 250) in the liquid phase, that was heated to 50°C to dissolve the gelatine powder. Three different concentrations were tested: 5, 10 and 15 w/vol % with respect to the liquid phase. The gelatine solutions were mixed with the CPC powder at liquid to powder ratios of 1.2 ml/g, 1.3 ml/g and 1.4 ml/g for 5, 10 and 15% gelatine respectively. For the preparation of the hybrid gelatine/HA MC, olive oil was heated at 60 °C, above the gelatine gelling temperature, and, after adding the CPC paste, the emulsion was formed by mechanical stirring at 900 rpm. After emulsification, an ice-cold washing solution with the same composition stated before (0.01% surfactant in 0.9% NaCl aqueous solution) was added to the oil in order to extract the MC and simultaneously decrease the temperature of gelatine below its gelling point. MC were further cross-linked by immersing the MC in a solution of 1-ethyl-3,3(3-dimethylaminopropyl)carbodiimide (EDC, Fluka 39391) (1.15% w/v) and N-Hydroxysuccinimide (Aldrich 13,067-2) (0.03M) at a molar ratio 2:1. Since the MC were prepared at a speed of 900 rpm, with olive oil and with fine cement, the code OF900 was still used, incorporating GEL in front of it with its corresponding concentration, making the code 5% GEL/OF900, 10% GEL/OF900 and 15% GEL/OF900.

### 5.3.2. Microcarriers characterization

The size distribution of the MC was characterized by Laser diffraction (LS 13 320 Beckman Coulter), dispersing the MC in ethanol for the analysis. An optical microscope (Leica QWin) coupled to an image analysis software (Omnimet and Image J) was also used to further characterise the morphological features of the MC. In addition to the MC size distribution, this technique allowed to evaluate the sphericity of the MC, as well as to estimate their envelope surface area, an important parameter to be taken into account

when performing the cell culture studies. Scanning electron microscopy (SEM, JEOL JSM-840) and field emission SEM (FE-SEM, Hitachi H-4100FE) were used to investigate the microstructure of the different MC. The samples were previously sputtered with gold or carbon to avoid charging effects. Mercury intrusion porosimetry (MIP, Autopore IV Micromeritics) was carried out to examine the porosity content (open porosity) and to determine the pore size distribution within the MC. The MC specific surface area was measured by N<sub>2</sub> adsorption according to the BET method (ASAP 2020 Micromeritics). The MC phase composition was evaluated by X-ray diffraction analysis (XRD, Philips MRD). Ni-filtered Cu K<sub>α</sub> radiation was used. The step-scanning was performed with an integration time of 50 s at intervals of 0.017° (2θ). Indexing of the peaks was carried out by means of JCPDS cards 29-359 for α-TCP and 9-432 for HA. The relative amounts of the different phases present in the samples just after the emulsion process and after 7 days in Ringers solution were estimated on the basis of the peak intensity variation by means of the external standard method, as previously described<sup>26</sup>, having pure α-TCP as the external standard.

### 5.3.3. Cell cultures

Human osteoblast-like Saos-2 cells were used as cell model. The medium used and the protocols followed are the same as the ones described in section 3.3.2.

Two types of MC were selected for cell cultures: pure inorganic MC, coded as HA-MC (the previously described OF900 series was selected) and hybrid gelatine/HA MC, containing 5% gelatin coded as GEL/HA-MC (the previously described 5% GEL/OF900). For the preparation route, it is important to know the speed and type of oil used, indicated with the code OF900, but for the biological characterization it was not. Actually, the two MC were prepared at the same speed and with the same type of oil, being the main difference the presence or absence of gelatine. Therefore, with the codes HA-MC and GEL/HA-MC, the differences in the MC composition can be tracked more easily. These codes in the cell culture make easier comparing results and refereeing to these MC in Chapter 6 and 7. To have a narrower size distribution range, the MC were sieved between 80 and 297 μm. Control glass MC (Glass MC Beads, Sigma G2892) with diameters between 90 and 150 μm (coded as CTRL-MC) were also used for comparison. All materials were sterilized with ethylene oxide. Taking into

account that the size distribution of the different series studied was not the same, it was necessary to adjust the mass of MC introduced in each well, in order to make sure that the surface available for cell attachment was the same in each MC series. This was done by using the values obtained for the envelope surface area measured for the different MC as reported in the previous section. No statistically significant differences were found between the HA-MC and the GEL/HA-MC envelope surface areas, with a mean value of  $295 \pm 19.5 \text{ cm}^2/\text{g}$ , whereas the CTRL-MC presented an external surface area of  $475 \pm 19.0 \text{ cm}^2/\text{g}$ . Taking this into account, the mass of MC introduced in the wells was 0.039 g for HA-MC and GEL/HA-MC and 0.024 g for CTRL-MC. Prior to cell seeding, the MC were soaked in ethanol in order to favour wettability of the samples, rinsed with PBS three times and afterwards pre-soaked in medium for 24 hours.

Saos-2 cells from nearly confluent flasks were harvested as described above and seeded in 24 well ultra-low attachment plates (Costar 3473) containing the samples in the amount of 200.000 cells per well, which represented approximately  $17.000 \text{ cell}/\text{cm}^2$  of MC surface. Afterwards, 1.5 ml of complete medium was added, changed after 24 hours and then changed every 48 hours.

### *5.3.3.1. Overall cell morphology*

To follow the overall morphology of adhering living cells, fluorescence images were obtained after fluorescein diacetate staining (FDA, Invitrogen F1303) at different times (1, 7 and 14 days). The protocol followed was the same as the one described in section 3.3.4.3.

Cell morphology was further characterized by means of SEM. The protocol followed was the same as the one described in section 3.3.4.4.

### *5.3.3.2. Cell proliferation*

Relative cell numbers were evaluated at 1, 7, and 14 days by the lactate dehydrogenase (LDH) assay. The protocol followed was the same as the one described in section 3.3.4.1.

### 5.3.3.3. *Cell differentiation*

The retention of osteoblastic phenotype was evaluated by measuring alkaline phosphatase activity. The protocol followed was the same as the one described in section 3.3.4.2.

### 5.3.3.4. *Statistical analysis*

The cell experiments were performed twice using three replicates for each MC composition. Statistical analysis was carried out with significance of 5%. One way analysis of variance (ANOVA) with Fisher post-hoc test was conducted. The data are expressed as mean  $\pm$  standard deviation.

## 5.4. Results

### 5.4.1. Inorganic Microcarriers

The effects of the oil viscosity, rotation speed and initial particle size on the MC mean size and sphericity, are shown in Figure 5.3a, where the results of the  $2^3$  factorial design are summarized. In fact, as shown by the evolution of the sphericity and the mean MC size, no emulsion was really formed when sunflower oil was used with the coarse CPC at 900 rpm and with the fine one at 600 rpm. Instead, proper emulsions were formed for all the experimental conditions with the olive oil. In this case, the most significant effect was the reduction of the CPC particle size, that resulted in a decrease of the MC size ( $p < 0.05$ ). The stirring speed also had a significant effect on the MC size, an increase of which, from 600 rpm to 900 rpm, resulted in a significant reduction of the MC mean size ( $p < 0.05$ ). In all cases, a reduction in MC size was accompanied by a reduction in the dispersion of the MC size. The MC obtained in olive oil, as observed by optical microscopy, are shown in Figure 5.3b-e, which confirms the trends pointed out in Figure 5.3a.

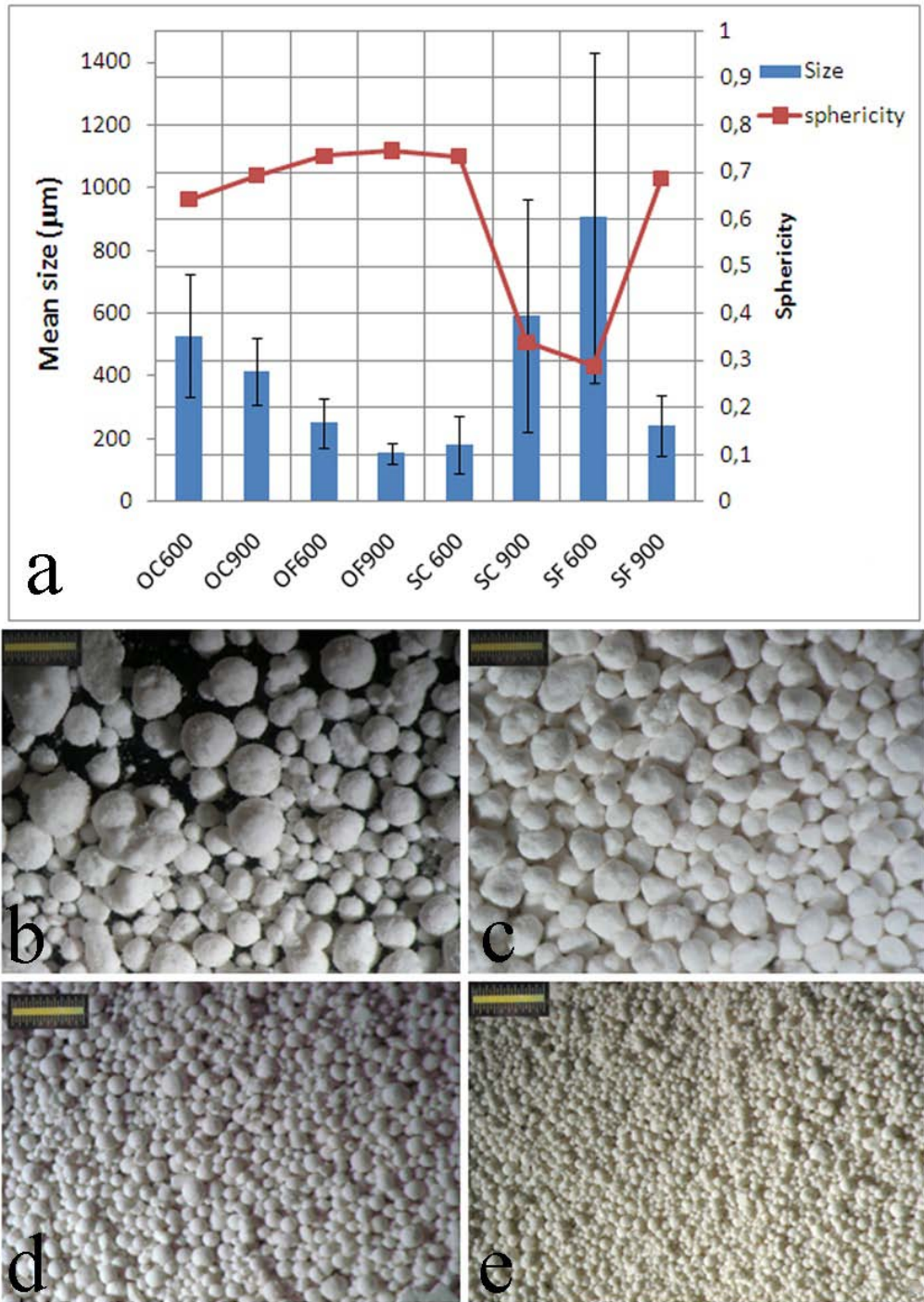


Figure 5.3. Mean size and sphericity of the microcarriers obtained by the different processing conditions tested in the factorial design (a). Optical microscopy images of the samples prepared by emulsion in olive oil: b) OC600, c) OC900, d) OF600 and e) OF900. Scale bar corresponds to 1 mm.

Figure 5.4a shows the MC size distribution, as measured by laser diffraction for the MC obtained with olive oil at 900 rpm, with different CPC particle sizes. The OF900 MC showed a monomodal and narrower distribution than the OC900 MC, which showed a

multimodal distribution. Moreover, the median size was smaller for the OF900 (180.8  $\mu\text{m}$ ) than for the OC900 (204.1  $\mu\text{m}$ ).

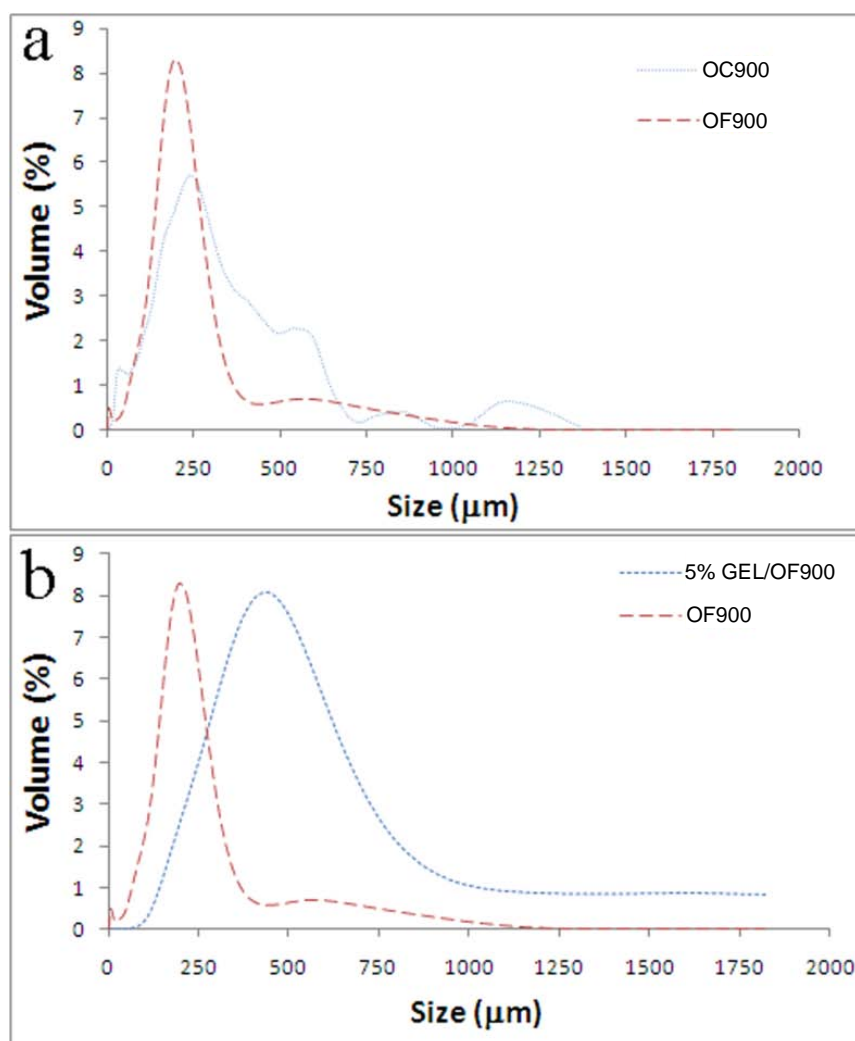


Figure 5.4. Size distribution of the microcarriers measured by laser diffraction: a) OC900 and OF900 and b) OF900 and 5% GEL/OF900.

The X-Ray diffraction patterns of the OF900 MC just after the emulsion process, and after soaking in Ringer's solution for 7 days are shown in Figure 5.5. After the emulsion process, the MC contained  $\alpha$ -TCP as the main phase and also HA, with relative amounts of 73.3 and 26.7 wt% respectively. As expected, the  $\alpha$ -TCP was nearly completely hydrolysed to HA after immersion in Ringer's solution for 7 days, when only a residual amount of 4.8 wt%  $\alpha$ -TCP was detected.

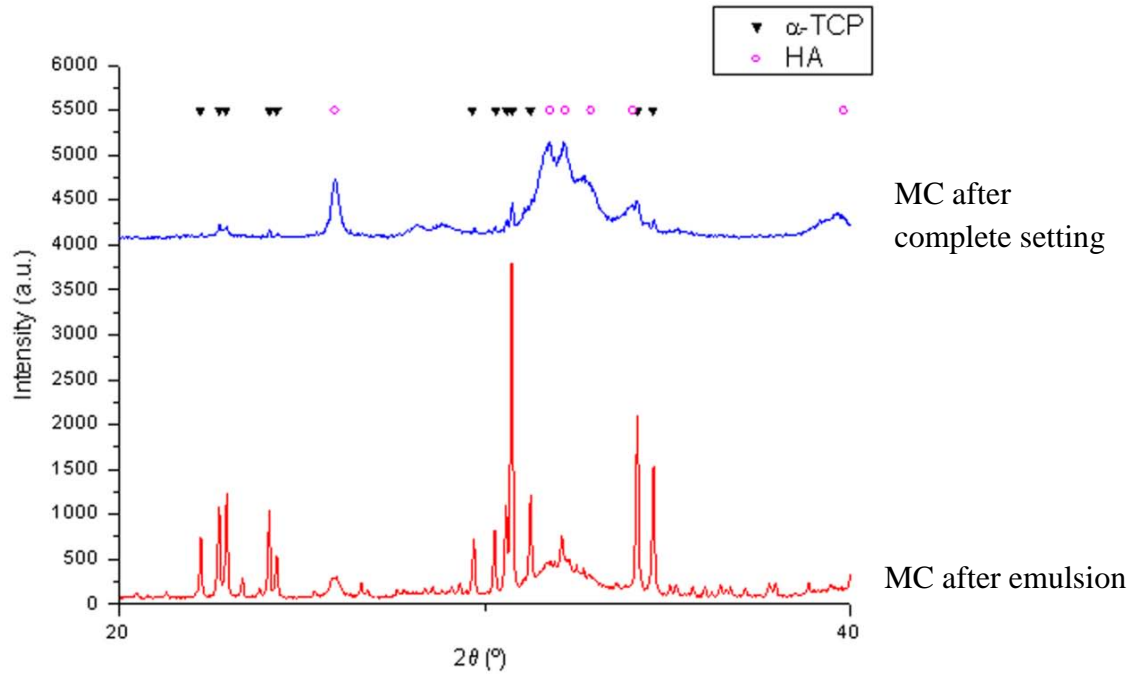


Figure 5.5. X-ray diffraction patterns of the microcarriers right after the emulsion preparation and after 7 days soaking in aqueous solution.

The broad peaks of the HA formed were consistent with the small crystal size revealed by SEM observations as shown in Figure 5.6 a) and c), which corresponds to the OF900 MC after hydrolysis. Moreover, comparison with the MC obtained with the coarse CPC powder (Figures 5.6b and d) revealed that the microstructure of the MC strongly depended on the particle size of the CPC powder used, the size of the HA crystals being much smaller when the fine CPC was used. These differences were consistently reflected in a higher specific surface area ( $27.85 \text{ m}^2/\text{g}$ ) for the OF900 MC than for the OC900 MC ( $19.94 \text{ m}^2/\text{g}$ ) as measured by  $\text{N}_2$  adsorption.

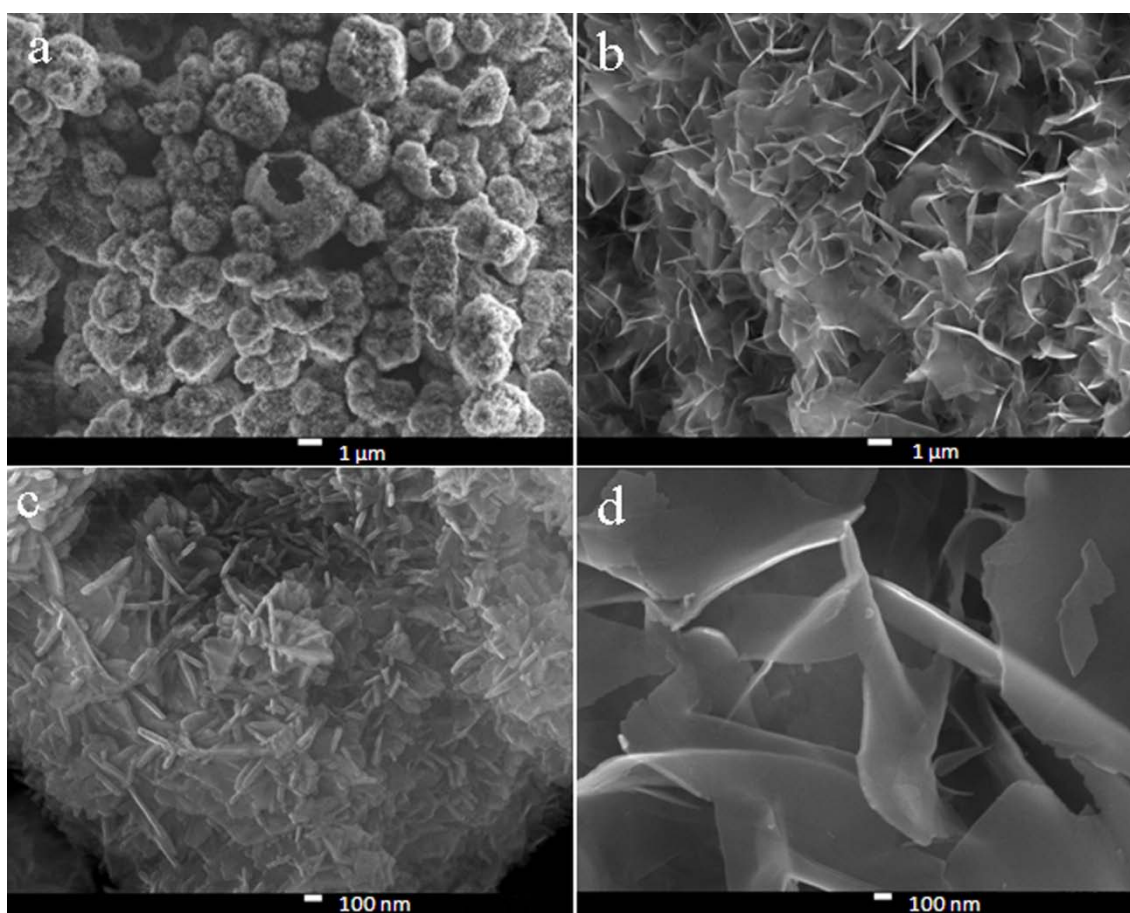


Figure 5.6. SEM images showing the different microstructures of the microcarriers prepared either with fine CPC powder (OF900): a) and c); and coarse CPC powder (OC900): b) and d).

### 5.4.2. Gelatine-Hydroxyapatite Microcarriers

As shown in Figure 5.7 a) and b), the hybrid MC presented higher sphericity and were bigger in size than the inorganic ones, all of them prepared with fine powder. When the amount of gelatin was increased, the mean size of the MC did not change, but the dispersion of the size increased. Therefore, the 5% GEL/OF900 were selected as the most promising hybrid GEL/OF900 MC and were compared with the OF900. The laser diffraction results (Figure 5.4b) revealed that the particle size distribution of the 5% GEL/OF900 MC was monomodal, as in the case of the OF900 MC, but it was broader and shifted to higher MC diameters. The median particle size was 431.6  $\mu\text{m}$  for the 5% GEL/OF900 MC, in front of 180.8  $\mu\text{m}$  for the OF900 MC. It is also worth highlighting the absence of particles smaller than 50  $\mu\text{m}$  in the gelatin containing MC, whereas in the case of the HA MC, a small peak was detected in the range of 1 to 12  $\mu\text{m}$ . SEM observations allowed to correlate this result with the presence of some debris particles that had been detached from the MC, that were observed in the case of the inorganic



MC but not in the gelatin-containing MC. The microstructure of the gelatin-containing MC is shown in Figure 5.7c, and consists of crystal agglomerates, embedded in a gelatin matrix, still present in the MC after 7 days of immersion in Ringers solution. The XRD patterns confirmed that, as for the inorganic MC, in the gelatin containing MC the  $\alpha$ -TCP transformation to HA was also complete after soaking in Ringer's solution for 7 days.

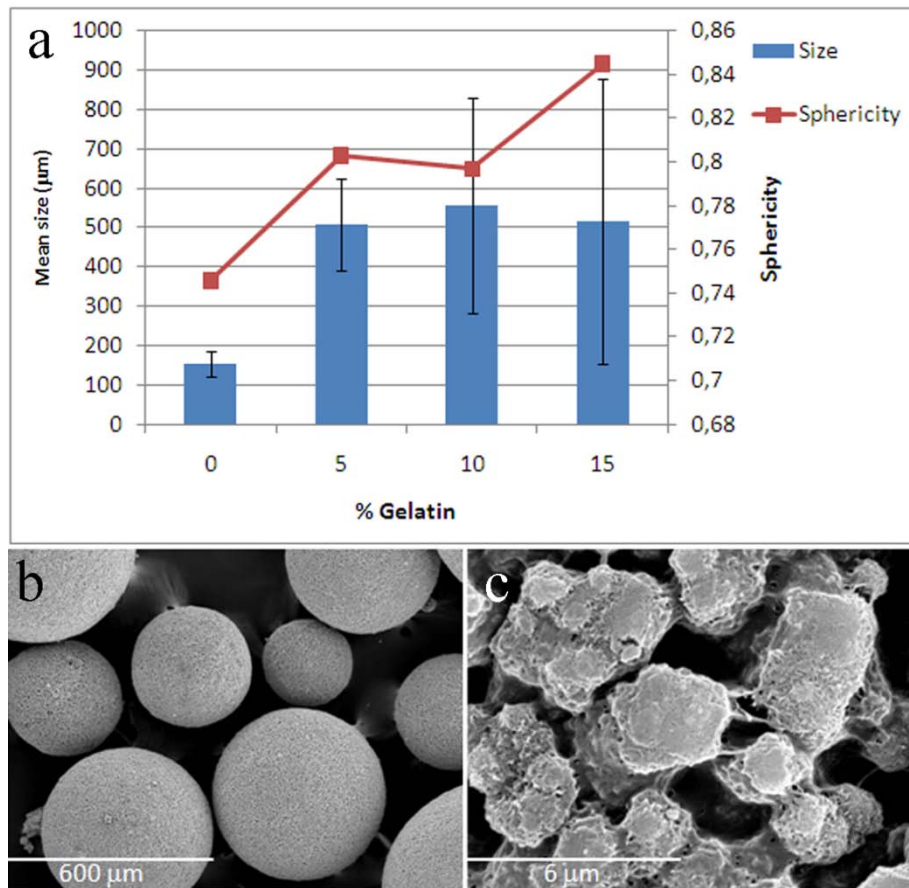


Figure 5.7. a) Mean size and sphericity of the hybrid microcarriers obtained with different gelatin concentrations with fine CPC at 900 rpm in olive oil, being 5% GEL/OF900, 10% GEL/OF900 and 15% GEL/OF900; b) SEM image of 5% GEL/OF900; c) higher magnification of the surface, showing gelatin covering the HA crystals.

The pore size distribution curves measured by MIP for the OF900 and 5% GEL/OF900 MC are plotted in Figure 5.8. The pore size distribution was similar in both cases, presenting a maximum between 0.5 and 5 µm, although also a certain population of smaller pores, between 6 nm (the lower detection limit for the MIP used) and 0.5 µm was observed. The total open porosity was higher for the gelatin containing MC (67%) than for the completely inorganic MC (47%).

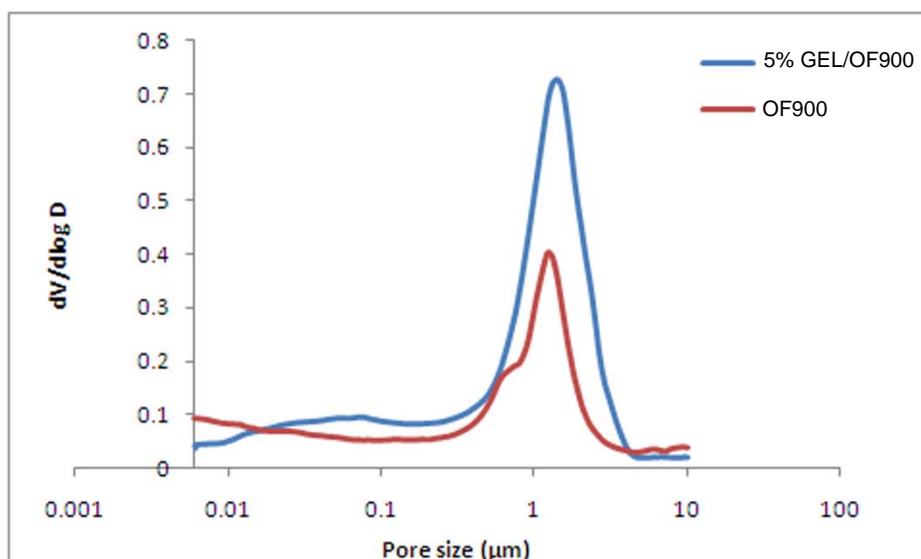


Figure 5.8. Pore size distribution of OF900 and 5% GEL/OF900 microcarriers measured by MIP.

### 5.4.3. Cellular response

The adhering Saos-2 cells at the first 24 h of incubation visualised by fluorescent microscopy after FDA staining are shown in Figure 5.9. Most pronounced initial adhesion was found on GEL/HA-MC (the previously characterized 5% GEL/OF900) (Figure 5.9b) in comparison to both pure HA-MC (the previously described OF900) (Figure 5.9a) and glass CTRL-MC (Figure 5.9c). Considering that under these conditions, only the vital cells convert FDA in a fluorescent analogue, the MC are not toxic for cells in this stage of culture. On CTRL-MC, adhering cells tended to interact over the beads, inducing their aggregation, particularly the smaller ones (Figure 5.9c).

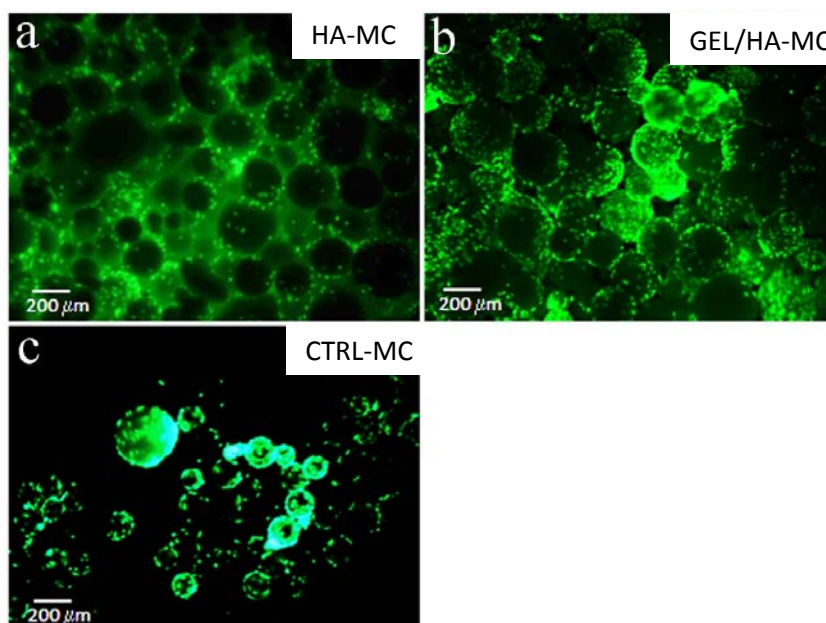


Figure 5.9. Overall cell morphology of SaOs-2 at 24 hours of incubation on different MC visualized by fluorescence after FDA staining : a) HA-MC, b) GEL/HA-MC and c) CTRL-MC

Due to the fact that the cell cultures were performed in a static environment, at low culture times, the cells were non-homogenously distributed throughout the surface of the MC. However, as cell proliferation advanced, they progressively tended to colonize the MC, resulting eventually in a more homogeneous distribution.

The average cell numbers after 1, 7 and 14 days of culture estimated via LDH assay is shown in Figure 5.10. After one day, the amount of cells was significantly higher in the GEL/HA-MC ( $p < 0.05$ ), confirming the results observed fluorescence staining with FDA, while for both the HA-MC and the CTRL-MC, the amount of non adhering cells in the suspension was higher. At day 7, however, the number of proliferating cells notably increased for both, the CTRL-MC and the GEL/HA-MC, while remained very close to day 1 for the HA-MC. However at day 14, the cell numbers increased significantly in all samples following the same ratio. The CTRL-MC showed again the highest proliferation, followed by the GEL/HA-MC, which displayed a higher cell number than the HA-MC, and these differences were statistically significant ( $p < 0.05$ ).

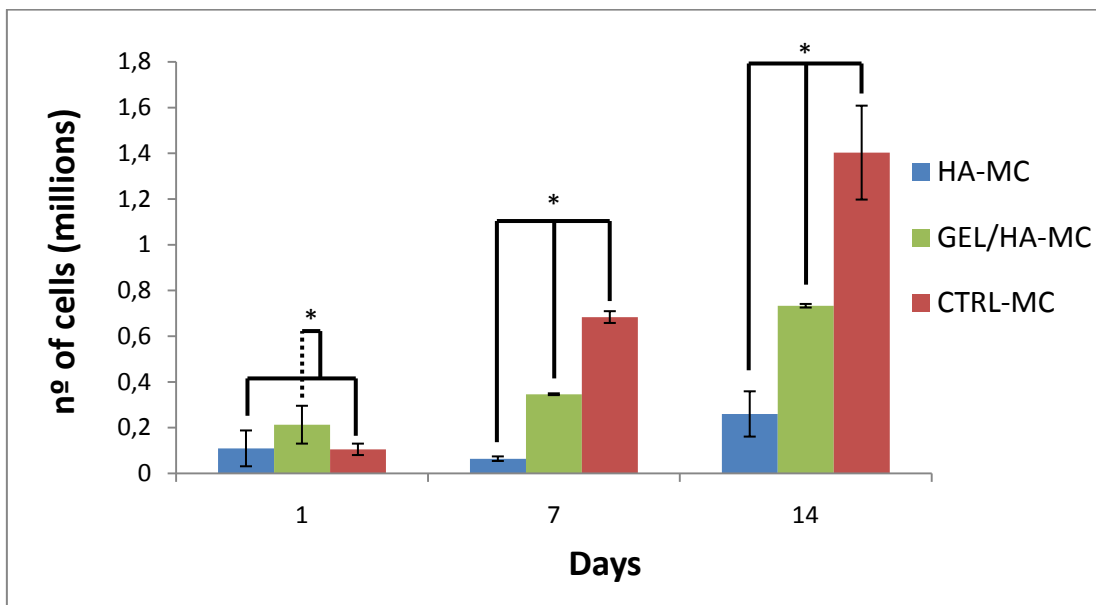


Figure 5.10. Cell proliferation at 1, 7, and 14 days as measured by LDH in direct contact experiments of Saos-2 cells on the HA-MC, GEL/HA-MC and the control CTRL-MC. All results are shown as the mean  $\pm$  standard deviation ( $n=3$ ). Asterisk (\*) indicates significant differences ( $p < 0.05$ ).

Figure 5.11 a and b, show that after 2 weeks, the Saos-2 grew better on GEL/HA-MC. Although some MC were nearly completely covered by cells (Figure 5.11 c and d), others had few cells and, in general, it can be stated that they did not form confluent layer on either HA-MC nor GEL/HA-MC, which is expectable under our static

conditions, where only the upper part of MC are exposed to cells. Nevertheless, the osteoblasts maintained their viability on both HA-MC and GEL/HA-MC, including CTRL-MC. The SEM images revealed that Saso-2 cells are more and better spread on GEL/HA-MC (Figure 5.11 d and f) versus pure HA-MC (Figure 5.11 c and e).

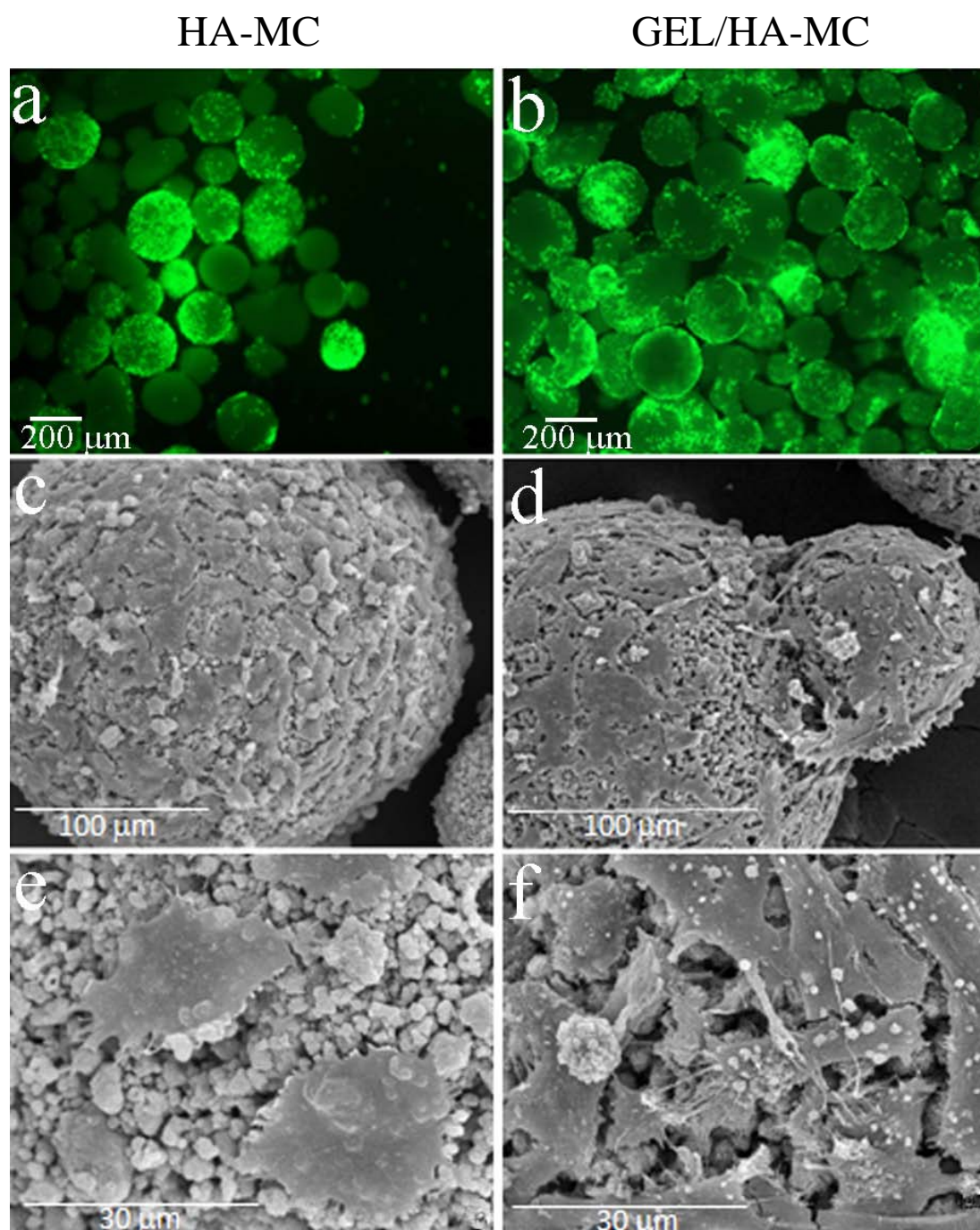


Figure 5.11. Morphology of Saos-2 cells on hydroxyapatite MC (HA-MC), a, c and e) and gelatin/hydroxyapatite MC (GEL/HA-MC), b, d and f) after 14 days of culture. a) and b) fluorescence images after FDA staining; c) - d) SEM images.

The cells on CTRL-MC showed a different morphology. The visibly higher amount of Saos-2 cells (Figure 5.12 a) resulted in almost confluent layer of viable cells formed on

some of the beads, particularly on the smaller ones. The osteoblasts tended to grow in aggregates (Figure 5.12 b), extending protrusions through which they contacted each other from the same and even neighbouring beads.

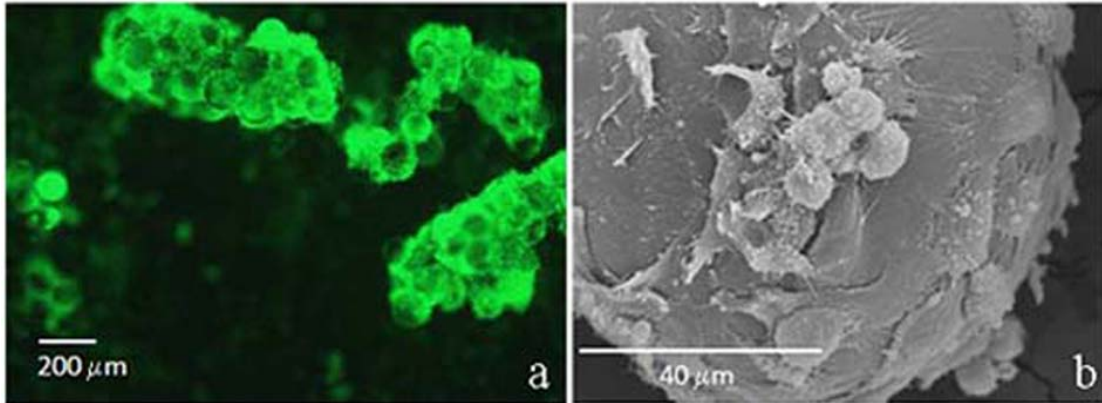


Figure 5.12. Morphology of Saos-2 cells on control glass microcarriers after 14 days of culture. a) Fluorescence images after FDA staining; b) SEM image.

Figure 5.13 reveals a common trend for increase in ALP activity of Saos-2 cells on different MC. Initially, the ALP activity was higher on HA-MC, followed by GEL/HA-MC and the CTRL-MC. After 7 days however, there was a strong increase on CTRL-MC and a smaller for both the HA-MC and GEL/HA-MC. At 14 days of culture, however, the ALP activity was similar for all three series, not showing statistically significant differences among them. Thus, whereas on HA-MC and GEL/HA-MC there was a continuous increase in the ALP activity, for the CTRL-MC, the maximum was reached after 7 days, decreasing slightly afterwards.

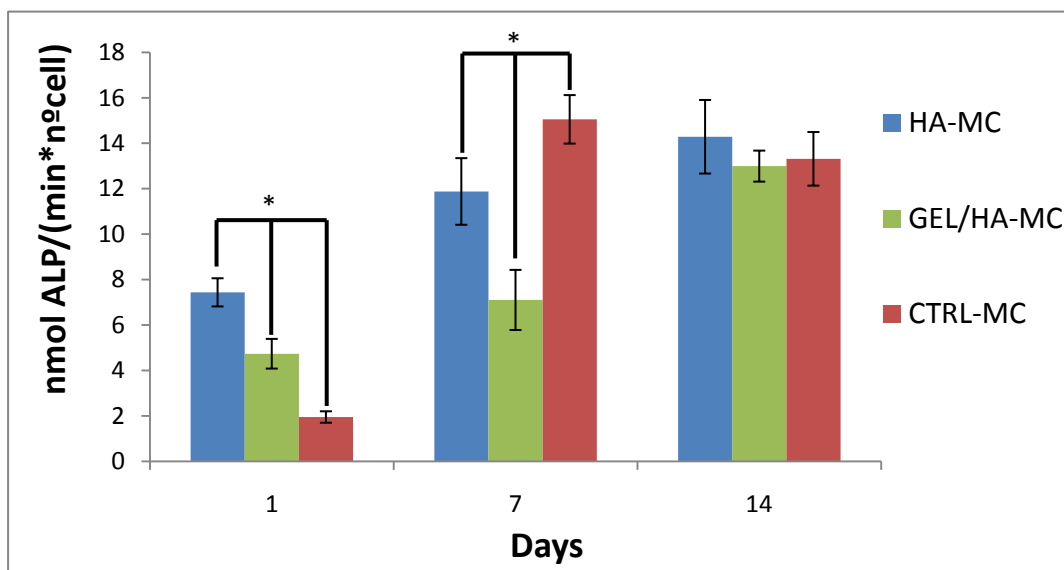


Figure 5.13. Alkaline Phosphatase activity measured in direct-contact experiments on CTRL-MC, HA-MC and GEL/HA-MC. Results were normalized with respect to cell number. Asterisk (\*) indicates significant differences ( $p < 0.05$ ).

## 5.5. Discussion

The results obtained showed that, the oil emulsion of a CPC hydraulic paste is a good method to fabricate HA or hybrid MC. Specifically, this strategy was assessed using an  $\alpha$ -TCP based CPC as the hydrophilic phase and different oils as the hydrophobic phase. Interestingly, no emulsifying agent was needed to form the emulsion.

A first requirement to form the emulsion is to have a calcium phosphate hydraulic paste with the adequate rheological properties, i.e. it must be able to flow in the oil matrix. This means that, high liquid to powder ratios are needed. However, high L/P ratios result in longer setting times, increased porosity and lower mechanical properties of the microcarriers. Setting times are especially relevant since they will determine the time required to stabilize the microcarriers. Longer setting times imply longer emulsion times, until the microcarriers are stabilized. Therefore, a compromise must be reached which ensures, on one hand, the adequate fluidity of the slurry, and on the other, adequate setting times and mechanical properties of the microcarriers.

The stabilization of the MC was achieved through the hydrolysis of the  $\alpha$ -TCP particles into a calcium deficient HA, as shown by XRD (Figure 5.5), which is a self-setting reaction in the sense that leads to the consolidation of the paste. It was shown that, according to the XRD results, after the emulsion process, which took 1 hour and 3 additional hours for complete sedimentation of the MC at the bottom of the flask, the MC contained already a 26.7 wt% of HA, confirming that the hydrolysis of the  $\alpha$ -TCP was already on course, acting as the stabilizing mechanism of the MC. In the case of the gelatin-containing MC, an additional mechanism contributed to the stabilisation of the MC: the gelatin gel transition that takes place around 38-40°C<sup>27</sup>. During the processing of the gelatin-HA MC, the occurrence of this transition contributed to the MC stabilization, making it unnecessary to wait for the CPC setting reaction to take place. Moreover, the addition of gelatin contributed to an increase of the MC sphericity (Figure 5.6). This can be attributed to the emulsifying ability of gelatin and its colloid protective features that prevented MC aggregation<sup>28</sup>. In fact, it is well known that, due to its amphiphilic character gelatin is a surface active molecule that can adsorb on O/W interfaces<sup>29</sup>.

The analysis of the factorial design performed with the HA-MC allowed extracting some conclusions on the influence of different processing parameters on MC properties. The oil viscosity had a high influence on the formation of the emulsion. Thus, when vaseline oil was used, the CPC slurry was not able to flow inside the oil due to the high oil viscosity, the ceramic particles sedimenting at the bottom of the beaker. On the other hand, when the oil viscosity was too low, which was the case of the sunflower oil, very big and non-spherical structures were formed. This can be related to the flow regime, as determined by the Reynolds number, a dimensionless parameter that gives a measure of the ratio of inertial forces to viscous forces in a fluid. In a cylindrical vessel stirred by a central rotating paddle, the Reynolds number (Re) is:

$$Re = \frac{\rho ND^2}{\mu}$$

where  $\rho$  is the density of the oil in  $\text{Kg/m}^3$ ,  $N$  is the rotational speed (revolutions per second),  $D$  is the diameter of the vessel in meters and  $\mu$  is the viscosity of the oil in  $\text{N*s/m}^2$ . The values of the Reynolds numbers for the different experimental conditions are summarized in Table 5.1. The transition Reynolds number is in the range of 2300<sup>30</sup>. Below this value, there is a laminar flow and above it, it becomes turbulent. In our experimental conditions, the Reynolds number for the oil with the highest viscosity (vaseline oil) was low, corresponding to a laminar flow. For the sunflower oil, the flow was partly turbulent, leading to the coalescence of the MC in a random way. In this case, there was a significant interaction between the oil viscosity and the consistency of the hydraulic phase, determined by the particle size of the powder, and it was difficult to control the final MC sizes and shapes, having in general lower sphericity, bigger sizes and bigger dispersion (Figure 5.3). The best results were obtained when the viscosity had an intermediate value (olive oil), with higher Reynolds numbers but within the laminar regime. For the beads obtained by emulsion in olive oil, as the speed increased the size was reduced (Figure 5.3), which is in agreement with the results found by other authors for gelatin-apatite MC<sup>12</sup>.

	Viscosity (cP)	Stirring speed (rpm)	Reynolds number
<i>Sunflower oil</i>	~40	600	2292.5
		900	3438.8
<i>Olive oil</i>	~80	600	1095.2
		900	1642.9
<i>Vaseline oil</i>	~200	600	436.5
		900	654.75

Table 5.1. Reynolds number in the different experimental conditions studied.

On the other hand, as a general trend, it was observed that when decreasing the particle size in the CPC slurry, the size of the MC decreased and the sphericity increased (Figure 5.3). This can be related to the effect of the particle size of the CPC powder on its reaction kinetics, and specifically its setting time<sup>23,31,32</sup>. The shorter setting time of the fine CPC led to a faster MC consolidation, avoiding MC fusion or aggregation during the period of mechanical agitation, which resulted in more spherical MC as compared to the coarse CPC. The particle size of the CPC also affected the final MC microstructure as observed in Figure 5.5, this being explained by the different degree of supersaturation attained from the dissolution of the fine or coarse  $\alpha$ -TCP particles<sup>32</sup>.

A key feature of the MC structure is the pore size distribution, which is especially relevant for drug delivery applications. Taking into account that the MC are obtained by a low temperature process, the drug or bioactive molecules could be either incorporated in the CPC paste prior to the emulsion, or after MC fabrication, by impregnation. In both cases, not only is the total interconnected porosity relevant, but so are the pore dimensions and pore size distribution relevant<sup>23,24</sup>. The pore size distribution function was similar for the MC obtained with fine CPC either in the presence or in absence of gelatin, in both cases presenting a maximum porosity centered around 1.4  $\mu\text{m}$ . However, the total porosity was higher for the gelatin containing MC. This was attributed to the higher liquid to powder ratio used, namely 1.2 ml/g for the 5% GEL/OF900 MC in front to 0.8 ml/g for the OF900 MC, which has been previously shown to result in an increased porosity in the micrometric range<sup>23</sup>. In fact, the pore size obtained in the MC, could allow not only the incorporation of small molecular weight drugs, but also larger molecules such as proteins. Indeed, it has been shown that CPC with pore sizes in the same range of those in the MC, allowed albumin penetration,



whereas smaller pore sizes prevented the absorption of the protein, therefore limiting loading capacity of the substrate<sup>23</sup>.

The gelatin containing microcarriers showed a higher sphericity (Figure 5.7). This can be attributed to the emulsifying ability of gelatine, due to its amphiphilic character, having polar and non-polar groups in its structure. This makes gelatine a surface/interfacial active molecule that can adsorb on O/W interfaces with various hydrophobic segments penetrating into the oil phase, and decreasing the surface tension. In fact, surface tension plays an important role in the formation of the microcarriers. As gelatine concentration is increased, surface energy is decreased<sup>29</sup>, approaching the surface energy of olive oil. An additional advantage of gelatin is that, it can prevent particle aggregation because of the colloid protective feature gelatine has<sup>33</sup>. In our case, the fact that gelatin was dissolved in PBS increased the polarity of the dissolution, enhancing its effect as surface active agent.

Besides the previously mentioned processing advantages, the addition of gelatin in the MC significantly improved their biological performance, enhancing cell adhesion due to the better exposure of RGD sequences in gelatin<sup>34</sup>, which together with other collagen specific adhesive sequences, e.g. GFOGER motif in the  $\alpha$ I domain<sup>35</sup>, are directly involved in cell adhesion recognized by both  $\alpha$ 1 $\beta$ 1 and  $\alpha$ 2 $\beta$ 1 integrins<sup>35,36</sup>.

The number of cells after 1 day was significantly higher on the gelatin containing MC when compared to both the control and the inorganic MC, and cell proliferation was also significantly higher in the gelatin containing MC than in the inorganic ones. This behaviour is in good agreement with previous results reported for CPC/gelatin composites<sup>37,38</sup> and gelatin/nanoHA composites<sup>39</sup>, and can be attributed to the exposed RGD sequence contained in gelatin, which is involved in the integrin-dependent cell adhesion<sup>35,36</sup>. Another aspect that can contribute to the improved cell response is that, gelatin increased the cohesion of the MC, avoiding the release of small particles, as revealed by laser diffraction (Figure 5.4). Conversely, when cell were cultured on the inorganic HA-MC, some particles were found in the wells. Negative effects of CPC debris particles on osteoblast activity have already been reported for particle sizes below 10  $\mu$ m<sup>40</sup>.

It is important to note that the two types of MC analysed in the *in vitro* study were obtained with fine powder CPC, which after setting form nanometric HA crystals, with a very high surface area. It has been previously reported that this kind of microstructure elicits low proliferation rates compared to TCPS or even to HA with bigger crystal sizes<sup>41,42</sup>. This could explain the lower proliferation rates of osteoblasts on the HA containing MC compared to the CTRL-MC. Interestingly, other studies reported also decreased cell attachment and proliferation when the specific surface of OCP microscaffolds was increased<sup>43</sup>. Despite the lower proliferation rate compared to that of the CTRL, both the CPC MC were able to sustain cell attachment and proliferation. This, together with the fact that HA is an osteoconductive material, able to guide bone ingrowth *in vivo*, make these MC, good candidates for bone regeneration applications. Moreover, an enhanced biodegradability is expected in the case of the gelatin containing MC, as a result of both the higher porosity and the degradability of gelatin itself<sup>44</sup>.

The results shown in figure 5.12, suggest that cell differentiation was accelerated in the HA containing microcarriers, especially on the pure HA-MC. The cells growing on these MCs showed higher ALP activity even at the early stages of culturing compared to the control MC. At 14 days, however the ALP activity was similar for all series. These results correlate well with our previous data, showing enhanced cell differentiation of osteoblast-like MG63 cells when cultured on low temperature hydroxyapatite substrates that have a very similar composition and topography to those of the HA-MC<sup>42</sup>. In that study, the enhancement of cell differentiation was attributed to the specific substrate topography. Focusing on the effect of gelatine, previous works report a slight increase of differentiation due to gelatine incorporation in the HA<sup>38</sup>. However, it has to be considered that the ALP activity is provided as absolute values (of p-nitrophenol)<sup>38</sup>, whereas in the present work the values were normalised by the number of cells and if the total amount of p-nitrophenol are compared, the trend is the same.

Collectively, our results suggest an enhanced functional activity of osteoblast when cultured on GEL/HA-MC. The differences in the morphology are remarkable even at 1 day of culture in which cells appear to attach (Figure 5.8) and spread better on GEL/HA MC than on CTRL-MC and HA-MC. Similar results were found with cells on gelatine cement composite material when compared to a normal cement<sup>37</sup>. The differences in cell morphology are still maintained at 14 days of culture, where osteoblasts are better

spread on GEL/HA-MC in comparison to pure HA-MC (Figure 5.11 f vs e). Moreover, cells present distinct dorsal activity manifested by development of fibril-like features, presumably reflecting the formation of new ECM. It is in accordance with other studies showing that different types of cells when cultured on cement develop a rounded shape with few phyllopodia, but when gelatine is present, cells become more flattened and spread<sup>38</sup>. However, it does not correlate well with the observed tendency for equalisation of ALP activity for all samples at the 14 days of culture – a fact that may be attributed to the insufficient culture conditions. It seems that higher amount of cells on MCs need facilitated diffusion of nutrients and gases, therefore using spinner flasks might be required in a future work.

## **5.6. Conclusions**

An optimized protocol for the preparation of HA and hybrid gelatine/HA MC from the emulsion of CPC slurries in oil has been presented. The formation of the MC is based on the setting reaction of the CPC, which hardens inside the hydrophobic phase. Our results show that these MC are suitable for culturing osteoblast-like cells, thus representing a promising scaffold for bone tissue engineering application. Gelatine incorporation in the aqueous phase, in addition to improving MC formation and stability, enhances the biological performance of the MC to support initial osteoblast interaction and subsequent growth.

## 5.7. References

1. Meijer GJ, de Bruijin JD, Koole R & van Blitterswijk CA. Cell-based bone tissue engineering. *PLoS Med* **4**, 260-265 (2007).
2. Malda J & Frondoza CG. Microcarriers in the engineering of cartilage and bone. *Trends in Biotechnology* **24**, 299-304 (2006).
3. van Wezel AL. Growth of cell-strains and primary cells on micro-carriers in homogeneous culture. *Nature* **216**, 64-65 (1967).
4. Komlev VS, Barinov SM & Koplík EV. A method to fabricate porous spherical hydroxyapatite granules intended for time-controlled drug release. *Biomaterials* **23**, 3449-3454 (2002).
5. Ginebra MP, Espanol M, Montufar EB, Perez RA & Mestres G. New processing approaches in calcium phosphate cements and their applications in regenerative medicine. *Acta Biomaterialia* **6**, 2863-2873 (2010).
6. Cheh XG *et al.* Preparation and biocompatibility of chitosan microcarriers as biomaterial. *Biochemical Engineering Journal* **27**, 269-274 (2006).
7. Chung TW, Huang YY & Liu YZ. Effects of the rate of solvent evaporation on the characteristics of drug loaded PLLA and PDLLA microspheres. *International Journal of Pharmaceutics* **212**, 161-169 (2001).
8. Ping H, Davis SS & Illum L. Chitosan microspheres prepared by spray drying. *International Journal of Pharmaceutics* **187**, 53-65 (1999).
9. Komlev VS *et al.* Porous spherical hydroxyapatite and fluorhydroxyapate granules: processing and characterization. *Science and Technology of Advanced Materials* **4**, 503-508 (2003).
10. Bohner M. Implant comprising calcium cement and hydrophobic liquid [US Patent]. 6642285 B1, 2003.

11. Wu TJ *et al.* Studies on the microspheres comprised of reconstituted collagen and hydroxyapatite. *Biomaterials* **25**, 651-658 (2004).
12. Kim HW, Yoon BH & Kim HE. Microsphere of apatite-gelatin nanocomposite as bone regenerative filler. *Journal of Materials Science: Materials in Medicine* **16**, 1105-1109 (2005).
13. Cancedda R, Giannoni P & Mastrogiacomo M. A tissue engineering approach to bone repair in large animal models and in clinical practice. *Biomaterials* **28**, 4240-4250 (2007).
14. Fischer EM, Layrolle P, Van Blitterswijk CA & De Bruijn JD. Bone Formation by Mesenchymal Progenitor Cells Cultured on Dense and Microporous Hydroxyapatite Particles. *Tissue Engineering* **9**, 1179-1188 (2003).
15. Mankani MH, Kuznetsov SA, Fowler B, Kingman A & Robey PG. In Vivo Bone Formation by Human Bone Marrow Stromal Cells: Effect of Carrier Particle Size and Shape. *Biotechnology and Bioengineering* **72**, 96-107 (2001).
16. Bohner M & Baumgart F. Theoretical model to determine the effects of geometrical factors on the resorption of calcium phosphate bone substitutes. *Biomaterials* **25**, 3569-3582 (2004).
17. Paul W & Sharma ST. Development of porous spherical hydroxyapatite granules: application towards protein delivery. *Journal of Materials Science: Materials in Medicine* **10**, 383-388 (1999).
18. Qiu Q, Ducheyne P & Ayyaswamy PS. Fabrication, characterization and evaluation of bioceramic hollow microspheres used as microcarriers for 3-D bone tissue formation in rotating bioreactors. *Biomaterials* **20**, 989-1001 (1999).
19. Wu C & Chang J. Bonelike apatite formation on carbon microspheres. *Material Letters* **61**, 2502-2505 (2007).

20. Barrias CC, Ribeiro CC & Barbosa MA. Adhesion and proliferation of human osteoblastic cells seeded on injectable hydroxyapatite microspheres. *Key Engineering Materials* **254–256**, 877–880 (2004).
21. Bohner M *et al.* Synthesis and characterization of porous  $\beta$ -tricalcium phosphate blocks. *Biomaterials* **26**, 6099-6105 (2005).
22. Ginebra MP. Calcium Phosphate bone cements. In: Deb S, editor. Orthopaedic Bone Cements. Cambridge: Woodhead Publishing Limited; 2008. p 206-230.
23. Espanol M *et al.* Intrinsic porosity of calcium phosphate cements and its significance for drug delivery and tissue engineering applications. *Acta Biomaterialia* **5**, 2752-2762 (2009).
24. Ginebra MP, Traykova T & Planell JA. Calcium phosphate cements as bone drug delivery systems: A review. *Journal of Controlled Release* **113**, 102-110 (2006).
25. Emsley J, Knight CG, Farndale RW, Barnes MJ & Liddington RC. Structural basis of collagen recognition by integrin  $\alpha 2\beta 1$ . *Cell* **101**, 47-56 (2000).
26. Ginebra MP *et al.* Setting reaction and hardening of an apatitic calcium phosphate cement. *Journal of Dental Research* **76**, 905-912 (1997).
27. Hayashi A & Oh SC. Gelation of gelatin solution. *Agricultural and Biological Chemistry* **47**, 1711-1716 (1983).
28. Teng S, Chen L, Guo Y & Shi J. Formation of nano-hydroxyapatite in gelatin droplets and the resulting porous composite microspheres. *Journal of Inorganic Biochemistry* **101**, 686-691 (2007).
29. Johnston JH & Peard GT. The surface tension of gelatin solutions. *Biochemical Journal* **19**, 281-289 (1925).
30. Clements DJ. Food emulsions: Principles, practices and techniques. Boca Ratón: CRC Press; 2004.

31. Liu C, Shao H, Chen F & Zheng H. Effects of the granularity of raw materials on the hydration and hardening process of calcium phosphate cement. *Biomaterials* **24**, 4103-4113 (2003).
32. Ginebra MP, Driessens FCM & Planell JA. Effect of the particle size on the micro and nanostructural features of a calcium phosphate cement: a kinetic analysis. *Biomaterials* **25**, 3453-3462 (2004).
33. Teng S, Chen L, Guo Y & Shi J. Formation of nano-hydroxyapatite in gelatin droplets and the resulting porous composite microspheres. *Journal of Inorganic Biochemistry* **101**,686-691 (2007).
34. Anselme K. Osteoblast adhesion to biomaterials. *Biomaterials* **21**,667-681 (2000).
35. Zhang WM *et al.* Alpha 11beta 1 integrin recognizes the GFOGER sequence in interstitial collagens. *Journal of Biological Chemistry* **278**, 7270-7277 (2003).
36. Knight CG *et al.* Identification in collagen type I of an integrin alpha2 beta1-binding site containing an essential GER sequence. *Journal of Biological Chemistry* **273**, 33287-33294 (1998).
37. Bigi A *et al.* A biomimetic gelatin-calcium phosphate bone cement. *International Journal of Artificial Organs* **27**, 664-673 (2004).
38. Bigi A *et al.* Normal and osteopenic bone-derived osteoblast response to a biomimetic gelatin-calcium phosphate bone cement. *Journal of Biomedical Materials Research* **78A**, 739-745 (2006).
39. Kim HW, Kim HE & Salih V. Stimulation of osteoblast responses to biomimetic nanocomposites of gelatin-hydroxyapatite for tissue engineering scaffolds. *Biomaterials* **26**, 5221-5230 (2005).
40. Pioletti DP *et al.* The effects of calcium phosphate cement particles on osteoblast functions. *Biomaterials* **21**, 1103-1114 (2000).

41. Misiek DJ, Kent JN & Carr RF. Soft tissue responses to hydroxylapatite particles of different shapes. *Journal of Oral and Maxillofacial Surgery* **42**, 150-160 (1984).
42. Engel E *et al.* Discerning the role of topography and ion exchange in cell response of bioactive tissue engineering scaffolds. *Tissue Engineering* **14**, 1341-1351 (2008).
43. Shelton RM *et al.* Bone marrow cell gene expression and tissue construct assembly using octacalcium phosphate microscaffolds. *Biomaterials* **27**, 2874-2881 (2006).
44. Kuijpers AJ *et al.* *In vivo* compatibility and degradation of crosslinked gelatin gels incorporated in knitted Dacron. *Journal of Biomedical Materials Research* **51**, 136-145 (2000).



# **Chapter 6: Hydroxyapatite/collagen Microcarriers for Bone Tissue Engineering Applications**

## **6.1. Introduction**

Microcarriers (MC) were originally developed for culturing anchorage dependent cells in suspension<sup>1</sup> as was described in the previous chapter. Apart from their biotechnological applications, however, recent studies have shown their potential for tissue engineering purposes, as vectors for the delivery of cells or drug release vehicles<sup>2-6</sup>. Suspensions of MC can be easily injected or implanted in the diseased tissue, such as bone, and if they are colonized with cells, MC can function as scaffolds for bone tissue repair<sup>5</sup>. For this specific application, it is important to fabricate MC of a material that

has the ability to enhance bone ingrowth *in vivo*. In this context, the development of MC of osteoconductive and osteoinductive materials, such as calcium phosphates, can be especially useful<sup>7-9</sup>.

Hydroxyapatite (HA)/collagen based materials have been extensively used as substrates for bone tissue engineering as they mimic the extracellular bone matrix. Interesting results have been reported for this kind of materials, combining the osteoconductivity of HA with an enhanced recognition from the cells, provided by collagen incorporation<sup>10-16</sup>. Microspheres made of collagen and HA have been previously obtained by emulsion of a collagen solution in oil<sup>17-19</sup>. In these works however, the collagen was the continuous phase, its content ranging between 35 and 70 wt%, and the stabilization of the MC was achieved through chemical crosslinking. In the present work a novel approach is proposed, based on the emulsion of a collagen-containing calcium phosphate cement (CPC) paste in oil. The stabilization of the MC is achieved through the setting reaction of the CPC.

The setting reaction produces an entangled network of calcium deficient HA crystals<sup>20</sup>. Since the native type I collagen is soluble in acidic water solutions, it can be introduced in the system by dissolving it in the liquid phase of the CPC - a strategy that should allow the preparation of porous, protein-containing MC with high mineral content. Moreover, as the consolidation arises from the setting reaction of the inorganic phase, the cross-linking of the collagen should not be necessary. The high HA content is expected to enhance the osteogenic properties of the MC.

This chapter describes the synthesis of the above hybrid HA/collagen MC and their interaction with osteoblast-like Saos-2 cells. An additional point that is tackled in this work is the effect of the MC microstructure on the cell response, as it is well documented that microporosity and surface texture of bioactive ceramics can affect their biological performance, and even their osteoinductive properties<sup>9</sup>. It has been previously shown that micro and nanostructured HA can be obtained from an alpha tricalcium phosphate ( $\alpha$ -TCP) cement, by modifying the particle size of the starting cement powder<sup>21</sup>.

## 6.2. Objectives

The objective of the present work was to develop micro and nanosized HA/collagen MC. The fabrication of microcarriers constituted of CPC and collagen has not been previously reported. The effect of both, the presence of collagen, and the HA microstructure, on the cellular response, was evaluated culturing osteoblast like cells SaOs-2 for 14 days.

## 6.3. Materials and methods

### 6.3.1. Microcarrier preparation

The powder phase of the CPC was composed of  $\alpha$ -tricalcium phosphate ( $\alpha$ -TCP). The fabrication process applied was the same as the one described in section 2.3.1. Coarse and fine CPC were obtained according to the protocols described in section 2.3.1.

The liquid phase was prepared by dissolving bovine type I collagen in a 50 mM acetic acid aqueous solution at a concentration of 10 mg/ml. Collagen was obtained from bovine pericardium as described in section 2.3.2.1.

A ceramic slurry was prepared by mixing the CPC powder with the corresponding liquid phase at a L/P ratio of 0.8 ml/g. This means a collagen: $\alpha$ -TCP weight ratio of 0.8:100 for the collagen containing MC. The setting time of the CPC paste was measured by the Gilmore needle method according to the standard ASTM C266-99 (ASTM International C266-99, 2007).

An emulsion was formed by mixing both components with a mechanical stirrer (Heidolph BDC 2002), at 900 rpm, for a period of time equal to the setting time of the CPC paste. The setting times of the different CPC compositions are reported in Table 6.1.

	No collagen	Collagen
Coarse powder	100	108
Fine powder	48	90

*Table 6.1. Initial setting times (min) of the different CPC slurries prepared with coarse or fine powder and with or without collagen (10 mg/ml) in the liquid phase.*

The addition of collagen increased the viscosity and also the initial setting times, requiring longer emulsion times. In contrast, the use of fine powder allowed reducing the emulsion times. After their consolidation, the microcarriers were extracted by adding a 0.9 wt% sodium chloride and 0.01% surfactant (Triton X-100) aqueous solution. Afterwards, they were immersed in a 0.9 wt% sodium chloride solution for 7 days. Four series of MC were studied: two hydroxyapatite MC, produced with either the fine or the coarse powder (HAc and HAcf respectively) and the corresponding collagen-containing HA MC (COL/HAc and COL/HAcf).

### **6.3.2. Microcarriers characterization**

X-ray diffraction (XRD) was used to analyze the phases present in the MC and to assess if collagen modified the end product of the CPC. The MC were crushed and a powder diffraction pattern was obtained (Philips MRD, Cu K $\alpha$ , 40  $\mu$ A, 45 kV, scan step size 0.017 $^\circ$ , step time 50 s). The peaks were indexed using cards JCPDS-29-359 for  $\alpha$ -TCP and JCPDS-9-432 for apatite (Joint Committee on Powder Diffraction Standards, 1988). The specific surface area (SSA) of the MC was measured by N $_2$  adsorption according to the BET method (ASP 2020 Micromeritics).

An image analysis software (Ominimet and Image J) coupled to an optical microscope (Leica QWin) was used to determine MC size and sphericity. Moreover, this technique allowed estimating the envelope surface area of the MC, an important parameter to be taken into account when performing the cell culture studies. The size distribution of the MS was characterized by Laser diffraction (LS 13 320 Beckman Coulter), dispersing the MC in ethanol for the analysis. The morphology and microstructure of the MC was characterized by Scanning electron microscopy (SEM, JEOL JSM-840).

The presence of collagen and its distribution in the MC was studied using 3-(4carboxybenzoyl)quinoline- 2-carboxaldehyde (CBQCA, Invitrogen) as fluorescent marker. After rinsing the samples with abundant water in order to remove possible salts that could interfere in the fluorescence, they were then left reacting in a 1 mM CBQCA and 2 mM KCN aqueous solution for 90 minutes. Afterwards, samples were rinsed to remove the excess and the non-reacted dye, and observed in a confocal microscope (Leica TCS-SPE) with an emission of 490 nm.

### 6.3.3. *In vitro* culture test

The culture assay was performed in order to determine the viability of the MCs as potential cell carriers. Human osteoblast-like Saos-2 cells were used as cell model. The medium used and the protocols followed are the same as the ones described in section 3.3.2.

Prior to the cell culture studies, the MC were sieved between 100 and 297  $\mu\text{m}$  in order to have the same size distribution for the different series studied. Three types of MC were analyzed, namely HAf, COL/HAf and COL/HAc. It was not possible to test the HAc MC due to their bigger size and lower sphericity. Glass microspheres (Glass MC Beads, Sigma G2892) were used as control MC (CTRL), having a size range between 90 and 150  $\mu\text{m}$ . Materials were sterilized with ethylene oxide.

The MC were introduced in a twenty-four ultra-low attachment well plates. In order to favor wettability of the samples, MC were previously soaked in ethanol, rinsed with PBS three times and afterwards pre-soaked in medium for 24 hours prior to cell seeding. Taking into account that the size distribution of the MC obtained and the control MC was not the same, it was necessary to adjust the mass of MC introduced in each well, in order to make sure that the surface available for cell attachment was the same in each series. This was done by using the values obtained for the envelope surface area measured for the different MS, as reported in the previous section. Thus, the amount of MC introduced was 39 mg/well for the three series of MC and 24 mg/well for the CTRL MC. Saos-2 cells (200,000 cells/well) were seeded on the MC. Afterwards, 1.5 ml of complete medium was added, changed after 24 hours and then changed every 48 hours.

#### 6.3.3.1. *Morphology*

To follow the overall morphology of adhering living cells, fluorescence images were obtained after fluorescein diacetate staining (FDA, Invitrogen F1303) to monitor cell viability at different times after 1, 7 and 14 days. SEM images were also taken in order to characterize cell morphology. The protocols followed in each of the cases are described in section 3.3.4.3. and 3.3.4.4.

### 6.3.3.2. Cell proliferation

Relative cell numbers were evaluated at 1, 7, and 14 days by the lactate dehydrogenase (LDH) assay. The protocol used is described in section 3.3.4.1.

### 6.3.3.3. Cell differentiation

The retention of osteoblastic phenotype was evaluated by measuring alkaline phosphatase activity. The protocol used is described in section 3.3.4.2.

## 6.3.4. Statistical analysis

The cell experiments were performed twice using three replicates for each MC composition. Statistical analysis was carried out with significance of 5%. One way analysis of variance (ANOVA) with Fisher post-hoc test was conducted. The data are expressed as mean  $\pm$  standard deviation.

## 6.4. Results

### 6.4.1. Microcarrier characterization

Figure 6.1 shows the size distribution of the different MC. The collagen containing MC showed a broader particle size distribution, compared to their inorganic counterparts.

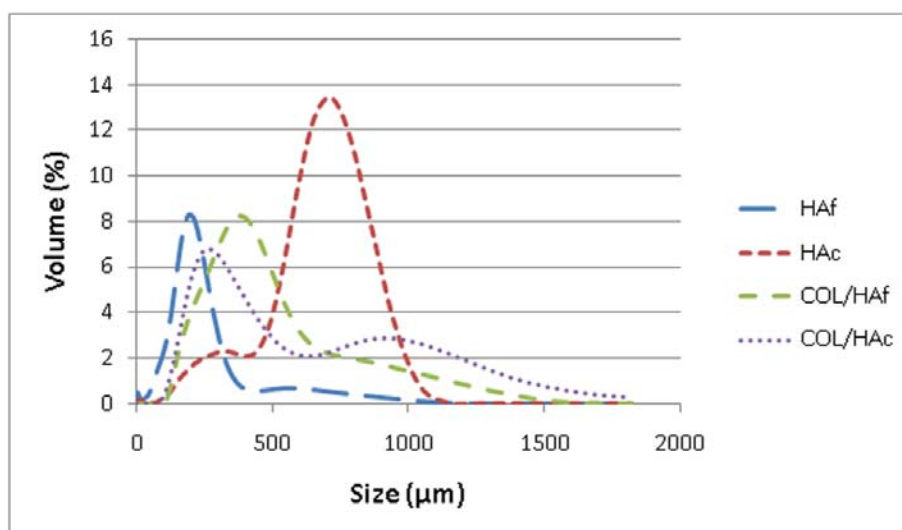


Figure 6.1. Particle size distribution of the different inorganic or collagen-containing MC measured by laser diffraction.

The median size and the sphericity measured by image analysis are summarized in Table 6.2. The median size of the two collagen-containing MC was similar and close to 350  $\mu\text{m}$ , being the effect of the size of the starting powder negligible. In contrast, the starting particle size of the ceramic powder had a strong effect on the size of the inorganic MC, resulting in a median size of around 650  $\mu\text{m}$  for the coarse powder (HAc) and 180  $\mu\text{m}$  for the fine powder (HAf). The sphericity was higher in the collagen-containing MC than in the inorganic MC.

<i>Sample</i>	<b>Median Size (<math>\mu\text{m}</math>)</b>	<b>Sphericity</b>	<b>SSA (<math>\text{m}^2/\text{g}</math>)</b>
<i>HAc</i>	652.3 $\pm$ 263.4	0.70 $\pm$ 0.05	22.25 $\pm$ 0.01
<i>HAf</i>	180.8 $\pm$ 149.2	0.76 $\pm$ 0.03	29.28 $\pm$ 0.08
<i>COL/HAc</i>	333.5 $\pm$ 344.3	0.87 $\pm$ 0.03	8.39 $\pm$ 0.07
<i>COL/HAf</i>	376.4 $\pm$ 240.7	0.88 $\pm$ 0.01	11.67 $\pm$ 0.06

Table 6.2. Median size, sphericity and specific surface area (SSA) of the different inorganic and collagen-containing microcarriers as a function of the particle size of the cement powder used.

The morphology and microstructure of the microcarriers are shown in Figure 6.2.

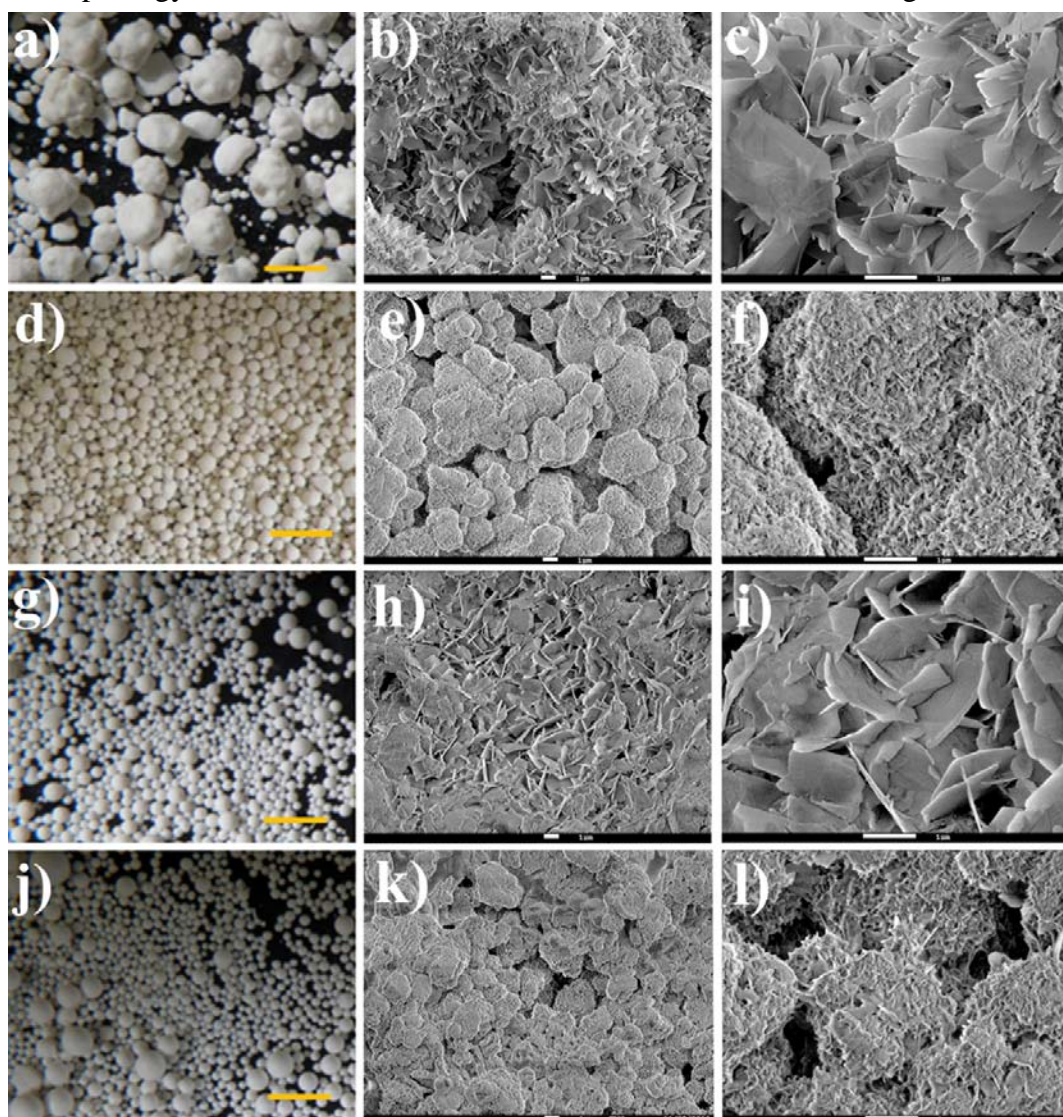


Figure 6.2. Optical and SEM images for the different MC: a), b) and c) HAc; d), e) and f) HAf; g), h) and i) COL/HAc; and j), k) and l) COL/HAf.

The microstructure of the inorganic MC consisted of entangled crystals, micrometric in size in the case of the HAc, and in the nanometric range in the HAc. When collagen was introduced in the MC, the HA crystals on the surface were still visible, retaining the same micro- or nanostructural features, although overall a flattened and less porous surface was observed. XRD results confirmed that the end product of the setting reaction of the CPC was HA in all cases (Figure 6.3). The presence of collagen did not hinder the complete hydrolysis of  $\alpha$ -TCP. However, when the coarse powder was used, the transformation was slower, as proved by a small amount of unreacted  $\alpha$ -TCP still present in the MC after 7 days (5.7% and 7.4% for the HAc and COL/HAc respectively).

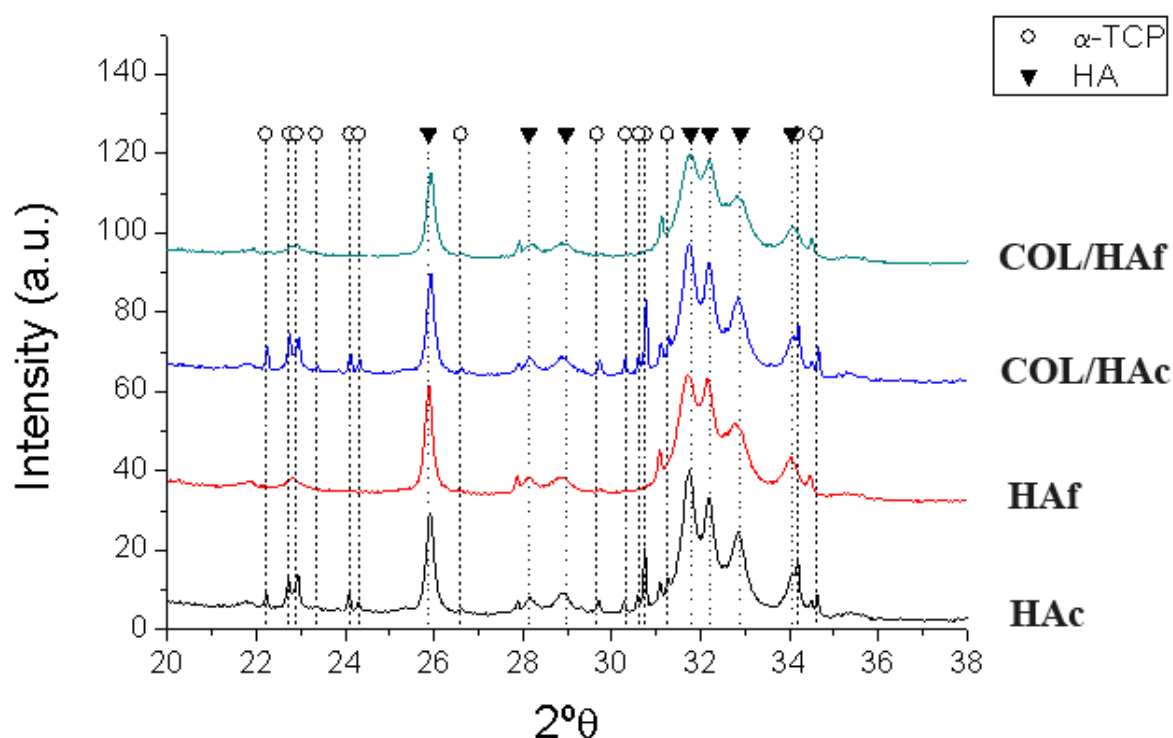


Figure 6.3. XRD patterns of the different microcarriers after 7 days immersion in a 0.9 wt% NaCl aqueous solution. In all cases hydroxyapatite was formed as a result of the setting reaction. Small amounts of unreacted  $\alpha$ -TCP were detected in the MC obtained with coarse powder (HAc and COL/HAc). The larger peak width in the HAf and COL/HAc MC is indicative of smaller crystallite size.

The fact that the XRD patterns of the MC obtained with the fine powder (HAf and COL/HAc) showed wider peaks was indicative of their lower crystallinity, in the sense of having smaller crystalline domains. These results were corroborated by the higher SSA values of the MC obtained with fine powders compared to those obtained with the



coarse ones, as reported in Table 6.2, indicating a smaller crystal size. The addition of collagen in the MC considerably reduced their SSA, suggesting that inside the MC the HA crystal network was partially wrapped in the polymer.

The distribution of collagen in the microcarriers after 7 days immersion in 0.9% NaCl aqueous solution, as assessed by fluorescence imaging, is shown in Figure 6.4. The homogenous green signal indicated that the collagen was retained and evenly distributed in the MC.

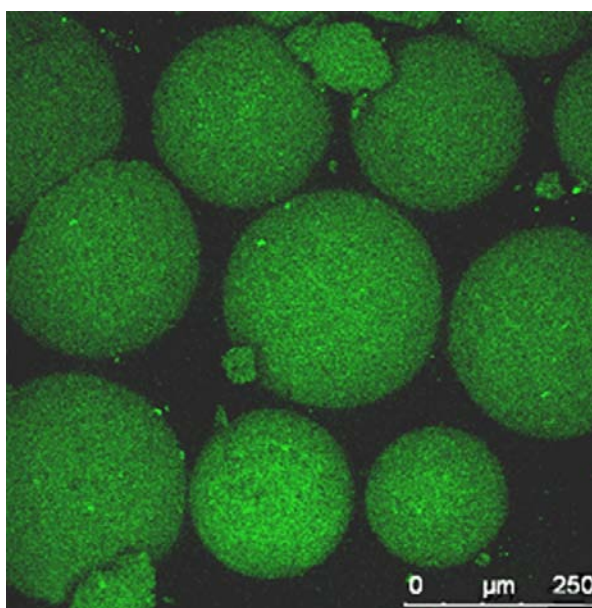


*Figure 6.4. Fluorescence images of coarse COL/HAc microcarriers showing the presence and homogenous distribution of collagen after 7 days immersion in 0.9 wt% NaCl aqueous solution. A fluorescent marker (CBQCA, Invitrogen) was used for collagen (green signal).*

## **6.4.2. *In vitro* culture test**

### *6.4.2.1. Overall cell morphology and proliferation*

The overall morphology of the viable Saos-2 cells after 1 day culturing on the different MC visualized by fluorescence after FDA staining is shown in Figure 6.5. Cells were able to attach on all types of MC. A lower number of cells were observed on the inorganic MC.

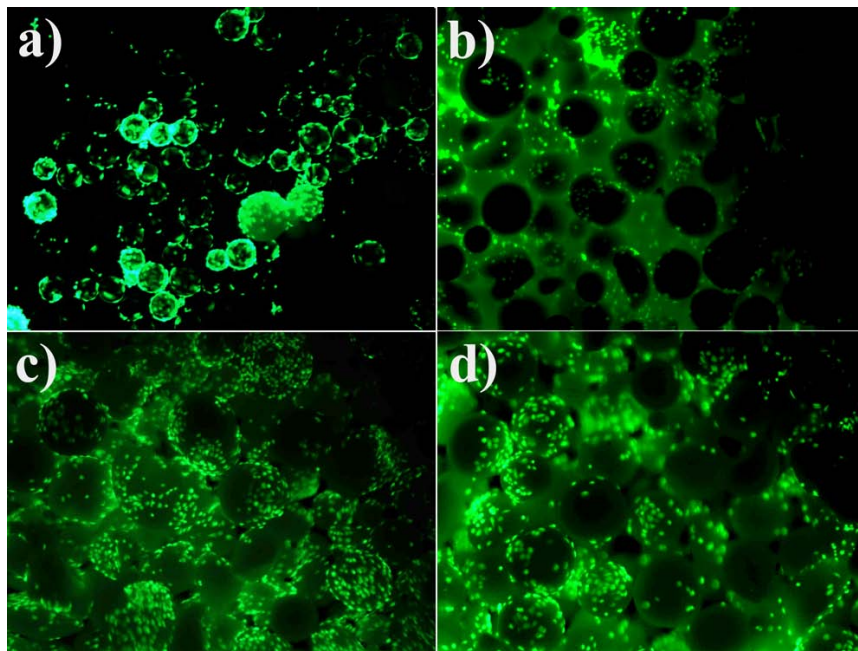


Figure 6.5. Overall morphology of Saos-2 cells after 1 day of culture on different MC visualized by FDA staining: a) CTRL-MC; b) HAF; c) COL/HAc; and d) COL/HAf.

Figure 6.6 represents the proliferation rate of Saos-2 cells grown on the different MC. After 24 hours of culture, the LDH assay did not reveal significant differences in cell number between the different MC. After seven days however, the cell number increased significantly except for the HAF MC, where no significant differences in cell number were observed compared to day 1. The CTRL and the collagen containing MC did present significantly higher values, being the highest for the CTRL MC, followed by COL/HAc, with no significant differences among them.

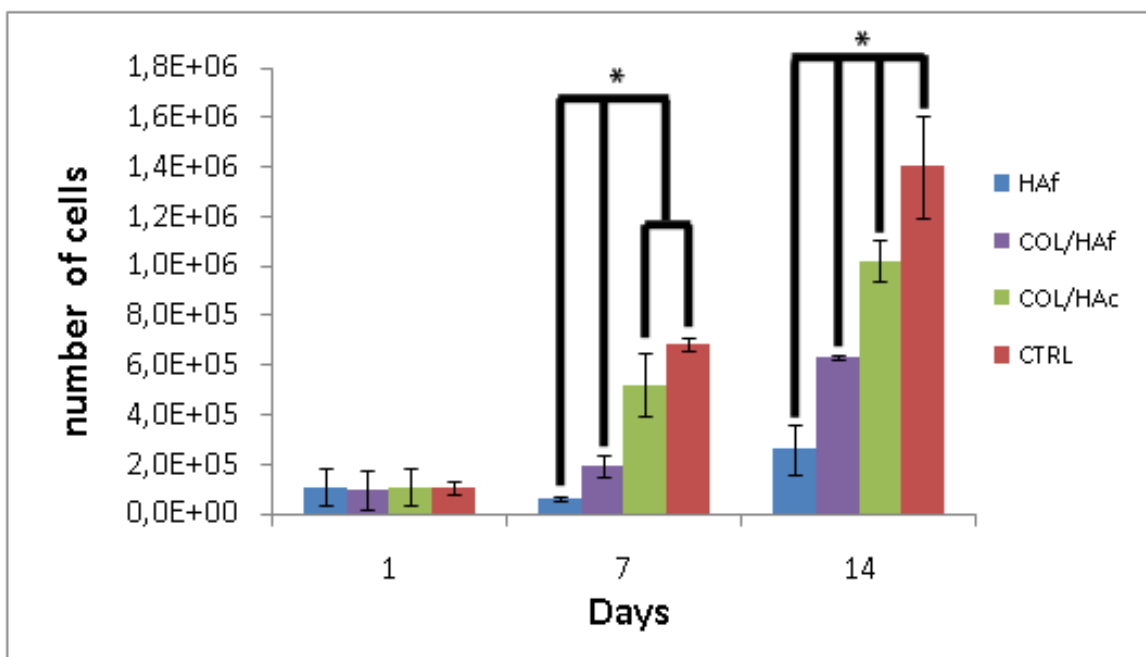


Figure 6.6. Cell proliferation on the microcarriers for different periods of time up to 14 days, measured by the LDH assay. Glass microspheres were used as a control.. Data are presented as the average  $\pm$  standard deviation. \*denotes significant differences for the different materials at a given time point ( $p < 0.05$ ).

A high number of adhered cells on collagen containing MC were also revealed by FDA staining, especially on the COL/HAc (Figure 6.7). SEM images showed a more flattened cell morphology in COL/HAf, as compared to COL/HAc.

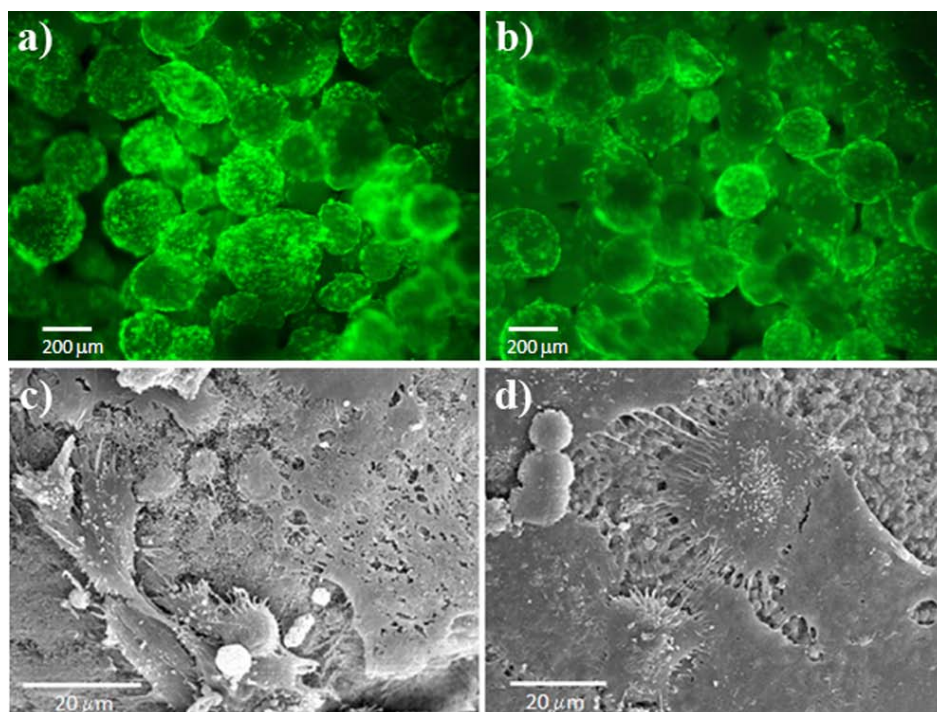


Figure 6.7. Saos-2 cells cultured on collagen-containing MC for 7 days. Fluorescent images of FDA stained cells (top) and SEM images (bottom): a) and c) COL/HAc; b) and d) COL/HAf.

Finally, after 14 days, the number of cells increased about twice for all samples compared to the 7 day value (Figure 6.6), including HAc MC. Most of the surface of the MC was covered with cells, although presenting slightly different morphologies on the different materials as revealed by SEM (Figure 6.8). On HAc, the cells were rounder, presenting low phyllopodial activity. Cells on CTRL MC showed long protrusions expanding throughout the surface of glass beads, although some cells tended to shrink. COL/HAc presented a more homogenous cell layer with elongated shaped cells tending to interact with each other, while on COL/HAc, cells showed a rather flattened morphology. Nevertheless, the rough aspect of their surface suggested a higher dorsal cell activity.

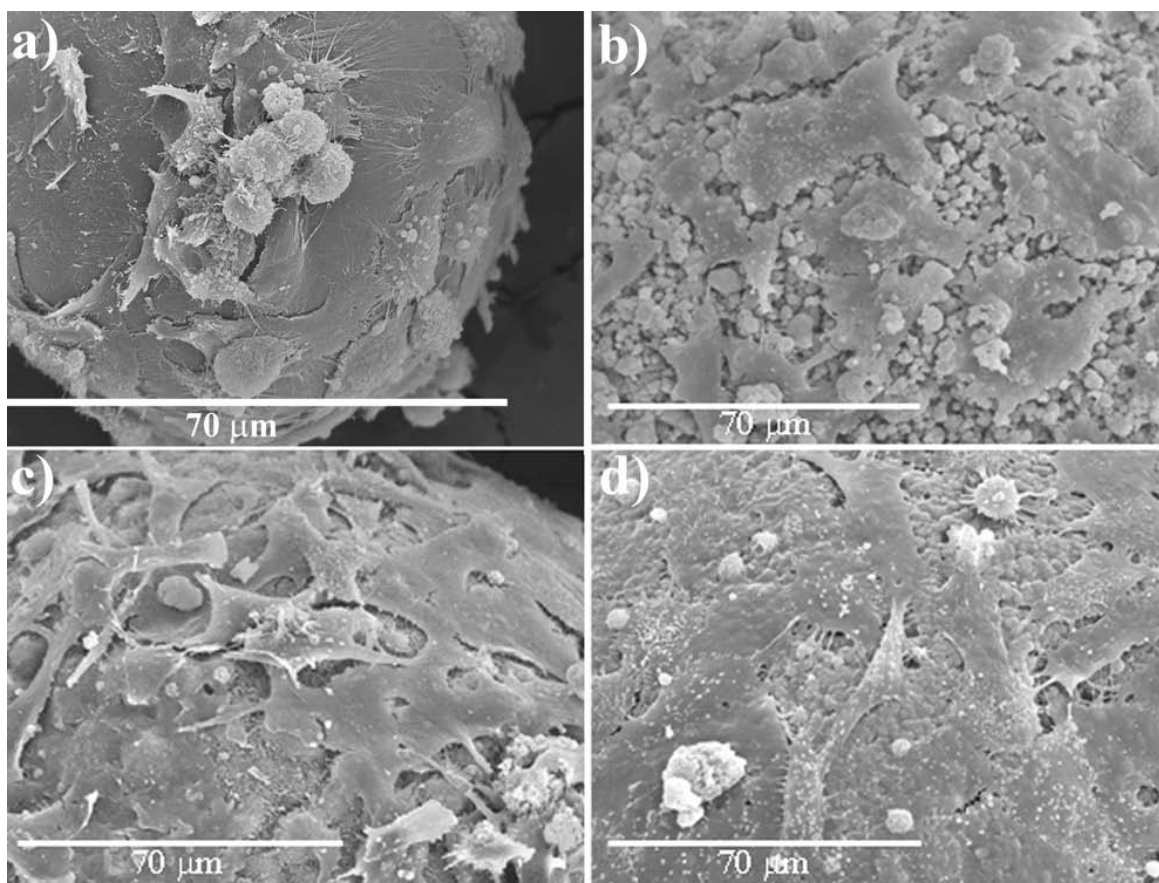


Figure 6.8. SEM images of Saos-2 cells on the different MC after 14 days of culture. a) CTRL-MC; b) HAf; c) COL/HAc; and d) COL/HAf.

#### 6.4.2.2. Cell differentiation

The ALP expressed by the cells at different time points is shown in Figure 6.9. Initially, after 1 day of culture, the three HA materials studied presented a similar ALP activity, whereas for the cells growing on the CTRL MC, the alkaline phosphatase activity was 4 to 5 times lower. After 7 days, COL/HAf showed a significantly higher ALP activity compared to HAf and COL/HAc MC. After 14 days, the differences were more pronounced and statistically significant with respect to all MC.

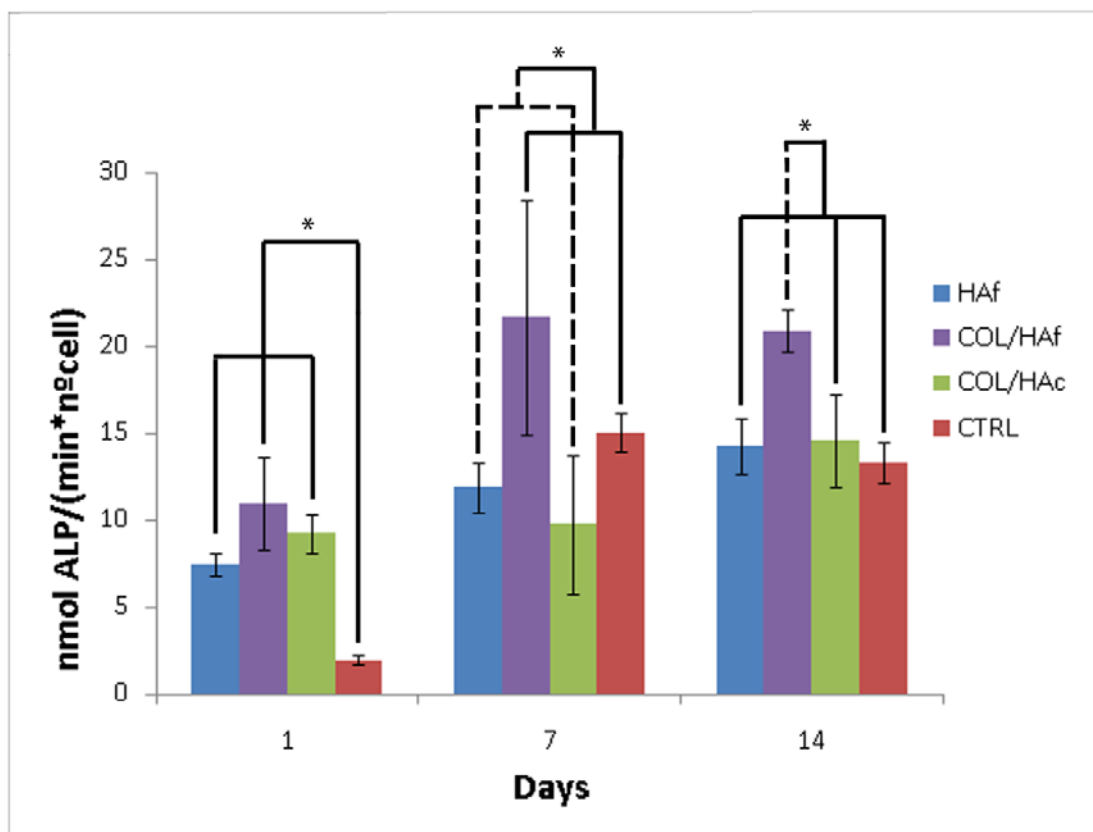


Figure 6.9. Alkaline phosphatase (ALP) expression level on the microcarriers after different periods of culturing. Data are normalized to the number of cells. \*denotes significant differences for the different materials at a given time point ( $p < 0.05$ ).

## 6.5. Discussion

In the present work, the setting reaction of a CPC was used as the stabilizing mechanism to produce microcarriers with high content of inorganic phase, through a water-in-oil emulsion. The method allowed the fabrication of collagen containing MC, by using a collagen solution as the liquid phase of the CPC.

A key issue was to determine the adequate emulsion times that ensured the consolidation of the MC. The setting time of the CPC slurry proved to be an appropriate parameter, since it gives an idea on when the water starts hydrolyzing the  $\alpha$ -TCP, obtaining a harder and stiffer structure<sup>22</sup>. The addition of collagen modified the CPC setting kinetics, as reflected by the increase of the setting times, and the emulsion time was accordingly modified (Table 6.1). In all cases, a high L/P was used, in order for the CPC slurry to flow inside the oil. However, since it is known that an increase in the L/P ratio results in longer setting times, higher porosity and impaired mechanical properties

of the CPC<sup>23</sup>, the lowest L/P value that ensured the formation of an emulsion was selected.

The presence of collagen resulted in a higher sphericity of the MC, with values close to 0.9 and median sizes near 300 microns (Figure 6.2, Table 6.2). This can be explained by the amphiphilic character of collagen and its subsequent surface active properties<sup>24</sup>. Moreover, in the presence of collagen, the sphericity and the size of the MC was not affected by the particle size of the powder, in contrast to what happened in the collagen-free slurries. In addition, the  $\alpha$ -TCP transformation into calcium deficient HA was not altered by the presence of collagen, as assessed by XRD (Figure 6.3).

From a biological point of view, two variables were shown to have a significant effect on the MC-cell interactions: the presence of collagen in the MC, even in a small amount (0.8 wt%) ; and the microstructure of the MC.

When comparing the morphology of the cells growing on the COL/HAf MC with those on the HAf MC, significant differences were observed. As expected, cell spreading was favored on the collagen-containing MC (Figure 6.8d) with respect to the collagen-free MC (Figure 6.8b). This behavior, which was also previously observed in Saos-2 cells cultured on nanoHA and collagen/nanoHA surfaces<sup>25</sup>, can be attributed to the cell-adhesion domain sequences contained in the collagen molecule (e.g., GFOGER) that play a key role in cell attachment through binding of the integrin  $\alpha 2\beta 1$ <sup>26</sup>. It is also in agreement with other studies showing that the presence of collagen type I induced osteoblastic differentiation that might be associated with the improved adhesion, mediated by collagen interaction with  $\alpha 2\beta 1$  integrin<sup>27-29</sup>. Conversely, the enhanced dorsal activity that was observed when Saos-2 cells were cultured on the COL/HAf MC might be attributed to the higher levels of ALP activity (Figure 6.9).

The microstructure of the MC, which was modified by changing the particle size of the  $\alpha$ -TCP powder in the ceramic slurry, also had a significant effect on cell behavior. As shown in Figure 6.2, the coarse  $\alpha$ -TCP resulted in micrometric calcium deficient HA, whereas in the fine  $\alpha$ -TCP, nanometric HA was obtained. When collagen was added, the presence of either nanometric or micrometric HA crystals was still evident in the COL/HAf and COL/HAc respectively (Figure 6.2 h,i,l), resulting in a significant effect on cell proliferation and differentiation (Figures 6.6 and 6.9). This cell behavior is in

agreement with our previous results obtained with calcium deficient HA, analogous to the mineral component of the MC presented here, where a slower cell proliferation and enhanced ALP activity was observed in fine nanometric HA substrates compared to the micrometric ones<sup>30</sup>. Accordingly, Shelton *et al*<sup>31</sup>, in a study on the interactions of bone marrow cells with an octacalcium phosphate scaffold found a direct correlation between cell proliferation and crystal size. It has also been shown that very sharp and small crystal sizes inhibit cell growth due to the lowered initial cell attachment<sup>32</sup>.

## 6.6. Conclusions

A new approach for preparing collagen-containing HA MC was described based on the emulsion of a CPC in oil. MC with high mineral content and tailored microstructures were obtained. The addition of collagen resulted in an increased cell proliferation. A synergistic effect was found between the presence of collagen and the nanosized HA crystals, which resulted in an enhanced ALP activity for the collagen-containing nanoHA MC.

## 6.7. References

1. Van Wezel AL. Growth of cell-strains and primary cells on micro-carriers in homogeneous culture. *Nature* **216**, 64-65 (1967).
2. Freiberg S & Zhu XX. Polymer microspheres for controlled drug release. *International Journal of Pharmaceutics*, **282**, 1-18 (2004).
3. Brandon G, Santoni G, Pluhar E, Motta T & Wheeler DL. Hollow calcium phosphate microcarriers for bone regeneration: In vitro osteoproduction and ex vivo mechanical assessment. *Biomedical Materials Engineering* **5**, 277-289 (2007).
4. Ng EY, Ng WK & Chiam SS. Optimization of Nanoparticle Drug Microcarrier on the Pharmacokinetics of Drug Release: A Preliminary Study. *Journal of Medical Systems* **32**, 85-92 (2008).
5. Malda J & Frondoza G. Microcarriers in the engineering of cartilage and bone. *Trends in Biotechnology*, **24**, 299-304 (2006).
6. Malda J, Kreijveld E, Temenoff JS, van Blitterswijk CA & Riesle J. Expansion of human nasal chondrocytes on macroporous microcarriers enhances redifferentiation. *Biomaterials* **24**, 5153-5161 (2003).
7. Cancedda R, Giannoni P & Mastrogiacomo M. A tissue engineering approach to bone repair in large animal models and in clinical practice. *Biomaterials* **28**, 4240-4250 (2007).
8. Fischer EM, Layrolle P, Van Blitterswijk CA, De Bruijin JD. Bone formation by mesenchymal progenitor cells cultured on dense and microporous HA particles. *Tissue Engineering* **9**, 1179-1188 (2003).
9. Yuan H, *et al.* Osteoinductive ceramics as synthetic alternative to autologous bone grafting. *Proceedings of the National Academy of Sciences* **107**, 13614-13619 (2010).



10. Schliephake H *et al.* Use of a mineralized collagen membrane to enhance repair of calvarial defects in rat. *Clinical and Oral Implants Research* **15**, 112-118 (2004).
11. Kikuchi M *et al.* Biomimetic synthesis of bone-like nanocomposites using the self-organization mechanism of hydroxyapatite and collagen. *Composite Science Technology* **64**, 819-825 (2004).
12. Chaozong L, Zhiwu H & Czernuszka JT. Gradient collagen/nanohydroxyapatite composite scaffold: Development and characterization. *Acta Biomaterialia* **5**, 661-669 (2009).
13. Shunji Y *et al.* Three-dimensional porous hydroxyapatite/collagen composite with rubber-like elasticity. *Journal of Biomaterial Science Polymer Edition* **18**, 393-409 (2007).
14. Miyamoto Y *et al.* Basic properties of calcium phosphate cement containing atelocollagen in its liquid or powder phases. *Biomaterials* **19**, 707-715 (1998).
15. Tamimi F *et al.* Brushite-collagen composites for bone regeneration. *Acta Biomaterialia* **4**, 1315-1321 (2008).
16. Moreau JL, Weir MD & Xu HH. Self-setting collagen-calcium phosphate bone cement: mechanical and cellular properties. *Journal of Biomedical Materials Research A* **91**, 605-613 (2009).
17. Hsu FY, Chueh SC & Wang YJ. Microspheres of hydroxyapatite/reconstituted collagen as supports for osteoblast cell growth. *Biomaterials* **20**, 1931-1936 (1999).
18. Wu TJ *et al.* Studies on the microspheres comprised of reconstituted collagen and hydroxyapatite. *Biomaterials* **25**, 651-658 (2004).
19. Kim HW, Gu HJ & Lee HH. Microspheres of collagen-apatite nanocomposites with osteogenic potential for tissue engineering. *Tissue Engineering* **13**, 965-973 (2007).

20. Ginebra MP, Espanol M, Montufar EB, Perez RA & Mestres G. New processing approaches in calcium phosphate cements and their applications in regenerative medicine. *Acta Biomaterialia* **6**, 2863-2873 (2010).
21. Ginebra MP, Driessens FC & Planell JA. Effect of the particle size on the micro and nanostructural features of a calcium phosphate cement: a kinetic analysis. *Biomaterials* **25**, 3453-3462 (2004).
22. Ginebra MP *et al.* Setting reaction and hardening of an apatitic calcium phosphate cement. *Journal of Dental Research* **76**, 905-912 (1997).
23. Espanol M *et al.* Intrinsic porosity of calcium phosphate cements and its significance for drug delivery and tissue engineering applications. *Acta Biomaterialia* **5**, 2752-2762 (2009).
24. Zayas JF. *Functionality of Proteins in Food*. Springer-Verlag, Berlin, Germany (1997).
25. Zhu X, Eibl O, Scheideler L & Geis-Gerstorfer J. Characterization of nano hydroxyapatite/collagen surfaces and cellular behaviors. *Journal of Biomedical Materials Research A* **79**, 114-127 (2006).
26. Heino J. The collagen family members as cell adhesion proteins. *Bioessays* **29**, 1001-1010 (2007).
27. Mizuno M, Fujisawa R & Kuboki Y. Type I collagen-induced osteoblastic differentiation of bone-marrow cells mediated by collagen-alpha2beta1 integrin interaction. *Journal of Cell Physiology* **184**, 207-213 (2000).
28. Salaszyk RM, Williams WA, Boskey A, Batorsky A & Plopper Ge. Adhesion to vitronectin and collagen I promotes osteogenic differentiation of human mesenchymal stem cells. *Journal of Biomedical Biotechnology* **2004**, 24-34 (2004).

29. Carvalho RS, Kostenuik PJ, Salih E, Bumann A & Gerstenfeld LC. Selective adhesion of osteoblastic cells to different integrin ligands induces osteopontin gene expression. *Matrix Biology* **22**, 241-249 (2003).
30. Engel E *et al.* Discerning the role of topography and ion exchange in cell response of bioactive tissue engineering scaffolds. *Tissue Engineering* **14**, 1341-1351 (2008).
31. Shelton RM *et al.* Bone marrow cell gene expression and tissue construct assembly using octacalcium phosphate microscaffolds. *Biomaterials* **27**, 2874-2881 (2006).
32. Liu Y, Shelton R, Gbureck U & Barralet J. Influence of calcium phosphate crystal morphology on the adhesion, spreading, and growth of bone derived cells. *Journal of Biomedical Materials Research A* **90**, 972-980 (2009).

# Chapter 7: Dynamic *In Vitro* Characterization of Injectable CPC Microcarriers

## 7.1. Introduction

In the previous chapters the fabrication of HA, GEL/HA and COL/HA MC has been presented and their cell response in static conditions has been assessed. However, culturing the MC in static conditions has the main drawback of having a low seeding efficiency as well as the impossibility of having high number of cells in culture due to the limited culture medium. Therefore, the way to increase the seeding efficiency of the cells on the MC was explored. The dynamic culture allows for homogenous cell culture conditions and an improved gas liquid oxygen transfer<sup>1</sup>. The dynamic culture consists on placing the MC on a spinner flask, into which the MC and the cells are introduced

under gentle stirring. The gentle agitation allows MC and cells to be resuspended. In order to do so, dynamic MC culture in spinner flasks was developed with the aim of enhancing cell adhesion and proliferation on the whole MC surface. One of the drawbacks that had to be faced was the high density of ceramics that makes difficult this type of spinner flask culture system<sup>2</sup>. Indeed, most MC used in this type of dynamic culture are polymeric, avoiding therefore problems of sedimentation<sup>3-6</sup>. Hollow ceramic MC have also been developed as a method to overcome the problem<sup>7-9</sup>. Since in our MC the density is high compared to conventional polymeric MC, one of the objectives was to assess if the dynamic *in vitro* culture could be done with the CPC MC.

In this chapter, the GEL/HA-MC were selected and compared with the HA-MC in the dynamic conditions. The reason for selecting the GEL/HA-MC was that, as seen on the static condition tests in the previous chapters, the number of cells initially adhered was higher than in the rest of the materials. The explanation can be found in the fact that in gelatin, the anchorage of the cells was through an RGD dependent mechanism in which the integrin  $\alpha 5\beta 1$  interacts with the RGD sequence. In the case of collagen, the binding domains were different and the mechanism was completely RGD independent. Since the goal was to have a high number of cells initially adhered, gelatin was chosen as the additive in the composites MC.

Furthermore, a system was explored that could allow the injection of the cell-seeded MC. Injectable hydrogels have been used to deliver cells into the site of defect due to their similarity with the ECM. These gels can be mixed with the cells *in vitro* and can then be injected, being able to gelify *in situ*, forming a three dimensional structure with cells. The most common gels used are collagen<sup>10,11</sup>, chitosan<sup>12,13</sup>, alginate<sup>14-16</sup> and hyaluronan<sup>17,18</sup> among others. Their main drawback is that they present low mechanical properties and high degradation rate, as well as high flowability if the gels are not properly crosslinked.

On the other hand, microcarriers can also be combined with an appropriate gel to form an injectable 3D macroporous structure. The approach in this case would be to seed the cells on the MC and afterwards combine them with a gel to be able to inject the MC<sup>19</sup>. A possible drawback may be the uncontrolled movement of the MC *in vivo*<sup>20</sup>. For this reason, a combination of a gelling gel with the MC was thought as an optimum cell-loaded MC delivery system.

In this approach, the vehicle that is intended for delivering the MC into the defects should not damage the cells. In the present study, sodium alginate was selected since it has been previously studied as a vehicle inside of which cells are able to survive<sup>14-16</sup>. Moreover, an interesting feature of the alginate gels is that they are able to spontaneously crosslink in the presence of calcium ions<sup>21,22</sup>. Therefore, the rationale would be that, once the gel is injected in the defect, in the presence of calcium from the plasma, the sodium alginate would instantaneously gelify, avoiding microcarrier migration<sup>20</sup>. Therefore, the use of the sodium alginate gels was considered as an interesting approach for further clinical applications.

## **7.2. Objective**

The main objective of this chapter was to establish a protocol to culture cells on HA-MC and GEL/HA-MC in a dynamic culture. The dynamic culture was compared with that obtained in static culture conditions. A second objective was to assess the feasibility of using sodium alginate as a vehicle for MC delivery.

## **7.3. Materials and methods**

### **7.3.1. Materials**

The materials used in this chapter were those previously synthesized in Chapter 5 using CPC made of fine powder using either x10 PBS (HA-MC) or a 5% gelatin solution (GEL/HA-MC), both described in Chapter 5, section 5.3.1. As a control, Cytodex 3 microcarriers (CYTODEX, Percely Biolytica AB) were used, which are DEAE-dextran microspheres covered with collagen. The MC were sized by sieving in a range between 80 and 297  $\mu\text{m}$ .

### **7.3.2. Culturing cells on the MC in dynamic cultures**

Human osteoblast-like Saos-2 cells were used as cell model. The medium used and the protocols followed were the same as the ones described in section 3.3.2.

The MC containing HA were sterilized with ethanol, whereas the CYTODEX MC were initially hydrated in PBS for 3 hours and then sterilized with autoclave, according to the manufacturer's description (GE Healthcare, Instructions 18-1119-79AD).

The spinner flasks used had a capacity of 125 ml and had a magnetic stirrer attached inside to be able to rotate the MC and the cells (Wheaton). The spinner flasks and the agitation system (Wheaton Micro-system) are shown in Figure 7.1. The spinner flasks were coated with a special silicon solution in heptane (Sigmacote, SL2, Sigma) that prevented the adhesion of cells and MC to the surface of the spinner flask. The amount of MC introduced in each spinner flask was 300 mg, as recommended by the CYTODEX manufacturer (GE Healthcare, Instructions 18-1119-79AD). In the HA containing MC, 300 mg were also introduced and, in order to favour wettability, MC were previously soaked in ethanol and rinsed with PBS three times. All MC were then left in contact with 50 ml of medium for 24 hours prior to cell culture. This volume of medium was the one used in the initial 24 hours of cell seeding as described below.



Figure 7.1. Spinner flask and rotating system used for the dynamic culture. The whole system was placed inside the incubator for the period of time the culture lasted.

Saos-2 cells were harvested from nearly confluent flasks as described in Chapter 3, section 3.3.2 and seeded on the MC at a final number of  $10^7$  cells, as recommended by the CYTODEX manufacturer (GE Healthcare, Instructions 18-1119-79AD) and previous studies<sup>3,4,23,24</sup>. The protocol for the cell seeding and the different agitation cycles are illustrated in Figure 7.2. Initially, the MC (represented as the black spheres) in the spinner flask were agitated at 40 rpm to have the MC in suspension, time in which the cells (represented by the red dots) were seeded through one of the lateral arms

of the spinner flask. After introducing the cells, repeating cycles of rotation and idle positions were carried out. For period times lower than 24 hours, the repeating cycles consisted of 2 minutes of agitation at 40 rpm, followed by 30 minutes of no agitation. During these repeating cycles the cells were allowed to attach to the MC. After 24 hours, the medium volume was adjusted from the initial 50 ml to 100 ml. From that point, the protocol consisted of combining periods of 2 minutes of agitation at 40 rpm with 120 minutes of no agitation, obtaining MC covered with cells. The process was repeated for 3 or 14 days depending on the type of experiment performed, as described below. The medium was changed every second day, replacing 50 ml of each flask with fresh medium. As an internal control, the same materials were used in static culture in the same way as described in Chapter 5.

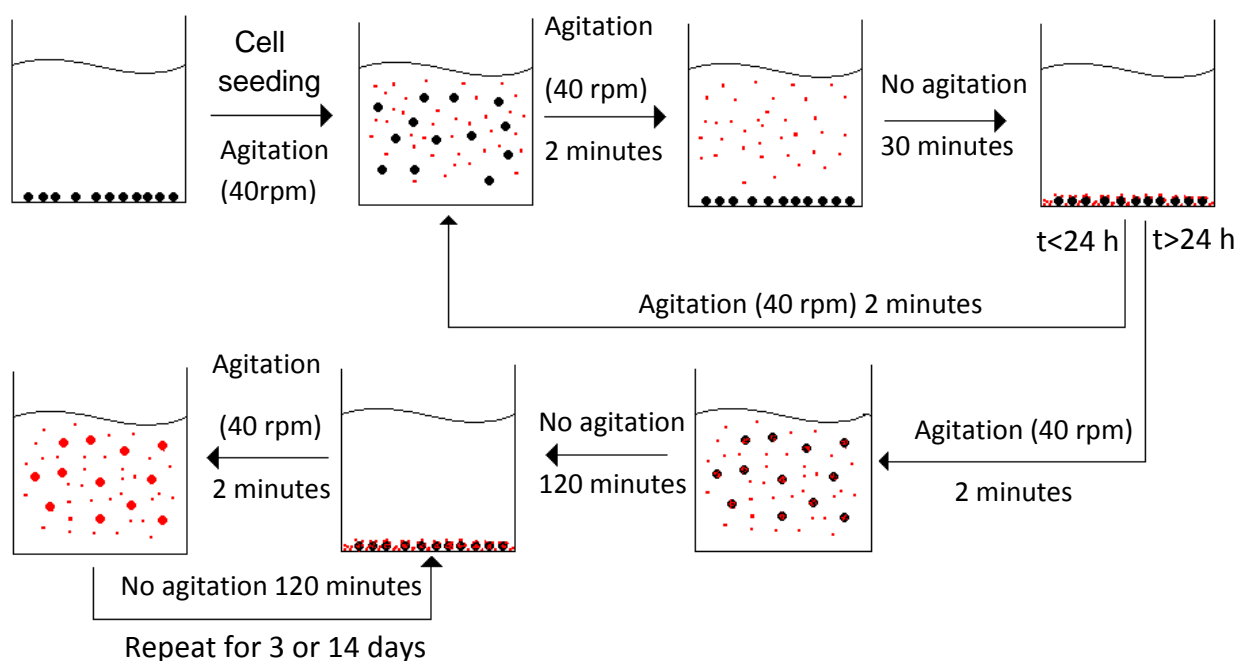


Figure 7.2. Scheme of the seeding mechanism onto MC in a dynamic culture system. Initially cell seeding was performed in suspension. For the first 24 hours of culture, repeating periods for 2 minute agitation at 40 rpm and 30 minutes of no agitation were performed. After 24 hours, the repeating periods combined agitation for 2 minutes at 40 rpm and no agitation periods of 120 minutes. The MC are represented by the black circles and the cells with the red dots.

In order to determine which was the rotation speed that would be most favourable for cell adhesion and would not disintegrate the different MC, the speed of 40 rpm was compared to 80 rpm for 24 hours. Cell viability was observed by means of fluorescent microscopy after FDA staining.



Once the rotation speed was chosen, two main types of experiments were done:

- A short-term study in which cell proliferation, SEM and fluorescence microscopy observations were performed at 6, 24 and 72 hours of culture. The experiment was done twice.
- A long-term study, in which cell proliferation, fluorescence microscopy and SEM observations were performed at 1, 7 and 14 days of culture. The experiment was done once.

### *7.3.2.1. Cell proliferation*

Cell proliferation was measured by means of the LDH assay. At each time point (6, 24 and 72 hours), a volume of 1 ml containing MC in suspension was extracted in triplicates from the spinner flask and introduced in a 24 well plate. The MC were then washed twice with PBS and left with 1 ml of PBS, freezing the plate afterwards. The values were then adjusted with the appropriate dilutions. The protocol followed was the same as that explained in section 3.3.4.1. The results of cell number were then normalized by the amount of MC in each ml in terms of MC weight.

### *7.3.2.2. Cell morphology*

The cell morphology was observed by fluorescence microscopy after FDA staining and SEM and was carried out with the same protocol described in sections 3.3.4.3 and 3.3.4.4. One milliliter aliquots were extracted with a pipette to determine cell morphology.

### *7.3.2.3. Statistical analysis*

Statistical analysis was carried out with significance of 5%. One way analysis of variance (ANOVA) with Fisher post-hoc test was conducted. The data were expressed as mean  $\pm$  standard deviation.

### 7.3.3. MC-containing alginate gels

A 2% sodium alginate solution was used as a vehicle for delivering the MC. Sodium alginate is an anionic polysaccharide that has a high viscosity, which is directly proportional to the concentration of the solution. When put in contact with water, it dissolves. Nevertheless, if the solution is put in contact with a calcium solution, it is able to create a gel with a gum texture being able to absorb high amounts of water. The MC-containing gel was characterized in terms of injectability, microstructure and porosity. Three different MC were used and their particle size distribution is shown in Figure 7.3:

- HA-MC with a size range between 100 and 300  $\mu\text{m}$ .
- Small GEL/HA-MC with a size range between 100 and 300  $\mu\text{m}$ , coded as GEL/HA-MCs.
- Big GEL/HA-MC with a size range between 300 and 590  $\mu\text{m}$ , coded as GEL/HA-MCb.

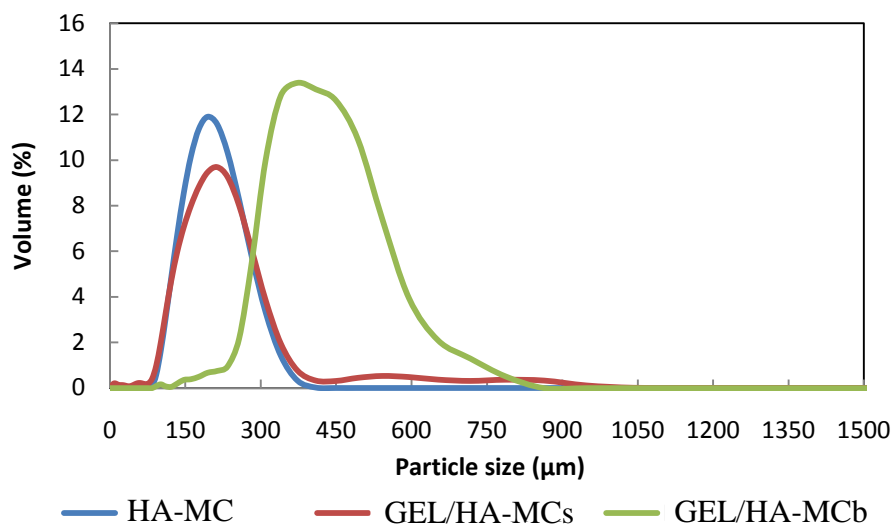


Figure 7.3. Microcarriers size distribution for the different types of MC and the different sieving.

The different MC were mixed with a 2% sodium alginate solution at a ratio alginate/MC of 2 ml/g. The mixture was then introduced in a syringe and injected into Teflon moulds, having a diameter of 6 mm and a height of 12 mm. The moulds containing the mixture were frozen overnight at  $-4^{\circ}\text{C}$  and lyophilized overnight.

The lyophilized constructs were analyzed by MIP in order to determine the total porosity and to observe the pore size distribution, following the protocol described in section 2.3.4.7.

## 7.4. Results

### 7.4.1. Dynamic culture

It was observed that the HA-containing MC had higher tendency to sediment at the bottom of the flask at 40 rpm than the CYTODEX due to their higher skeletal density (~2.85 g/ml for HA containing MC and 1.02 g/ml for CYTODEX). Therefore, it was explored if higher rotating speeds would resuspend more the MC, and therefore increase cell viability, or if on the other hand, cell viability would be reduced at higher speeds. Agitation speeds of 40 rpm and 80 rpm were compared.

As shown in Figure 7.4, the fluorescence images indicated that cell adhesion after 24 hours in the GEL/HA-MC was high at 40 rpm (Figure 7.4a and b), whereas at 80 rpm (Figure 7.4c and d) was very low. Moreover, some MC were broken at 80 rpm. Therefore, in spite of the sedimentation problem, 40 rpm was the selected speed.

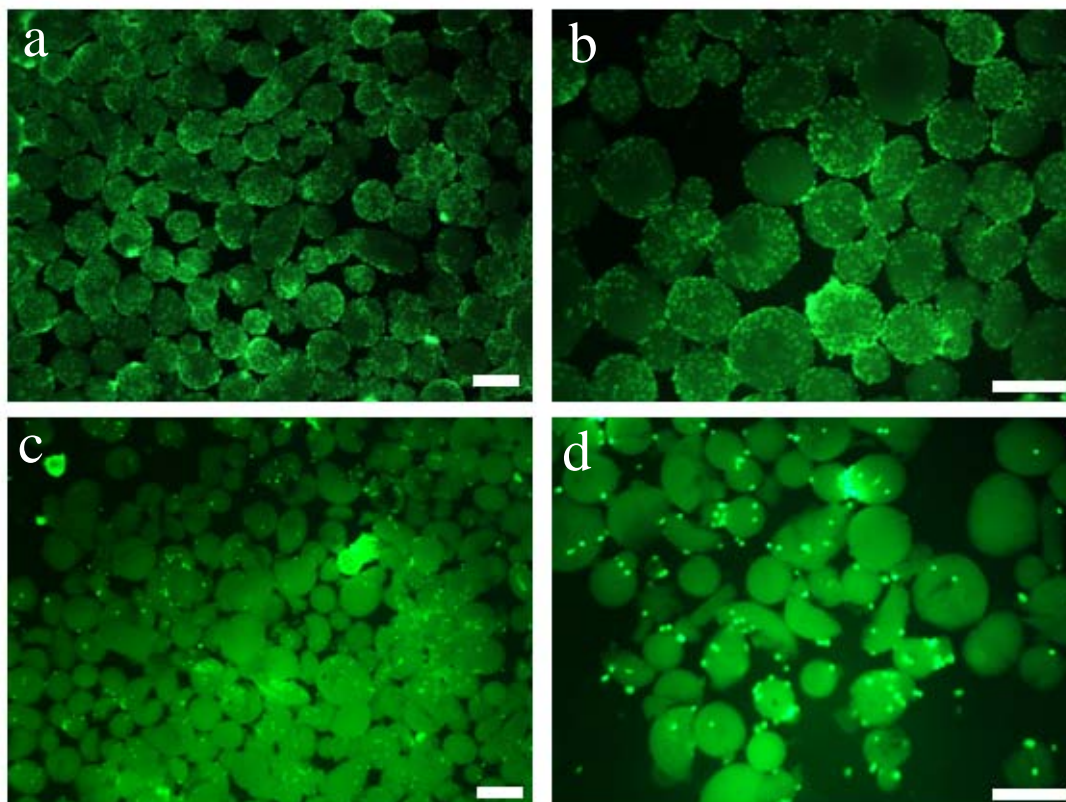


Figure 7.4. FDA staining for the GEL/HA-MC in dynamic culture for 24 hours at two different speeds: a) and b) 40 rpm, c) and d) 80 rpm. Bar = 200  $\mu$ m.

### 7.4.1.2. Short-term dynamic and static cultures

The general cell morphology was observed by fluorescence microscopy after FDA staining and SEM. Cell proliferation was afterwards quantified and compared with the static cultures.

The images obtained with FDA staining after 6, 24 and 72 hours of culture, both in static and dynamic cultures are shown in Figure 7.5. In the dynamic culture, the amount of cells was higher than in the static culture, for both the HA-MC and GEL/HA-MC.

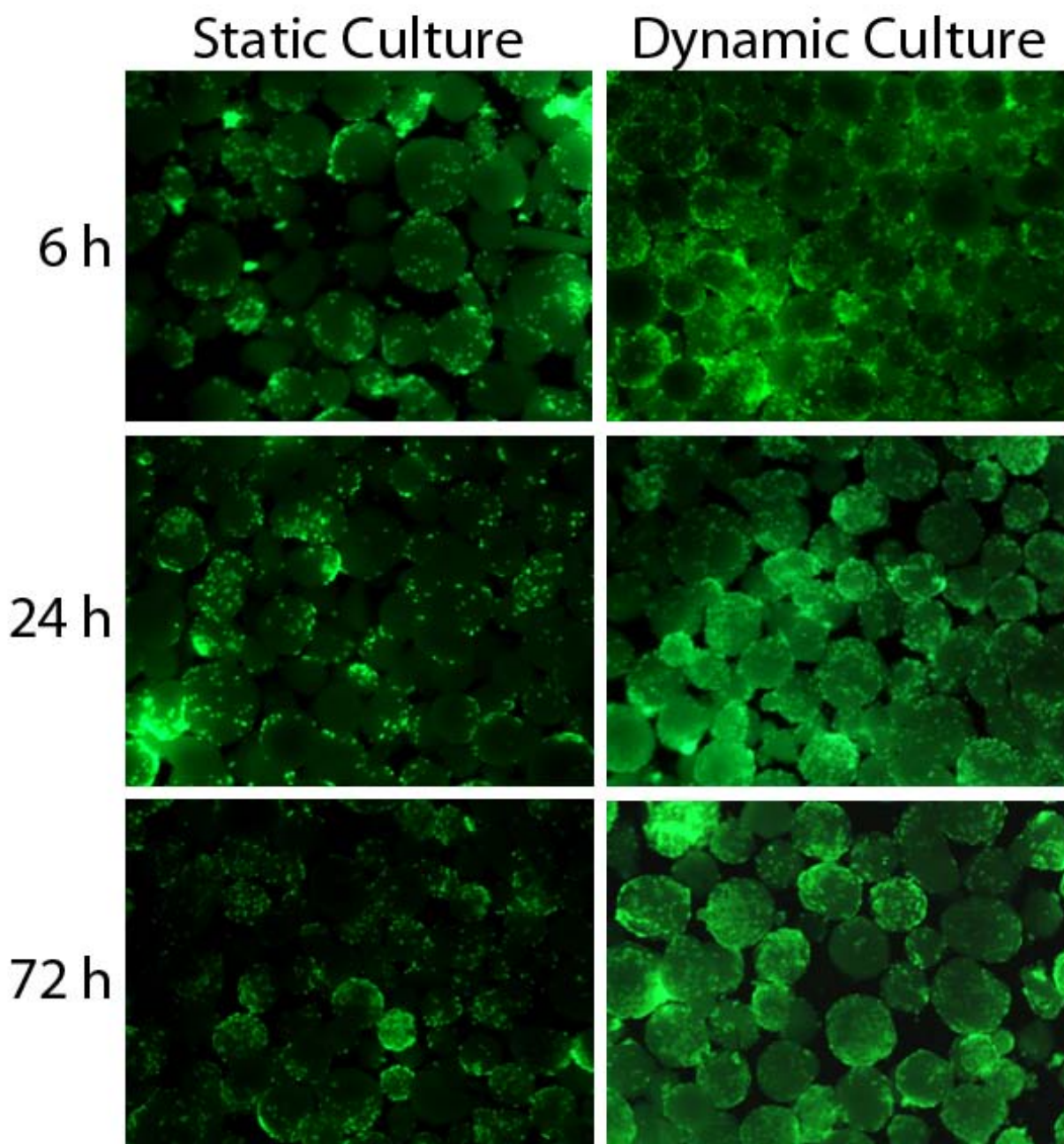


Figure 7.5. Comparison of FDA staining images for HA-MC after 6, 24 and 72 hours in dynamic and static culture. Bar = 200  $\mu\text{m}$ .

A similar trend was observed for the GEL/HA-MCh the differences did not seem as clear (Figure 7.6.).

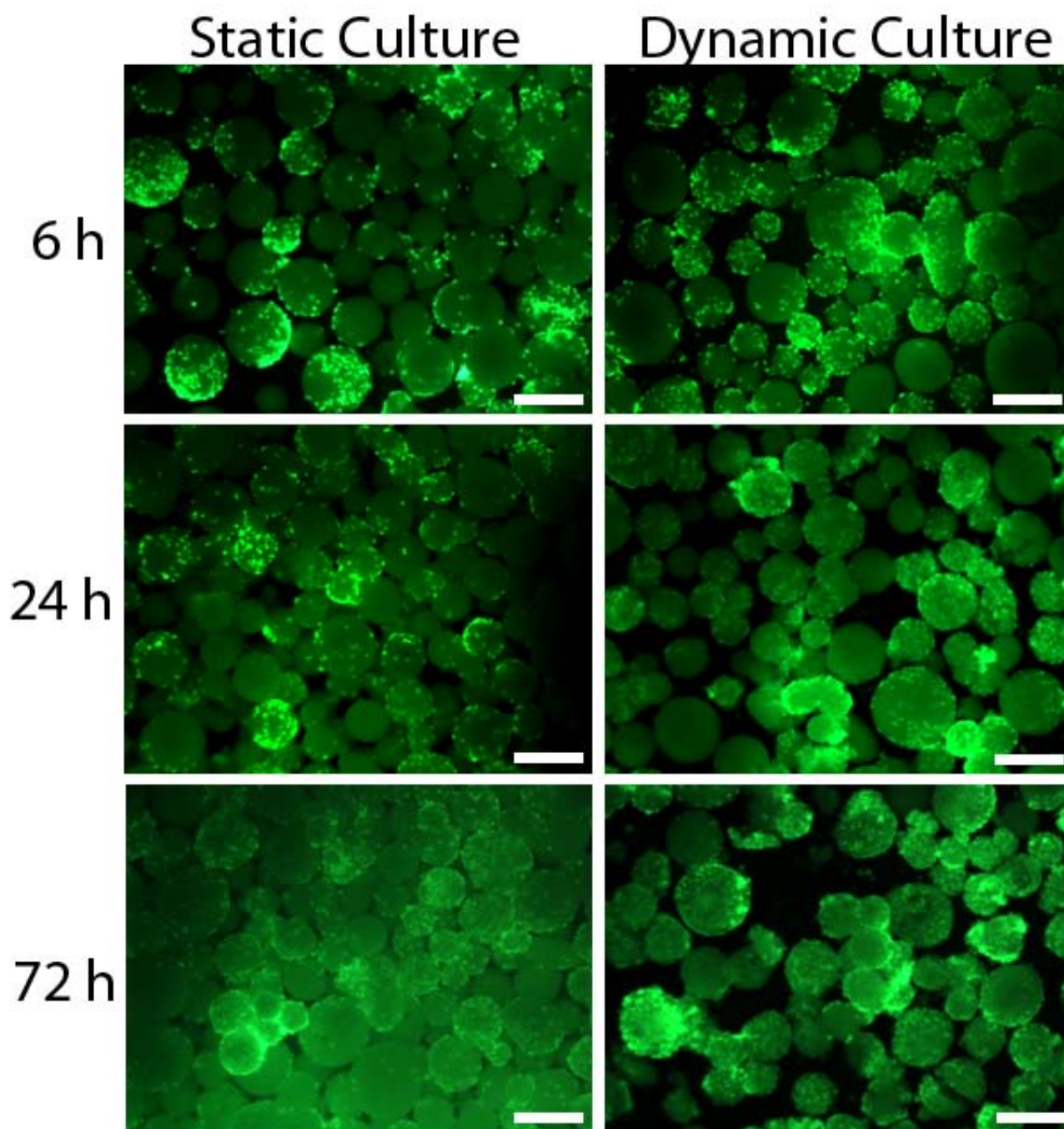


Figure 7.6. Comparison of FDA staining images for GEL/HA-MC after 6, 24 and 72 hours in dynamic and static culture. Bar = 200  $\mu$ m.

Figure 7.7 shows the fluorescent images obtained in dynamic and static culture for the CYTODEX. In this case a much more marked difference was observed between them, due to the ability of the MC to spin and move at the same pace as the cells.

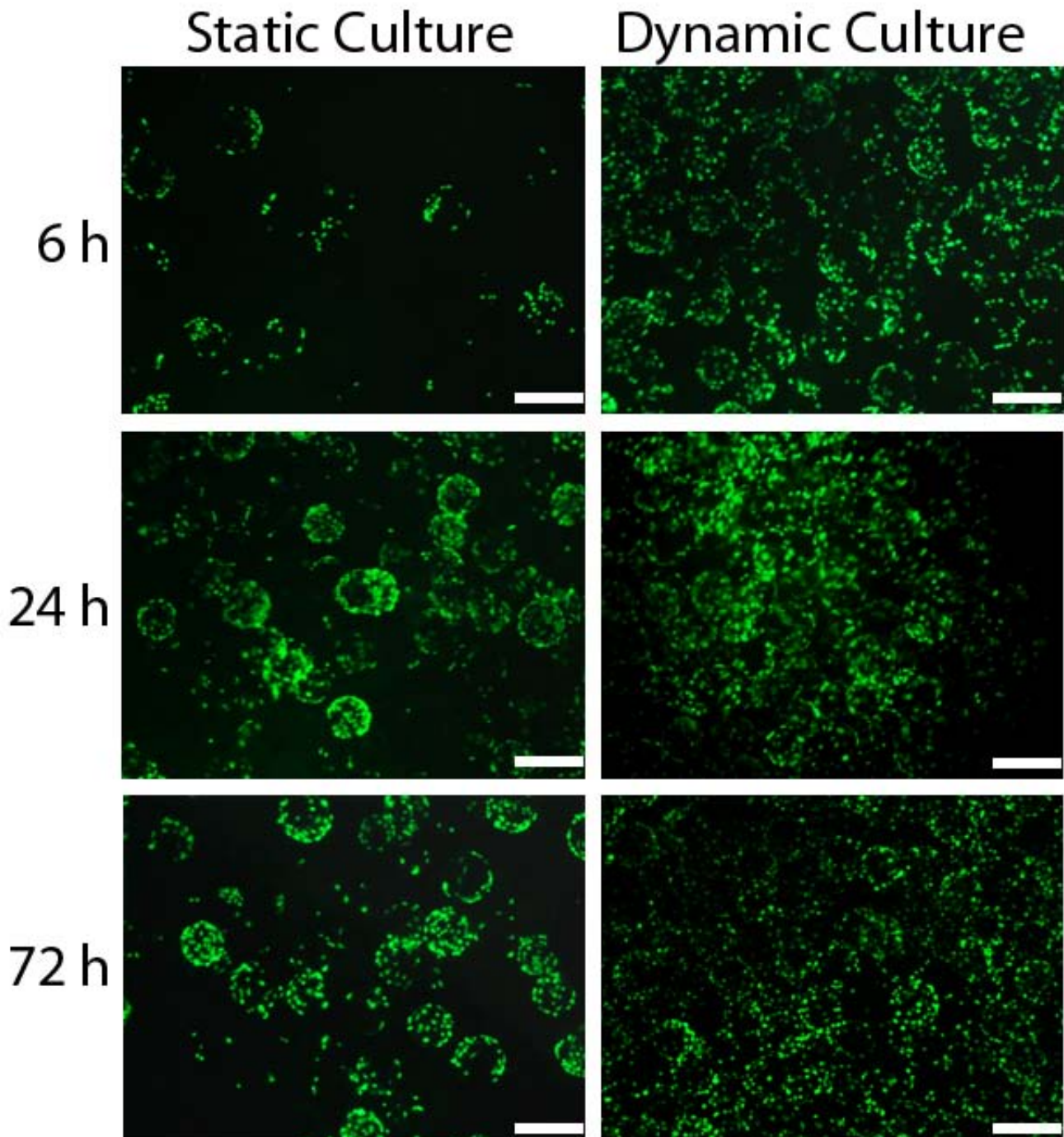


Figure 7.7. Comparison of FDA staining images for CYTODEX after 6, 24 and 72 hours in dynamic and static culture. Bar = 200  $\mu\text{m}$ .

Figure 7.8 shows the cell morphology observed by SEM. The images shown correspond to the HA-MC. At low magnifications it can be seen that, as time advances, the structure of the MC seemed to disintegrate (Figure 7.8 a, b and c). The longer time the MCs were in culture, the structure became more damaged, with fragment detachment. On the other hand, at higher magnifications, the cell morphology was observed. At 6 hours, some cells were seen (Figure 7.8d) and after 24 hours cell number considerably increased (Figure 7.8e). At 72 hours, cells were able to contact different MC through their protrusions, and established some connections among them (Figure 7.8f).

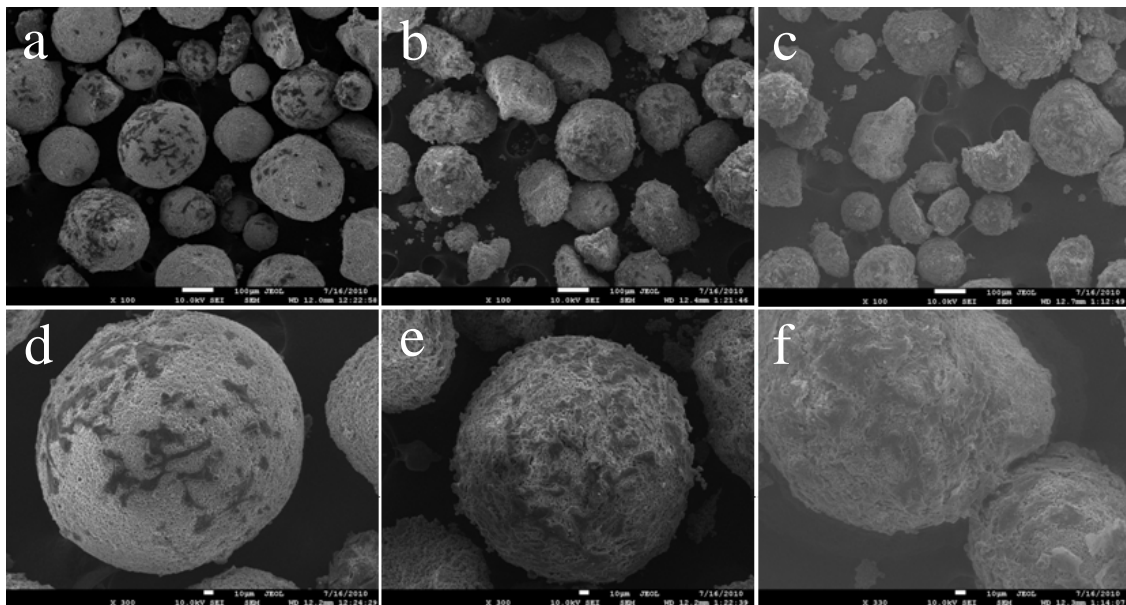


Figure 7.8. SEM images for HA-MC for the different times: a) and d) 6 hours, b) and e) 24 hours, c) and f) 72 hours. Bar a), b) and c) 100  $\mu\text{m}$ . Bar d), e) and f) 10  $\mu\text{m}$ .

Cell proliferation at 6, 24 and 72 hours measured by LDH is shown in Figure 7.9a. In the static culture, the trend was similar for the HA-MC and GEL/HA-MC, in which no proliferation was observed. For CYTODEX, cells grew exponentially. There were no statistically significant differences between HA-MC and GEL/HA-MC at any time point, whereas these two materials were significantly different with CYTODEX at 24 and 72 hours.

The proliferation of the dynamic culture is shown in Figure 7.9b. After 6 hours there were no significant differences between HA-MC and GEL/HA-MC. But after 24 hours and 72 hours, the differences between both of them became significant ( $p < 0.05$ ). It is also worth highlighting that the differences between the HA-MC and the CYTODEX

were significant in all cases, whereas there were only significant differences between CYTODEX and GEL/HA-MC at the 6 hour period.

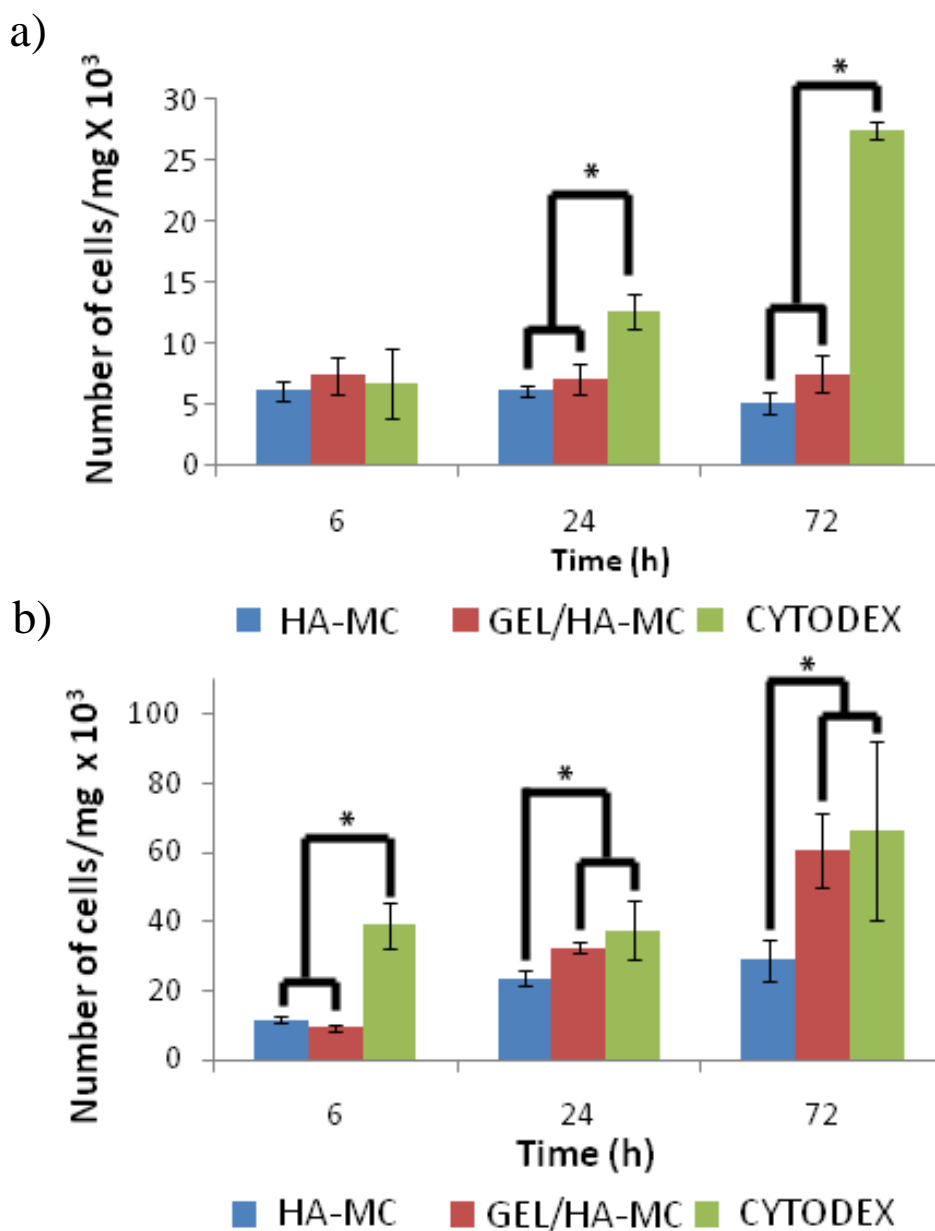


Figure 7.9. Proliferation for 6, 24 and 72 hours measured with LDH for HA-MC, GEL/HA-MC and CYTODEX in a) static culture and b) dynamic culture. \* denotes significant differences ( $p < 0.05$ ).

#### 7.4.1.1. Long-term dynamic culture

The fluorescence images after FDA staining images of the different MC after 1, 7 and 14 days of culture are shown in Figure 7.10. At low culture times, the MC were able to move easily around the spinner flask and were resuspend when the spinner flask was



stirred. However, at 7 days, as evidenced by the FDA images, the MC tended to agglomerate (Figure 7.10). This was visually observed by sedimentation of big clusters of MC at the bottom of the flask. Since the MC were at the bottom of the flask, cells tended to start proliferating in the interface between the different MC and tended to aggregate them, therefore the resuspension upon stirring was hindered.

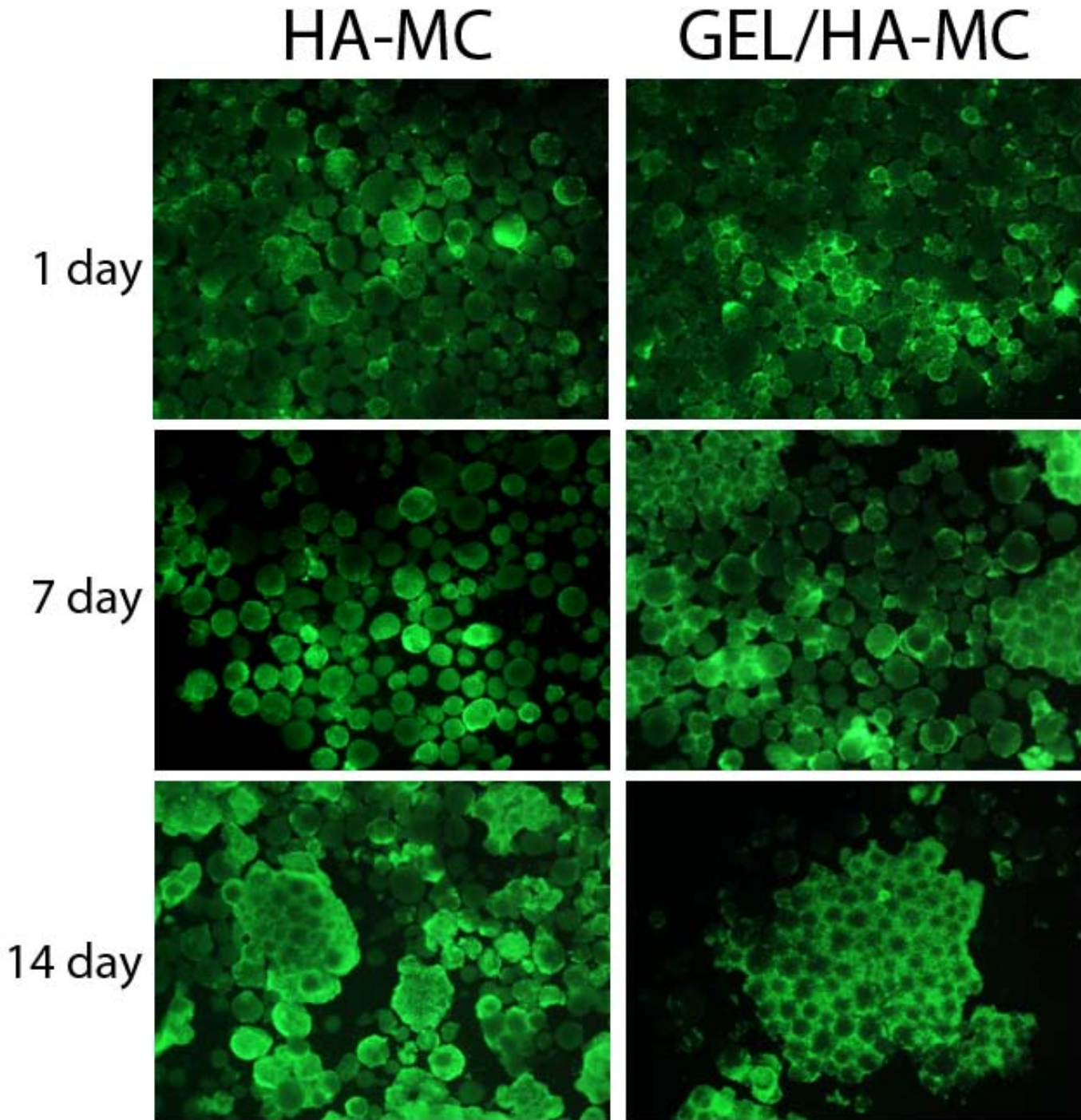
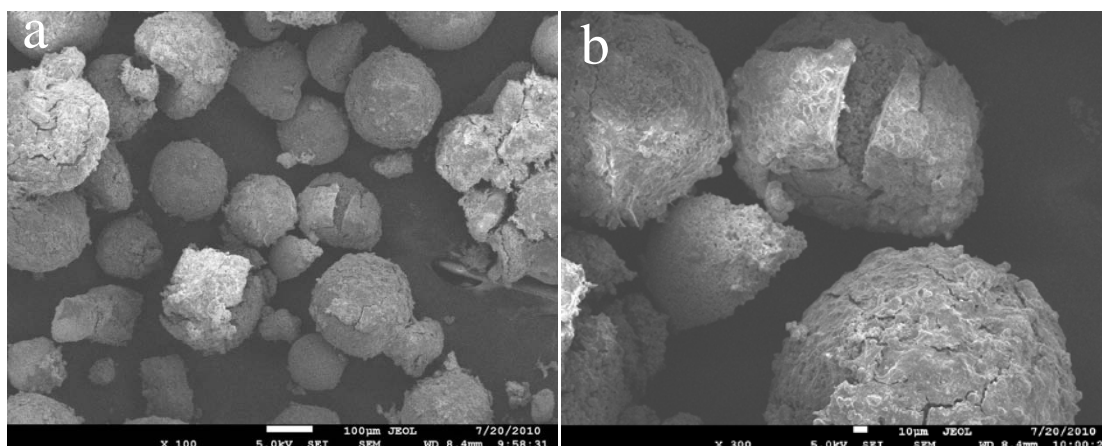


Figure 7.10. Fluorescence images after FDA staining images obtained at 1, 7 and 14 days for the HA-MC and GEL/HA-MC. Bar = 200  $\mu$ m.

After 14 days of culture, the distribution of cells on the MC was rather heterogeneous. Whereas some MC had plenty of cells on top of them, other had few or no cells (Figure 7.11).



*Figure 7.11. SEM image after 14 days of dynamic culture for the HA-MC. a) Low magnification of the different MC presenting some MC with cells and some MC with no cells. b) Higher magnifications of MC covered with several layers of cells on top of the MC.*

The results of cell proliferation measured by LDH in static culture are shown in Figure 7.12a. Low number of cells were found for the HA-MC at 1 and 7 days of culture. The number of cells in the HA-MC considerably increased after 14 days compared to 1 and 7 days. A higher cell number at 1 and 7 days in the GEL/HA-MC compared to HA-MC was observed. There were no significant differences in the number of cells between HA-MC and GEL/HA-MC after 14 days.

In the dynamic culture, the trend was different to the static as shown in Figure 7.12b. At 1 day, there were statistically significant differences between HA-MC and GEL/HA-MC. After 7 days, the amount of cells was higher in the case of HA-MC than on the gelatin containing MC, whereas after 14 days, the trend was the opposite and the amount of cells was higher for the gelatin containing MC, being the differences significant in both cases.

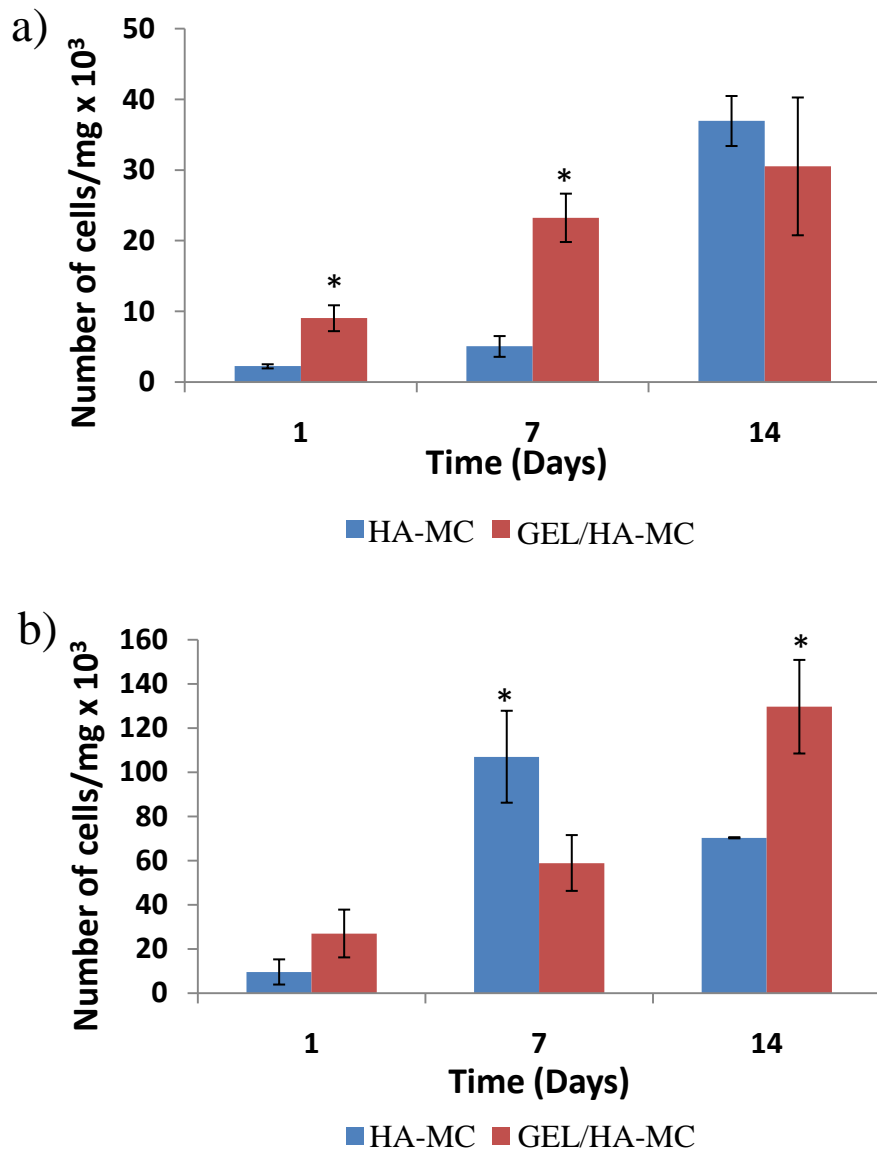


Figure 7.12. Proliferation for 1, 7 and 14 days measured with LDH for HA-MC and GEL/HA-MC in a) static culture and b) dynamic culture. \* denotes significant differences ( $p < 0.05$ ).

### 7.4.2. MC-containing alginate gels

The MC were then combined with sodium alginate gel to assess their ability to be injected. All the MC were injectable when mixed with a 2% sodium alginate solution. The sodium alginate gel was also able to adapt to the mould in which it was injected. Once the gel was extracted and lyophilized, the MC were shown to form well defined cylinders, demonstrating that the gel had been able to adapt to the walls of the moulds.

The samples were lyophilized and observed by stereoscope as shown in Figure 7.13. The cross-section of the samples presented a structure composed of MC aggregation.

The outside of the lyophilized MC containing gel showed that the different MC were placed together and linked through the alginate gels. At higher magnifications, it was observed that the different MC were not in contact with surrounding MC, but were separated by the alginate gel.

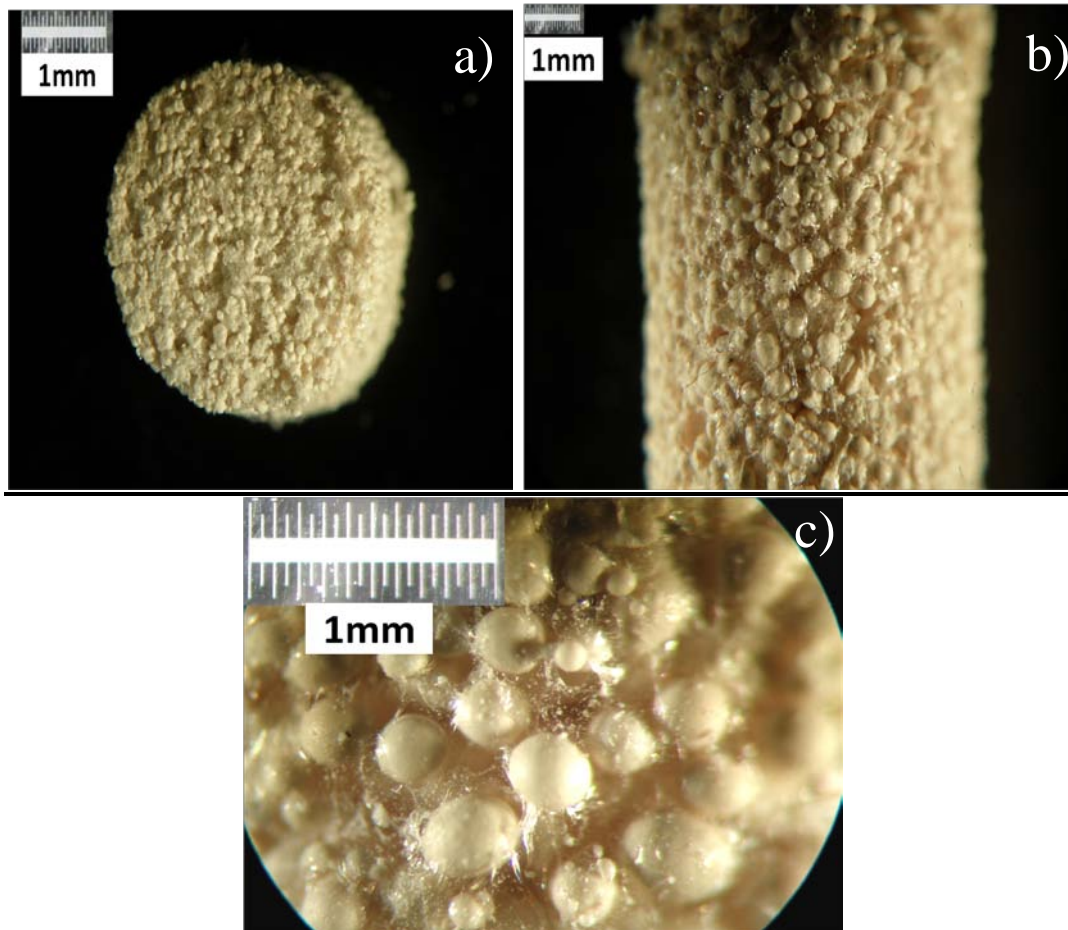


*Figure 7.13. Optical images of the constructs obtained with the alginate and GEL/HA-MCs showing a) the top surfaces, b) the lateral surface and c) top surface at higher magnifications.*

SEM images of the lyophilized gels are shown in Figure 7.14. The morphology was similar for the HA-MC and the GEL/HA-MCs, but different to the GEL/HA-MCb (Figure 7.14). The gaps between MC in the latter case were bigger.

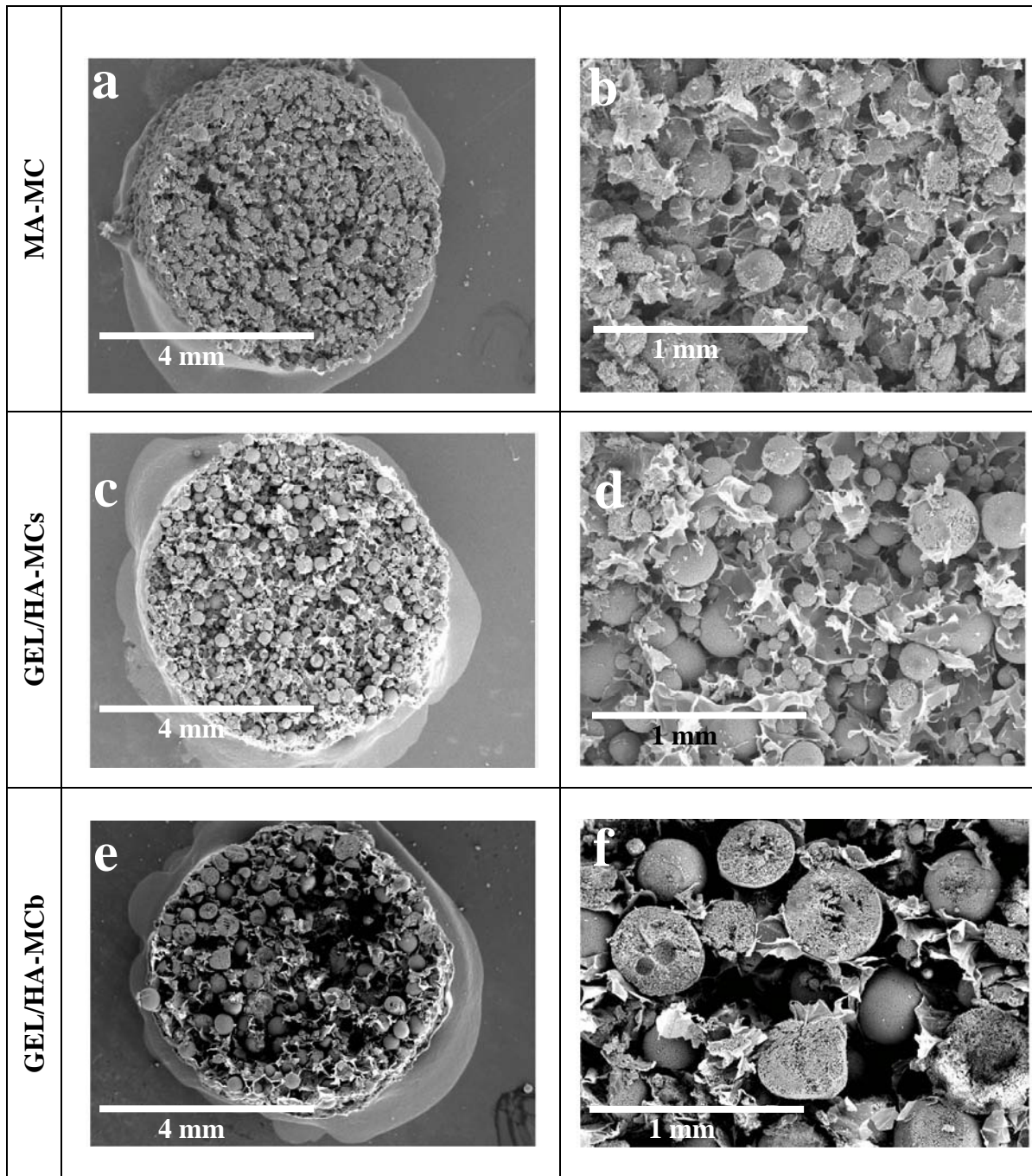


Figure 7.14. SEM images for the different constructs obtained from the mixing with alginate. a) and b) HA-MC construct, c) and d) GEL/HA-MCs construct, e) and f) GEL/HA-MCb construct.

The total porosity of the samples and the pore size distribution were measured by MIP. The results are shown in Figure 7.15. It can be seen that, as expected, the bigger the MC size, the bigger the gaps between them, and therefore, the bigger the pore size observed (Figure 7.15a). In the case of the HA-MC and the GEL/HA-MCs, the pore size was in the range between 6 and 100  $\mu\text{m}$ , having its peak in the range of 30 to 40  $\mu\text{m}$ . However, in the GEL/HA-MCb, the pore size distribution ranged between 10  $\mu\text{m}$  and 160  $\mu\text{m}$ ,

having its peak at a value of 65  $\mu\text{m}$ . Furthermore, the same graphic is shown in logarithmic scale (Figure 7.15b), showing at low pore size the pores corresponding to the intrinsic porosities of the MC, as was already shown in Chapter 5.

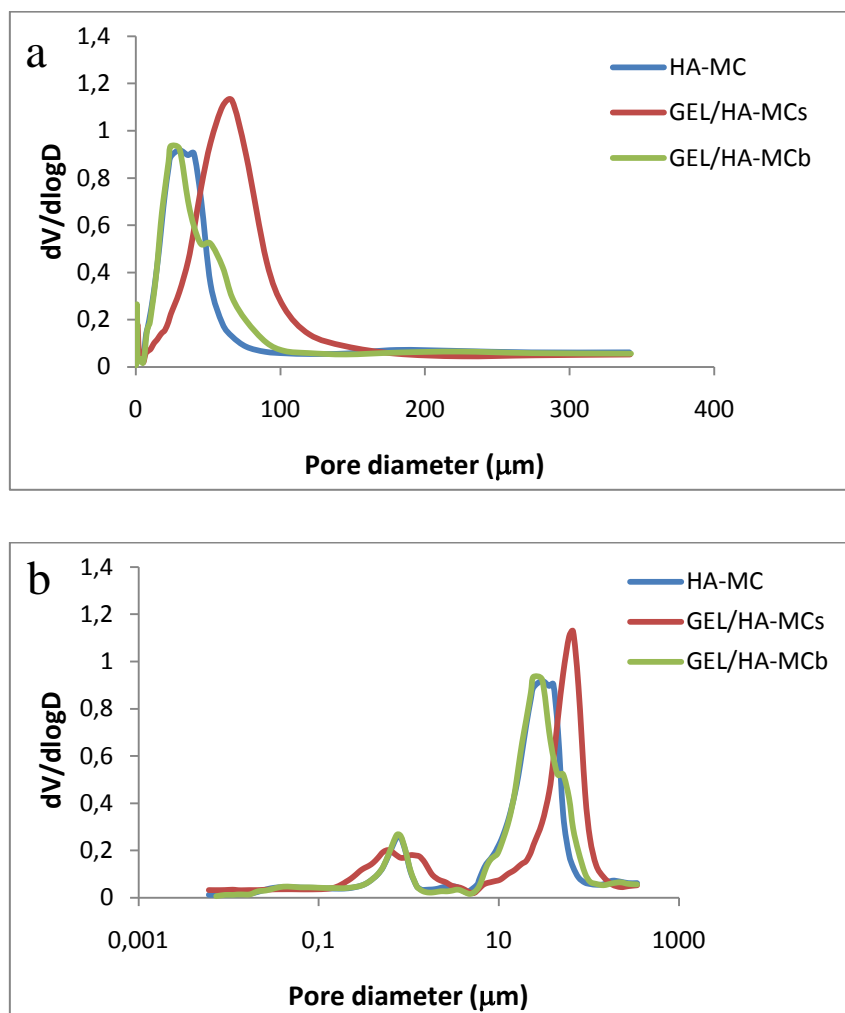


Figure 7.15. Pore size distribution for the HA-MC, GEL/HA-MCs and GEL/HA-MCb construct. a) Lineal scale and b) logarithmic scale.

Although presenting considerably different pore size distributions, the total porosity of the samples was similar in all cases (Table 7.1).

Sample	% Porosity
HA-MC	73.9
GEL/HA-MCs	74.2
GEL/HA-MCb	74.1

Table 7.1 Porosity of the different constructs obtained with the microcarriers.

## 7.5. Discussion

The dynamic cultures are of importance in several fields and have been widely used to expand cells on MC instead of the typical culture flasks<sup>25-28</sup>. There are two main applications for the use of MC as shown in Figure 7.16. MC can be designed so that cells are able to attach on them in order to obtain high number of viable cells for further experiments, or they can be designed so that cells attach on them for further implantation of the MC loaded with the cells into the defect site. This is the approach proposed in this Thesis.

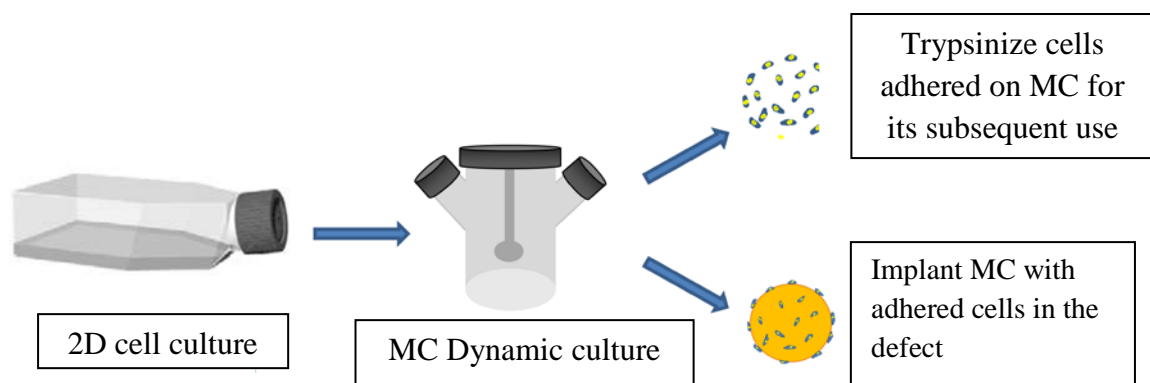


Figure 7.16. Representation of the use of MC. Cells are cultured on 2D cell culture on T-flasks. These anchorage dependent cells may attach to microcarriers in a dynamic culture. The microcarriers can be used, depending on the material and the purpose, as a way to obtain a high amount of viable cells due to the high surface available for cells to attach, or can be directly implanted into a defect to deliver a biomaterial with and elevated amount of cells.

An important issue is that depending on the MC nature, the gentle agitation can be insufficient to resuspend the MC. Polymeric MC, present low densities and are resuspended easily<sup>5,6</sup>. However, ceramics present higher densities, which may provoke sedimentation of the MC at the bottom of the flask. Actually, this is considered as one of the main drawbacks when using calcium phosphate MC in dynamic cultures, since their density is higher compared to the culture medium. In order to decrease the density of the MC, attempts have been made to fabricate hollow HA MC<sup>29,30</sup>.

In order to enhance MC resuspension, the effect of using a high rotation speed (80 rpm) was analyzed. As shown in Figure 7.3, the results showed a higher number of cells in the different MC seeded at 40 rpm compared to the cells seeded on the MC at 80 rpm.

Furthermore, the number of MC with cells on top was higher in the 40 rpm seeded MC. Moreover, MC were shown to fracture after the 24 hour initial experiment for the 80 rpm speed. It was concluded that, although the higher speeds gave rise to a higher resuspension of the MC in the medium, the higher speed was detrimental for cell viability and MC integrity. Therefore, the 40 rpm speed was selected for the dynamic cultures.

It has been documented that speed influences adhesion and proliferation on MC<sup>3,4</sup>. It was observed that speeds around 40 and 60 rpm gave the highest values of proliferation for Vero cells on Cytodex MC, whereas lower or higher speeds decreased the number of proliferating cells<sup>3,4</sup>. This can be related to the fact that cells can be damaged by strong collisions during agitation at high rotating speeds<sup>31</sup>. Therefore, equilibrium has to be found between rotating speed, cell viability and MC integrity.

The 40 rpm speed did not resuspend the HA MC as much as in the case of the polymer. That is, in the case of CYTODEX, the MC were dispersed in all the volume, or in other words, they were resuspended to the highest height of the flask as seen in Figure 7.17. For the HA-containing MC, the MC only reached a small height as observed in Figure 7.17. The black arrows represent the height the MC were able to reach in each case, whereas the red arrows represent the height cells reached. In both cases, the red arrows are the same length, indicating that the height reached for the cells is the same in both cases.

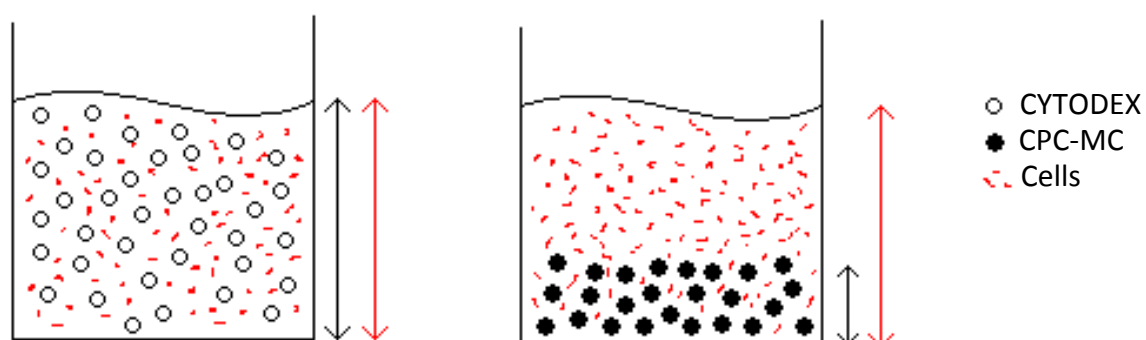


Figure 7.17. Representation of the suspension ability of the different MC (Cytodex and CPC-MC) upon stirring. The black arrows represent the total height the MC are resuspended, whereas the red arrows represent the height into which the cells are resuspended.



Nevertheless, the conclusion that was extracted from the results was that it was more favorable for cell viability to have a lower rotation speed that would not damage the cells, instead of having higher rotating speeds that would not allow for cells to adhere and survive on the MC.

One of the goals of this chapter was to apply the spinner flask dynamic culture system to the HA containing MC and compare it with the static culture system. However, the two systems are very different, and therefore, direct comparison is difficult. Table 7.2 summarizes the main values for the parameters in each of the two culturing conditions. The values for the dynamic culture were selected according to the CYTODEX manufacturer and to previous studies<sup>3,4,23</sup>. The fact of having a big volume of medium in the spinner flask allowed for a higher number of cells to be introduced. However, the number of cells that can be seeded in the well plate in static was limited because of the medium volume and of the available space.

	Static	Dynamic
<i>MC Weight (mg)</i>	39	300
<i>MC Surface (cm<sup>2</sup>)</i>	11.8	82.5
<i>Cells seeded</i>	2x10 <sup>5</sup>	10 <sup>7</sup>
<i>Medium (ml)</i>	1	100
<i>Cells/surface of MC (cells/cm<sup>2</sup>)</i>	16,949	121,212
<i>Cells/weight of MC (cells/mg)</i>	5,128	33,333

Table 7.2. Comparison between the different parameters of cell culture in static and dynamic culture.

Moreover, it was interesting to carry out two different types of experiments: short-term and long-term. For the short-term culture, the differences between the dynamic and the static cultures were quite significant. In order to compare the dynamic and static culture easier, the values for the different MC were combined in Figure 7.18. In the HA-MC and GEL/HA-MC in static cultures, the proliferation was very low. In the 3 day period, no increase in cell number was observed. This is related with the intrinsic properties of the material and with the low seeding efficiency of the MC. Cells seeded on HA and similar materials have in general low attachment ratios due in some cases to the surface roughness<sup>32,33</sup>. Therefore, proliferation is usually delayed and the amount of cells on the material is low at short times. Regarding the seeding efficiency, in static it is usually low<sup>26</sup> since cells may fall in the gaps between the MC. This is because once the cells are

seeded, the cells that are able to attach on the MC survive, whereas the ones that sediment on the bottom of the non-adhesive well, die. Furthermore, if the cells that sediment on top of the MC are moved by any reason (e.g. well plate movement into incubator), cells that had sedimented on top of the MC may also fall to the bottom of the well, therefore reducing even more its seeding efficiency.

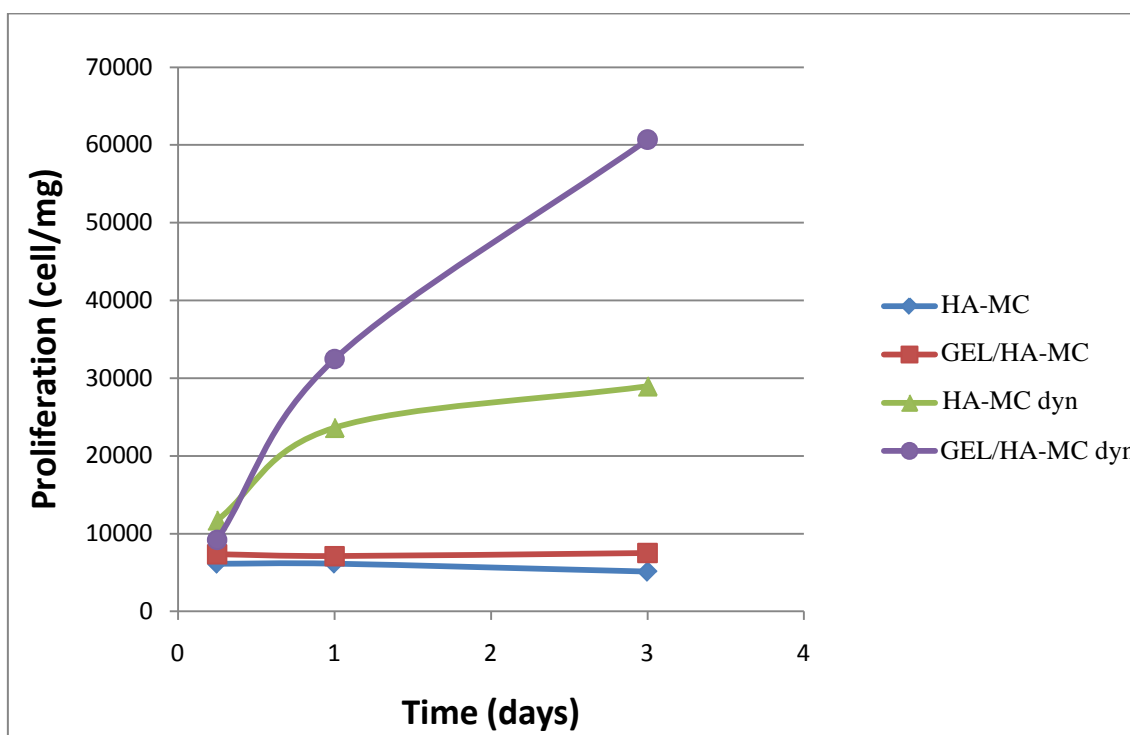


Figure 7.18. Comparison between the dynamic and static culture for HA-MC and GEL/HA-MC after 3 days of culture.

On the other hand, the dynamic culture system at short times clearly showed an increase in the number of cells from 6 hours to 24 and 72 hours for both HA-MC and GEL/HA-MC (Figure 7.18). The materials were the same as the materials prepared for the static culture. Therefore, the differences in cell number are not due to the materials, but to the seeding mechanism. There were also clear differences when comparing the HA-MC and the GEL/HA-MC in dynamic culture. Although under dynamic conditions the cell adhesion was promoted, the presence of gelatin promoted even more the adhesion of cells on these MC due to the RGD sequence on the gelatin as has already been discussed.

The results for the GEL/HA-MC were also compared to the CYTODEX (Figure 7.19). There were differences, especially in the static culture. In the static culture, as was

previously seen, GEL/HA-MC barely had an increase in cell number from 6 hours to 72 hours. For CYTODEX the cell number considerably increased after 72 hour compared to GEL/HA-MC, although it can be seen that the cell number after 6 hours is similar in both cases. Therefore, the number of cells initially adhered was similar, but due to the morphology of the material, cells were able to proliferate faster in the CYTODEX. CYTODEX presents surface properties that make these materials optimum for anchorage dependent cells to attach. CYTODEX are composed of DEAE-dextran and covered with collagen, presenting a relatively smooth surface. Therefore, the spiky morphology of the GEL/HA-MC was shown to be detrimental compared to the CYTODEX already in static culture.

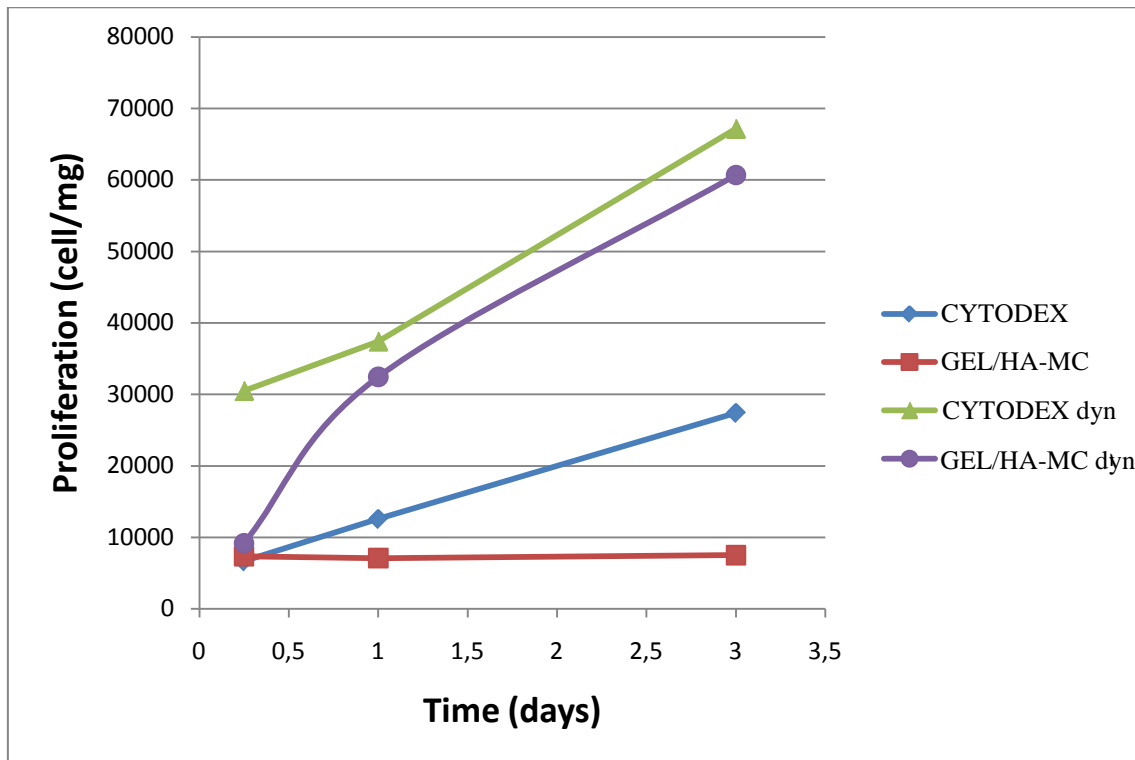


Figure 7.19. Comparison between the dynamic and static culture for CYTODEX and GEL/HA-MC after 3 days of culture.

On the other hand, when comparing the two materials in dynamic cultures, the differences were not as pronounced (Figure 7.19). There were a higher number of cells after 6 hours for CYTODEX compared to GEL/HA-MC, meaning that the seeding efficiency was higher for CYTODEX. Nevertheless, these differences disappeared after 24 and 72 hours. Actually, a very important observation that is worth highlighting is that the trend for the cells cultured on CYTODEX in dynamic and static was very

similar. It can be observed in Figure 7.19 that the curves in static and dynamic for CYTODEX have similar slopes. The only difference was the amount of cells loaded. However, in the GEL/HA-MC, the trend was very different between the dynamic and the static conditions. Therefore, the conclusion was that for GEL/HA-MC, the dynamic culture clearly increased the ability cells had to attach and proliferate, whereas for the CYTODEX, the MC had similar ability to attach and proliferate on the MC in static and dynamic culture.

In order to observe the effect at longer culture times, the 14 day culture was performed (Figure 7.20). Regarding cell proliferation, the results showed that the amount of cells was higher for the dynamic conditions as was already shown for the short term cultures. The main differences compared to the short term cultures, was that even though the system was also under gentle agitation, the MC aggregated among them. As can be seen in Figure 7.10, clusters of MC were formed after 7 and 14 days, with high amounts of cells. This aggregation took place once the cells achieved confluence on the surface of the MC.

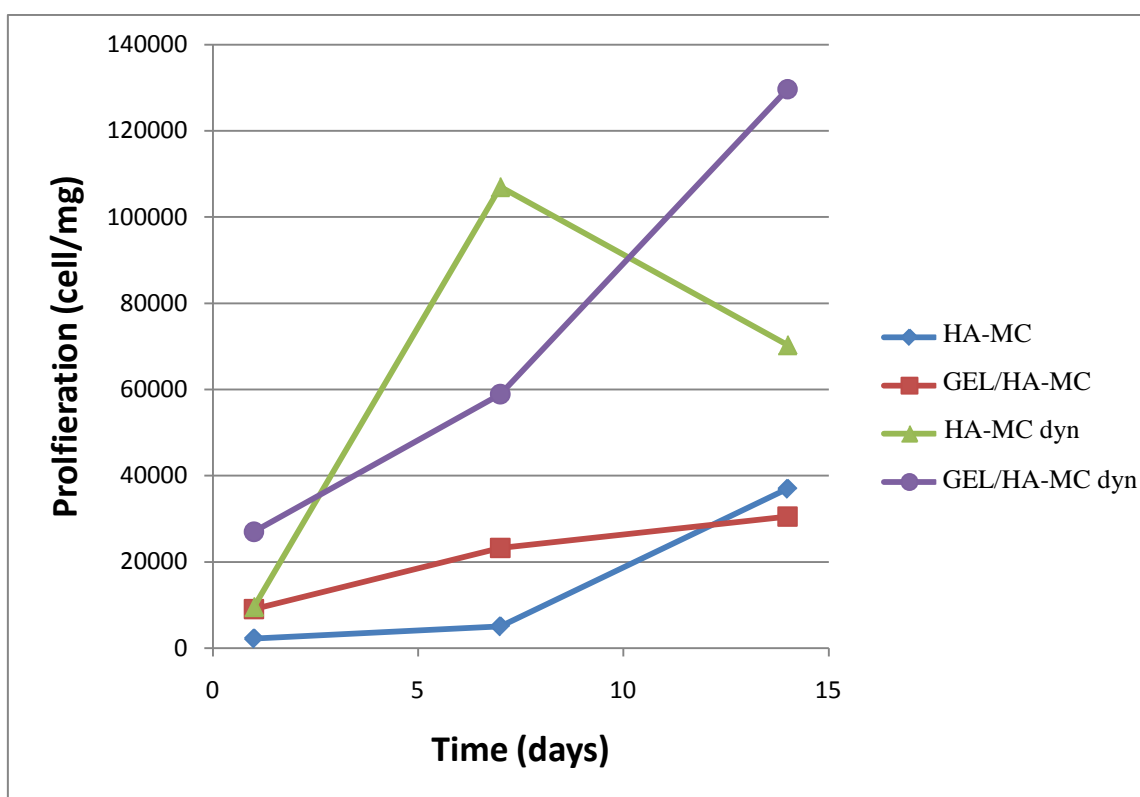


Figure 7.20. Comparison between the dynamic and static culture for HA-MC and GEL/HA-MC after 14 days of culture.

It was also observed by SEM in Figure 7.11, that cells were forming confluent cell layers on top of the MC. The fact of having some MC with several monolayers of confluent cells on top of the MC could also affect the phenotypic expression of these cells, since it is known that when cells are submitted to different types of stress, these are able to differentiate into different types of cell lineage<sup>34</sup>.

Nevertheless, in some cases, the aggregation of the MC can be exploited to obtain hybrid cell/material constructs. The degree of aggregation can be controlled by regulating different culture conditions such as mixing intensity<sup>27,35</sup>, oxygen tension<sup>36</sup> or duration of culture<sup>35</sup> among others. The aggregation is actually demonstrating that cells are being able to proliferate and create ECM in order to make the different MC aggregate. An example of aggregation has been previously described, in which it was shown that chondrocyte seeded MC cultured for less than two weeks in a spinner culture, provided constructs suitable for injection; these chondrocyte-MC aggregates could be delivered, arthroscopically, into the cartilage defect or could be used for meniscus reconstruction<sup>35,37</sup>.

Regarding the injectability of the gels containing the MC, it was important to select a gel that, in addition to enhance injectability, would not jeopardize cell viability. It was shown that the sodium alginate gel was a good system to allow for the injection of the MC. The total porosities were similar when using the different size MC. Nevertheless, GEL/HA-MCb had a higher pore size distribution which would allow for cells to migrate from the inside the MC to the surrounding tissue (Figure 7.15). Similar results were previously reported, where it was seen that as the microsphere size was increased, the pore size was increased for PLLA and PLAGA microspheres<sup>38,39</sup>. Actually, the remaining porosity in the gels is of great importance since it is necessary for nutrient diffusion as well as for cell migration. The amount of MC incorporated in the gels was 2 ml/g, which represent 31% of MC weight in the composite. In a previous study, a 6% alginate gel incorporated 40% wt of HA MC<sup>40</sup>, presenting reasonable injectability, presenting a similar behavior to that found in the present Chapter. When the amount of MC was increased to 60 % of HA microspheres<sup>40</sup>, problems of injectability appeared. The conclusion is that equilibrium must be found between the amount of the microspheres incorporated, the porosity and the ability to inject the microspheres.

Similar material to the present injectable alginate-MC composed of  $\beta$ -TCP microspheres and alginate gel was shown to sustain cell growth and differentiation and that once implanted *in vivo* it was able to adapt to the bone irregularities<sup>41</sup>. Nevertheless, in this previous study, the approach was slightly different, since the microspheres were used as a system to increase the mechanical properties of the gel and to increase the osteoconductivity of the composite. The cells were then combined with the alginate gel and then mixed with the microspheres, whereas our approach would be to load the microcarriers with cells and then combine them with the gel to inject them.

Regarding the cell viability, alginate gels have been previously used to encapsulate directly cells and implant them<sup>42</sup>, the cells maintaining their viability within the crosslinked gel<sup>43,44</sup>. Some problems of low cell adhesion were assessed for these types of gels, when the gels were crosslinked with calcium<sup>21,22</sup>. If the crosslinking was done with other ions, such as iron, enhancement of the cell adhesion was observed<sup>45</sup>. In any case, alginate has been proved as a biocompatible and biodegradable material for its use in tissue engineering and regenerative medicine<sup>46,47</sup>. Alginate may degrade as fast as desired controlling different parameters, especially its crosslinking ability<sup>48-50</sup>.

## 7.6. Conclusions

The results have shown an increase in dynamic cultures compared to the static ones. It was seen that it is of high importance to select an adequate speed for the culture in dynamic system, since the speed plays a key role in the survival of the cells as well as on the microcarriers integrity. The dynamic culture was shown to be a valid system to increase the ability of cells to attach to the HA containing MC. Short culture times were a good system to obtain HA containing MC with cell cultured on top of them. Nevertheless, if an aggregation of MC is desired through cell contacting, longer time periods may be used. These MC were injectable when mixed with sodium alginate solutions and can be used as injectable microscaffolds.

## 7.7. References

1. Freed LE, Vunjak-Novakovic C & Langer R. Cultivation of cell-polymer cartilage implants in bioreactors. *Journal of Cellular biochemistry* **51**, 257 (1993).
2. Malda J & Frondoza CG. Microcarriers in the engineering of cartilage and bone. *Trends in Biotechnology* **24**, 299-304 (2006).
3. Hirstenstein M & Clark J. Tissue culture in medical research. Pergamon Press, Oxford, (1980).
4. Wu SC. Influence of hydrodynamic shear stress on microcarrier-attached cell growth: cell line dependency and surfactant protection. *Bioprocess Engineering* **21**, 201-206 (1999).
5. Chung HJ, Kim IK, Kim TG & Park TG. Highly open porous biodegradable microcarriers: In vitro cultivation of chondrocytes for injectable delivery. *Tissue Engineering* **14**, 607-615 (2008).
6. Overstreet M, Sohrabi A, Polotsky A, Hungerford DS & Frondoza CG. Collagen microcarrier spinner culture promotes osteoblast proliferation and synthesis of matrix proteins. *In Vitro Cellular Devices in Biology* **39**, 228-234 (2003).
7. Qiu QQ, Ducheyne P & Ayyaswamy PS. Fabrication, characterization and evaluation of bioceramic hollow microspheres used as microcarriers for 3-D bone tissue formation in rotating bioreactors. *Biomaterials* **20**, 989-1001 (1999).
8. Park JS *et al.* Evacuated calcium phosphate spherical microcarriers for bone regeneration. *Tissue Engineering* **16A**, 1681 (2010).
9. Hong SJ, Yu HS & Kim HW. Preparation of porous bioactive ceramic microspheres and in vitro osteoblastic culturing for tissue engineering applications. *Acta Biomaterialia* **5**, 1725 (2009).
10. Sams AE, Monir RR, Wootton JA, Mohammed H & Nixon AJ. Local and remote matrix responses to chondrocyte-laden collagen scaffold implantation in

- extensive articular cartilage defects. *Osteoarthritis and Cartilage* **3**, 61-70 (1995).
11. Taguchi T *et al.* Encapsulation of chondrocytes in injectable alkali-treated collagen gels prepared using poly(ethylene glycol)-based 4-armed star polymer. *Biomaterials* **26**, 1247-1252 (2005).
  12. Chenite A *et al.* Novel injectable neutral solutions of chitosan from biodegradable gels in situ. *Biomaterials* **21**, 2155-2161 (2000).
  13. Chung HJ *et al.* Synthesis and characterization of Pluronic grafted chitosan copolymer as a novel injectable biomaterial. *Current Applied Physics* **5**, 485-488 (2005).
  14. Paige KT, Cima LG, Yaremchuk MJ, Vacanti JP & Vacanti CA. Injectable cartilage. *Plastic Reconstruction Surgery* **96**, 1390-1400 (1995).
  15. Stevens MM, Qanadilo HF, Langer R & Shastri VP. A rapid-curing alginate gel system: utility in periosteum-derived cartilage tissue engineering. *Biomaterials* **25**, 887-894 (2004).
  16. Balakrishnan B & Jayakrishnan A. Self-cross-linking biopolymers as injectable in situ forming biodegradable scaffolds. *Biomaterials* **26**, 3941-3951 (2005).
  17. Park YD, Tirelli N & Hubbell JA. Photopolymerized hyaluronic acid-based hydrogels and interpenetrating networks. *Biomaterials* **24**, 893-900 (2003).
  18. Shu XZ, Liu YC, Palumbo FS, Luo Y & Prestwich GD. In situ crosslinkable hyaluronan hydrogels for tissue engineering. *Biomaterials* **25**, 1339-1348 (2004).
  19. Wang C, Gong Y, Lin Y, Shen J & Wang DA. A novel gellan gel-based microcarrier for anchorage-dependent cell delivery. *Acta Biomaterialia* **4**, 1226-1234 (2008).
  20. Hong Y, Gong Y, Gao C & Shen J. Collagen-coated polylactide microcarriers/chitosan hydrogel composite: injectable scaffold for cartilage regeneration. *Journal of Biomedical Materials Research* **85A**, 628-637 (2008).



21. Smetana K Jr. Cell biology of hydrogels. *Biomaterials* **14**, 1046-1050 (1993).
22. Rowley JA, Malambayan G & Mooney DJ. Alginate hydrogels as synthetic extracellular matrix materials. *Biomaterials* **20**, 45-53 (1999).
23. Yang Y, Rossi FMV & Putnins EE. Ex vivo expansion of rat bone marrow mesenchymal stromal cells on microcarriers beads in spin culture. *Biomaterials* **28**, 3110-3120 (2007).
24. Malda J, Kreijveld E, Temenoff JS, van Blitterswijk CA & Riesle J. Expansion of human nasal chondrocytes on macroporous microcarriers enhances redifferentiation. *Biomaterials* **24**, 5153-5161 (2003).
25. Melero-Martin JM, Dowling MA, Smith M & Al-Rubeai M. Expansion of chondroprogenitor cells on macroporous microcarriers as an alternative to conventional monolayer systems. *Biomaterials* **27**, 2970-2979 (2006).
26. Schop D *et al.* Expansion of human mesenchymal stromal cells on microcarriers: growth and metabolism. *Journal of Tissue Engineering and Regenerative Medicine* **4**, 131-140 (2010).
27. Frondoza C, Sohrabi A & Hungerford D. Human chondrocytes proliferate and produce matrix components in microcarrier suspension culture. *Biomaterials* **17**, 879-888 (1996).
28. Malda J *et al.* Expansion of bovine chondrocytes on microcarriers enhances redifferentiation. *Tissue Engineering* **9**, 939-948 (2003).
29. Doctor J *et al.* Evaluating microcarriers for delivering human adult mesenchymal stem cells in bone tissue engineering. *Developmental Biology* **247**, 505 (2002).
30. Qiu Q, Ducheyne P & Ayyaswamy P. 3D bone tissue engineered with bioactive microspheres in simulated microgravity. *In vitro Cellular Developmental Biology Animals* **37**, 157-165 (2001).

31. Lakhota S & Paputsakis ET. Agitation induced cell injury in microcarrier cultures, protective effect of viscosity is agitation intensity dependent: experiments and modeling. *Biotechnology and Bioengineering* **39**, 95 (1992).
32. Zhang W, Walboomers XF, Van Osch G, Van den Dolder J & Jansen JA. Hard tissue formation in a porous HA/TCP ceramic scaffold loaded with stromal cells derived from dental pulp and bone marrow. *Tissue Engineering* **14**, 285-294 (2008).
33. Bjerre L, Bünger C, Baatrup A, Kassem M & Mygind T. Flow perfusion culture of human mesenchymal stem cells on coralline hydroxyapatite scaffolds with various pore sizes. *Journal of Biomedical Materials Research* **97A**, 251-263 (2011).
34. Altman G *et al.* Cell differentiation by mechanical stress. *FASEB* **16**, 270-272 (2002).
35. Shikani AH *et al.* Propagation of human nasal chondrocytes in microcarrier spinner culture. *American Journal of Rhinology* **18**, 105-112 (2004).
36. Malda J *et al.* Effect of oxygen tension on adult articular chondrocytes in microcarrier bioreactor culture. *Tissue Engineering* **10**, 987-994 (2004).
37. Tan H, Wu J, Huang D & Gao C. The design of biodegradable microcarriers for induced cell aggregation. *Macromolecular Bioscience* **10**, 156-163 (2010).
38. Borden M, Attawia M, Khan Y & Laurencin CT. Tissue engineered microsphere-based matrices for bone repair: design and evaluation. *Biomaterials* **23**, 551-559 (2002).
39. Borden M, El-Amin SF, Attawia M & Laurencin CT. Structural and human cellular assessment of a novel microsphere-based tissue engineered scaffolds for bone repair. *Biomaterials* **24**, 597-609 (2003).
40. Oliveira SM *et al.* Characterization of polymeric solutions as injectable vehicles for hydroxyapatite microspheres. *AAPS PharmSciTech* **11**, 852-858 (2010).

41. Matsuno T *et al.* Preparation of injectable 3D-formed  $\beta$ -tricalcium phosphate bead/alginate composite for bone tissue engineering. *Dental Materials Journal* **27**, 827-834 (2008).
42. Hunt NC & Grover LM. Cell encapsulation using biopolymer gels for regenerative medicine. *Biotechnology Letters* **32**, 733-742 (2010).
43. Trivedi N *et al.* Islets in alginate macrobeads reverse diabetes despite minimal acute insulin secretory responses. *Transplantation* **71**, 203-211 (2001).
44. Park JK & Chang HN. Microencapsulation of microbial cells. *Biotechnology Advances* **18**, 303-319 (2000).
45. Machida-Sano I, Matsuda Y & Namiki H. In vitro adhesion of human dermal fibroblasts on iron cross-linked alginate films. *Biomedical Materials* **4**, 1-8 (2009).
46. Wang L *et al.* Evaluation of sodium alginate for bone marrow cell tissue engineering. *Biomaterials* **24**, 3475-3481 (2003).
47. Becker TA, Kipke DR & Brandon T. Calcium alginate gel: a biocompatible and mechanically stable polymer for endovascular embolization. *Journal of Biomedical Materials Research* **54**, 76-86 (2001).
48. Matthew IR, Browne RM, Frame JW & Millar BG. Subperiosteal behavior of alginate and cellulose wound dressing materials. *Biomaterials* **6**, 275-278 (1995).
49. Iannuccelli V *et al.* Biodegradable intraoperative system for bone infection treatment 0.2. In vivo evaluation. *International Journal of Pharmaceutics* **143**, 187-194 (1996).
50. Wu SF, Suzuki Y, Tanihara M, Ohniihi K & Endo K Nishimura Y. Repair of facile nerve with alginate sponge without suturing: an experimental study in cats. *Scandinavian journal of plastic reconstruction hand surgery* **36**, 135-140 (2002).

# Conclusions and Future Perspectives

## Conclusions

### *Injectable Calcium phosphate cements with collagen*

1. The injectable calcium phosphate with collagen in its liquid phase was successfully fabricated and characterized.
2. The presence of collagen in the CPC slightly delayed the initial hydrolysis of the  $\alpha$ -TCP. The two main factors that determined this behavior were directly related with the acetic acid and to the higher viscosity of the collagen solution compared to water.
3. The analysis by XRD revealed the complete hydrolysis of  $\alpha$ -TCP to CDHA in the presence of collagen, meaning that the reaction was not affected in terms of the final product.
4. During the setting reaction of the collagen-CPC in water, collagen was not released after 7 days, even if it was not crosslinked.
5. The initial conformation of collagen was controlled obtaining fibrillised and solubilized collagen. The distribution of this collagen in the CPC after the setting reaction was different depending on this initial collagen conformation, obtaining homogenous distribution for the solubilized collagen and heterogeneous distribution for the fibrillised collagen.
6. The presence of solubilized collagen increased the injectability of the paste.
7. Collagen did not affect the compressive strength of the CPC at low collagen concentrations (10 mg/ml), but as the collagen concentration was increased (50 mg/ml), the compressive strength was decreased.
8. Cell proliferation was enhanced in the presence of solubilized. ALP activity was high in the presence of the CPC. Collagen did not have a significant effect on ALP activity, although the ALP pattern changed, obtaining the maximum ALP value after 1 day, whereas in the absence of collagen, the maximum was obtained at 7 days.

*Collagen-Calcium phosphate cement scaffolds*

1. Macroporous collagen scaffolds with increasing amounts of CPC were fabricated. The collagen scaffold served as a template for the CPC to deposit on top of it.
2. The transformation of  $\alpha$ -TCP into CDHA took place inside the collagen matrix.
3. The scaffolds were able to sustain adhesion, proliferation and differentiation of mesenchymal stem cells. As the amount of CPC was increased, the proliferation initially decreased, whereas the ALP activity increased.
4. A plasmid encoding BMP7 was incorporated into the scaffolds and it resulted in an increase in cell number. The amount of BMP7 expressed was significant, but did not differ when changing the amount of plasmid incorporated.

*Calcium phosphate cement Microcarriers*

1. Viable MC made of CPC mixed with collagen and gelatin were prepared. The size, shape and porosity were tailored by changing the composition of the CPC and the emulsion parameters, such as oil viscosity or agitation speed.
2. The presence of the biopolymers (collagen or gelatin) increased the sphericity of the MC.
3. The MC had a high porosity (~60% depending on the MC composition), in a range of pore size between 0.5 and 5  $\mu\text{m}$ , which would be useful for drug delivery applications.
4. Cells cultured on the MC showed a higher cell adhesion in the presence of gelatin compared to the rest of the materials, whereas after 14 days, collagen had the highest values of cell proliferation.
5. The dynamic culture of MC in spinner flasks allowed cell adhesion and proliferation of cells on the MC, having higher rates of proliferation compared to the static cultures.

**Future Perspectives**

The results obtained in the present thesis are promising in the field of tissue engineering and regenerative medicine. To be able to increase their potentially in this field, it would be of great interest to be able to incorporate some type of signaling to these CPC, such

as antibiotics or drugs. This could enhance bone regeneration in the site of defect or prevent infections once implanted. Furthermore, in order to enhance the angiogenesis, the dense calcium phosphate cements could be prepared as macroporous in order to allow for blood vessels to penetrate the whole material. This could be done by foaming the liquid phase of the CPC, being collagen the liquid phase. Since collagen is a protein and presents amphiphilic properties, it has similar properties to surfactants and can therefore form stable foams that can then be mixed with the powder to form macroporous CPC foams.

Regarding the work on macroporous scaffolds made of collagen and calcium phosphate cement and its use as gene delivery vehicle, they also showed promising results. In order to verify if these scaffolds would allow bone to grow ectopically, the scaffolds loaded with the BMP7 gene could be implanted *in vivo* in an animal model in order to observe if bone growth would take place outside of a bone region. Nevertheless, the efficiency of the plasmid incorporated as well as the amount of protein expressed need to be optimized. One of the approaches would be to further protect the gene inside the scaffold so that cells do not degrade the gene once it penetrates the cell membrane. For this purpose, the scaffold preparation can be modified, such as combining the gene with the CPC powder in order to obtain a paste slurry with gene and CPC, which would then be mixed with the collagen slurry to obtain a CPC/gene-collagen slurry, which upon the freeze-drying would give as a result the CPC-collagen scaffolds incorporating a gene in the matrix of the scaffold.

Microcarriers would be the ideal candidate to be used as drug delivery system. These have demonstrated to have microporosity suitable for releasing antibiotics, drugs or growth factors. The advantage of using these CPC MC is that the drug could be delivered through two main systems, such as the incorporation in the CPC paste for a supposed long deliver, or can also be incorporated by adsorption on the MC. The release would depend on the microporosity of the MC, which can also be tailored according to the CPC formulation. Furthermore, cells could also be seeded on top of the MC as was observed, and the combination of the cells with osteogenic potential, with the osteoconductive calcium phosphate and a drug/growth factor with osteoinductive potential, would lead to an ideal tissue engineering scaffold. An osteoinductive growth factor that could be used are those described in Chapter 4, being BMP-7 or BMP-2.

Furthermore, even though these MC have already been implanted in vivo, it would also be interesting to implant these MC combined with cells, incorporating an osteoinductive signal such as the mentioned BMP-7 and inject them through minimally invasive surgery with the studied alginate gel. This would confirm the viability of this composite as a promising biomaterial for tissue regeneration.